NASA TECHNICAL NOTE

AIRFRAME, WING, AND TAIL AERODYNAMIC CHARACTERISTICS OF A 1/6-SCALE MODEL OF THE ROTOR SYSTEMS RESEARCH AIRCRAFT WITH THE ROTORS REMOVED

Raymond E. Mineck and Carl E. Freeman

Langley Directorate,
U.S. Army Air Mobility R&D Laboratory
Langley Research Center
Hampton, Va. 23665

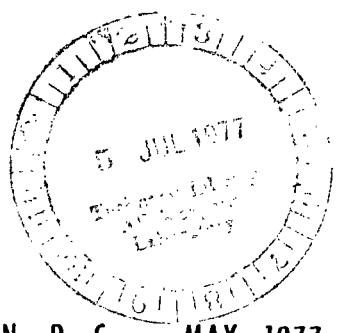

NATIONAL AERONAUTICS AND SPACE ADMINISTRATION • WASHINGTON, D. C. • MAY 1977

1. Report No.	2. Government Accession No.	3. Recipient's Catalog No.
NASA TN D-8456		

4. Title and Subtitle
AIRFRAME, WING, AND TAIL AERODYNAMIC CHARACTERISTICS OF A 1/6-SCALE MODEL OF THE ROTOR SYSTEMS RESEARCH AIRCRAFT WITH THE ROTORS REMOVED

5. Report Date
May 1977

6. Performing Organization Code

7. Author(s)
Raymond E. Mineck and Carl E. Freeman

8. Performing Organization Report No.
L-11201

9. Performing Organization Name and Address
Langley Directorate, USAAMRDL
NASA Langley Research Center
Hampton, VA 23665

10. Work Unit No.
505-10-21-05

11. Contract or Grant No.

12. Sponsoring Agency Name and Address
National Aeronautics and Space Administration
Washington, DC 20546
and
U.S. Army Air Mobility R&D Laboratory
Moffett Field, CA 94035

13. Type of Report and Period Covered
Technical Note

14. Army Project No.
1L161102AH45

15. Supplementary Notes

16. Abstract

A wind-tunnel investigation was conducted to determine the aerodynamic characteristics of the rotor systems research aircraft (RSRA) as the helicopter and the compound helicopter with the rotors removed. Data were obtained over ranges of angle of attack and angle of sideslip. Results are presented for the total loads on the airframe as well as the loads on the wing and the tail.

The results indicate that the RSRA with the rotors removed has stable static longitudinal and directional characteristics and has stable effective dihedral.

17. Key Words (Suggested by Author(s))	18. Distribution Statement
RSRA (rotor systems research aircraft) Compound helicopters	Unclassified - Unlimited Subject Category 02

19. Security Classif. (of this report)	20. Security Classif. (of this page)	21. No. of Pages	22. Price*
Unclassified	Unclassified	139	$6.00

*For sale by the National Technical Information Service, Springfield, Virginia 22161

AIRFRAME, WING, AND TAIL AERODYNAMIC CHARACTERISTICS OF A 1/6-SCALE MODEL OF THE ROTOR SYSTEMS RESEARCH AIRCRAFT WITH THE ROTORS REMOVED

Raymond E. Mineck* and Carl E. Freeman*
Langley Research Center

SUMMARY

A wind-tunnel investigation was conducted to determine the aerodynamic characteristics of the rotor systems research aircraft (RSRA) as the helicopter and the compound helicopter with the rotors removed. Data were obtained over ranges of angle of attack and angle of sideslip. Results are presented for the total loads on the airframe as well as the loads on the wing and the tail.

The results indicate that the RSRA has stable static longitudinal and directional characteristics and has stable effective dihedral. The wing provided a stabilizing contribution to the static longitudinal and directional stability but provided a destabilizing contribution to the effective dihedral. The auxiliary thrust engine nacelles provided a direct destabilizing increment to the longitudinal stability by acting as a lifting surface in front of the center of gravity and provided an indirect destabilizing increment by reducing the tail contribution to the longitudinal stability. The wing also reduced the tail contribution to the longitudinal stability. The tail provided a positive contribution to the longitudinal and directional stability and to the effective dihedral.

INTRODUCTION

NASA and the U.S. Army are jointly developing a unique research helicopter, the rotor systems research aircraft (RSRA). The RSRA is designed to obtain accurate data for development and validation of rotorcraft theory and for evaluating advanced rotor systems. It is equipped with a variable-incidence wing to load and unload the rotor, auxiliary thrust engines and drag brakes to cover a wide range of rotor propulsive force, and fly-by-wire controls to evaluate advanced flight control systems. The RSRA can be flown as a single-rotor helicopter, a compound helicopter, or a fixed-wing aircraft. Additional details of the RSRA may be found in reference 1.

Because the configuration is unique, four phases of wind-tunnel testing were conducted to determine and refine the aerodynamic characteristics of the RSRA. The Phase I test results indicated potential lateral and longitudinal stability problems with the rotors removed. (See ref. 2.) The Phase II and Phase III tests refined the configuration to improve the stability levels. (See refs. 2 and 3.) The Phase IV test investigated mutual interference effects of the wing, tail, and fuselage both with and without a main rotor. (See ref. 4.)

*Langley Directorate, U.S. Army Air Mobility R&D Laboratory.

The results from reference 4 for the configuration without the main rotor are analyzed herein.

SYMBOLS

The units used for the physical quantities defined in this paper are given in the International System of Units (SI) and parenthetically in U.S. Customary Units. Measurements and calculations were made in U.S. Customary Units. Conversion factors relating the two systems are presented in reference 5.

The longitudinal data on the airframe, wing, and tail are resolved in the stability-axis system and the lateral data in the body-axis system. Positive directions for the moments and forces are defined in figures 1(a), 1(b), and 1(c). The moment reference center for the airframe, wing, and tail was located 3.81 cm (1.5 in.) behind and 35.13 cm (13.83 in.) below the center of the rotor hub, which is the nominal aft center of gravity of the RSRA. Sign conventions used for the deflection angles of the control surfaces are shown in figure 1(d).

b	wing span, 2.29 m (90.0 in.)
$\bar{c}$	wing mean aerodynamic chord, 0.423 m (16.67 in.)
C_D	drag coefficient, D/qS
C_L	lift coefficient, L/qS
$C_{L_{i_w}}$	change in lift coefficient with wing incidence, dC_L/di_w, per deg
C_{L_α}	lift-curve slope, $dC_L/d\alpha$, per deg
C_l	rolling-moment coefficient, M_X/qSb
C_{l_β}	effective-dihedral parameter, $dC_l/d\beta$, per deg
C_m	pitching-moment coefficient, $M_Y/qS\bar{c}$
$C_{m_{i_t}}$	horizontal-tail effectiveness, dC_m/di_t, per deg
C_{m_α}	static longitudinal-stability parameter, $dC_m/d\alpha$, per deg
C_n	yawing-moment coefficient, M_Z/qSb
C_{n_β}	static directional-stability parameter, $dC_n/d\beta$, per deg
$C_{T,J}$	auxiliary jet engine thrust coefficient, T_J/qS
C_Y	side-force coefficient, F_Y/qS
D	drag, N (lbf); rotor diameter, 3.149 m (10.33 ft)

e	Oswald efficiency factor
F_Y	side force, N (lbf)
i_t	horizontal-tail incidence, deg
i_w	wing incidence, deg
L	lift, N (lbf)
M_X	rolling moment, N-m (lbf-in.)
M_Y	pitching moment, N-m (lbf-in.)
M_Z	yawing moment, N-m (lbf-in.)
q	free-stream dynamic pressure, Pa (lbf/ft^2)
S	wing area, 0.954 m^2 (10.27 ft^2)
T_J	total auxiliary engine thrust, N (lbf)
V	free-stream velocity, m/sec (ft/sec)
α	angle of attack, deg
β	angle of sideslip, deg
δ_f	flap deflection, deg
ε	downwash at lower horizontal tail, deg

Model components:

F_1	fuselage and ventral fin
F_2	fuselage and ventral fin with main-rotor pylon removed
H_C	compound horizontal tail
H_H	helicopter horizontal tail
J_1	flow-through nacelles
J_2	auxiliary thrust fans and nacelles
V	vertical tail
W_x	variable wing/flap settings:

W_1 $i_w = 0^o$, $\delta_f = 0^o$ W_2 $i_w = 7.5^o$, $\delta_f = 0^o$

W_4 $i_w = -9^o$, $\delta_f = 0^o$ W_5 $i_w = 0^o$, $\delta_f = 30^o$

W_6 $i_w = 7.5^o$, $\delta_f = 30^o$

Subscripts:

fus	fuselage
t	tail
w	wing

MODEL AND APPARATUS

The general rotor model system (GRMS) in the Langley V/STOL tunnel was used in this investigation. The external configuration was a 1/6-scale model of the RSRA. A detailed three-view sketch of the model is presented in figure 2(a). The dimensions and areas of the model components may be found in table I.

The exterior is identical with the Phase III model described in reference 3 except for the main-rotor pylon and the compound tail. The main-rotor pylon was widened 2.54 cm (1.00 in.). The upper horizontal tail of the compound tail had the same planform, but with an NACA 0015 airfoil section instead of the flat plate used in Phase III. The lower-horizontal-tail span was changed to 114.3 cm (45.0 in.). The various components of the model, such as the wings, auxiliary thrust engine nacelles, and the horizontal and vertical tails, were removable to simulate the RSRA in the helicopter or the compound helicopter configuration with the rotors removed. Transition grit was used on the wings, horizontal tail, vertical tail, and nose of the model to trip the boundary layer to turbulent flow.

The variable-incidence wing, which pivoted about the 3/4-root-chord location, could be set at incidence angles of -9^o, 0^o, and 7.5^o. The partial-span, single-slotted flaps were deflectable to 30^o. During these tests, in lieu of sealing the wing roots to the fuselage, large end plates were attached at the wing roots to allow the wing to be mounted on a six-component strain-gage balance. Having the wing mounted on this balance permitted direct measurement of wing loads.

The empennage was attached to the GRMS main structure with a strain-gage balance to measure the empennage loads directly. Loads on the empennage included loads on the tail cone from fuselage station 231.78 cm (91.25 in.) aft. At that point, a 0.28-cm (0.11-in.) gap in the tail cone allowed clearance for balance deflections. The upper horizontal tails could be removed from the vertical tail, and the vertical tail and lower horizontal tail could be removed from the tail cone. Details of the horizontal and vertical tails may be found in figure 2(b).

The vertical tail remained the same for both the helicopter and the compound helicopter. An upper horizontal tail H_H, which had an area of 0.091 m^2 (0.98 ft^2), was used for the horizontal tail for the helicopter. A compound

tail H_C consisting of a smaller upper horizontal tail, with an area of 0.046 m^2 (0.48 ft^2), and a lower horizontal tail, with an area of 0.228 m^2 (2.45 ft^2), was used for the compound helicopter.

Two removable auxiliary thrust engine nacelles were mounted on the fuselage. (See fig. 2(c).) Each nacelle contained a removable fan used to simulate the jet thrust. These fans, nacelles, and engine pylon fairings were the same as those used in reference 3. The engine pylon fairings were the modified minimum fairings.

Each fan had a stator and a rotor. A ring with turbine blades was attached to the rotor. Dry, high-pressure air directed onto the turbine blade tips drove the fan to produce thrust. Each nacelle had one static-pressure orifice and three total-pressure probes mounted in the fan exit of each engine. The three total-pressure probes were connected to a manifold. A pressure transducer was used to measure the difference between the total pressure and the static pressure to obtain an average reference dynamic pressure at the exit. This exit reference dynamic pressure was used to calibrate the engine thrust. During the investigation, the fans were removed from the nacelles for a "flow-through" mode.

A photograph of the model in the Langley V/STOL tunnel is shown in figure 3. The model was mounted on the airframe balance attached to a special model sting. This sting model support system allows high angles of attack and sideslip to be obtained and keeps the model near the center of the test section for pitch, roll, and yaw excursions. High-pressure air is piped into the model from an air plenum mounted directly below the total balance. This plenum is fed by an air line running through the center of the sting. A reverse double coil in this air line minimizes pressure effects and mechanical tare effects of the air line crossing the total balance.

The data recorded during the test consisted of averaged values taken from the strain-gage balances, air pressures, engine exit pressures, and wind-tunnel test conditions.

TEST CONDITIONS AND CORRECTIONS

This investigation was conducted in the Langley V/STOL tunnel, which is a closed-return, atmospheric tunnel with a test section measuring 4.42 m (14.50 ft) by 6.63 m (21.75 ft). Tunnel free-stream dynamic pressure was varied from 0 Pa (0 lbf/ft^2) to 2633 Pa (55 lbf/ft^2). All testing was conducted with the model close to the center line of the test section.

The auxiliary engine thrust was calibrated statically (zero wind speed) as a function of the exit dynamic pressure. However, at forward speeds the exit dynamic pressure should be equal to the free-stream dynamic pressure when the engine produces no thrust. To account for this, the free-stream dynamic pressure was subtracted from the exit dynamic pressure and this result was then used in the static calibration. This static calibration was the same type used in reference 3 to provide a direct comparison of the results from the two tests.

The engine thrusts were balanced for zero yawing moment at maximum thrust at static conditions.

The basic fuselage was tested with several combinations of the tail, wing, and jets to determine the aerodynamic contribution of each component. Five wing/flap settings were used for the compound helicopter: i_w/δ_f of $-9^\circ/0^\circ$, $0^\circ/0^\circ$, $0^\circ/30^\circ$, $7.5^\circ/0^\circ$, and $7.5^\circ/30^\circ$. The horizontal-tail incidence was set at 0° for all testing, except where noted. The auxiliary jet thrust coefficient was set at zero, trim, and alternate thrust levels (above or below trim thrust). For zero thrust, the dynamic pressure at the jet exit was set equal to the free-stream dynamic pressure at 0° angle of attack. At trim thrust, the thrust level was set for zero model drag ($C_D = 0$) at 0° angle of attack. For all cases, the fan rotational speed for the desired thrust level was held constant for the angle-of-attack or angle-of-sideslip variation.

Several corrections were made in the data reduction scheme to compensate for certain identifiable mechanical and aerodynamic interferences. Correction factors were obtained for (1) the effect of the air line crossing the airframe balance; (2) the effect of the model support system; (3) the effect of the proximity of the sting to the model; and (4) the effects of the wind-tunnel walls. The effect of the air line was determined by loading the balance statically with the air line crossing the balance and the air line removed. The effect of the model support system was determined by rotating the joints of the sting in such a way as to maintain a constant model attitude so that variations of model loads could be attributed to tunnel flow alterations caused by joint position. The effect of the proximity of the sting was estimated from unpublished data from Phase III tests. In these tests, a large tube was attached to the strut model support system in the same position as the sting mount of Phase IV. The methods described in reference 6 were used to account for the wall effects.

PRESENTATION OF RESULTS

The results of the wind-tunnel investigation have been presented in coefficient form. The wing, tail, and airframe forces and moments are all resolved about the same center of gravity and are nondimensionalized by the same factors. The longitudinal aerodynamic data are presented in figures 4 to 24; the lateral aerodynamic data, figures 25 to 42. The following table is a guide to the figures for the airframe, wing, and tail data:

	Figure for -		
	Airframe	Wing	Tail
Longitudinal aerodynamic characteristics:			
Comparison of Phase IV and Phase III	4 to 9		
Effect of empennage components	10		20
Effect of wing incidence and flap deflection	11	17	21
Effect of wing lift on fuselage lift		18	
Effect of auxiliary thrust nacelles	12		22
Effect of horizontal-tail incidence	13		23

	Figure for -		
	Airframe	Wing	Tail
Downwash at tail	14		
Effect of auxiliary engine thrust	15,16	19	24
Lateral aerodynamic characteristics:			
Comparison of Phase III and Phase IV	25		
Effect of vertical tail	26		37
Effect of horizontal tail	27		38
Effect of wing incidence and flap deflection without the tail	28	33	
Effect of wing incidence and flap deflection with the tail	29	34	39
Effect of auxiliary thrust nacelles	30		40
Effect of angle of attack	31	35	41
Effect of auxiliary engine thrust	32	36	42

DISCUSSION OF RESULTS

Longitudinal Aerodynamic Characteristics

Comparison of Phase IV and Phase III.- There were several differences in the external contours of the models used in Phase IV and Phase III. (See the section "Model and Apparatus".) The results from Phase III suggest that the data contain some interference effects arising from the model strut support. Because of the difference in the model external contours and the interference, five configurations were retested in Phase IV: the fuselage and vertical tail with (1) the wing; (2) the horizontal tail; (3) the wing and horizontal tail; (4) the wing and the jets; and (5) the wing, horizontal tail, and jets. The results for these configurations are presented in figures 4 to 8. The data for Phase III presented in figure 5(b) are for the 118.5-cm (46.67-in.) span lower horizontal tail; the data in figure 6 are for the 127.0-cm (50.0-in.) span lower horizontal tail. The data presented in figure 8 for Phase III are the average of the data for the 118.5-cm (46.67-in.) span tail and the 110.1-cm (43.33-in.) span tail.

In general, the longitudinal data from Phase III and Phase IV for either but not both the wing and the horizontal tail are in reasonable agreement (figs. 4, 5, and 7). With the wing on and the horizontal tail removed, the Phase IV data show a higher lift coefficient (by 0.03) and a nose-down pitching-moment-coefficient increment of 0.02. The model stalls at a higher angle of attack in Phase IV than in Phase III (fig. 4(a)). These differences may be caused by some of the changes in the model, by the differences in the auxiliary engine thrust levels, by the interferences from the model support system, or by small differences in the positions defined as 0° angle of attack or 0° wing or tail incidence. The data from figure 4 have been replotted in figure 9 to obtain the Oswald efficiency factor e. The results from Phase IV correspond to $e \approx 0.71$; whereas, the results from Phase III for 0° wing incidence correspond to $e \approx 0.98$ and for 7.5° wing incidence, to $e = 0.76$. It is not understood what

caused the small values of induced drag which led to the high value of e for 0° wing incidence in Phase III.

With the wing and tail on, the differences in lift and pitching-moment coefficients are larger than previously noted. (See figs. 6 and 8.) The lift coefficients are about 0.05 higher and the nose-down pitching-moment coefficients are about 0.13 more in Phase IV than in Phase III. As the wing incidence or flap deflection increases, the difference in lift and pitching-moment coefficients between Phase III and Phase IV increases. (See fig. 8.) For both phases, the static longitudinal stability C_{m_α} decreases near 0° angle of attack. A limited amount of data was obtained for an increased separation between the sting and tail. These data indicate that the sting interference on the tail moderately increases with increasing wing lift. Part of the stability degradation and part of the difference in lift and pitching moment may therefore be attributable to sting aerodynamic interference.

For the tail-on configurations, the difference in lift and pitching-moment coefficients may also be due to a difference in the tail angle of attack. (See figs. 6 and 8.) This could be caused by a difference in either tail incidence (that is, error in tail-incidence setting) or downwash at the tail between Phase III and Phase IV. Also, the difference in the auxiliary engine thrust level will affect the pitching moment because the thrust line is above the moment reference center. If the difference in model drag is used as an indication of the differences in model thrust, the pitching-moment data will be in closer agreement.

Airframe loads.- The model was tested with various components mounted on the fuselage to determine the aerodynamic contribution of each component and the mutual interference effects between the components. The lift-curve slope and static longitudinal stability were computed, and the results are presented in table II. The fuselage was tested with and without the empennage for the wings off and on, and the results are presented in figure 10. Adding the vertical tail to the fuselage has a negligible effect on the lift-curve slope or the static longitudinal stability. (See fig. 10(a).) The addition of the compound tail to the fuselage changed C_{m_α} from 0.011/deg to -0.052/deg. The lift-curve slope based on wing area for the fuselage with the compound tail was 0.020/deg. The addition of the helicopter tail changed the longitudinal static stability from 0.011/deg to -0.020/deg. The helicopter with either the helicopter tail or the compound tail but without the rotor has static longitudinal stability. The lift-curve slope based on wing area for the fuselage and the helicopter tail was 0.007/deg.

The addition of the compound horizontal tail to the fuselage with the wing adds a positive increment in pitching moment at 0° angle of attack. (See figs. 10(b) and 10(c).) This nose-up pitching-moment change is caused by the wing downwash at the tail. The static longitudinal stability is reduced to -0.0327/deg for 0° wing incidence with the flaps retracted (fig. 10(b)) and to -0.0248/deg for 7.5° wing incidence with the flaps deflected 30° (fig. 10(c)). The stability reduction is caused by an increase in $d\epsilon/d\alpha$ and a reduction in dynamic pressure at the tail.

The fuselage was tested with five wing/flap settings (combinations of wing incidence and flap deflection): -9°/0°, 0°/0°, 7.5°/0°, 0°/30°, and 7.5°/30°. These results are presented in figure 11 for the wing and (1) the fuselage, (2) the fuselage and compound tail, and (3) the fuselage, auxiliary thrust jets, and compound tail. The addition of the wing to the fuselage alone increases the static longitudinal stability, because the wing center of pressure is slightly aft of the moment reference center. (See fig. 11(a).) The lift-curve slope C_{L_α}, which is not dependent on wing incidence for the conditions tested, is about 0.074/deg with the flaps retracted and 0.076/deg with the flaps deflected. The maximum lift coefficient was larger for 0° wing incidence than for 7.5° wing incidence. This is attributed to increased fuselage lift. The change in lift coefficient with wing incidence $C_{L_{i_w}}$ was evaluated at 0° angle of attack. The calculated values were 0.065/deg with the flaps retracted and 0.068/deg with the flaps deflected. This value is less than that for the lift-curve slope because the change in fuselage lift is small when only the wing incidence is changed. These results are in good agreement with those obtained in reference 3.

The effect of wing incidence and flap deflection on the configuration with the compound tail installed is presented in figure 11(b). Increasing the wing incidence or deflecting the flaps increases the downwash and decreases the dynamic pressure at the tail. The increased downwash results in an incremental increase in pitching moment. In general, increasing the wing lift by increasing the wing incidence or flap deflection decreases the stability. This decrease in stability is larger with the auxiliary thrust engines installed. (See figs. 11(c) and 11(d).)

The effect of the auxiliary thrust engine nacelles is shown in figure 12. The wing incidence was set at 0°, the flaps were retracted, and the compound-tail incidence was set at 0°. The addition of flow-through nacelles decreased the static longitudinal stability from -0.0327/deg to -0.0132/deg. The lift-curve slope increased slightly from 0.086/deg to 0.090/deg. The effects of the nacelles with the fans (with $C_{T,J} = 0$) are similar to those for the flow-through nacelles.

The effect of horizontal-tail incidence on the longitudinal aerodynamic characteristics is presented in figure 13. The horizontal-tail effectiveness $C_{m_{i_t}}$ was evaluated from data for α between -5° and 5°. The effect of horizontal-tail incidence for the helicopter tail is presented in figure 13(a) The tail lift-curve slope, based on wing area, was 0.0071/deg and $C_{m_{i_t}}$ was -0.0329/deg. The variation of downwash with angle of attack was computed and the results, presented in figure 14, indicated a value for $d\epsilon/d\alpha$ of 0.098. This small value was expected because of the high position of the upper horizontal tail.

The effect of horizontal-tail incidence for the compound tail is presented in figures 13(b) and 13(c). The auxiliary thrust engines were installed and the

wing incidence and flap deflection were set at 0°. There were no data for the horizontal tail off for this configuration, so the tail-off data were computed by removing the loads measured on the tail balance from the loads measured on the main balance. The horizontal-tail effectiveness $C_{m_{i_t}}$ was -0.0418/deg at zero thrust and -0.0474/deg at trim thrust. Before comparing these results with those of reference 3, a correction should be made for the difference in tail spans. If a correction factor of 0.9 (the ratio of the tail span used in the present investigation to that used in ref. 3) is used, $C_{m_{i_t}}$ from reference 3 would be -0.0421/deg at zero thrust and -0.0450/deg at trim thrust. These results are in good agreement with the present investigation. Since $C_{m_{i_t}}$ becomes more negative with increasing thrust, it follows that the dynamic pressure at the tail increases with thrust.

No data were available for the upper horizontal tail of the compound tail on and the lower tail off. The contribution of the upper horizontal tail was estimated by using the contribution of the helicopter tail, corrected for the difference in area, and the result was added to the tail-off data. These estimated tail-off data were used to compute the downwash at the lower horizontal tail and the results, presented in figure 14, indicated a value for $d\varepsilon/d\alpha$ of 0.65 for zero thrust and 0.90 for trim thrust ($C_{T,J} = 0.18$).

The effect of auxiliary engine thrust level on the longitudinal aerodynamic characteristics is presented in figure 15 for wing incidence angles of 0° and 7.5° with the flaps retracted and deflected. The compound tail was set at 0° incidence. This configuration, which represents the compound helicopter, had static longitudinal stability for the wing incidence angles tested. In general, increasing the thrust coefficient increases C_{L_α} slightly and decreases C_{m_α} at negative angles of attack. The change in C_{L_α} comes from the component of thrust in the lift direction; the change in longitudinal stability comes from the increase in $d\varepsilon/d\alpha$ at the lower horizontal tail with thrust. The effect of thrust coefficient on the static longitudinal stability of the compound helicopter is summarized in figure 16.

Wing loads.- The wing balance measured the wing forces and moments directly. To make comparisons between the wing and airframe data easier, the wing data are nondimensionalized by the same factors as the airframe data, and the moment data are resolved about the same moment reference center. The effect of wing incidence on the wing longitudinal aerodynamic characteristics is presented in figure 17 for the auxiliary thrust nacelles on and off and the tail on and off. Without the nacelles or tail (fig. 17(a)), deflecting the flaps 30° for 0° wing incidence at 0° angle of attack produces a 0.50 change in wing lift coefficient and a nose-down increment of 0.37 in wing pitching-moment coefficient. The change in wing lift with angle of attack was 0.061/deg for the flaps retracted and 0.064/deg for the flaps deflected. The wing provides a stabilizing contribution to the longitudinal stability because the wing center of pressure is behind the moment reference center. The change in wing lift with wing

incidence was 0.0545/deg. This is smaller than the value obtained on the airframe because of the interference of the fuselage on the wing.

The lift on the fuselage was computed by removing the lift measured on the wing balance (fig. 17(a)) from the total lift measured on the airframe balance (fig. 11(a)). The results for the various wing/flap settings have been crossplotted in figure 18 for several values of fuselage angle of attack. The significance of these results is that the fuselage experiences an increase in lift induced by an increase in wing lift.

With the tail and nacelles on and the jets at $C_{T,J} = 0$, the results are slightly different (fig. 17(b)). The lift-curve slope for all wing/flap settings decreased slightly to 0.057/deg, although there was no significant change in the pitching-moment slopes. Deflecting the flaps 30° produces the same changes in pitching moment and lift as obtained with the nacelles and tail off.

The effect of the auxiliary engine thrust on the wing aerodynamic characteristics is presented in figure 19 for several wing/flap settings. In general, the addition of thrust increases the lift slightly except near stall, makes the pitching moment slightly more negative, and reduces the wing drag. The thrust does not affect the wing contribution to the longitudinal stability. The effects increase with increasing wing incidence or flap deflection.

Tail loads.- The tail balance measured the empennage forces and moments directly. As was done for the wing, the tail data are nondimensionalized by the same factors as the airframe data, and the moments are resolved about the same moment reference center. The aerodynamic characteristics of the helicopter tail and the compound tail on the fuselage alone are presented in figure 20. The tail lift and the tail contribution to the static longitudinal stability (difference between tail-on and tail-off stability) agree with the results from figure 10(a).

The effect of wing incidence and flap deflection is shown in figure 21. Adding the wing to the fuselage increases the downwash at the tail and reduces the tail contribution to stability. (See fig. 21(a).) The tail contribution to stability increases with angle of attack for 7.5° wing incidence at trim thrust. (See fig. 21(c).)

As shown in figure 22, the addition of the auxiliary thrust engine nacelles reduces the stability contribution of the tail from -0.039/deg to -0.030/deg. This stability reduction is about one-half of the reduction due to nacelles in the airframe pitching moment. (See fig. 12.) The other half arises from the nacelles and pylons acting as lifting surfaces in front of the center of gravity. As was the case for the airframe pitching moments, the difference between the effect of the flow-through nacelles and the nacelles with the fans at zero thrust ($C_{T,J} = 0$) is small.

The effect of horizontal-tail incidence is presented in figure 23. The horizontal-tail effectiveness and the tail contribution to stability are consistent with the results of figure 13.

The effect of increasing the auxiliary engine thrust level is presented in figure 24. The results show the same trends, but they do not show the stability reduction at small angles of attack that was found for the complete configuration (fig. 15). The tail provides more stability at angles of attack near stall as thrust is increased; this is especially notable in figure 24(d) for the 7.5°/30° wing/flap setting.

Lateral Aerodynamic Characteristics

Comparison of Phase IV and Phase III.- As was previously described, there were several differences in the external contours of the models used in Phase IV and Phase III. The only lateral aerodynamic data obtained in Phase III were for the compound helicopter with the 127.0-cm (50-in.) span lower horizontal tail. These results are presented with the results for the 114.3-cm (45-in.) span horizontal tail from Phase IV in figure 25. The decreased tail span of Phase IV had little or no effect on static directional stability $\left(\text{positive } C_{n_\beta}\right)$ but decreased the aircraft positive effective dihedral $\left(\text{negative } C_{l_\beta}\right)$ slightly, as would be expected. Slight differences in trim conditions which are evident in this figure may be attributed to discrepancies in rudder deflections, incidence of the two wing panels, or small imbalances in engine thrust.

Airframe loads.- Various components of the model were tested on the fuselage to determine the aerodynamic contribution of each. The effective dihedral and directional stability were evaluated between -5° and 5° of sideslip and are summarized in table II.

The effect of adding the vertical tail to the fuselage is presented in figure 26. As can be seen in this figure, the vertical tail contributes positive effective dihedral and static directional stability. The end-plate effect of the helicopter tail H_H and the compound tail H_C (fig. 27) increased the static directional stability. However, the location of the helicopter upper horizontal tail above the reference center of the model provided a positive increment to effective dihedral, whereas the lower horizontal tail of the compound tail decreased the effective dihedral.

The effect of wing incidence and flap deflection on the lateral aerodynamic characteristics of the model without the empennage is presented in figure 28. As was discussed in reference 3, the 7° geometric dihedral was counteracted by the position of the wing on the bottom of the fuselage. The effective dihedral becomes more positive as the wing incidence changes from -9° to 7.5°. Addition of the compound tail to the wing-body configuration produced positive effective dihedral and static directional stability (fig. 29).

The results of adding the auxiliary thrust engine nacelles to the wing-body-empennage configuration are presented in figure 30. The addition of the nacelles produced no significant differences in the lateral aerodynamic characteristics.

Angle-of-attack effects on the lateral aerodynamic characteristics are presented in figure 31. Generally, directional stability decreased with increasing angle of attack for the configurations given in this figure. However, positive effective dihedral decreased with increasing angle of attack when the engine nacelles and pylon fairings were off and increased when they were installed.

The effect of auxiliary engine thrust is presented in figure 32 for several wing/flap settings and angles of attack. Increasing the engine thrust reduced the positive effective dihedral and the static directional stability.

Wing loads.- Lateral aerodynamic characteristics of the wing are presented in figures 33 to 36. These figures represent wing loads for various total configurations of the model. From these figures, wing contributions to stability may be determined directly.

The effect of wing incidence and flap deflection on the wing lateral aerodynamic characteristics is presented in figure 33. The wing is providing a destabilizing increment to the effective dihedral in spite of the 7° geometric dihedral. This is due to the interference effect from the low wing placement on a relatively deep fuselage. Increasing the wing incidence increases the effective dihedral, as expected. The wing does provide a positive increment to the static directional stability.

The lateral aerodynamic characteristics of the wing on the compound helicopter without the rotors are presented in figure 34. A comparison of this figure with figure 33 illustrates the effect of the empennage and engine nacelles on the wing. For the two cases which are directly comparable, little or no effect on static directional stability is evident with the jets at $C_{T,J} = 0$. The nonzero values of rolling moment at $\beta = 0^{\circ}$ can be attributed to model asymmetries.

The effect of angle of attack on the lateral aerodynamic characteristics of the wing with the model in various configurations is presented in figure 35. Increasing the angle of attack of the model had a favorable effect on the wing contribution to both the effective dihedral and the static directional stability for the configurations tested. This effect is consistent with that in figure 33 for comparable values of wing incidence.

Auxiliary-thrust-induced effects on the wing lateral aerodynamic characteristics are presented in figure 36. Increasing the thrust level further degrades the effective dihedral of the wing.

Tail loads.- The effect of the vertical tail on the tail lateral aerodynamic characteristics is presented in figure 37. The data for the configuration with the vertical tail off (F_1) include loads on the ventral fin and the aft section of the tail cone. As would be expected, the addition of the vertical tail provides positive static directional stability and effective dihedral. Addition of the two horizontal-tail configurations (see fig. 38) had only a slight effect on directional stability. However, the positive effective dihedral was decreased by addition of the compound horizontal tail and increased by addition of the helicopter tail.

Wing interference on the model empennage is shown in figure 39. As can be seen in this figure, the wing downwash on the tail has a favorable effect on both effective dihedral and static directional stability by inducing a cleaner flow over the vertical-tail surface.

The auxiliary thrust engine nacelles and pylon fairings have insignificant effects on the empennage static directional stability (fig. 40).

The effect of angle of attack on the tail lateral aerodynamic characteristics is presented in figure 41. For the configurations which were tested, increasing the angle of attack decreased the tail contribution to the effective dihedral and directional stability as the empennage became immersed in the wake of the rotor pylon and fuselage.

Figure 42 presents the effect of the auxiliary engine efflux on the empennage. In general, increasing the thrust coefficient decreases the tail contribution to both the effective dihedral and the directional stability. This effect becomes significant at the higher wing/flap setting ($i_w = 7.5^o$; $\delta_f = 0^o$) because of the interaction of the jet efflux and wing downwash.

SUMMARY OF RESULTS

A wind-tunnel investigation was conducted to determine the airframe, wing, and tail aerodynamic characteristics of a 1/6-scale model of the RSRA with the rotors removed. The results of this investigation may be summarized as follows:

1. The helicopter and the compound helicopter had static longitudinal stability.

2. The direct effect of the wing was to provide a stabilizing increment and of the auxiliary thrust engine nacelles to provide a destabilizing increment to the static longitudinal stability.

3. The induced effect of the wing and of the engine nacelles reduced the tail contribution to the static longitudinal stability.

4. Both the helicopter and the compound helicopter showed positive effective dihedral and static directional stability.

5. In general, the induced effects of the wing downwash and the engine efflux reduced the positive effective dihedral and the static directional stability.

6. The wing provided a destabilizing increment to the effective dihedral, despite the positive geometric dihedral of the wing itself, and a positive increment to the static directional stability.

7. The direct effect of the vertical tail was to provide positive effective dihedral and static directional stability.

8. The results from the present investigation and those of NASA TN D-8198 are in reasonable agreement when the tail is off but differ when the tail is on.

Langley Research Center
National Aeronautics and Space Administration
Hampton, VA 23665
April 7, 1977

REFERENCES

1. Linden, A. W.; and Hellyar, M. W.: The Rotor Systems Research Aircraft - A Flying Wind Tunnel. AIAA Paper No. 74-1277, Oct. 1974.

2. Flemming, R.; and Ruddell, A.: RSRA Sixth Scale Wind Tunnel Test - Final Report. Doc. No. SER-72011 (Contract NAS1-13000), Sikorsky Aircraft Div., United Aircraft Corp., Dec. 4, 1974. (Available as NASA CR-144964.)

3. Mineck, Raymond E.; Freeman, Carl E.; and Hassell, James L., Jr.: Aerodynamic Characteristics of a 1/6-Scale Model of the Rotor Systems Research Aircraft With the Rotors Removed. NASA TN D-8198, 1976.

4. Mineck, Raymond E.; and Freeman, Carl E.: Aerodynamic Characteristics of a 1/6-Scale Powered Model of the Rotor Systems Research Aircraft. NASA TM X-3489, 1977.

5. Mechtly, E. A.: The International System of Units - Physical Constants and Conversion Factors (Second Revision). NASA SP-7012, 1973.

6. Heyson, Harry H.: Use of Superposition in Digital Computers To Obtain Wind-Tunnel Interference Factors for Arbitrary Configurations, With Particular Reference to V/STOL Models. NASA TR R-302, 1969.

TABLE I.- MODEL DATA

Fuselage:		
Length, m (ft)	3.057	(10.03)
Frontal area, m^2 (ft^2)	0.172	(1.85)
Wing:		
Airfoil section	NACA 63_2415	
Area, m^2 (ft^2)	0.954	(10.27)
Span, m (in.)	2.29	(90.0)
Mean aerodynamic chord, m (in.)	0.423	(16.67)
Aspect ratio	5.52	
Taper ratio	0.66	
Sweep of 25-percent-chord line, deg	3.0	
Dihedral, deg	7.0	
Flaps (each):		
Area, m^2 (ft^2)	0.074	(0.80)
Span, percent of wing semispan	49.0	
Chord, percent of local wing chord	33.0	
Aileron:		
Area, m^2 (ft^2)	0.047	(0.50)
Span, percent of wing semispan	34.0	
Chord, percent of local wing chord	34.0	
Vertical stabilizer:		
Airfoil section	NACA 0015	
Area, m^2 (ft^2)	0.294	(3.164)
Span, m (ft)	0.813	(2.67)
Aspect ratio	2.25	
Root chord, m (ft)	0.476	(1.56)
Rudder, percent of local chord	37.0	
Helicopter tail:		
Airfoil section	NACA 0015	
Area, m^2 (ft^2)	0.091	(0.98)
Span, m (ft)	0.674	(2.21)
Aspect ratio	5.15	
Root chord, m (ft)	0.183	(0.599)
Taper ratio	0.487	
Compound tail:		
Airfoil section	NACA 0015	
Area, m^2 (ft^2)	0.046	(0.48)
Span, m (ft)	0.44	(1.43)
Aspect ratio	4.29	
Root chord, m (ft)	0.128	(0.42)
Taper ratio	0.60	
Lower horizontal tail:		
Airfoil section	NACA 0015	
Area, m^2 (ft^2)	0.228	(2.45)
Span, cm (in.)	114.3	(45.0)
Aspect ratio	5.75	
Root chord, m (ft)	0.198	(0.65)
Taper ratio	1.00	
Ratio of elevator chord to tail chord	0.30	

TABLE II.- STABILITY DERIVATIVES FOR VARIOUS CONFIGURATIONS WITH THE ROTOR REMOVED

Configuration	C_{L_α} (a)			C_{m_α} (a)			C_{l_β} (b)			C_{n_β} (b)		
	Airframe	Wing	Tail	Airframe	Wing	Tail	Airframe	Wing	Tail	Airframe	Wing	Tail
F_1	0.001		0	0.0110		0.0008	0		0.0001	-0.0022		0.0006
F_1V	.001		0	.0110		.0008	-.0007		-.0006	.0015		.0042
F_1VH_H	.007		.005	-.0200		-.0298	-.0010		-.0008	.0018		.0044
F_1VH_C	.020		.016	-.0520		-.0617	-.0006		-.0005	.0022		.0048
F_1W_1	.074	0.061	-----	.0090	-0.0163	------	.0006	0.0007	------	-.0023	0.0002	------
F_1W_2	.074	.061	-----	.0077	-.0155	------	.0003	------	------	-.0025	------	------
F_1W_4	.074	.061	-----	.0060	-.0152	------	.0010	------	------	-.0015	------	------
F_1W_5	.076	.064	-----	.0094	-.0158	------	------	------	------	-------	------	------
F_1W_6	.076	-----	-----	.0112	-------	------	-.0001	------	------	-.0037	------	------
$F_1W_2VH_C$	.086	-----	.010	-.0327	-------	-.0389	-.0004	------	-.0009	.0028	------	.0063
$F_1W_6VH_C$	.086	-----	.010	-.0248	-------	-.0414	-.0010	.0002	-.0011	.0041	.0005	.0070
$F_1W_1VH_CJ_1$	.090	-----	.008	-.0132	-------	-.0305	-.0001	.0008	-.0008	.0026	.0003	.0050

[a]Evaluated between $\alpha = -5^o$ and 5^o.
[b]Evaluated between $\beta = -5^o$ and 5^o at $\alpha = 0^o$.

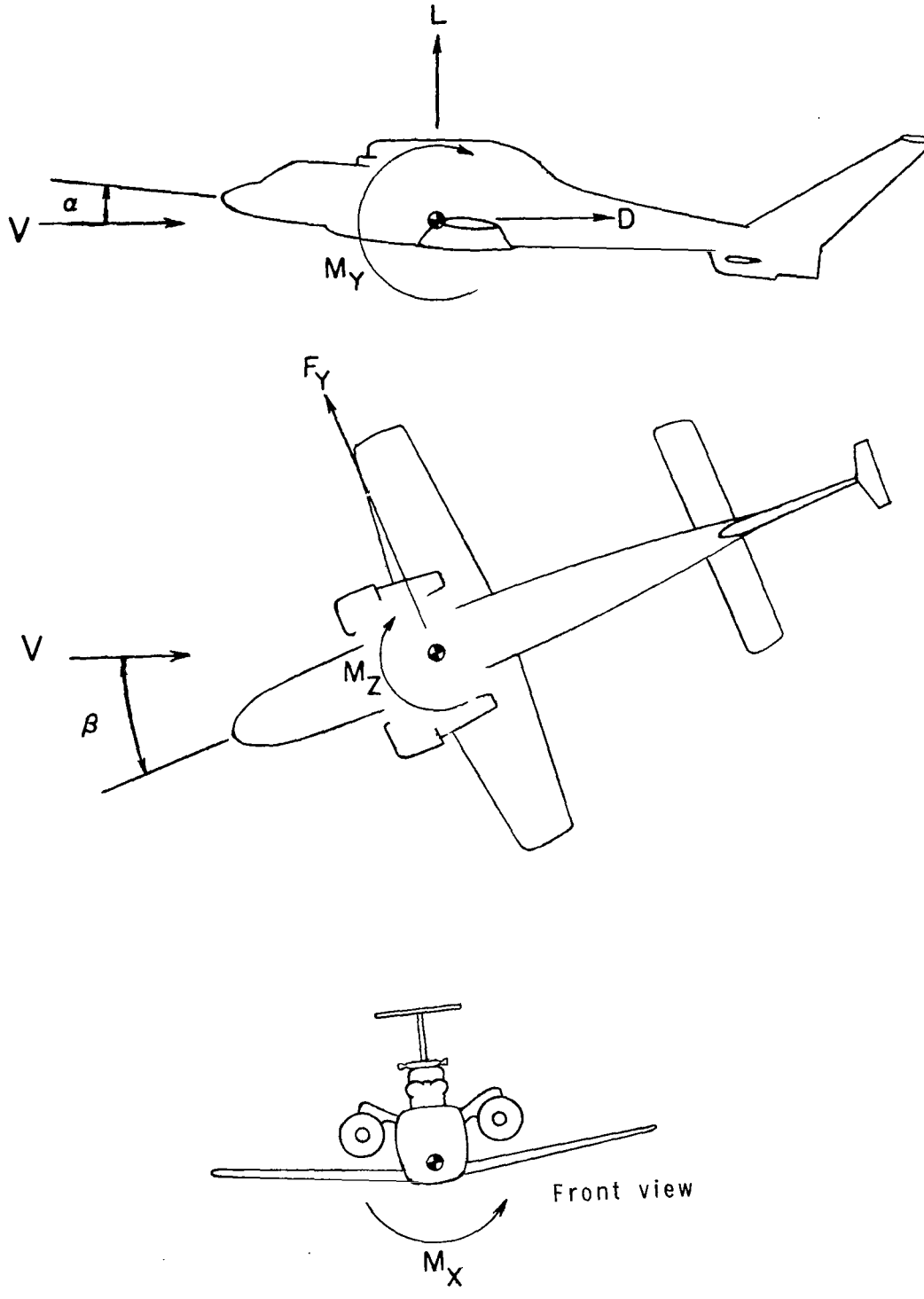

(a) Airframe.

Figure 1.- Sign convention for moments, forces, and angles. Positive directions are indicated by arrows.

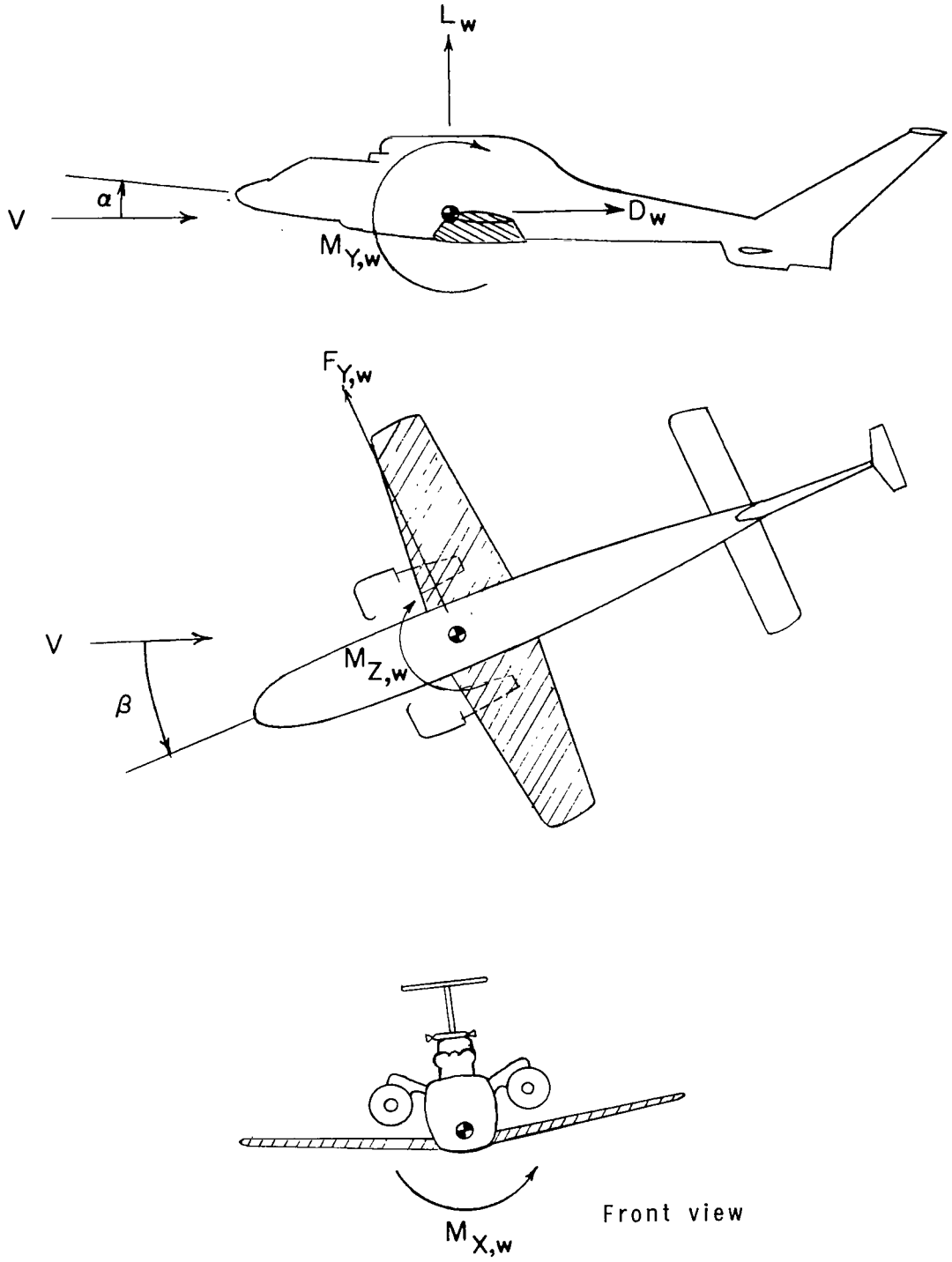

(b) Wing (hatched area).

Figure 1.- Continued.

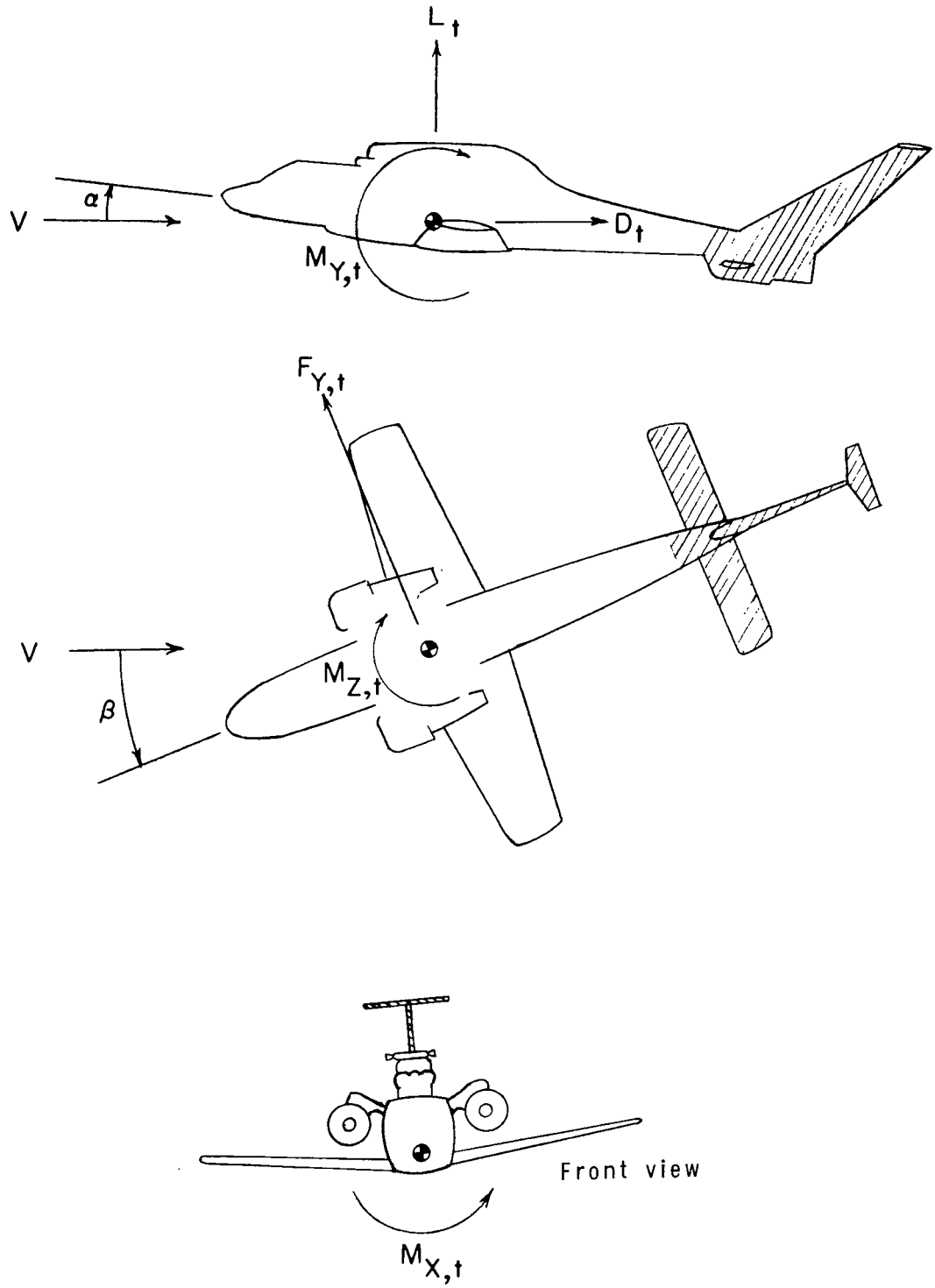

(c) Tail (hatched area).

Figure 1.- Continued.

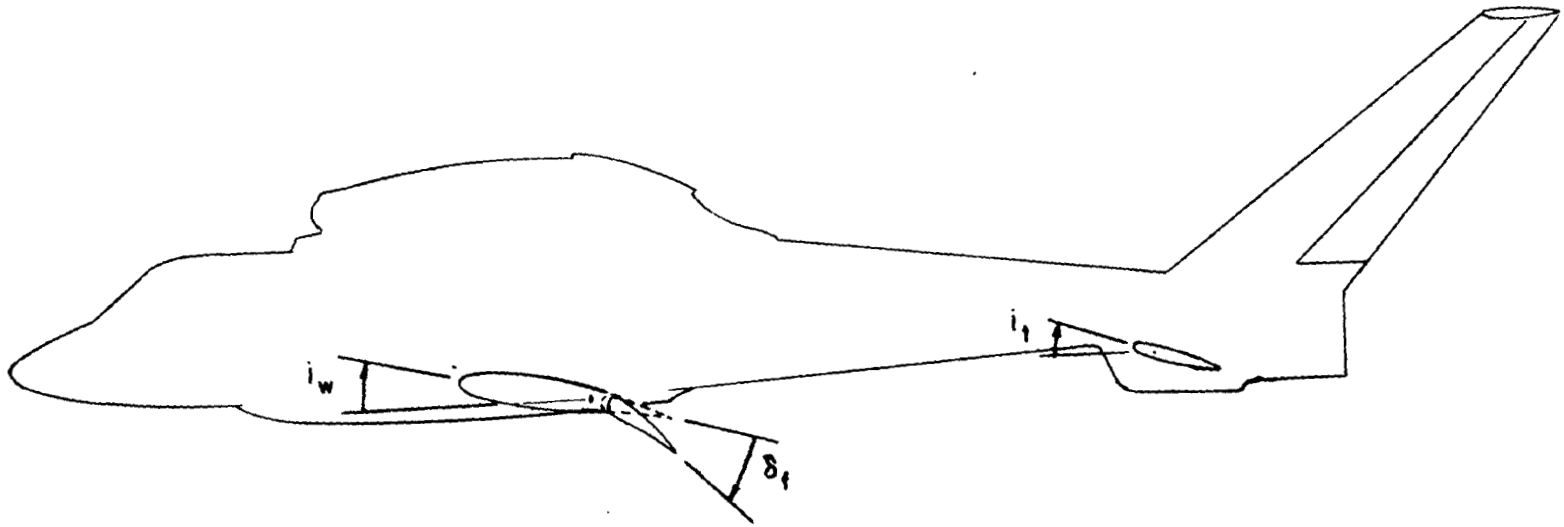

(d) Aerodynamic surfaces.

Figure 1.- Concluded.

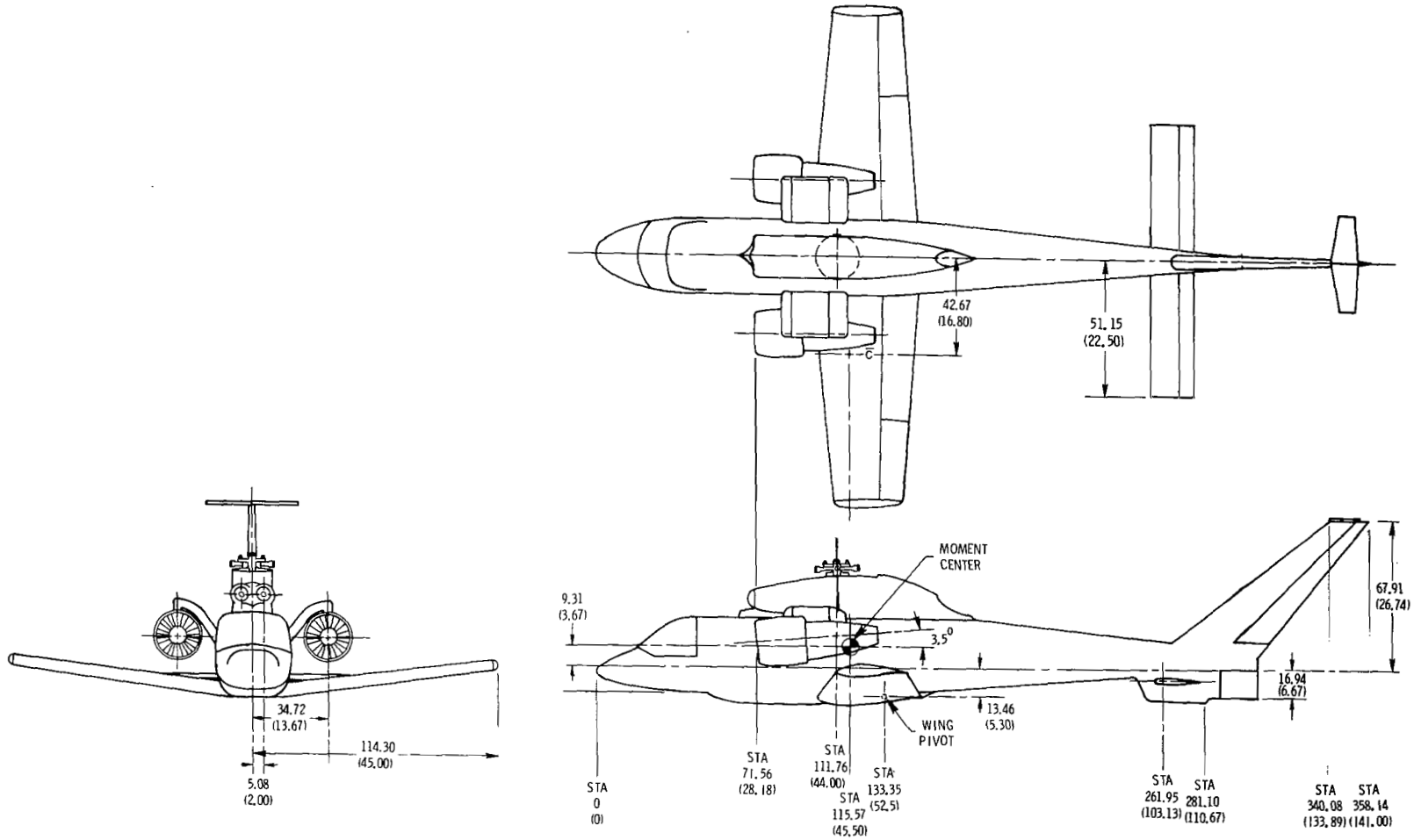

(a) Three-view sketch.

Figure 2.- Details of model. All dimensions shown in cm (in.) unless otherwise specified. (F.S., fuselage station; W.L., water line; B.L., buttock line.)

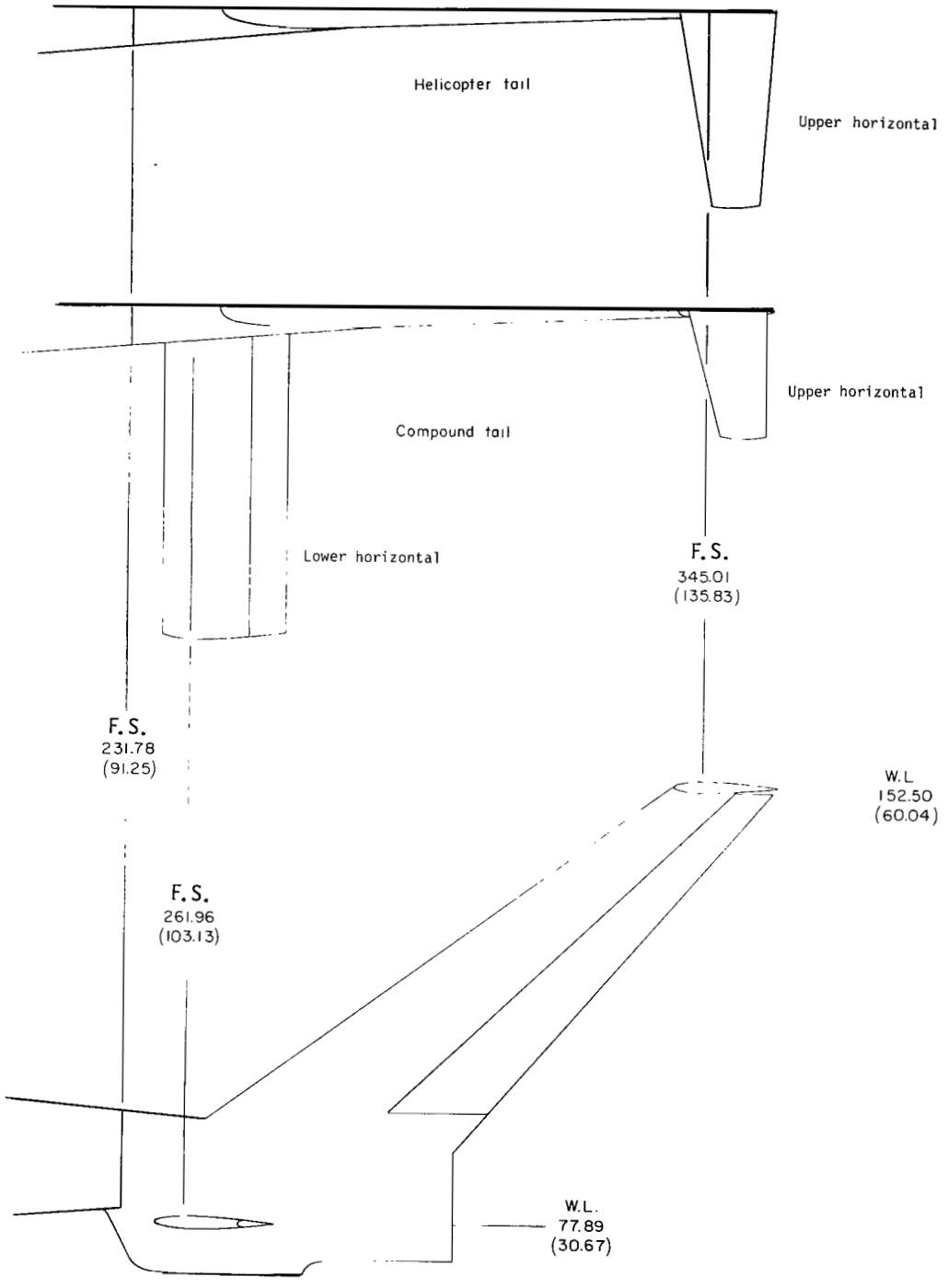

(b) Helicopter tail H_H and compound tail H_C.

Figure 2.- Continued.

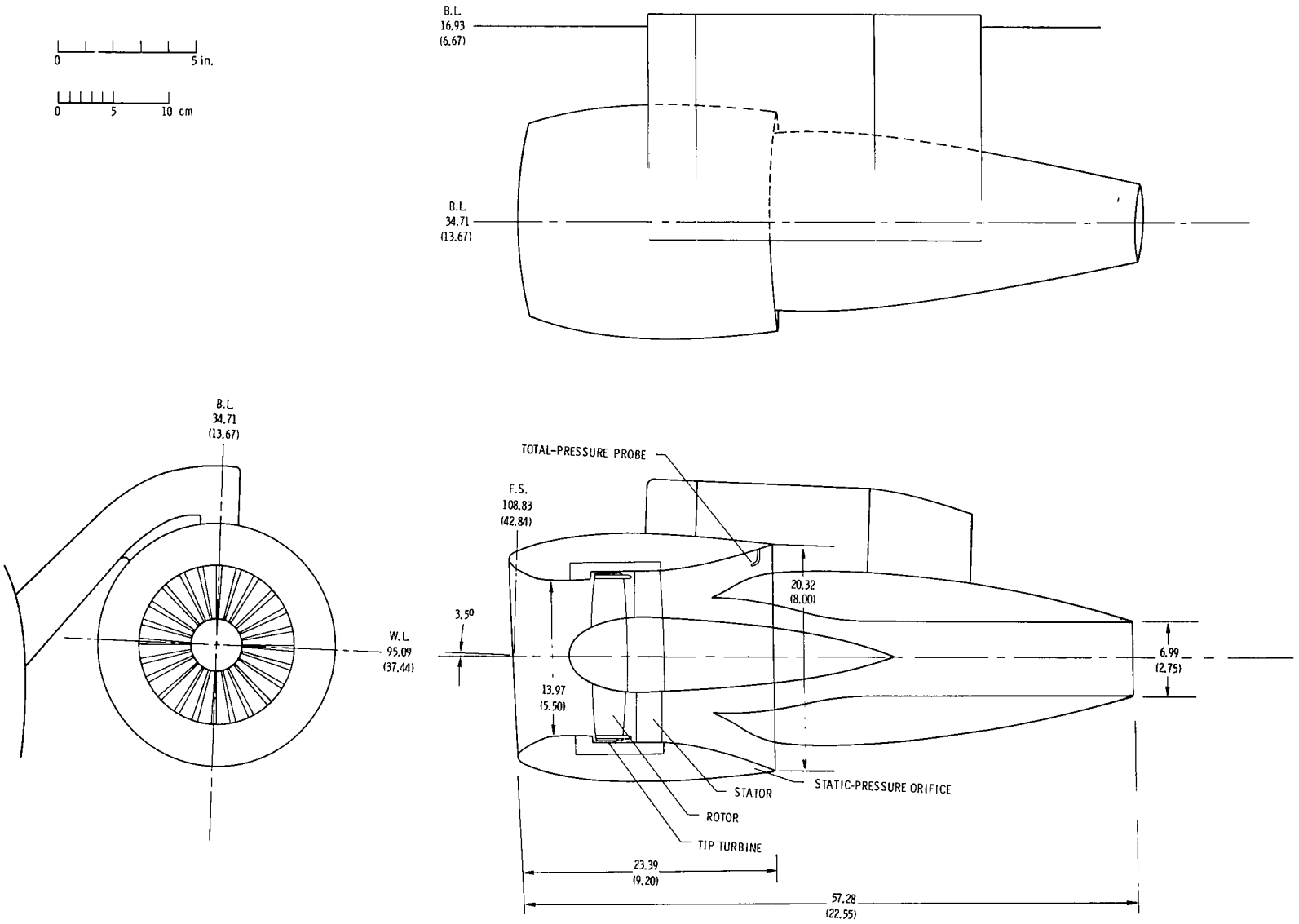

(c) Auxiliary thrust engine simulators.

Figure 2.- Concluded.

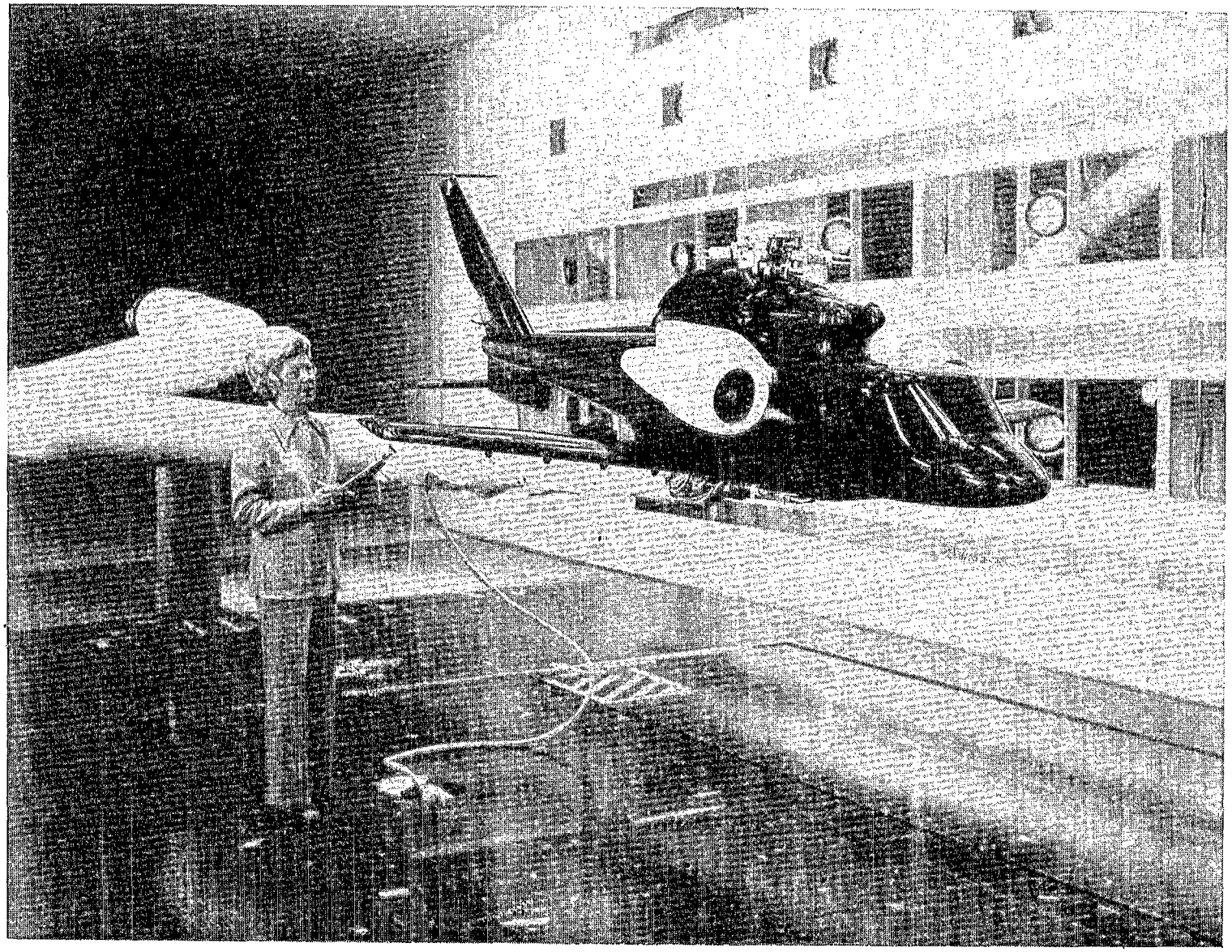

L-75-7507

Figure 3.- Model in Langley V/STOL tunnel.

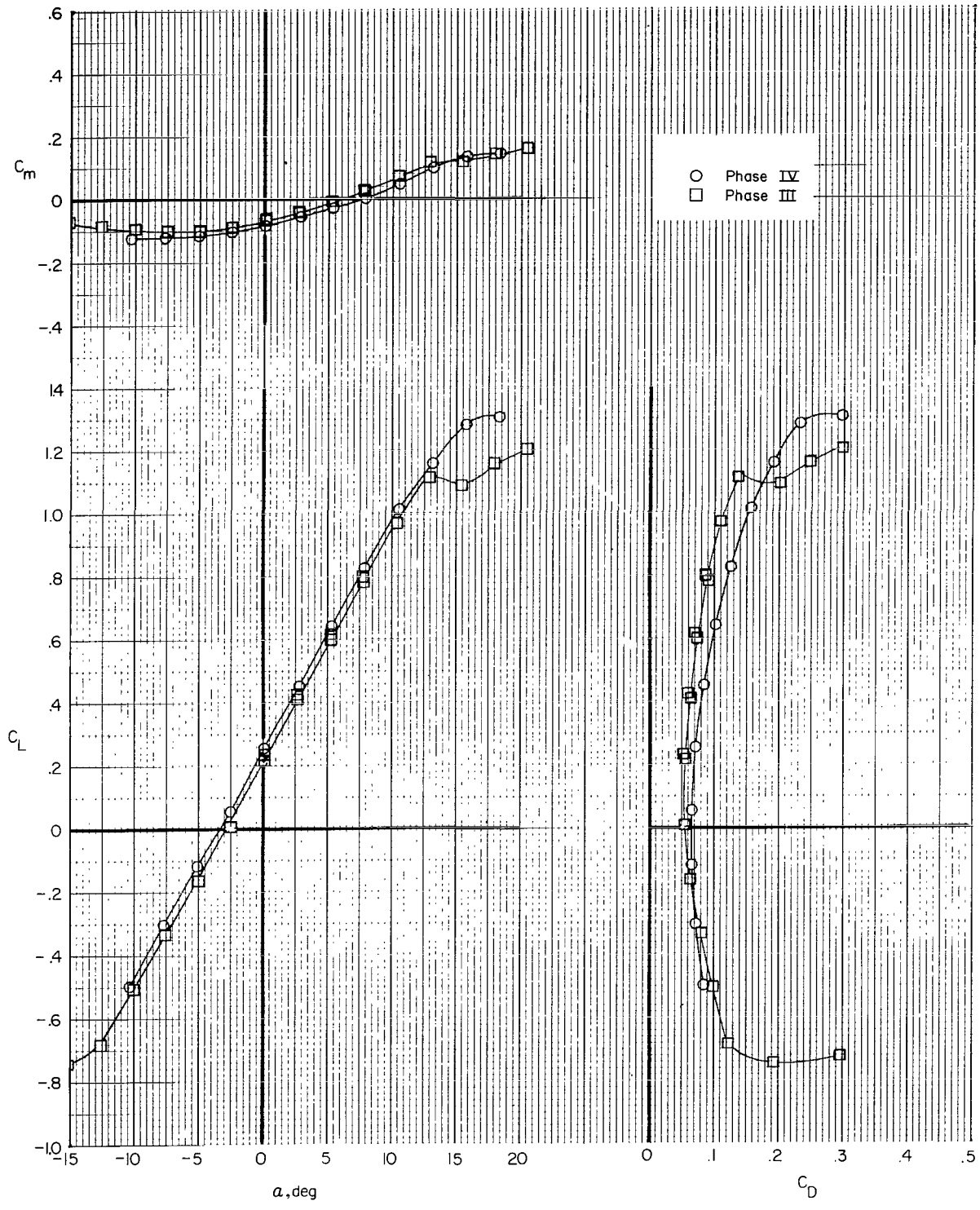

(a) $i_w = 0^o$; $\delta_f = 0^o$.

Figure 4.- Comparison of longitudinal aerodynamics from Phase IV and Phase III for fuselage, vertical tail, and wing (F_1W_XV).

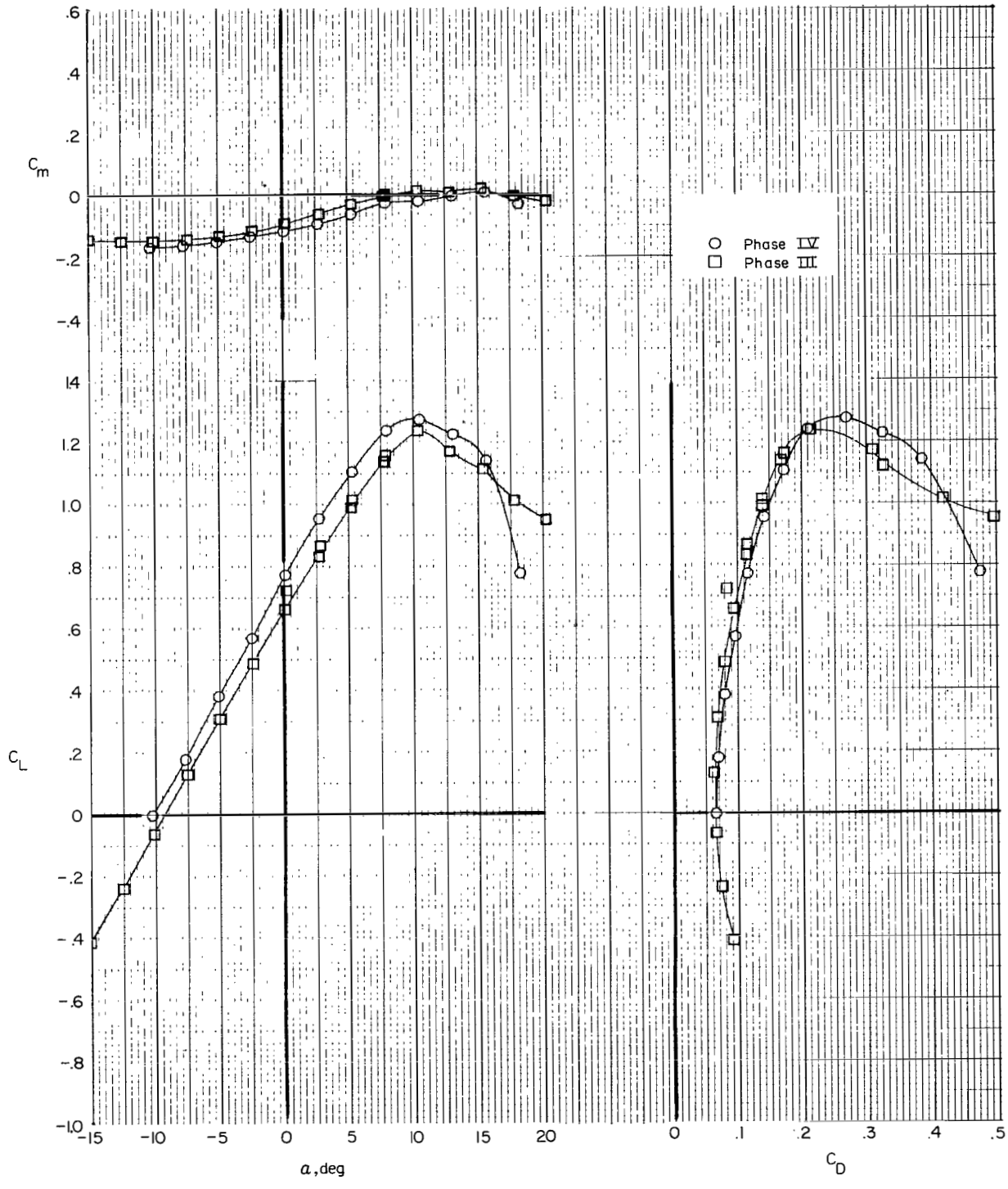

(b) $i_w = 7.5^\circ$; $\delta_f = 0^\circ$.

Figure 4.- Concluded.

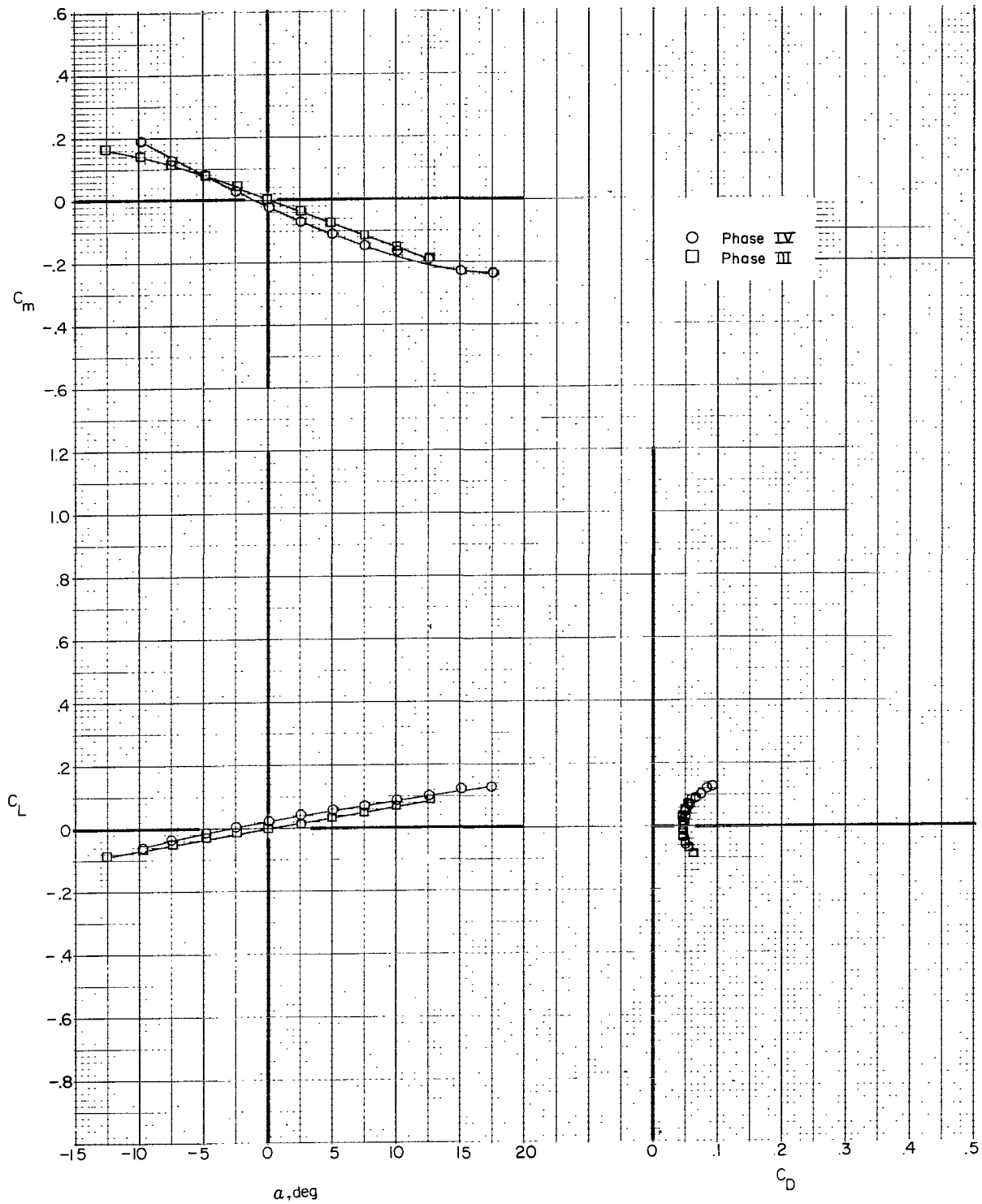

(a) Helicopter tail (F_1VH_H). (Phase III data for shortened vertical tail.)

Figure 5.- Comparison of longitudinal aerodynamics from Phase IV and Phase III for fuselage, vertical tail, and horizontal tail.

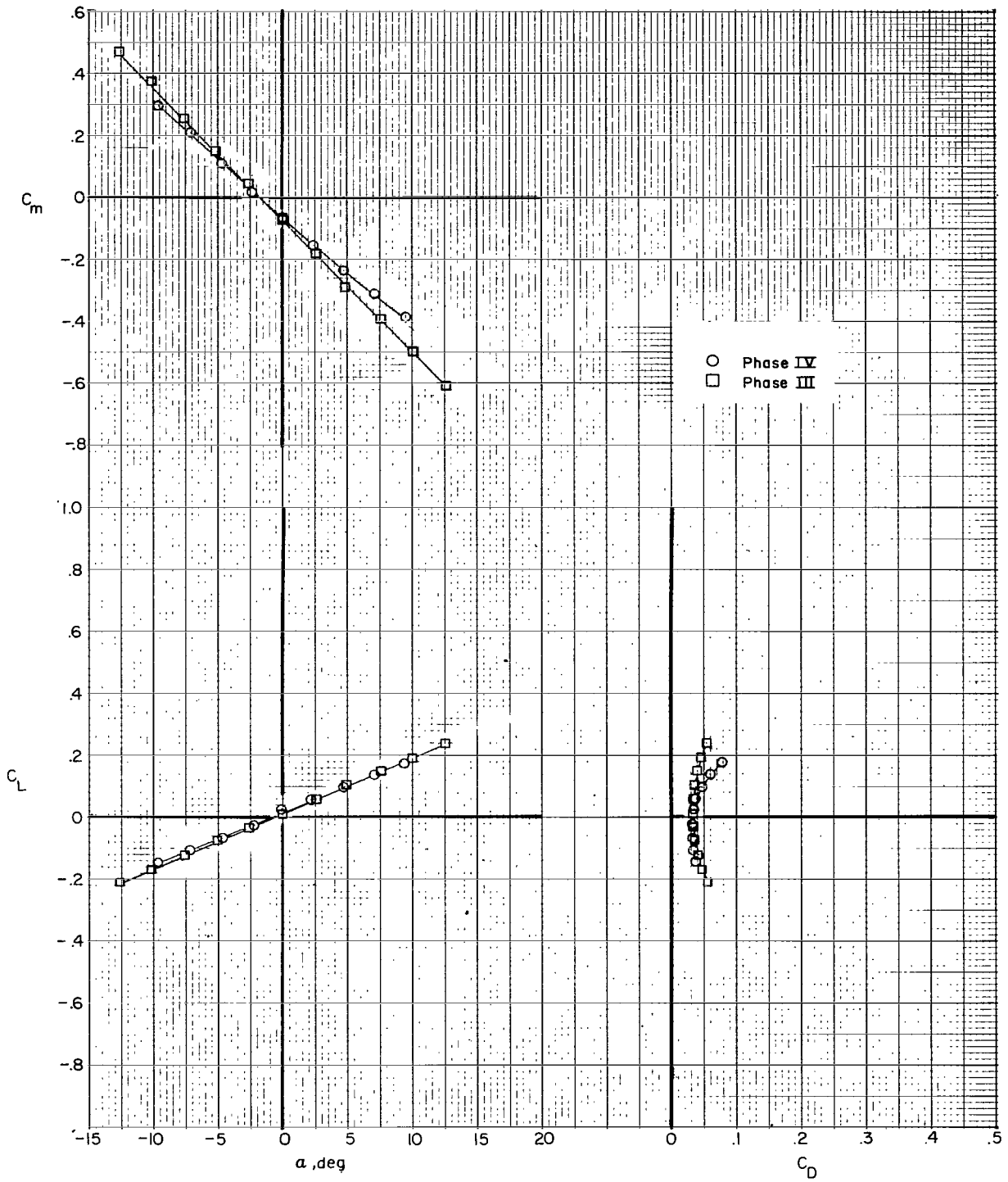

(b) Compound tail (F_2VH_C). (Phase III data for 118.5-cm (46.67-in.) span horizontal tail.)

Figure 5.- Concluded.

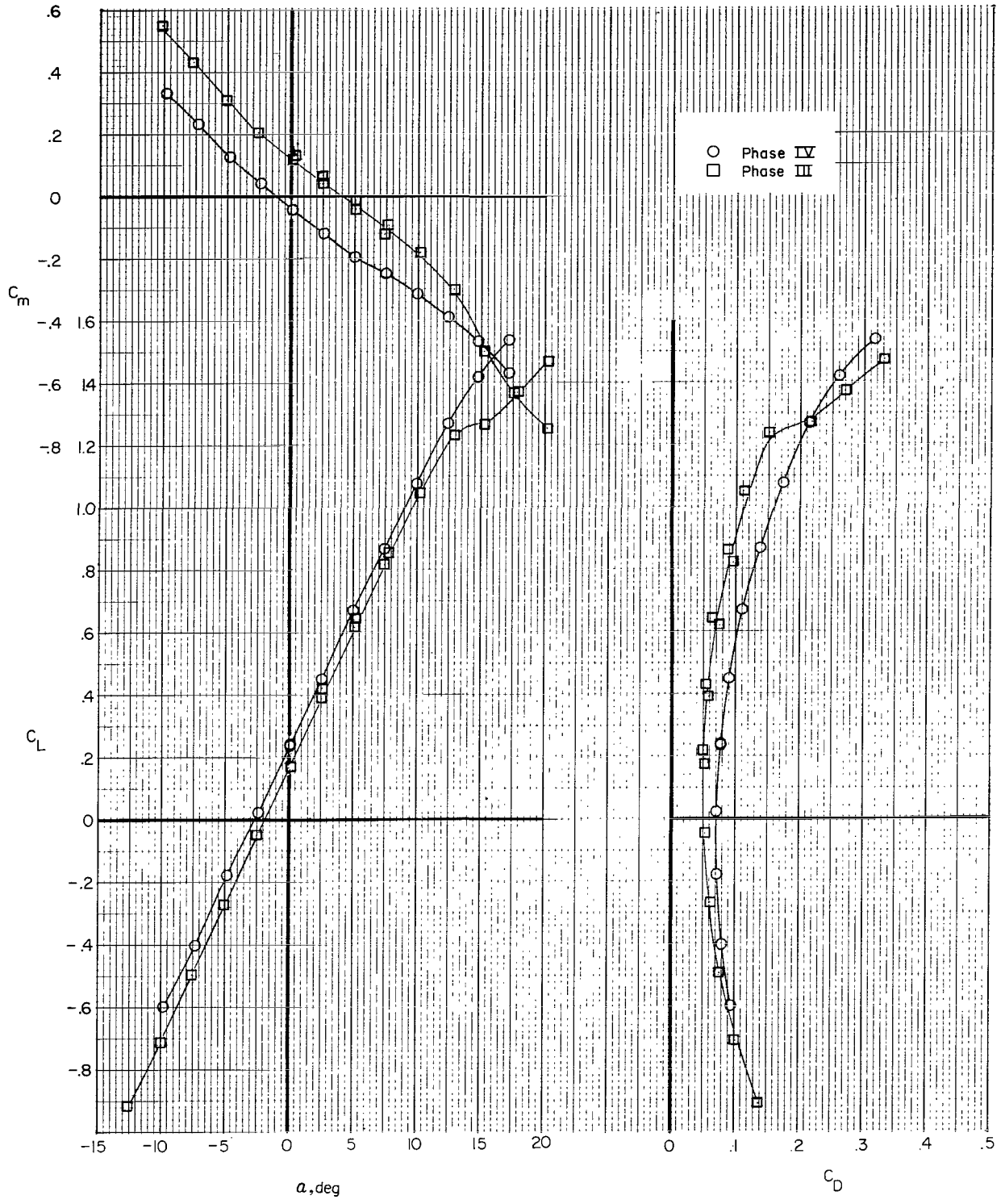

Figure 6.- Comparison of longitudinal aerodynamics from Phase IV and Phase III for fuselage, wing, vertical tail, and compound horizontal tail ($F_1W_1VH_C$). (Phase III data for 127.0-cm (50.0-in.) span horizontal tail.)

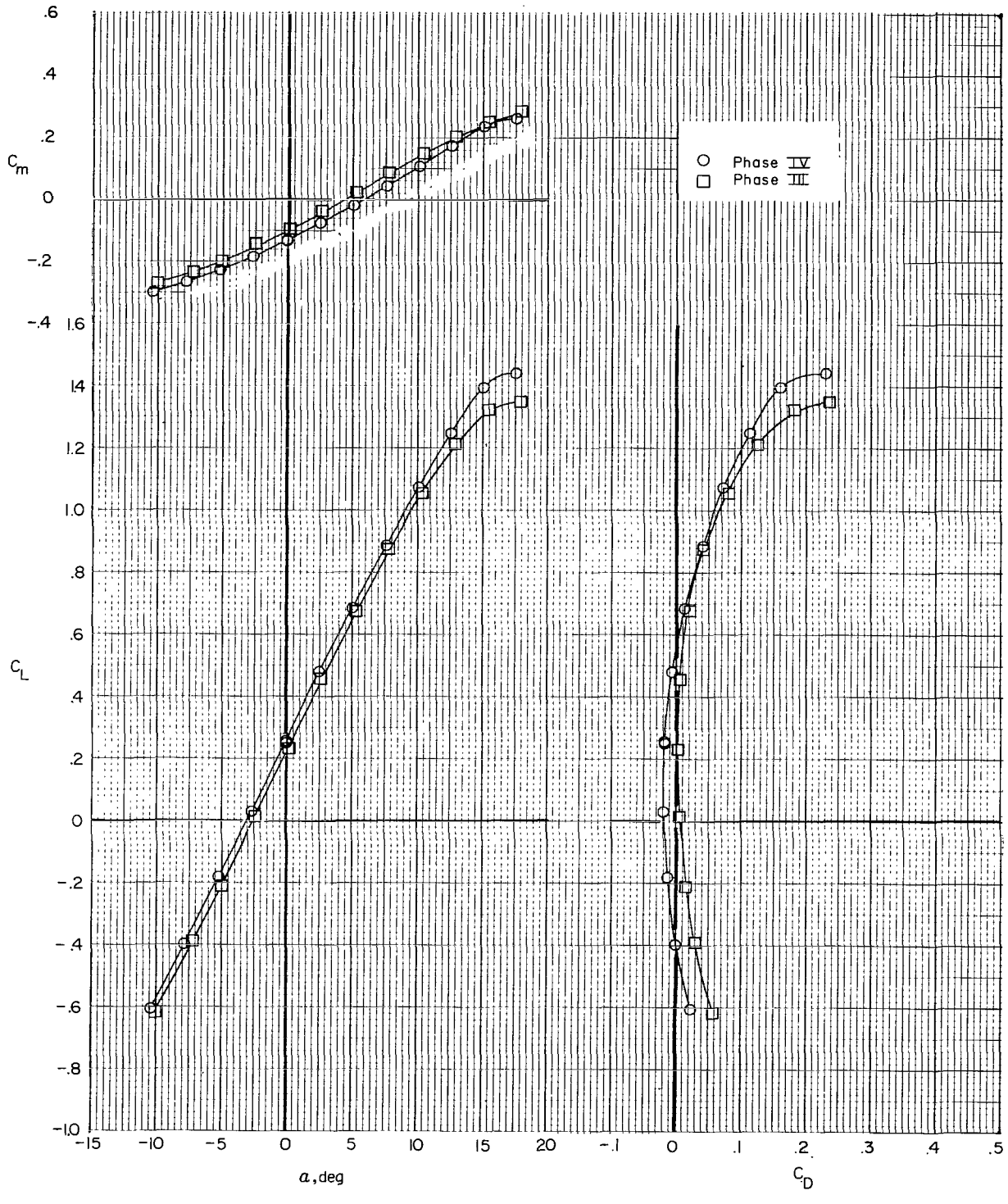

(a) $i_w = 0^o$; $\delta_f = 0^o$.

Figure 7.- Comparison of longitudinal aerodynamics from Phase IV and Phase III for fuselage, wing, vertical tail, and auxiliary thrust jets ($F_1W_xVJ_2$). Trim thrust.

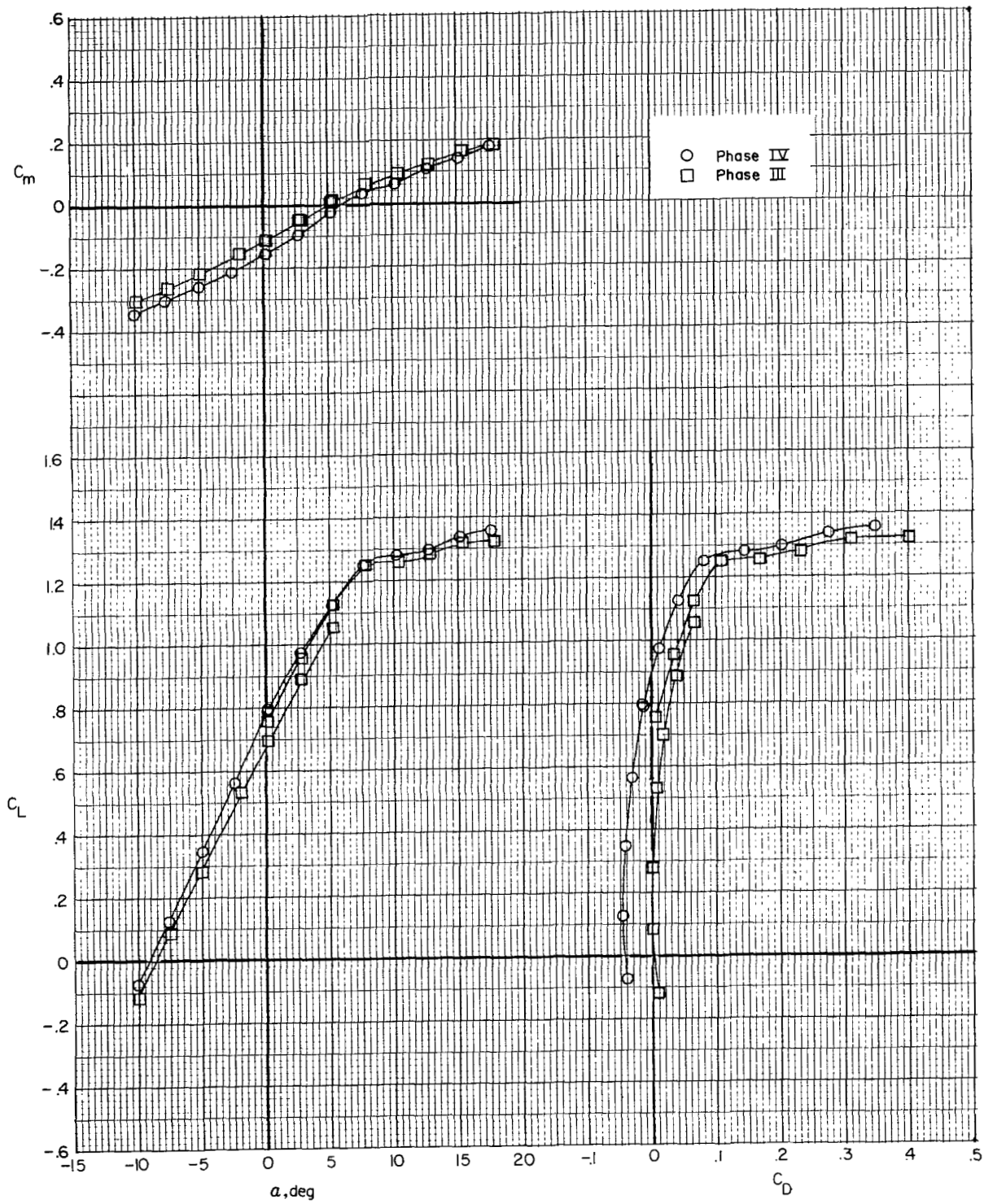

(b) $i_w = 7.5^o$; $\delta_f = 0^o$.

Figure 7.- Concluded.

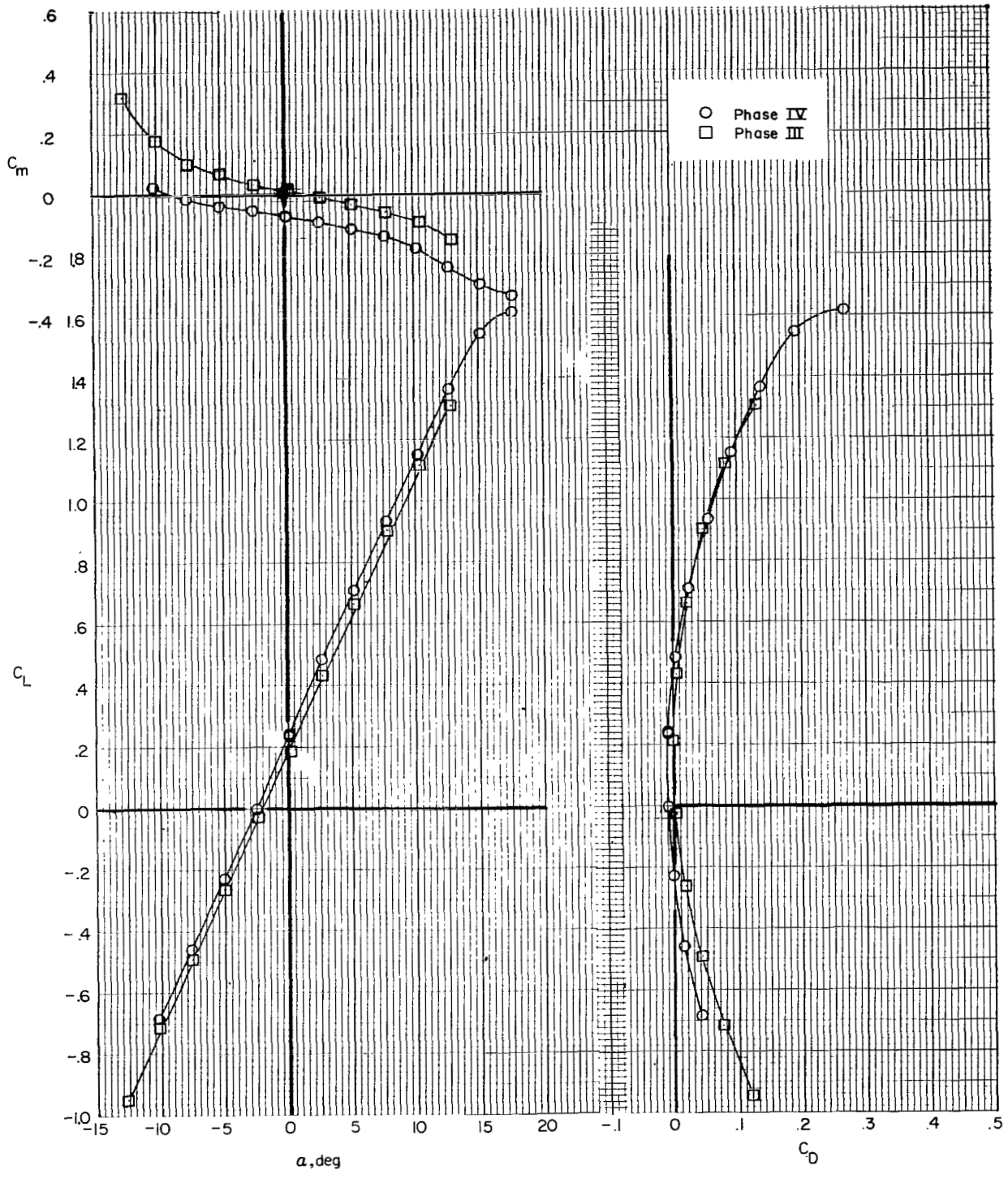

(a) $i_w = 0^o$; $\delta_f = 0^o$.

Figure 8.- Comparison of longitudinal aerodynamics from Phase IV and Phase III for fuselage, wing, vertical tail, compound horizontal tail, and auxiliary thrust jets ($F_1W_XVH_CJ_2$). Trim thrust. (Phase III data are average of data for the 118.5-cm (46.67-in.) span tail and the 110.1-cm (43.33-in.) span tail.)

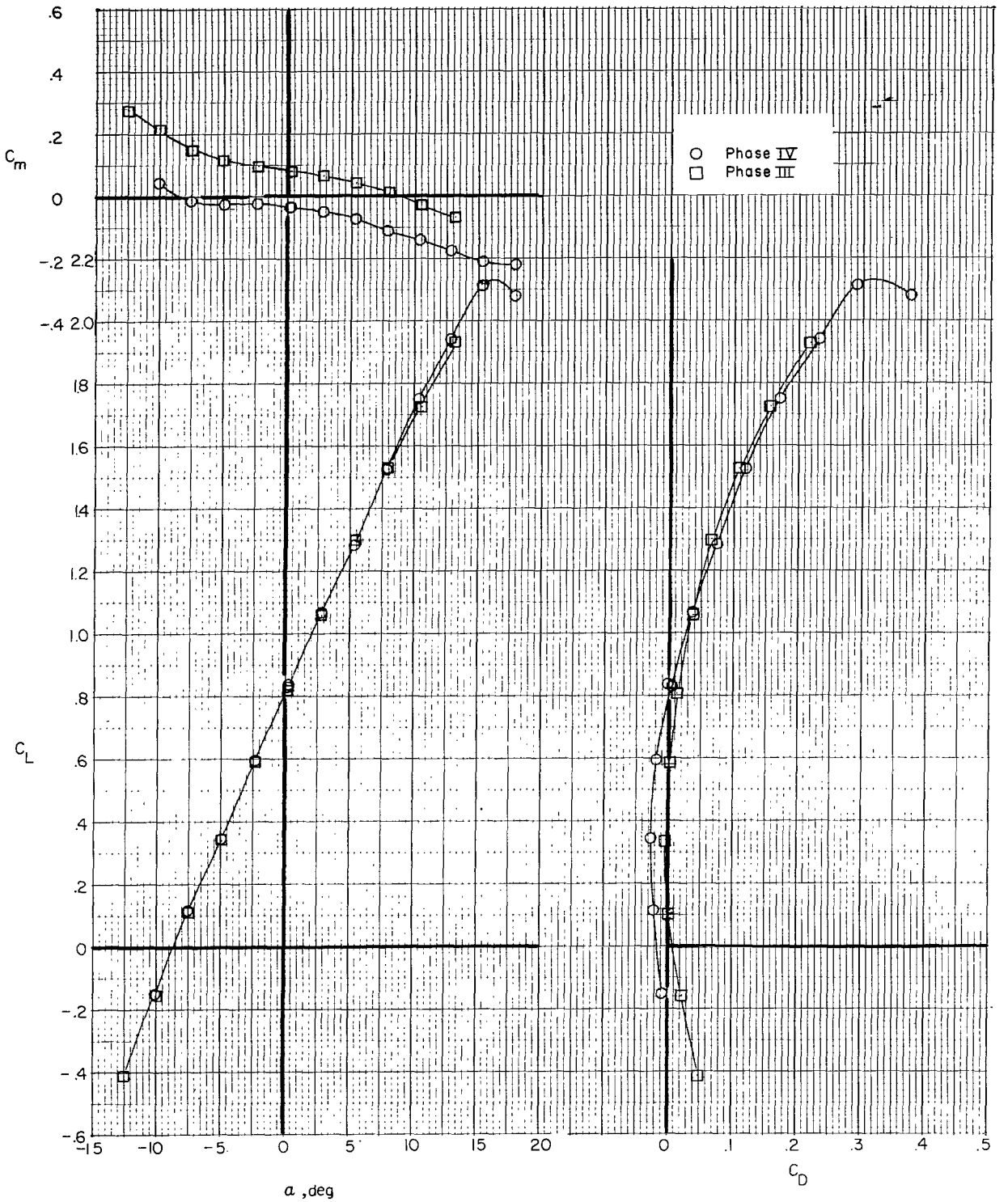

(b) $i_w = 0^o$; $\delta_f = 30^o$.

Figure 8.- Continued.

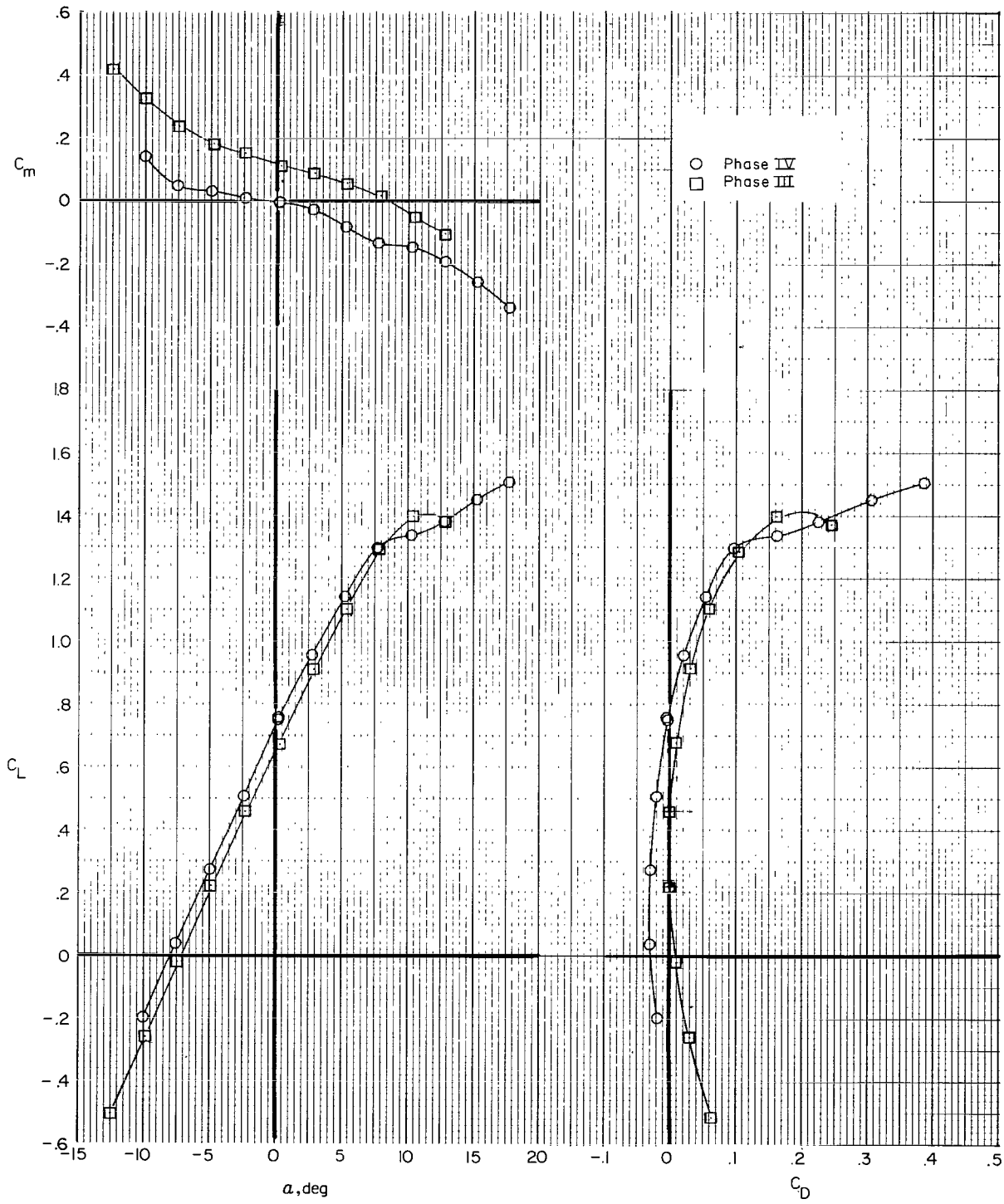

(c) $i_w = 7.5^\circ$; $\delta_f = 0^\circ$.

Figure 8.- Continued.

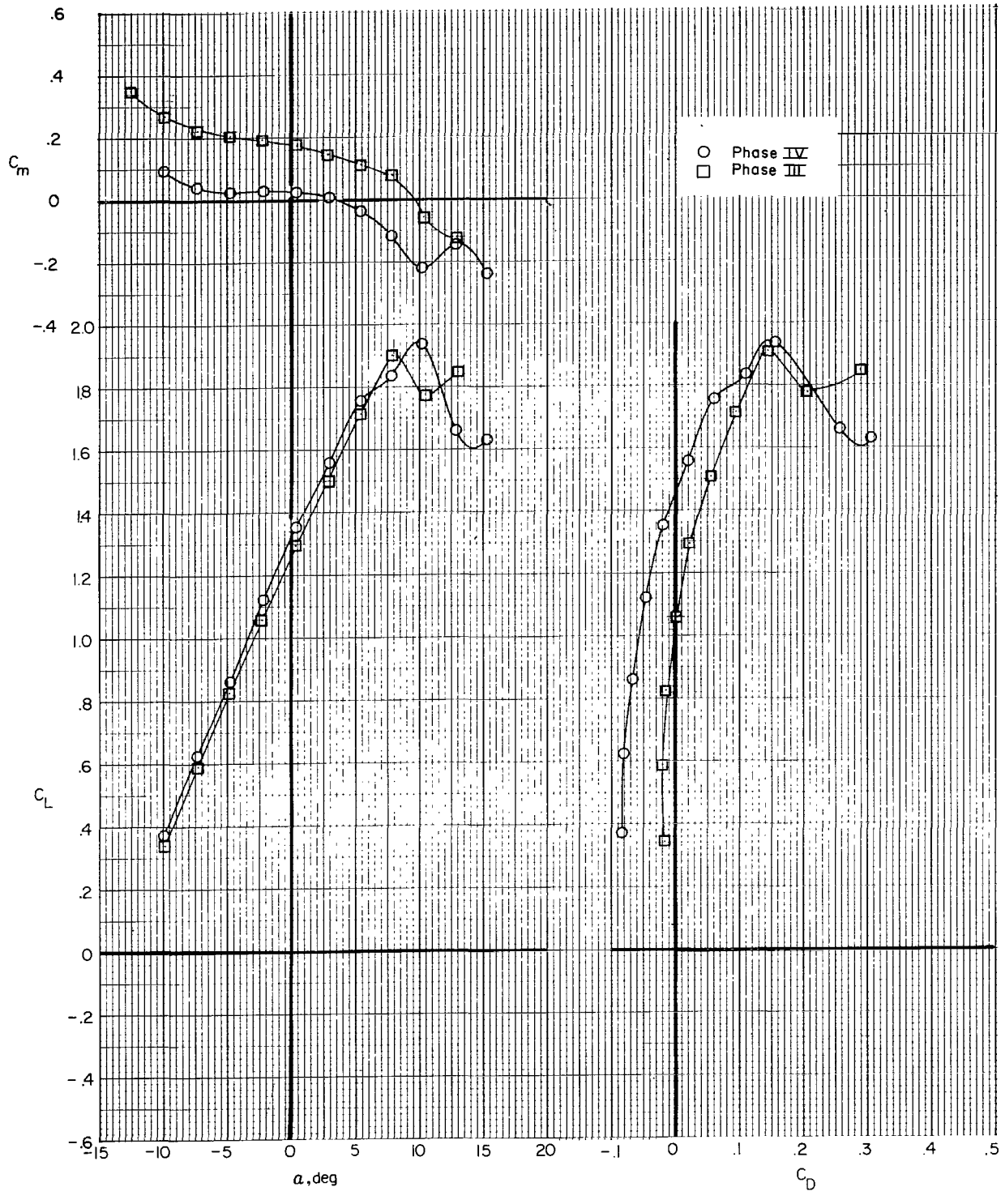

(d) $i_w = 7.5^\circ$; $\delta_f = 30^\circ$.

Figure 8.- Concluded.

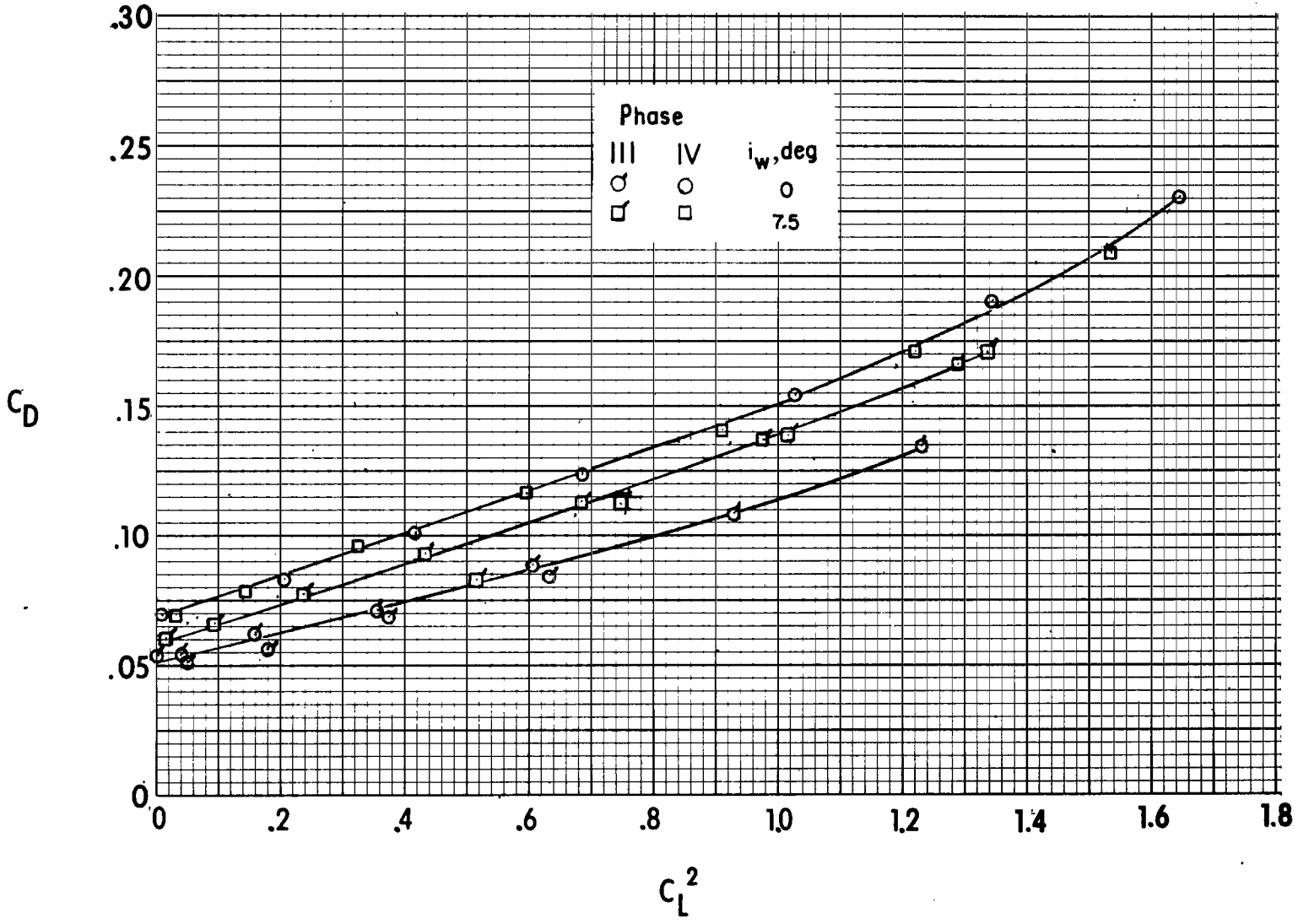

Figure 9.- Comparison of variation of drag with lift squared for Phase III and Phase V. F_1W_x; $\delta_f = 0^o$.

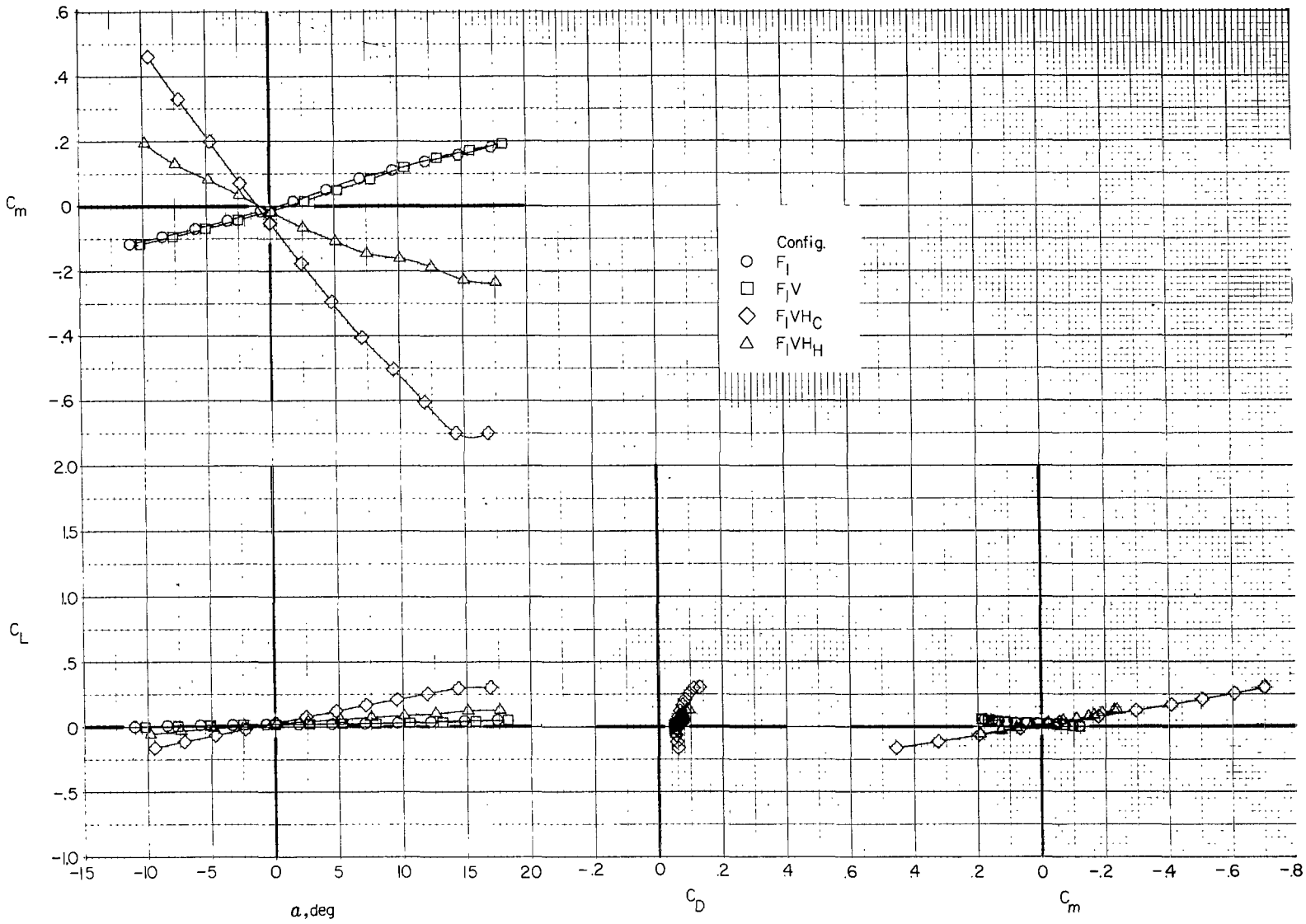

(a) Wing and jets removed.

Figure 10.- Effect of empennage components on longitudinal aerodynamics. $i_t = 0^o$.

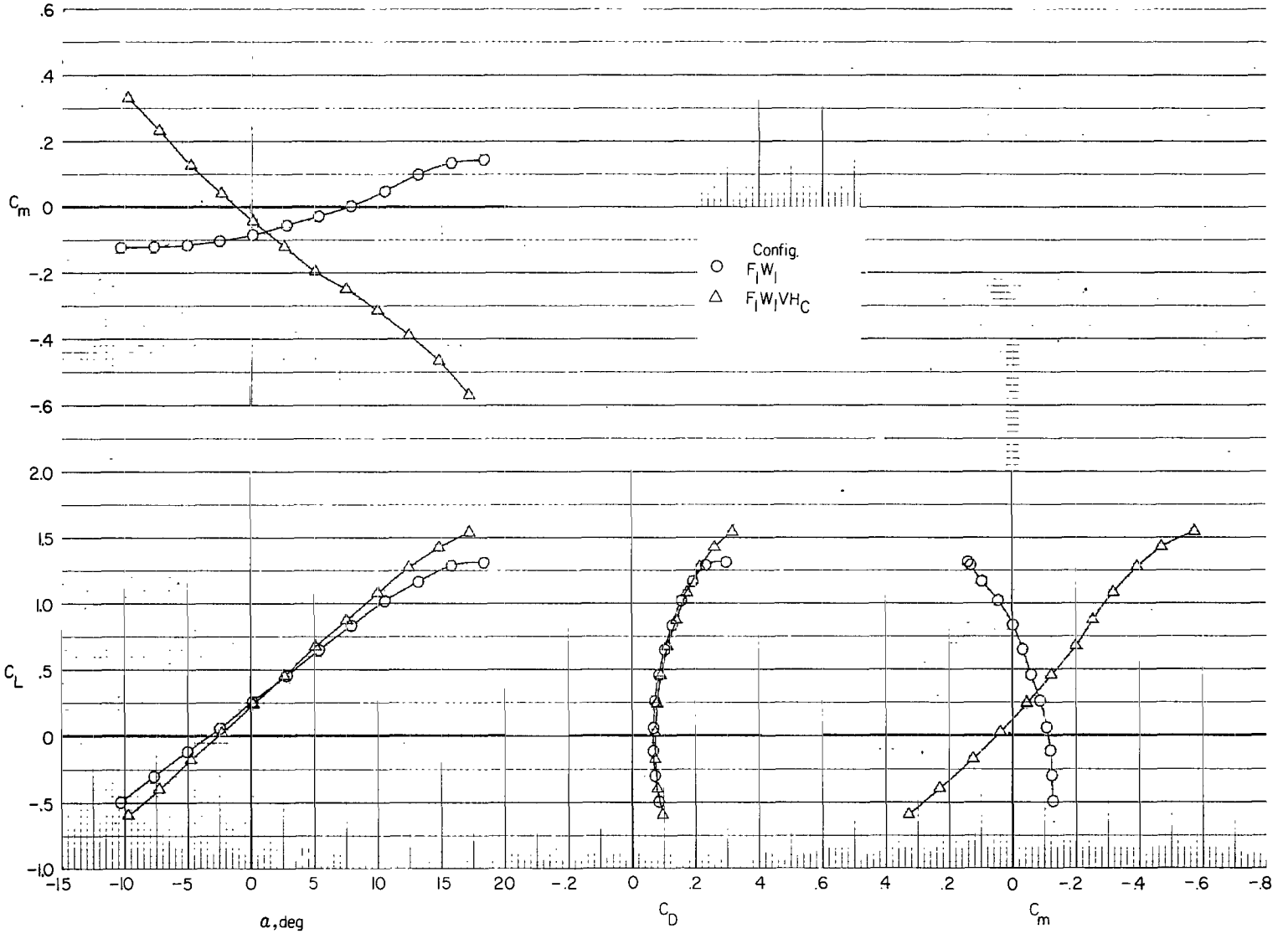

(b) i_w = 0°; δ_f = 0°; jets removed.

Figure 10.- Continued.

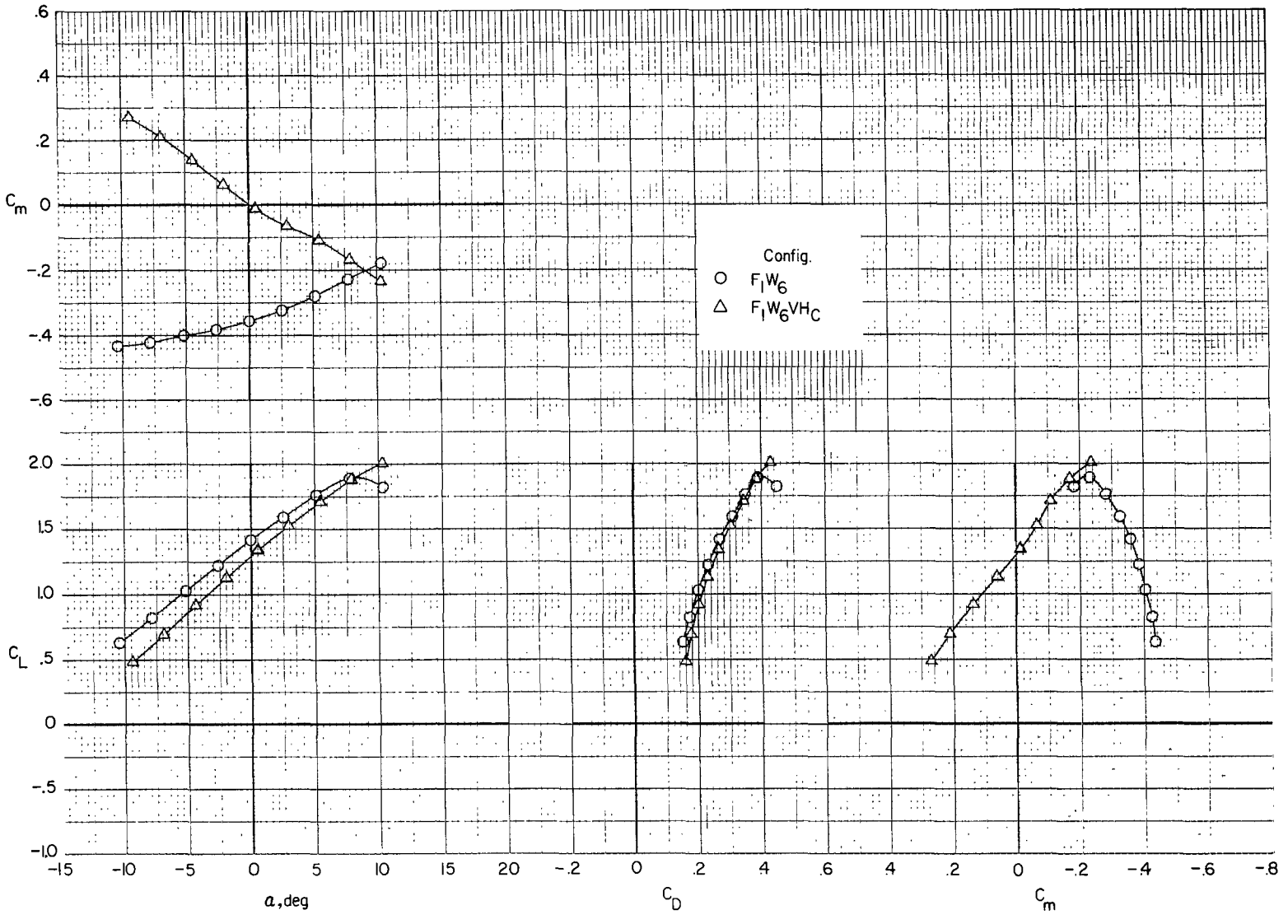

(c) i_w = 7.5°; δ_f = 30°; jets removed.

Figure 10.- Concluded.

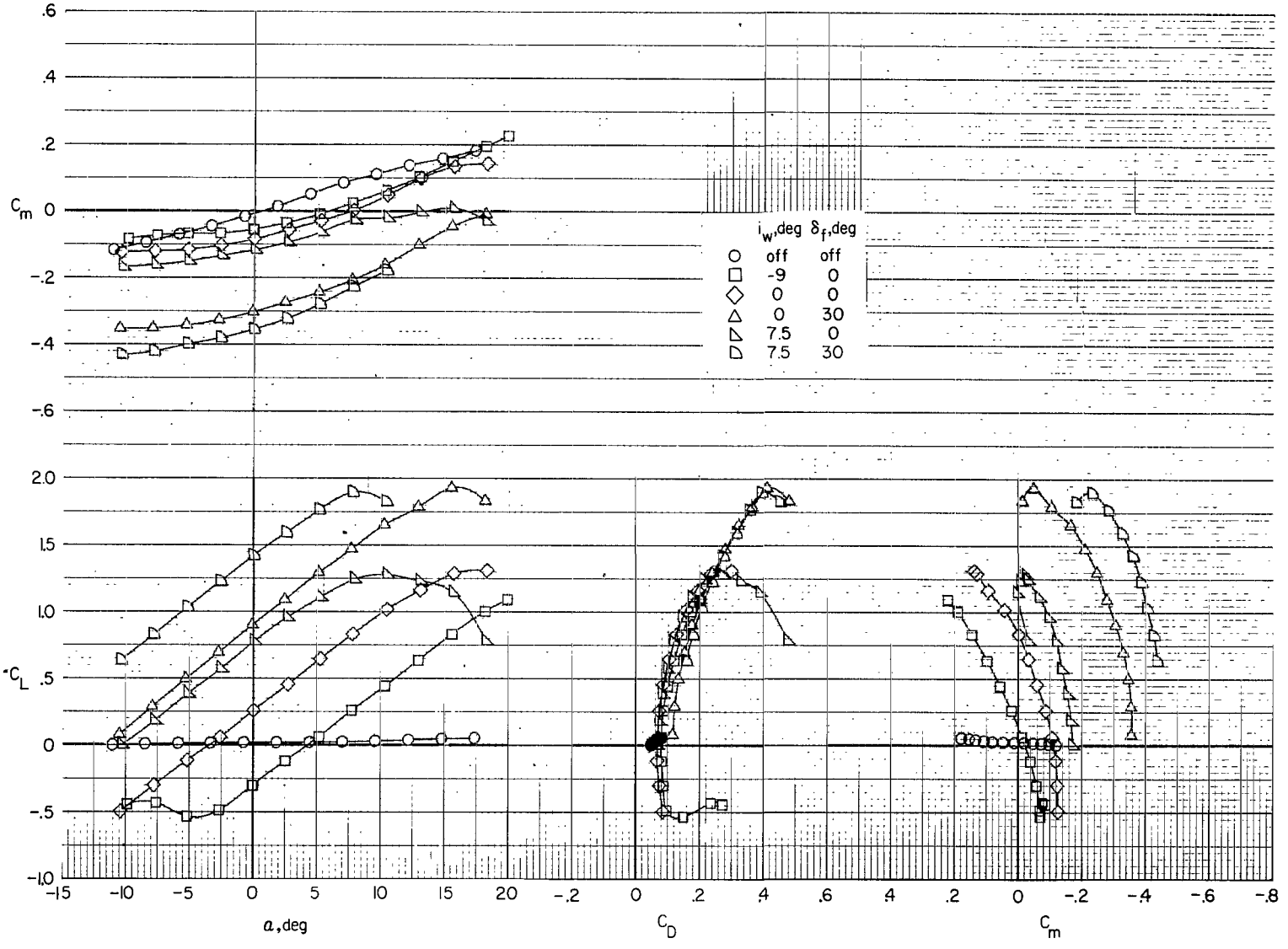

(a) Empennage and jets removed (F_1W_x).

Figure 11.- Effect of wing incidence and flap deflection on airframe longitudinal aerodynamics. $i_t = 0^o$.

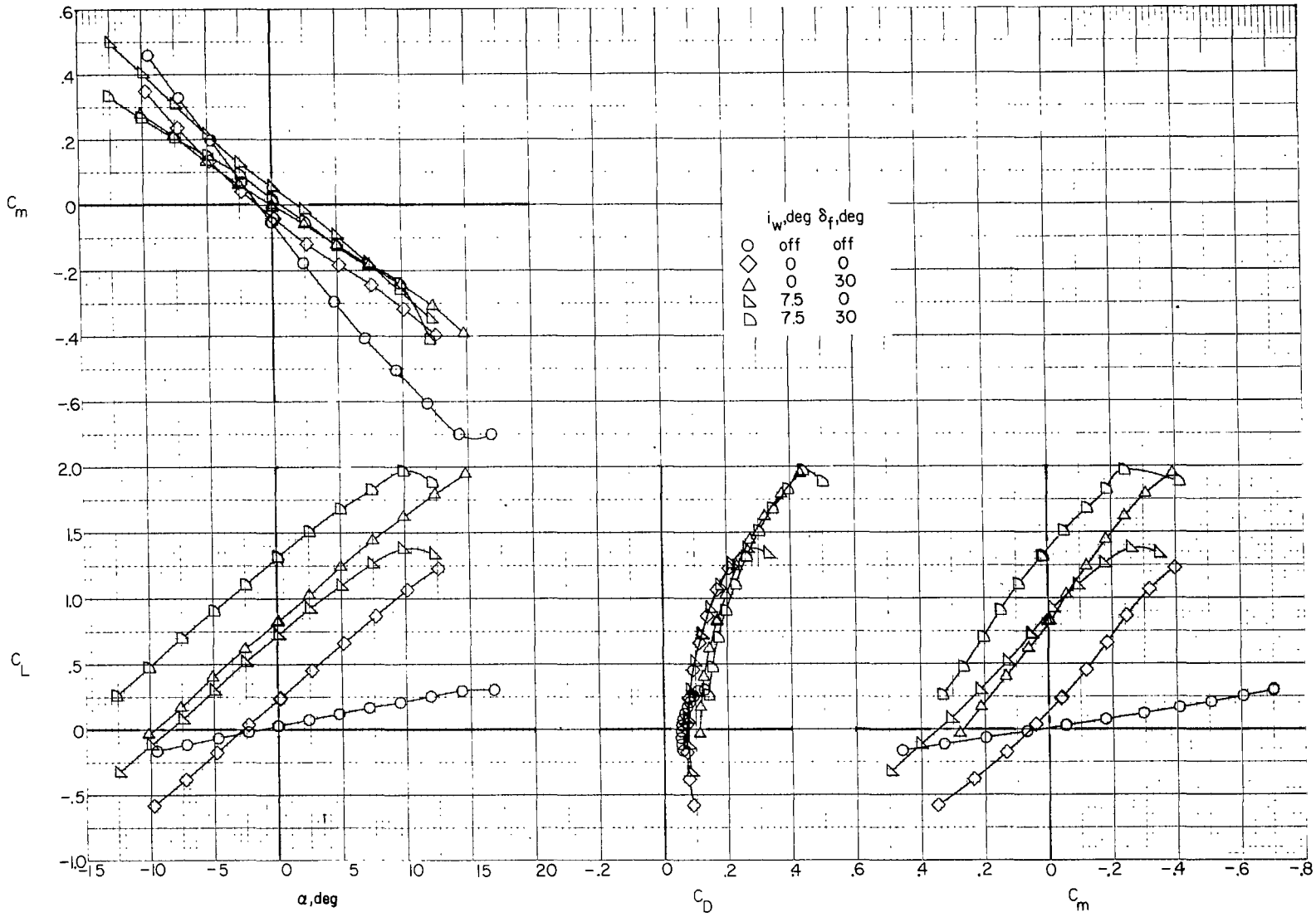

(b) Empennage on and jets removed ($F_1W_xVH_C$).

Figure 11.- Continued.

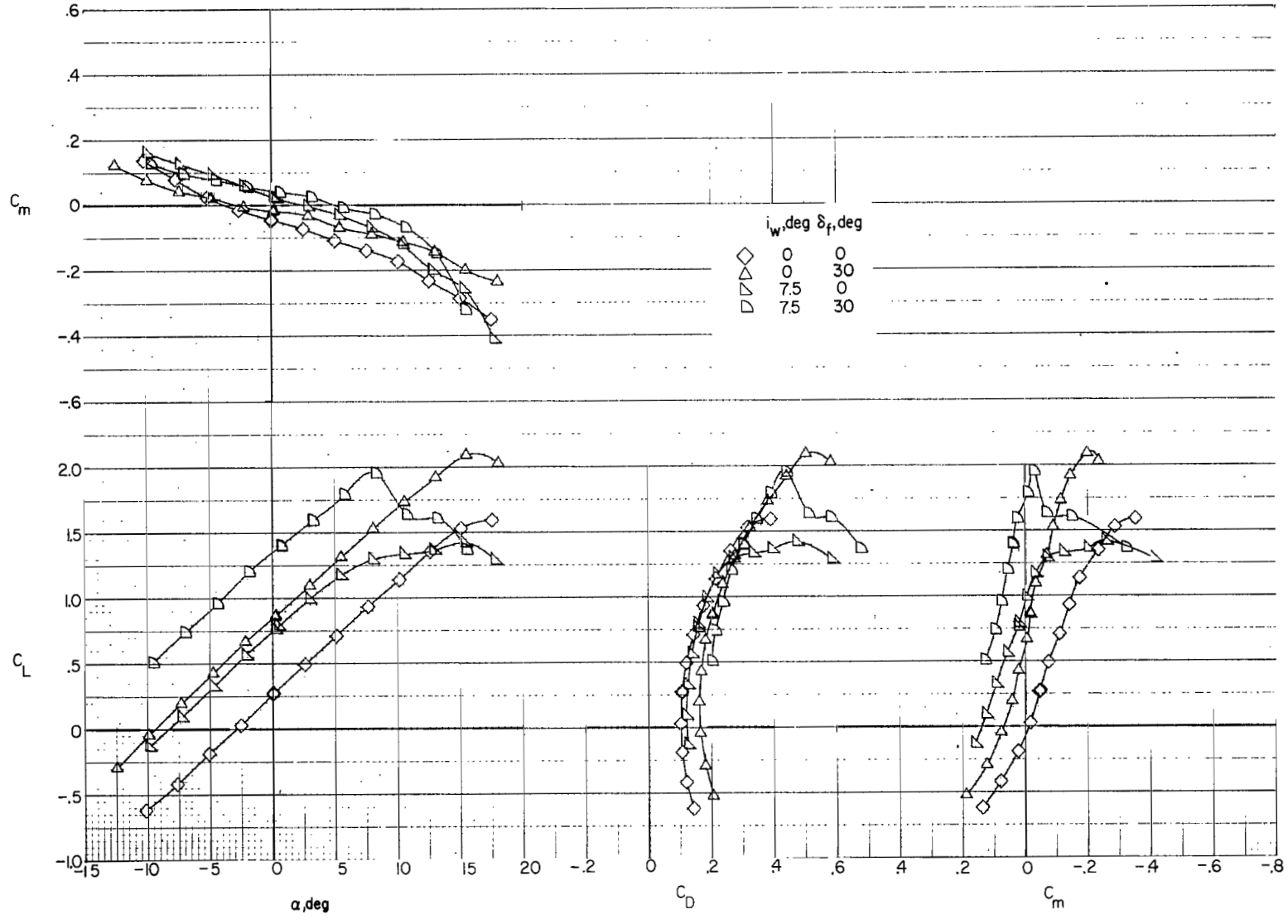

(c) Empennage and jets on ($F_1W_XVH_CJ_2$). $C_{T,J} \approx 0$.

Figure 11.- Continued.

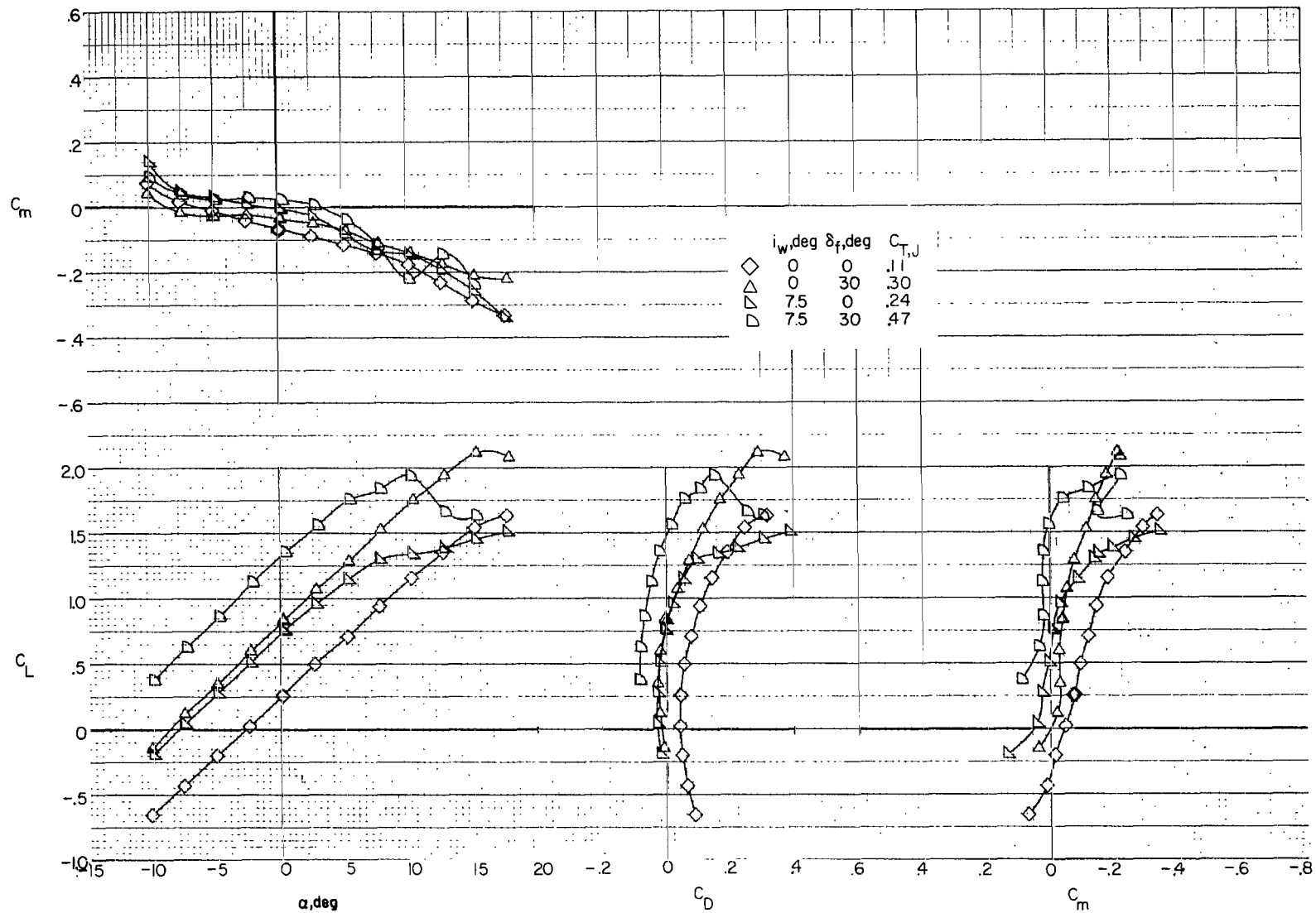

(d) Empennage and jets on ($F_1W_xVH_CJ_2$). Trim thrust.

Figure 11.- Concluded.

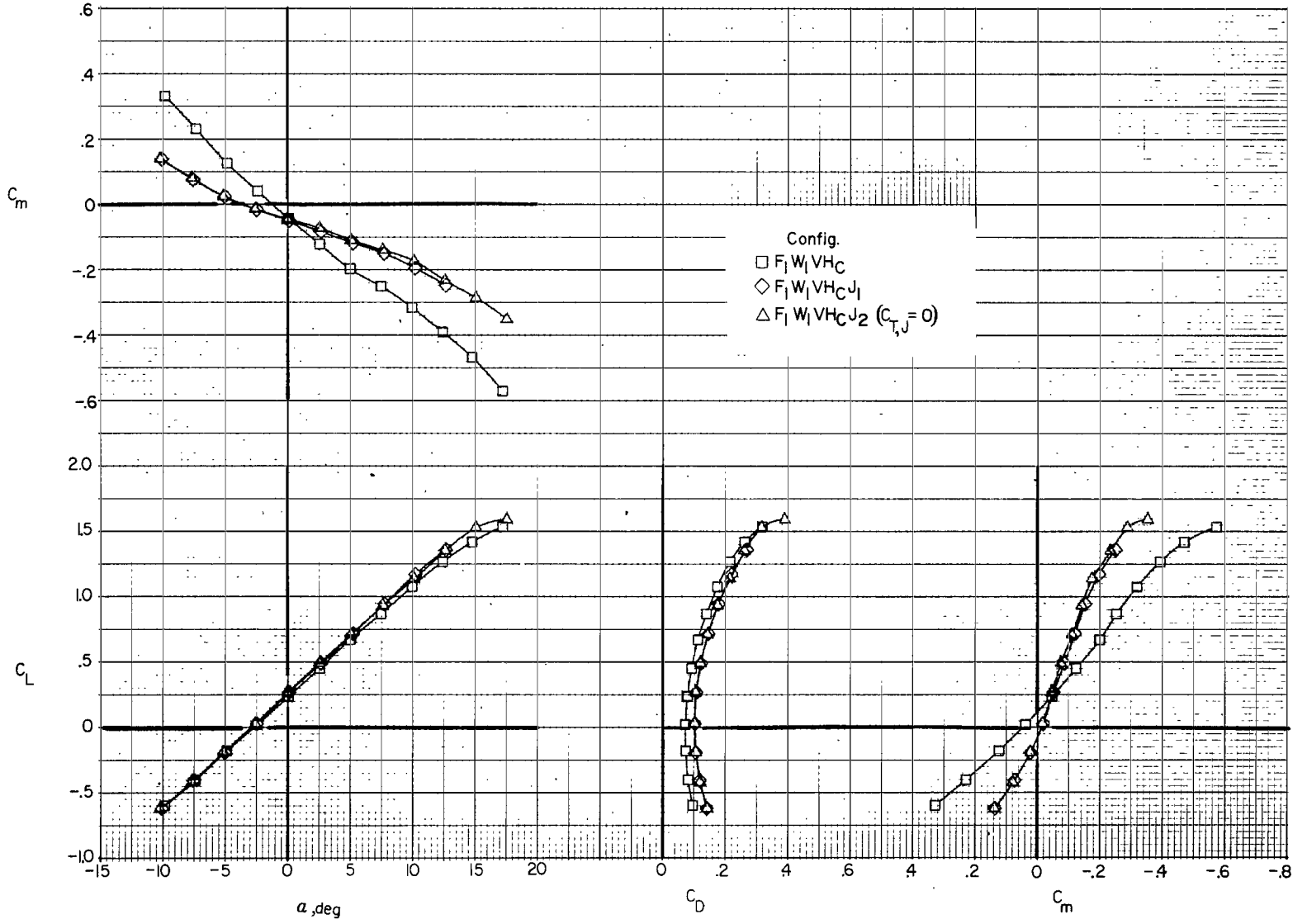

Figure 12.- Effect of auxiliary thrust engine nacelles on airframe longitudinal aerodynamics. $i_t = 0^o$.

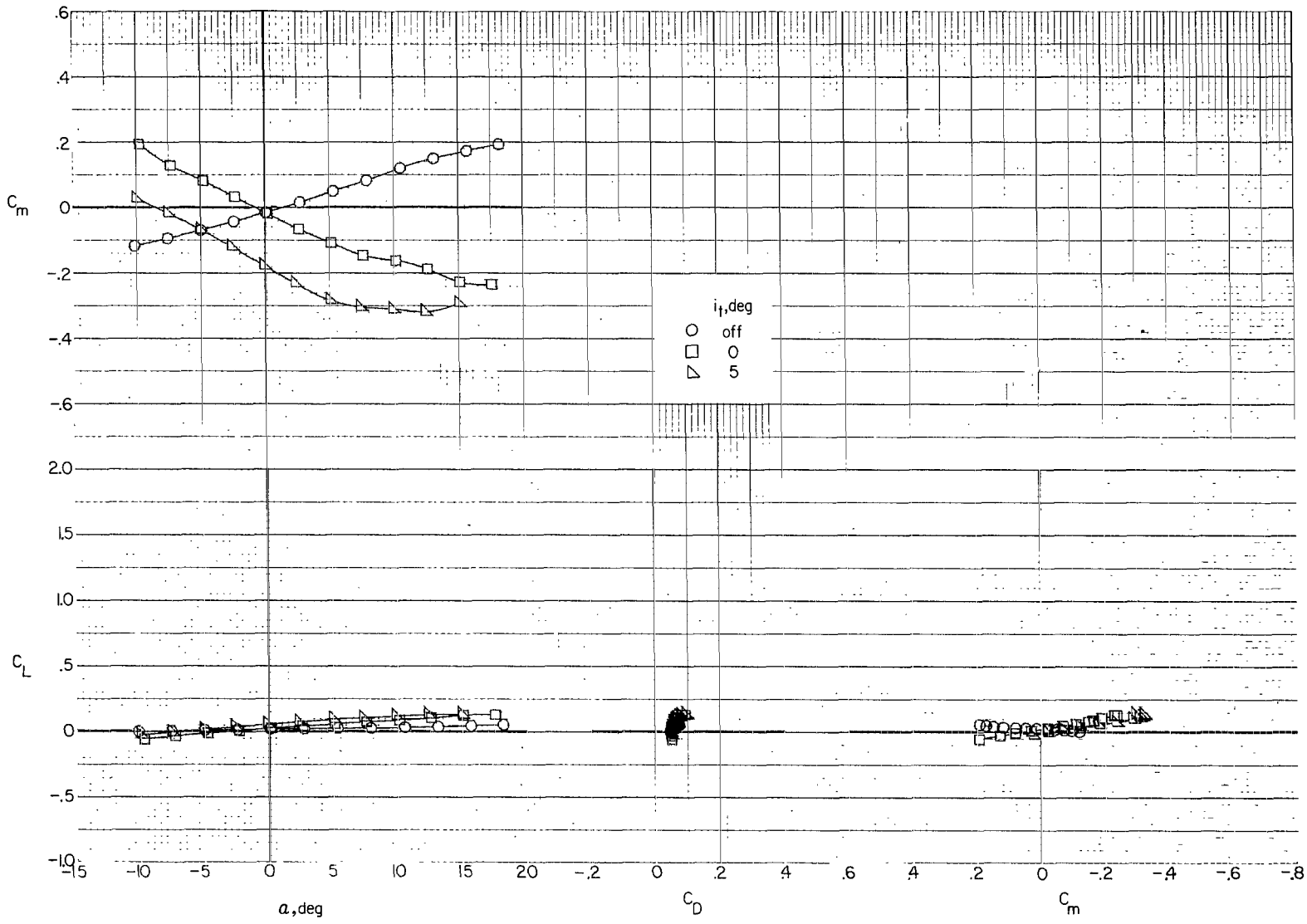

(a) Helicopter tail (F_1VH_H).

Figure 13.- Effect of horizontal-tail incidence on airframe longitudinal aerodynamics.

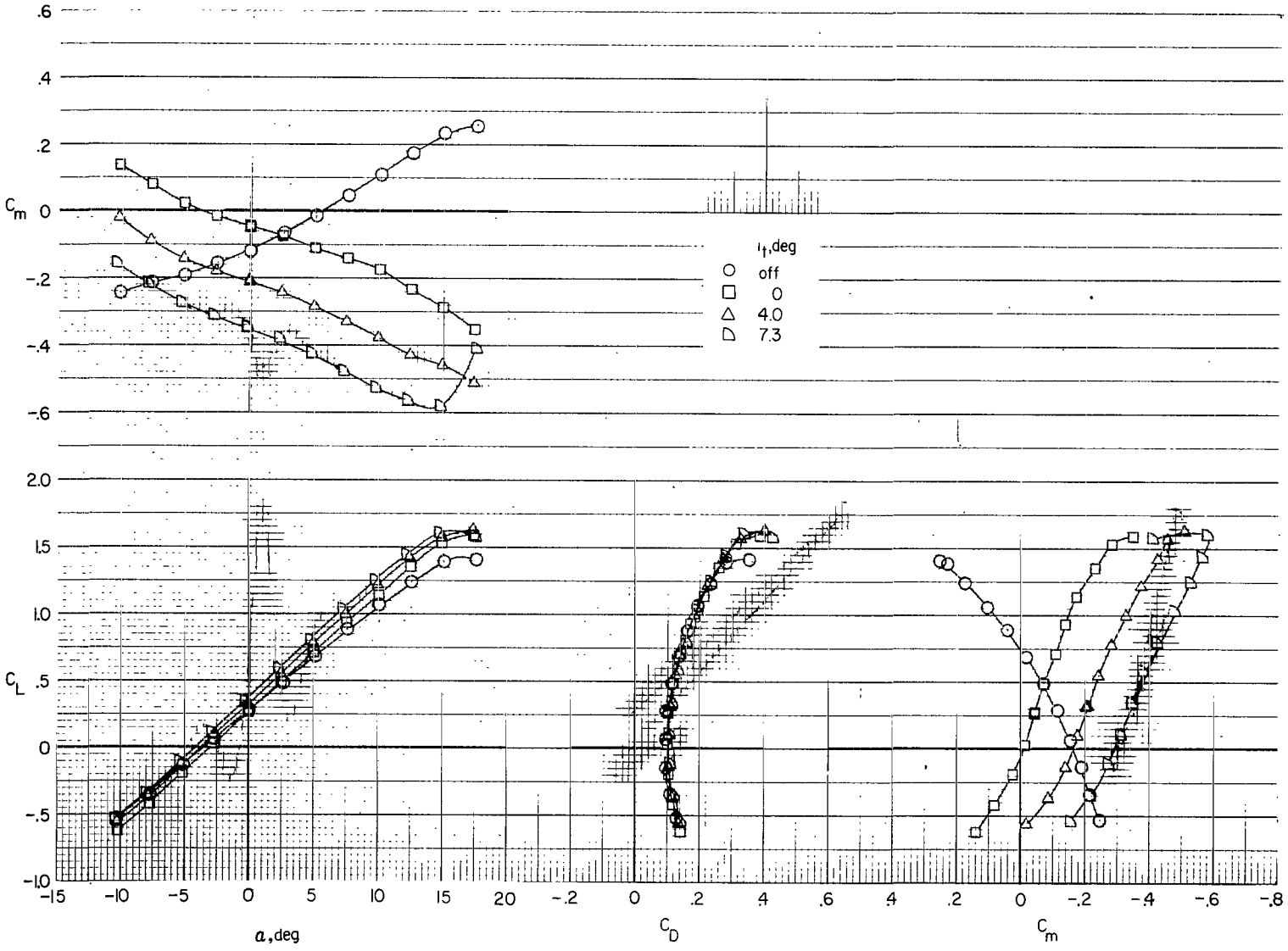

(b) Compound tail ($F_1W_1VH_CJ_2$). $C_{T,J} = 0$.

Figure 13.- Continued.

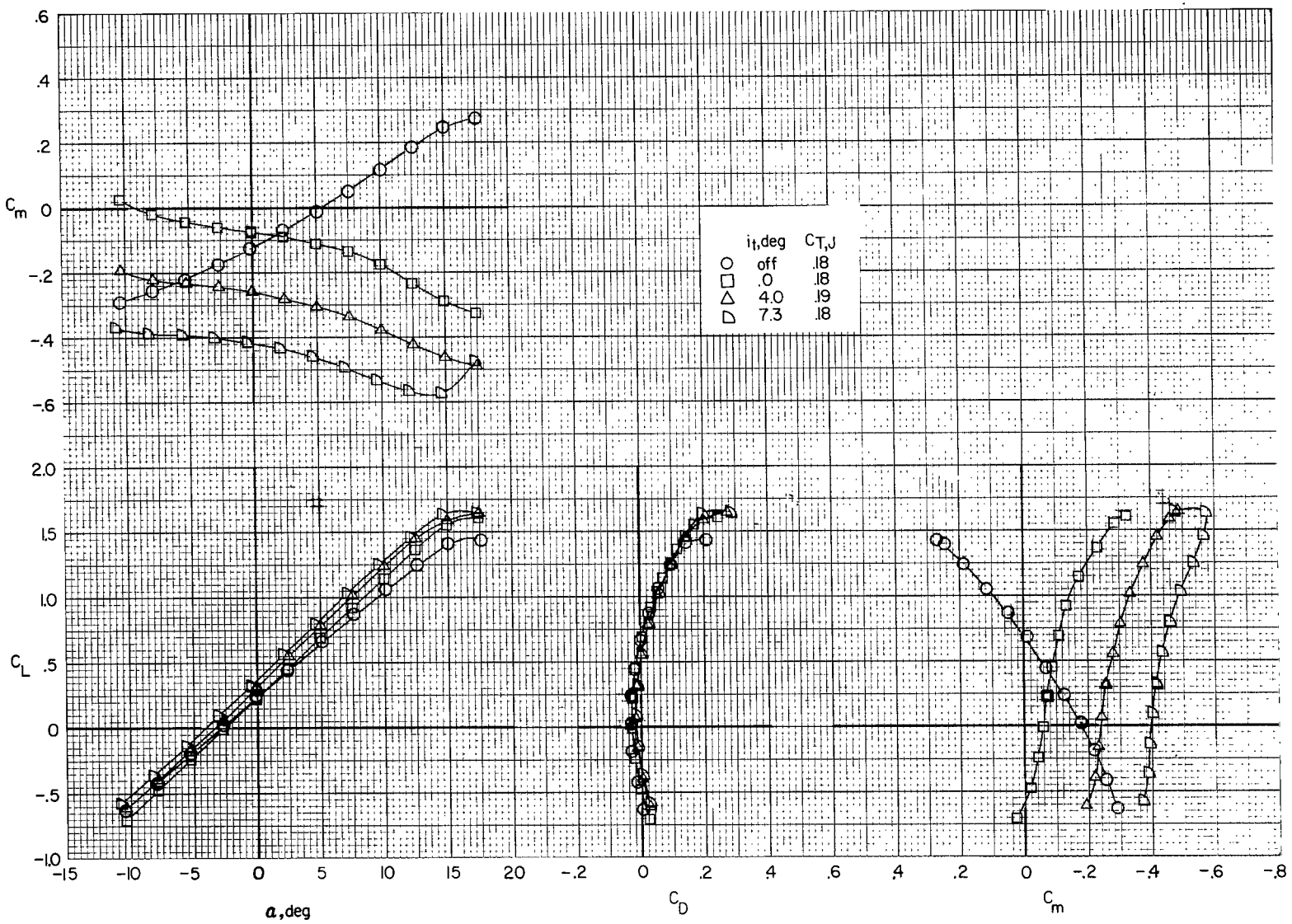

(c) Compound tail ($F_1W_1VH_CJ_2$). Trim thrust.

Figure 13.- Concluded.

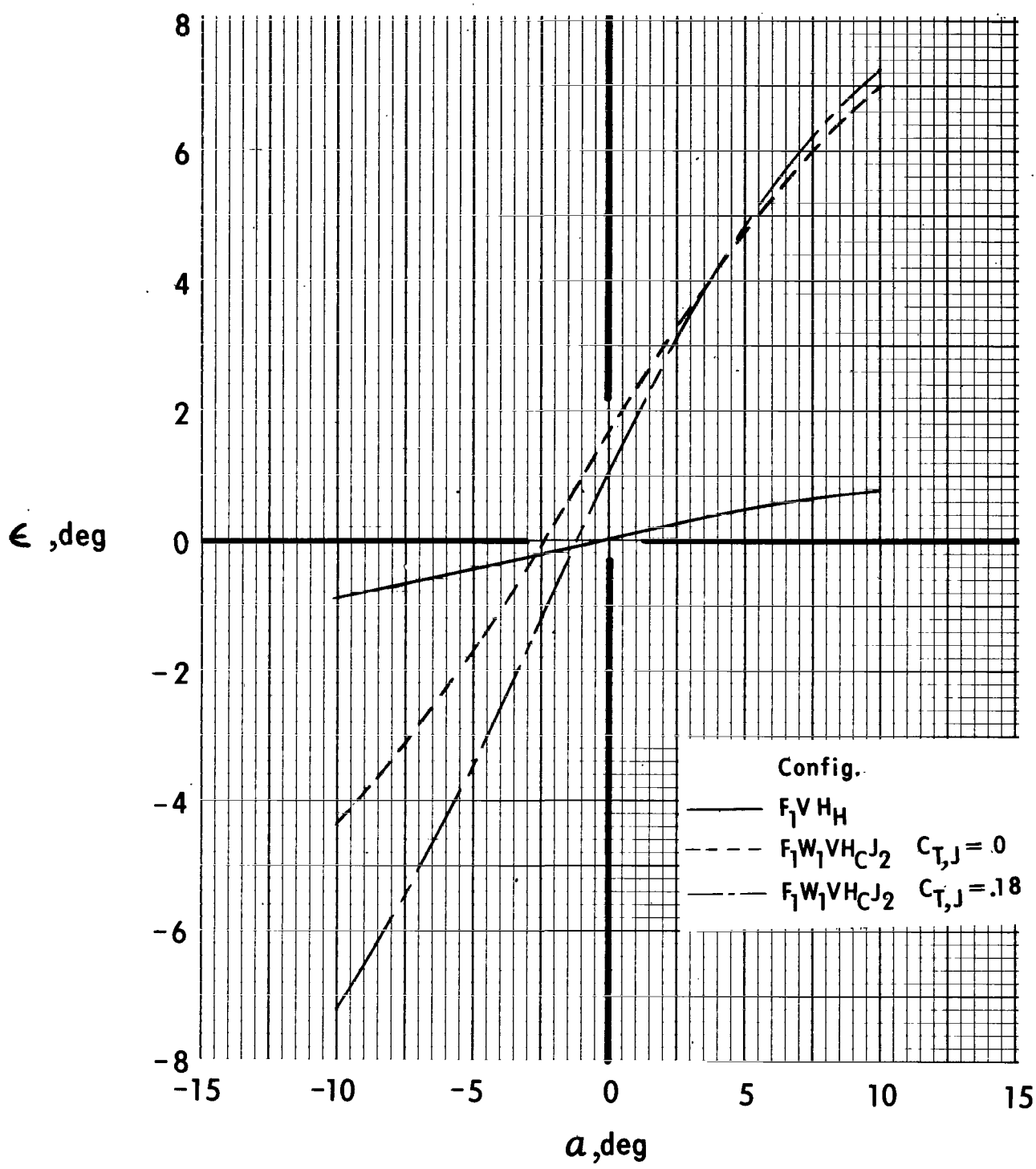

Figure 14.- Variation of downwash at tail with angle of attack for several configurations.

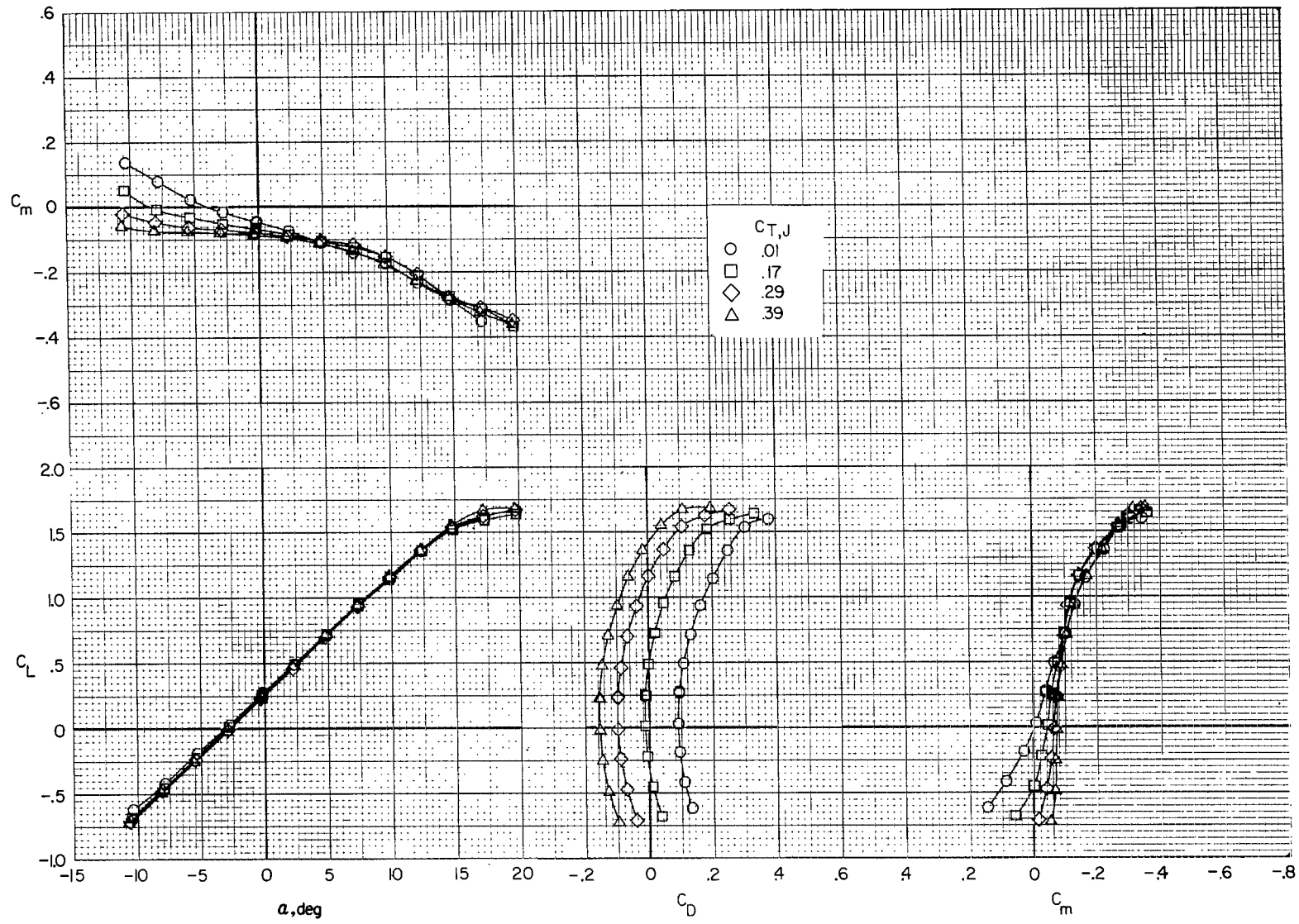

(a) $i_w = 0^o$; $\delta_f = 0^o$.

Figure 15.- Effect of auxiliary engine thrust level on airframe longitudinal aerodynamics. $F_1W_XVH_CJ_2$; $i_t = 0^o$.

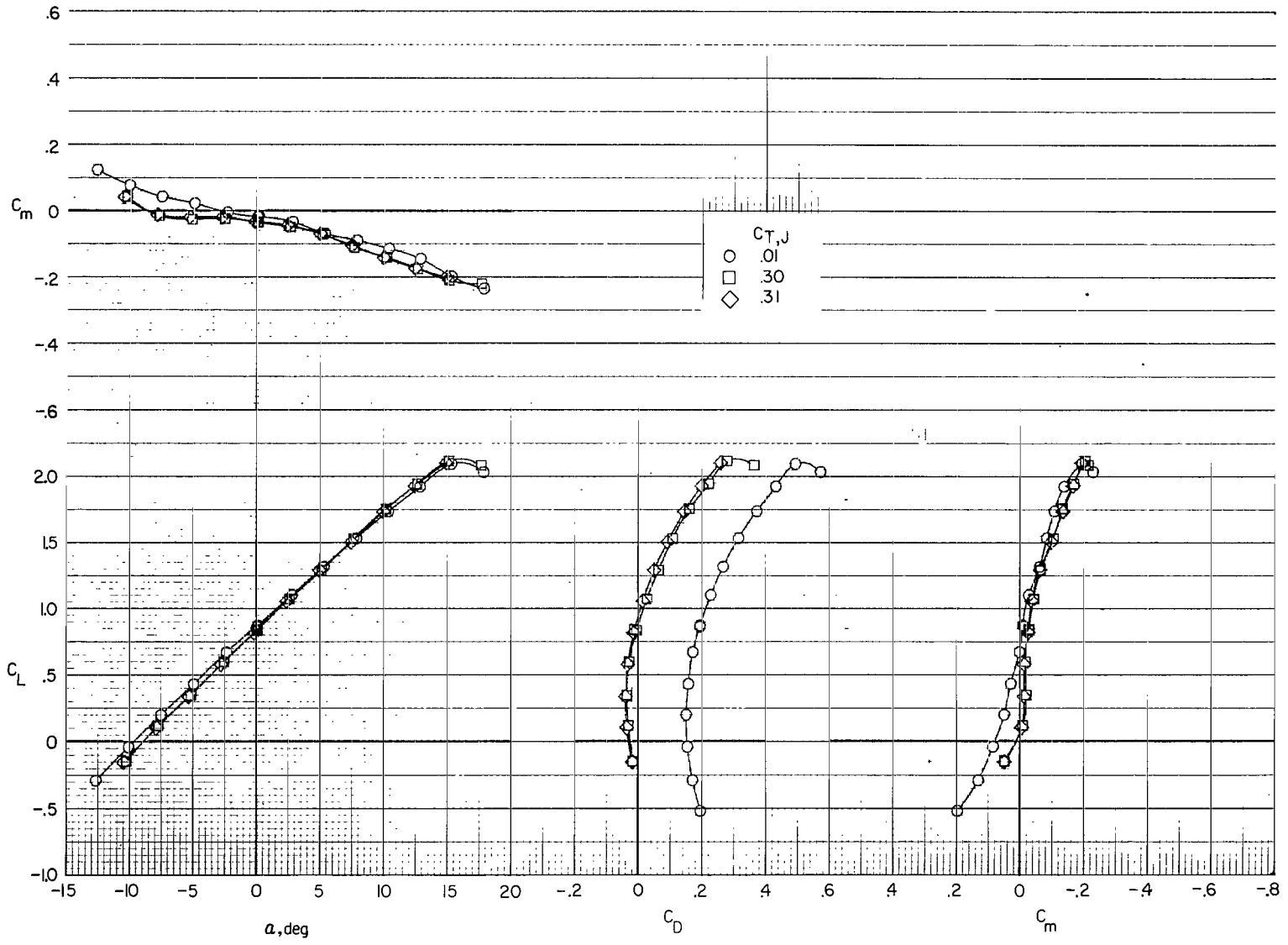

(b) $i_w = 0^o$; $\delta_f = 30^o$.

Figure 15.- Continued.

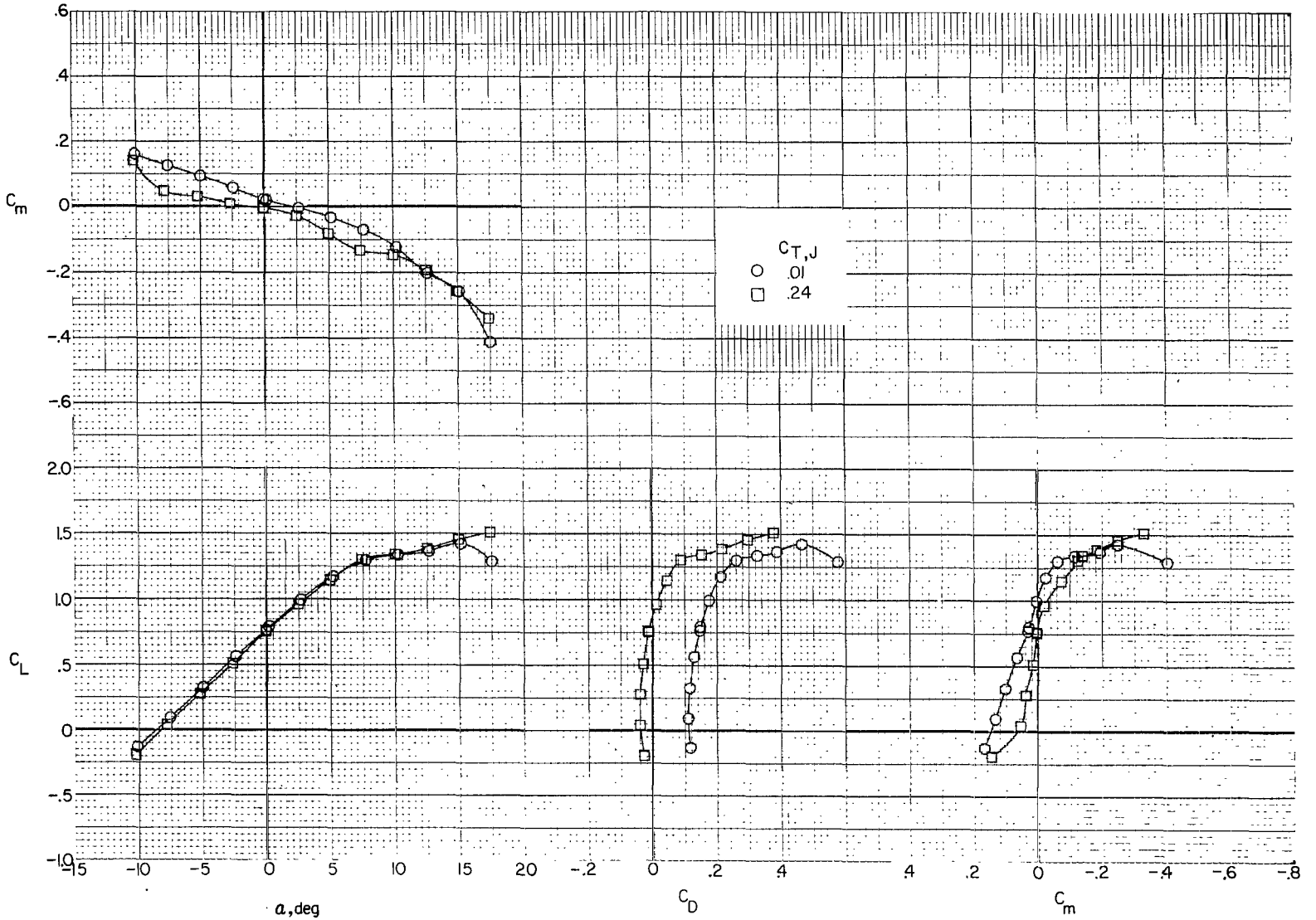

(c) $i_w = 7.5^o$; $\delta_f = 0^o$.

Figure 15.- Continued.

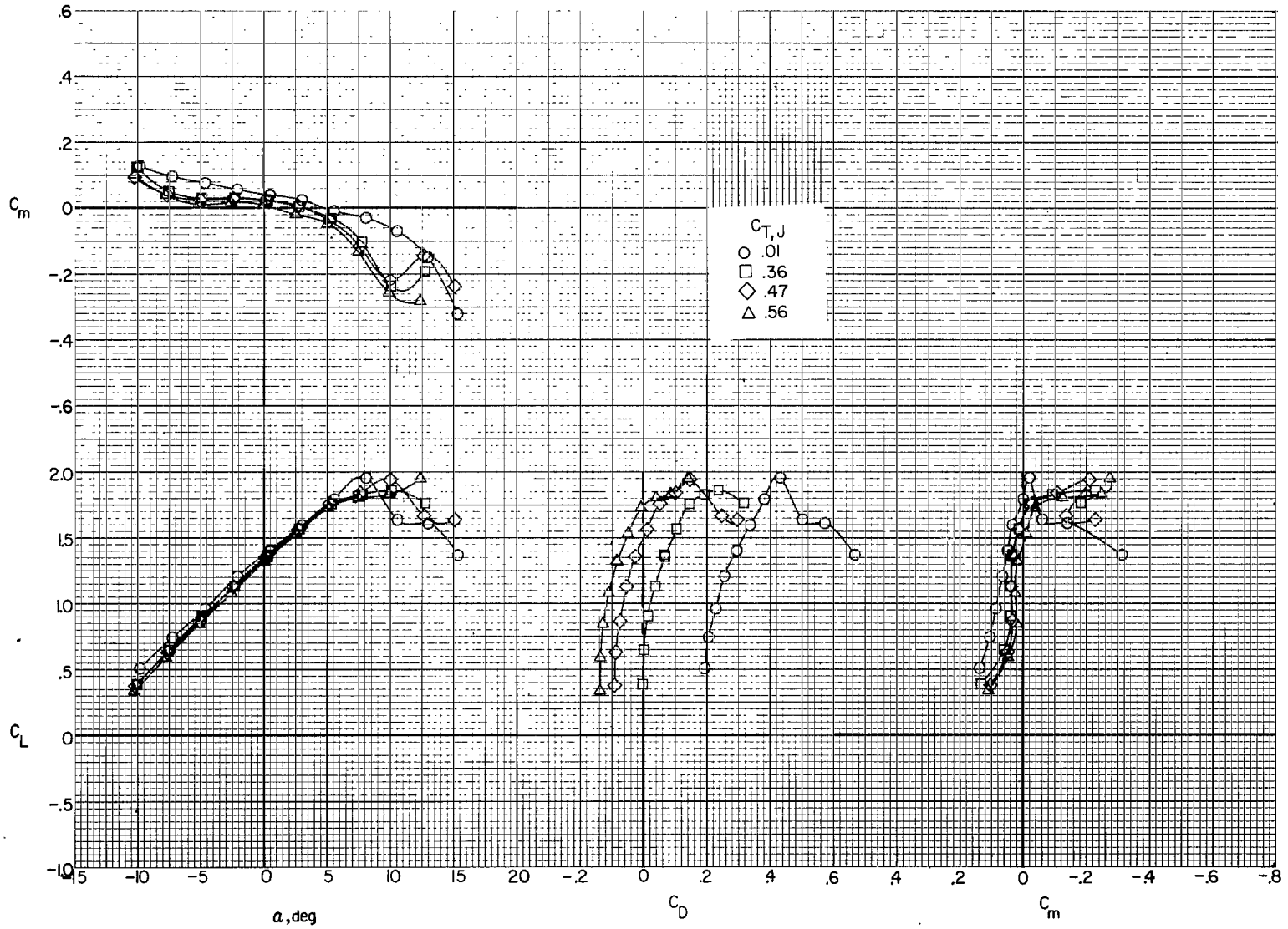

(d) $i_w = 7.5^o$; $\delta_f = 30^o$.

Figure 15.- Concluded.

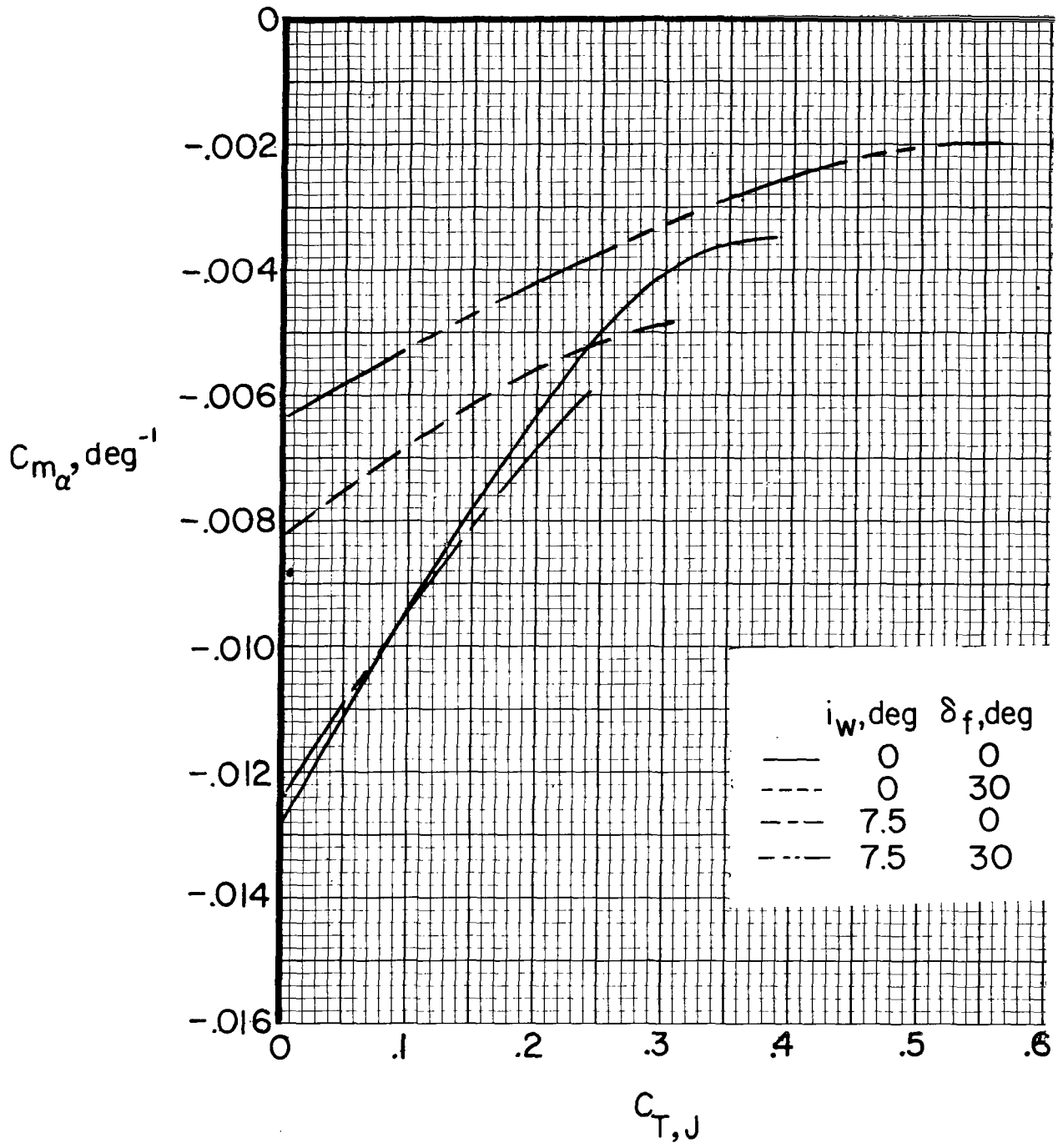

Figure 16.- Summary of effect of auxiliary engine thrust on static longitudinal stability of compound helicopter.

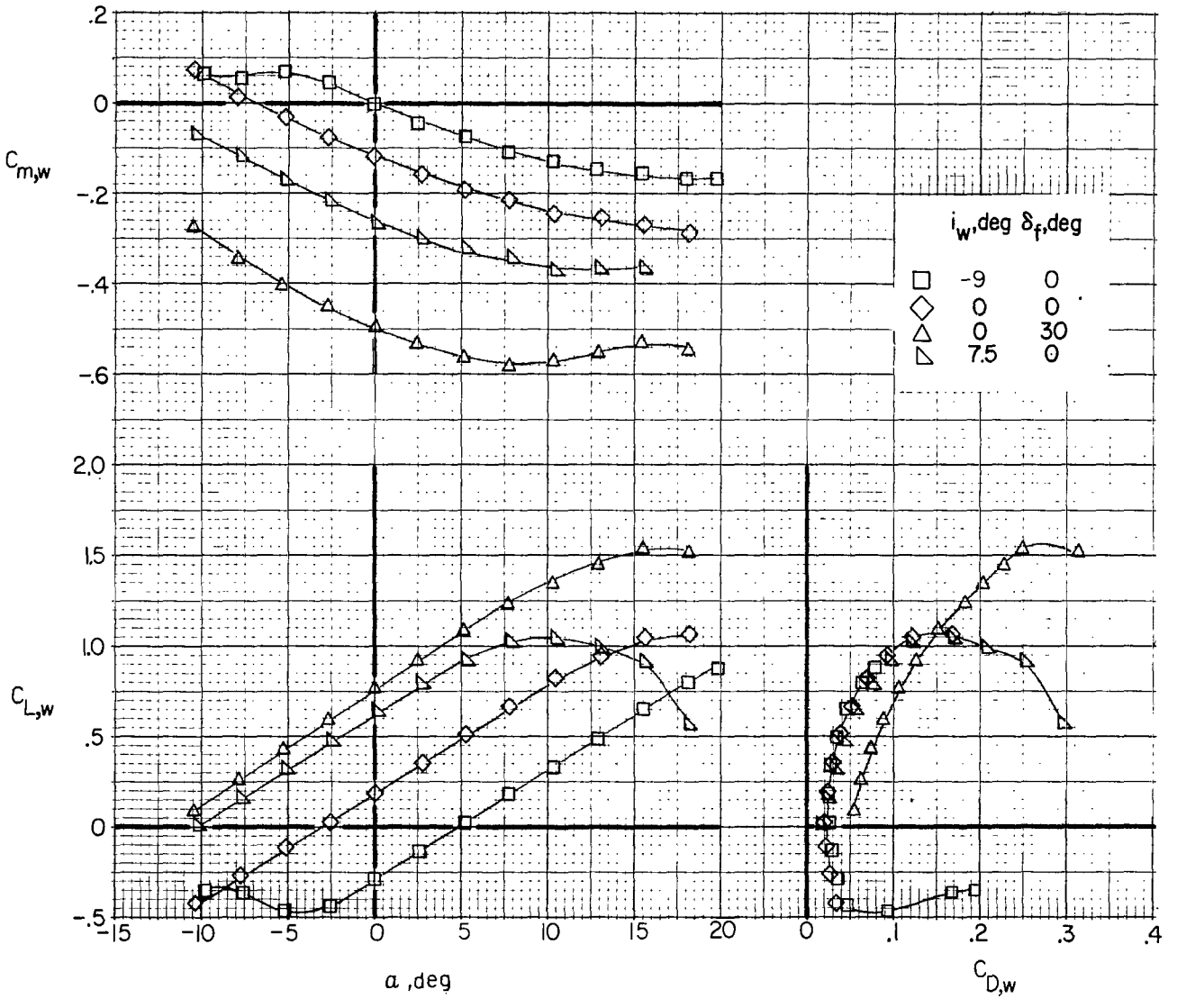

(a) Jets removed (F_1W_X).

Figure 17.- Effect of wing incidence and flap deflection on wing longitudinal aerodynamics.

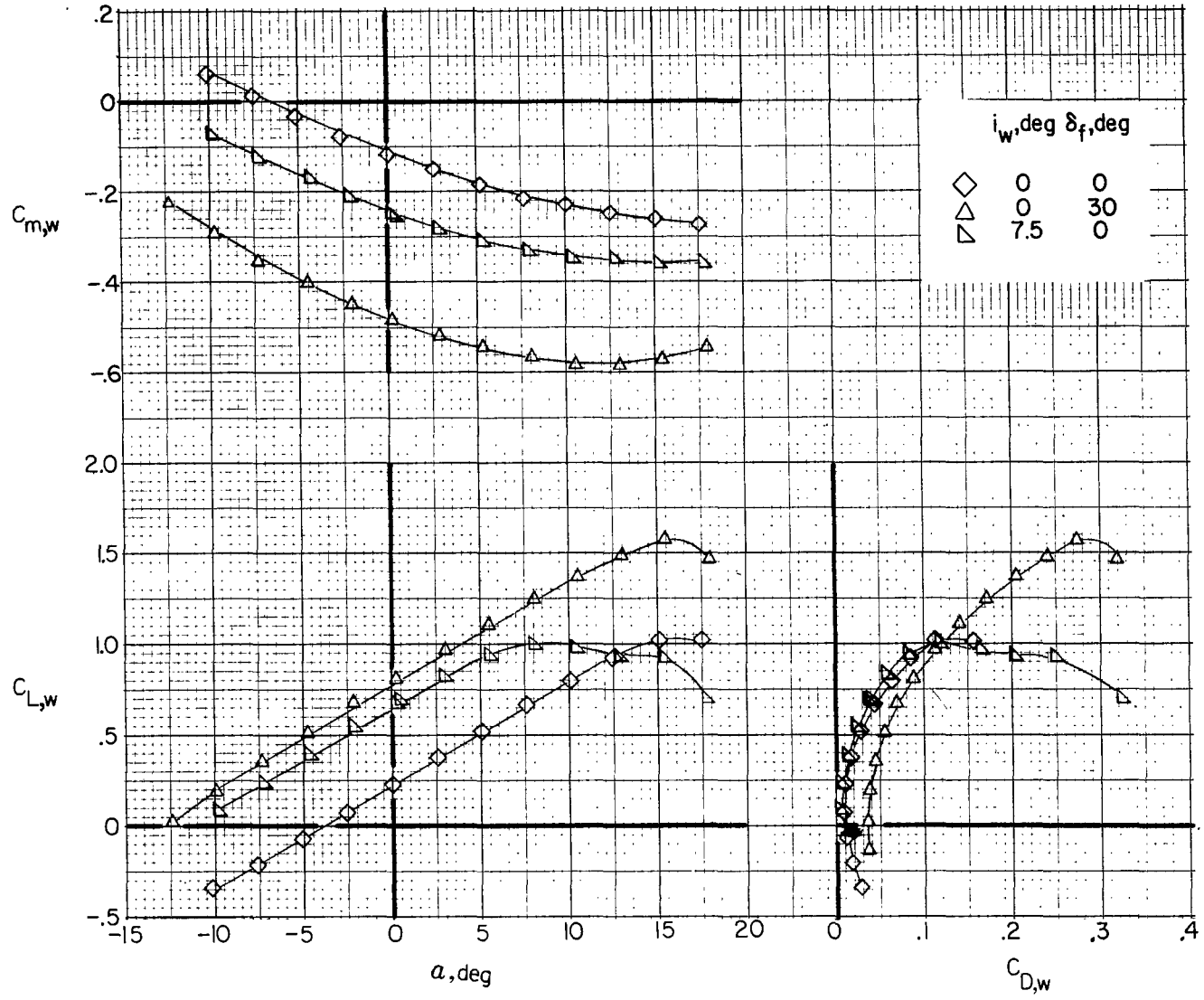

(b) Jets on ($F_1W_XVH_CJ_2$). $C_{T,J} = 0$.

Figure 17.- Concluded.

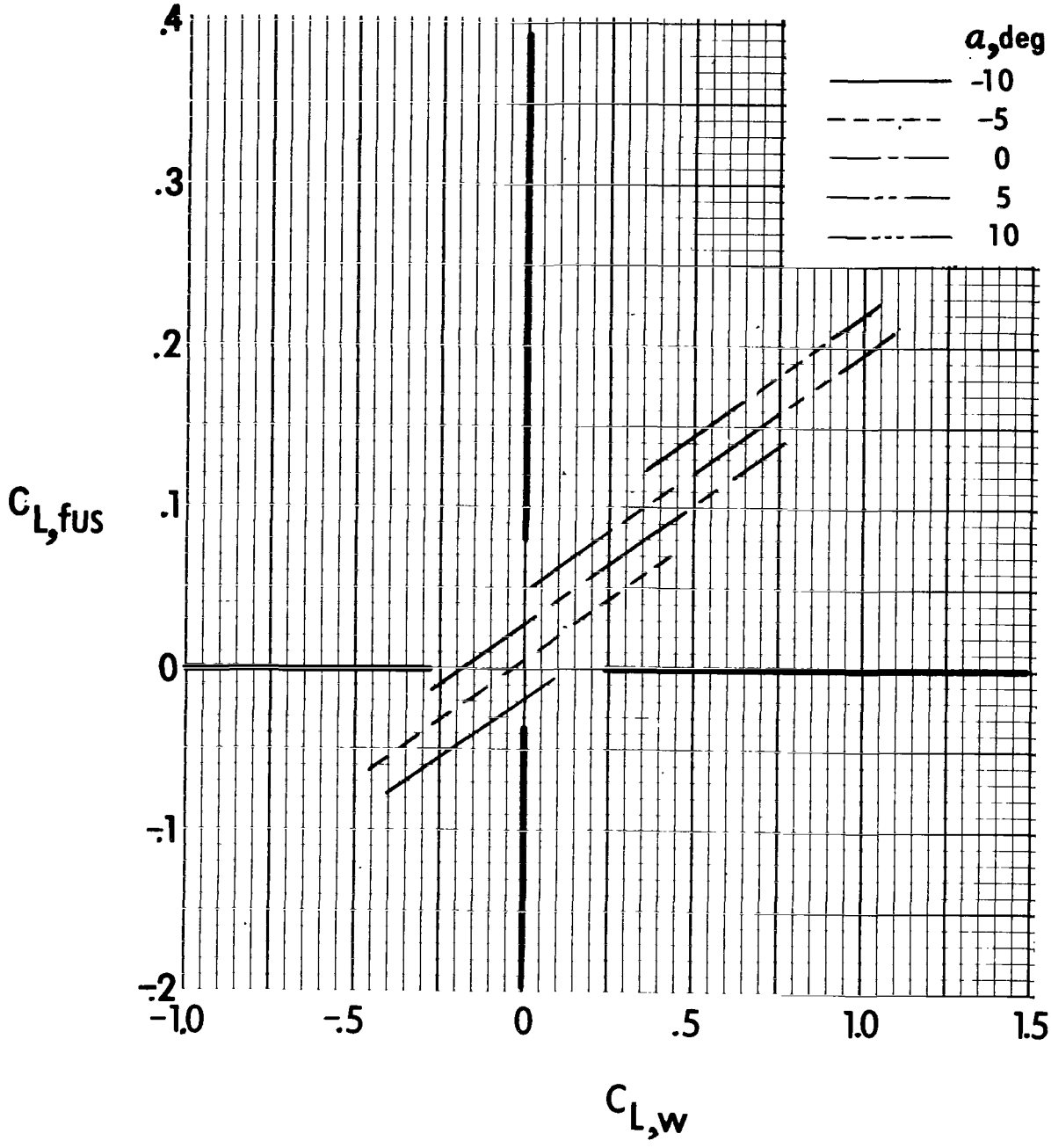

Figure 18.- Variation of fuselage lift coefficient with wing lift coefficient for several angles of attack. F_1W_x.

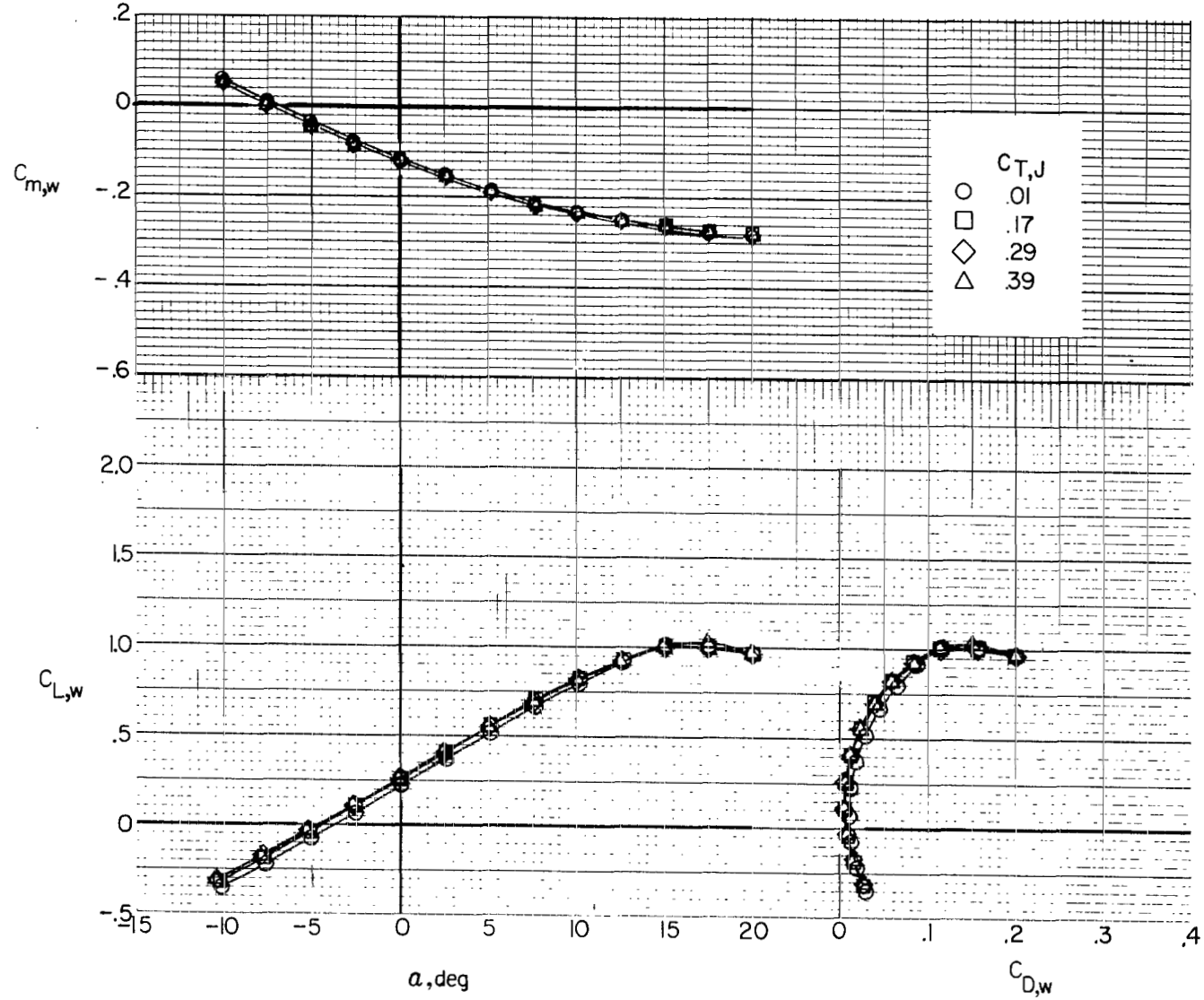

(a) $i_w = 0^o$; $\delta_f = 0^o$.

Figure 19.- Effect of auxiliary engine thrust on wing longitudinal aerodynamics.

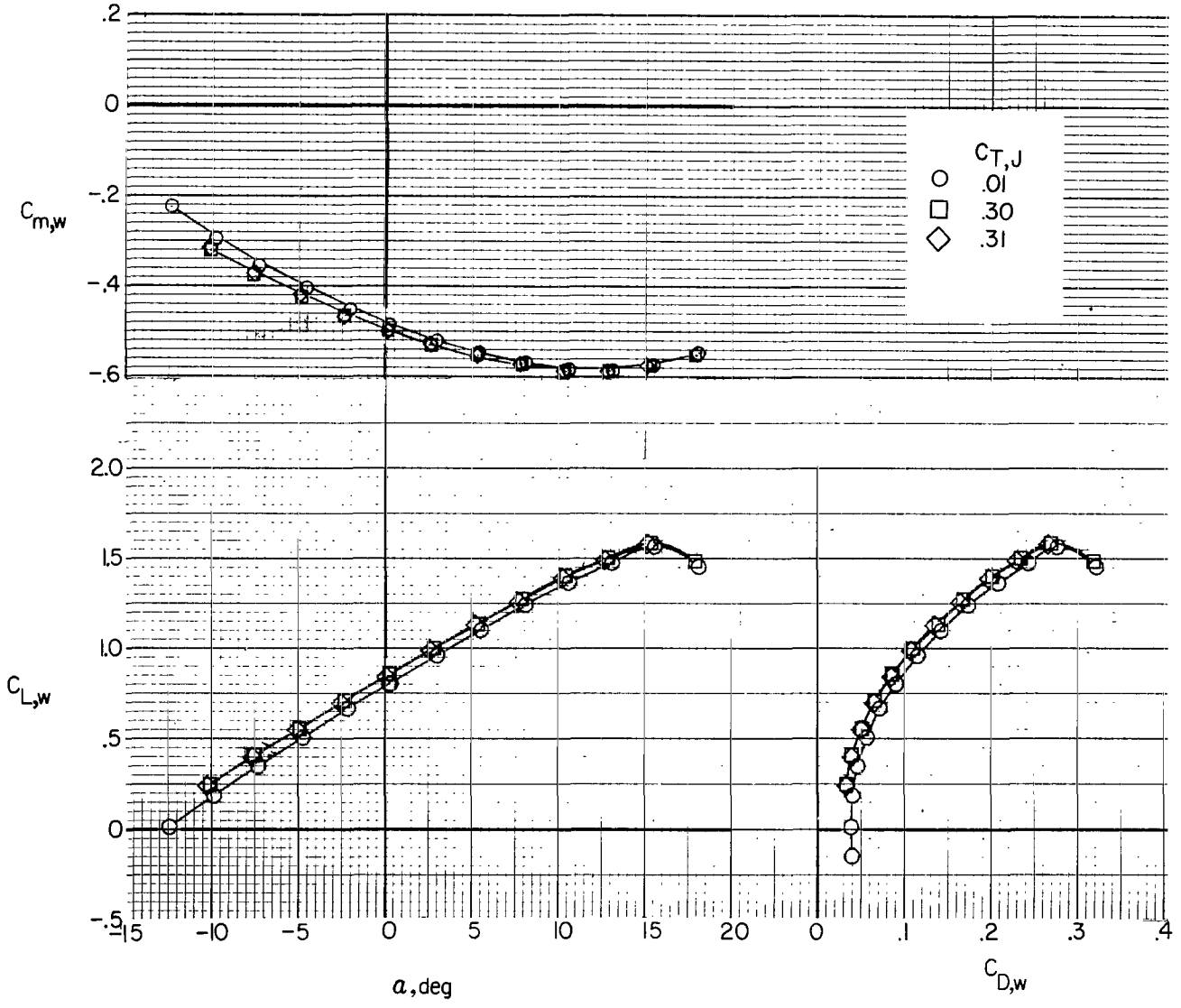

(b) $i_w = 0^\circ$; $\delta_f = 30^\circ$.

Figure 19.- Continued.

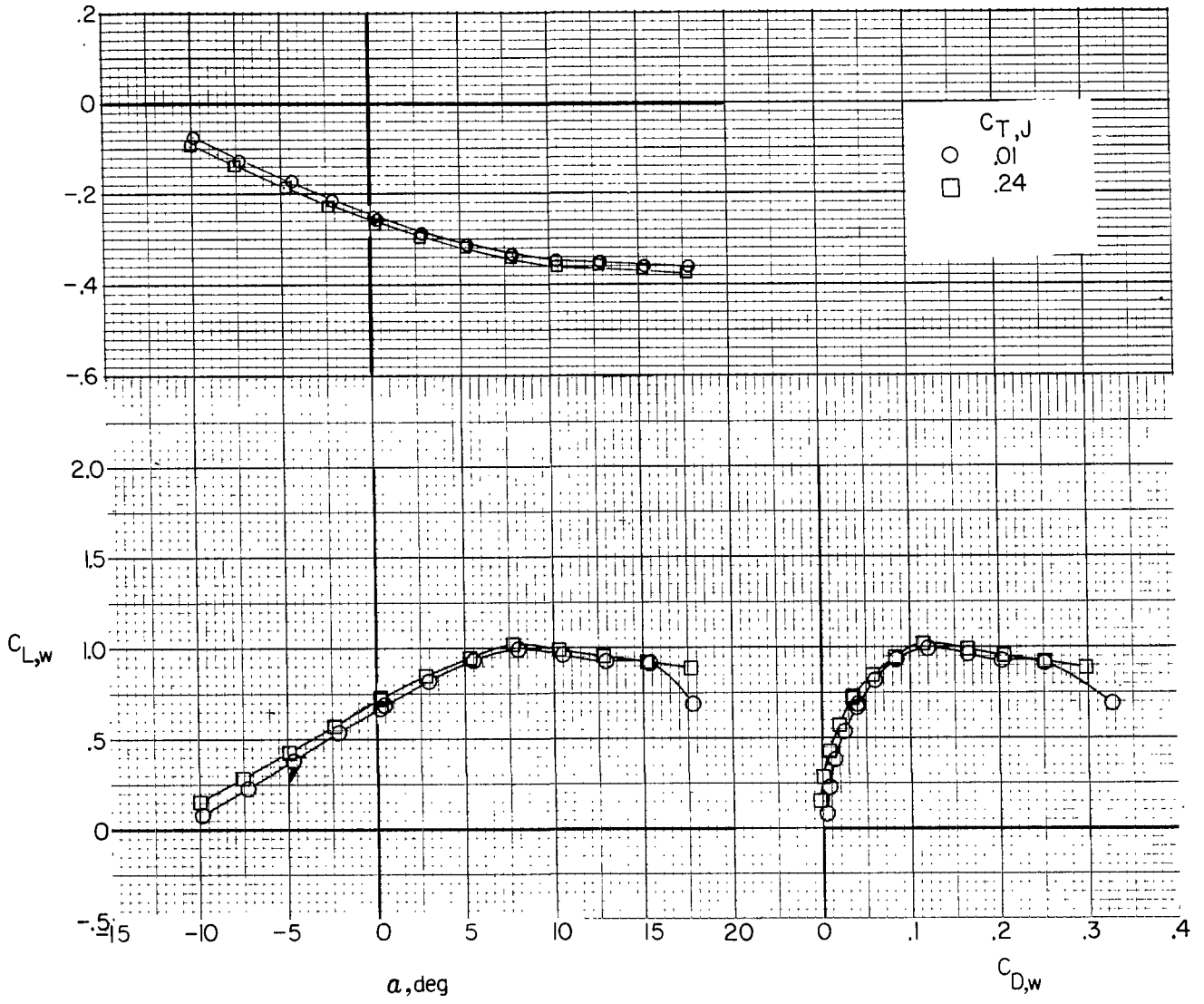

(c) $i_w = 7.5^o$; $\delta_f = 0^o$.

Figure 19.- Continued.

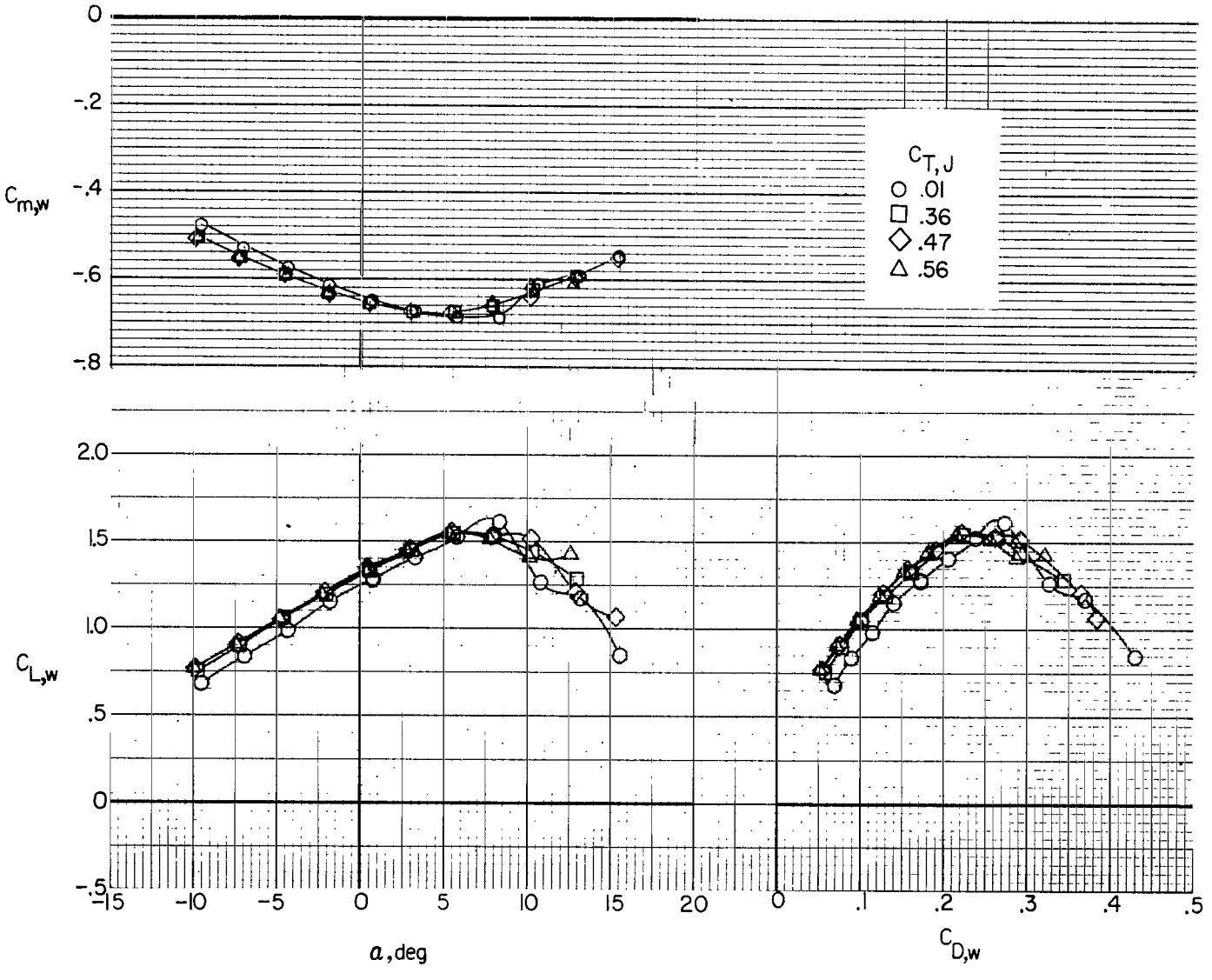

(d) $i_w = 7.5^o$; $\delta_f = 30^o$.

Figure 19.- Concluded.

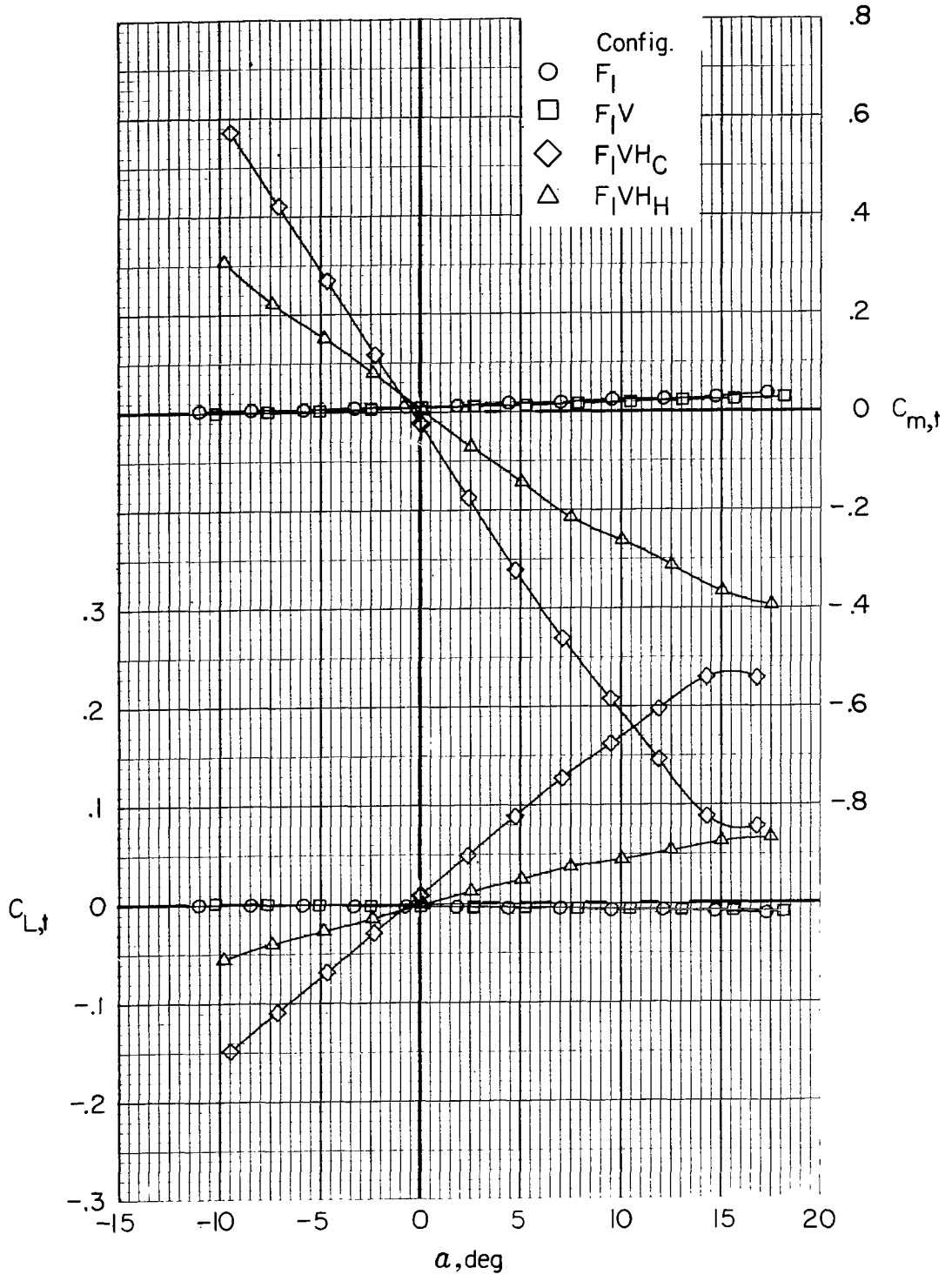

Figure 20.- Effect of empennage components on tail longitudinal aerodynamics with wing and jets removed. $i_t = 0^o$.

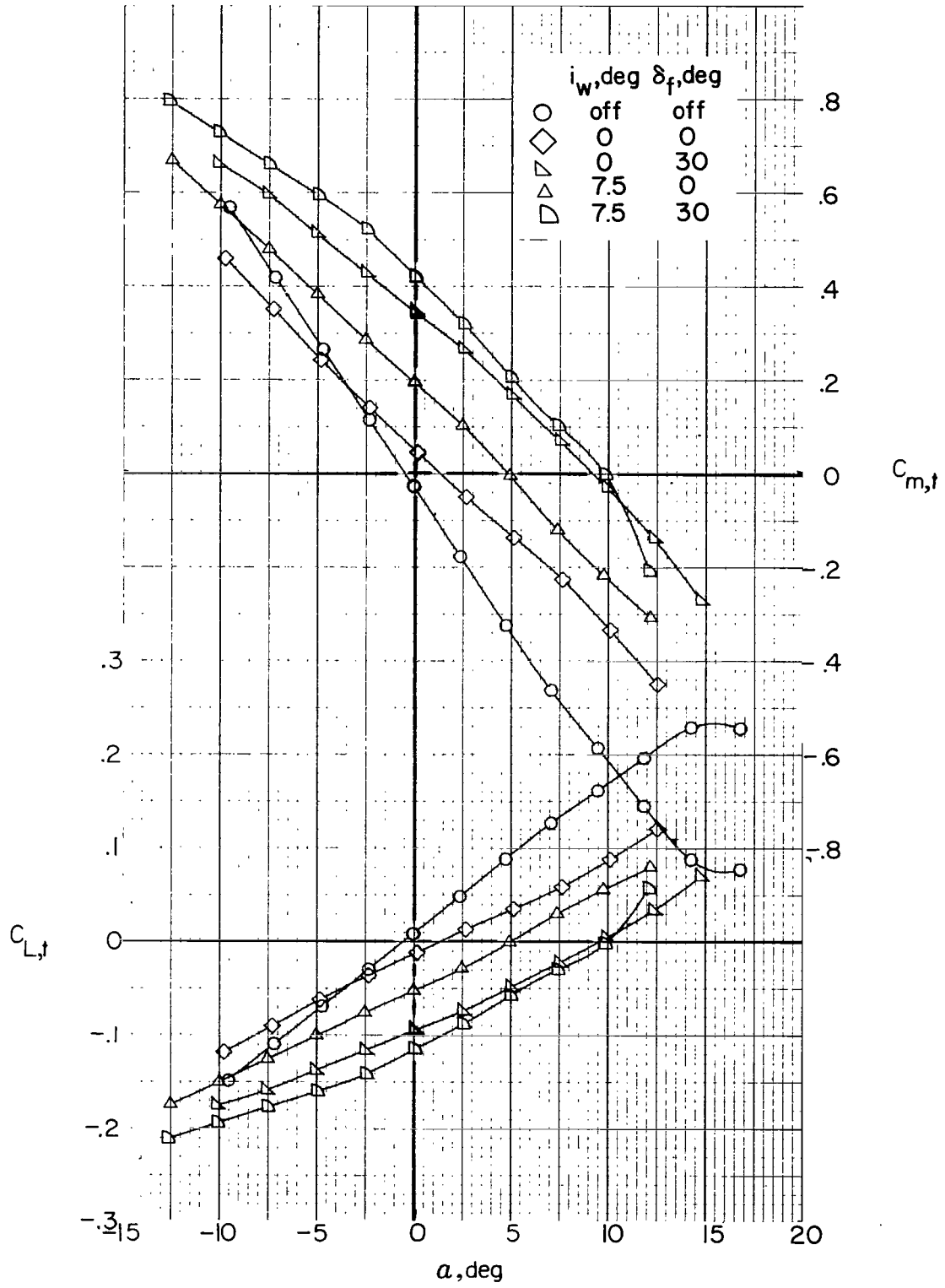

(a) Jets removed ($F_1W_xVH_C$).

Figure 21.- Effect of wing incidence and flap deflection on tail longitudinal aerodynamics. $i_t = 0^o$.

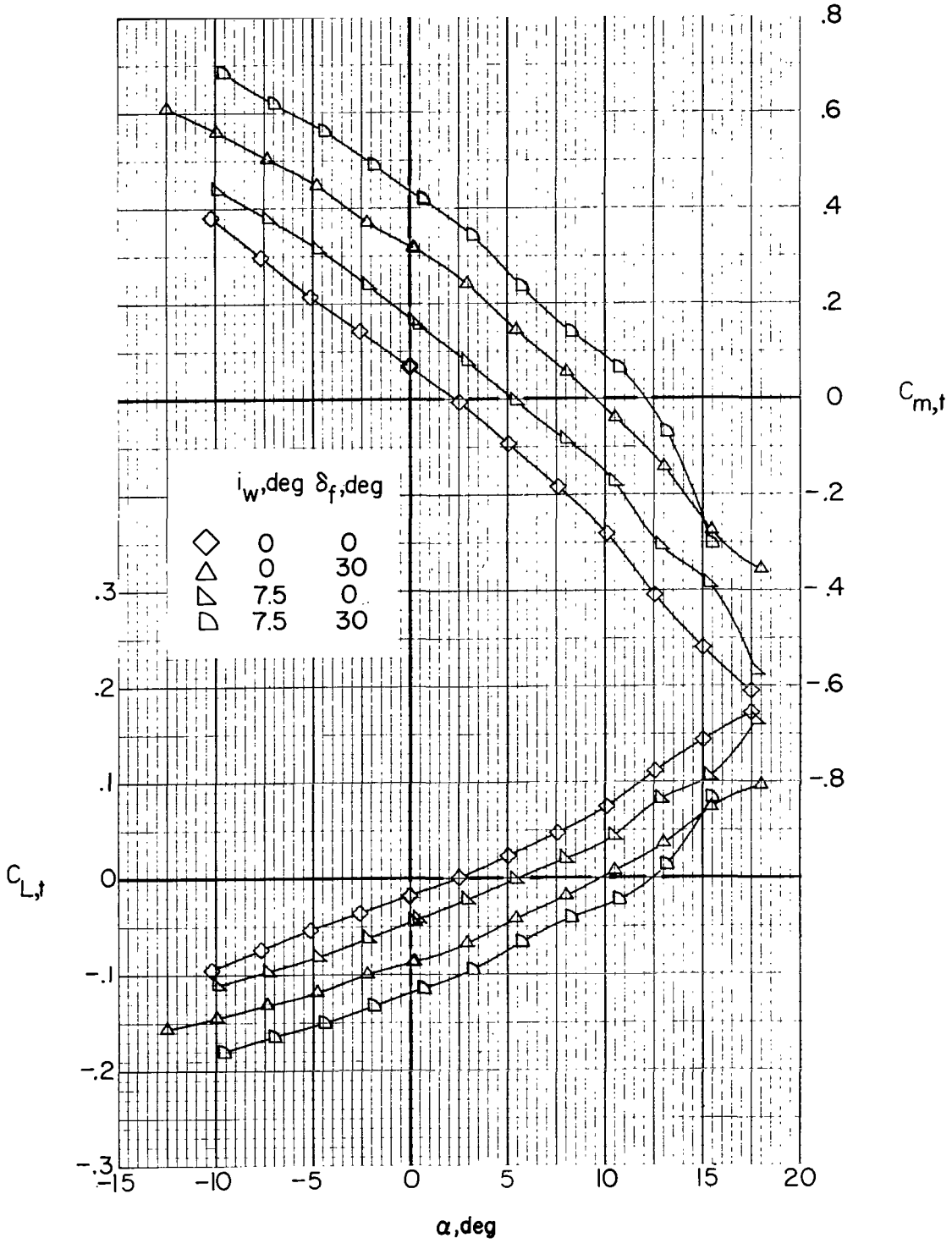

(b) Jets on ($F_1 W_X V H_C J_2$); $C_{T,J} = 0°$

Figure 21.- Continued.

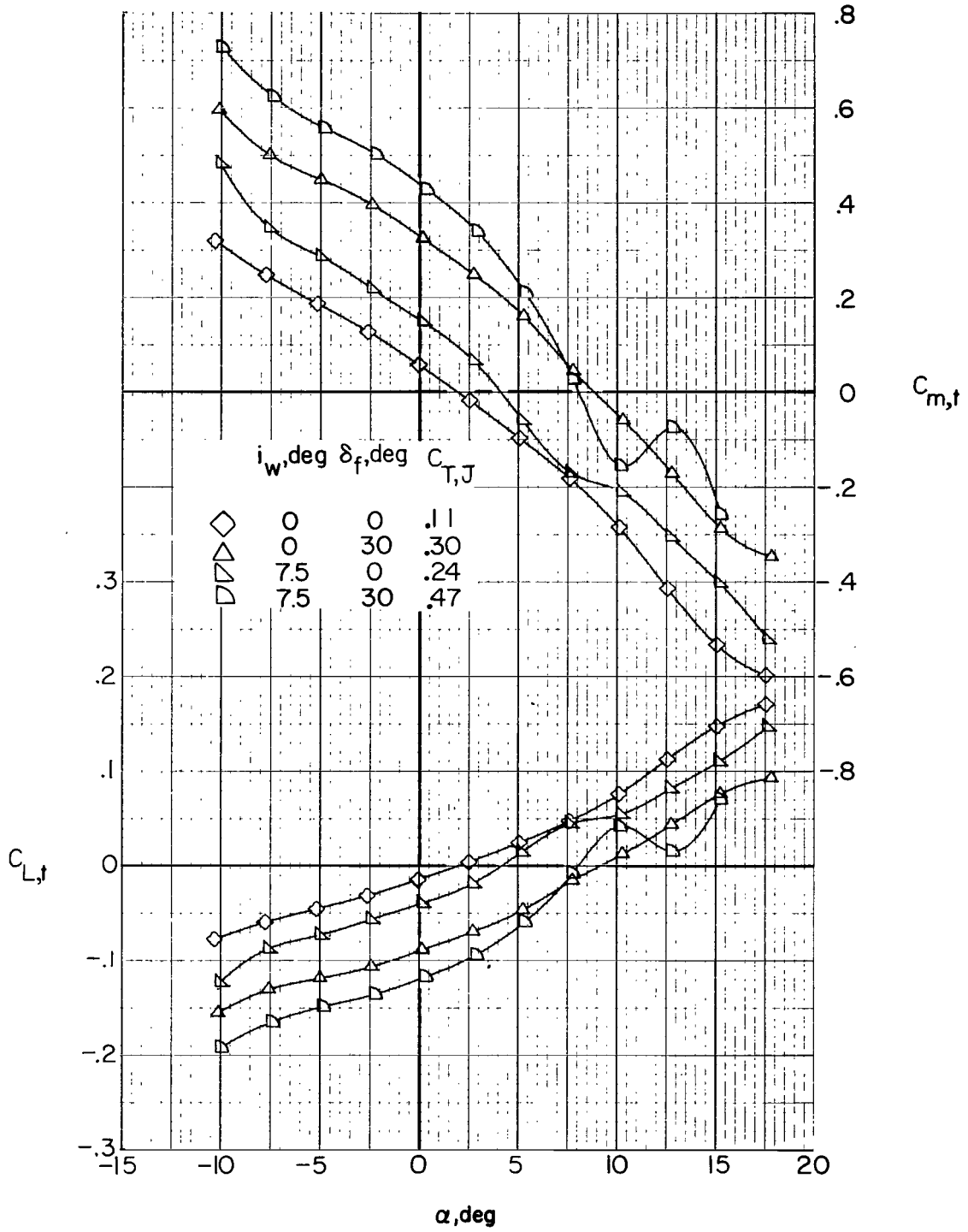

(c) Jets on ($F_1W_xVH_CJ_2$); trim thrust.

Figure 21.- Concluded.

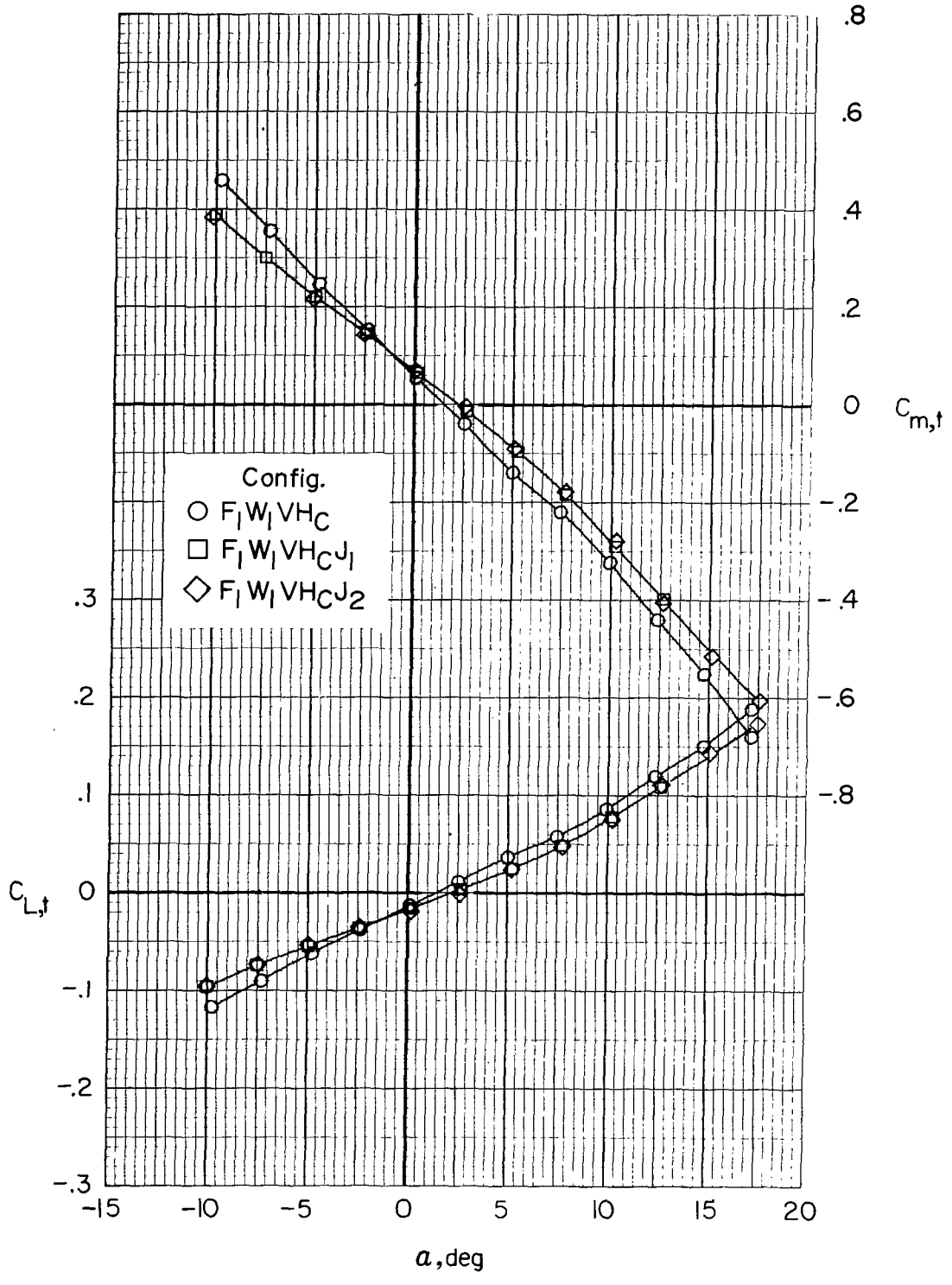

Figure 22.- Effect of auxiliary thrust engine nacelles on tail longitudinal aerodynamics. i_w = 0°; δ_f = 0°; i_t = 0°; $C_{T,J}$ = 0.

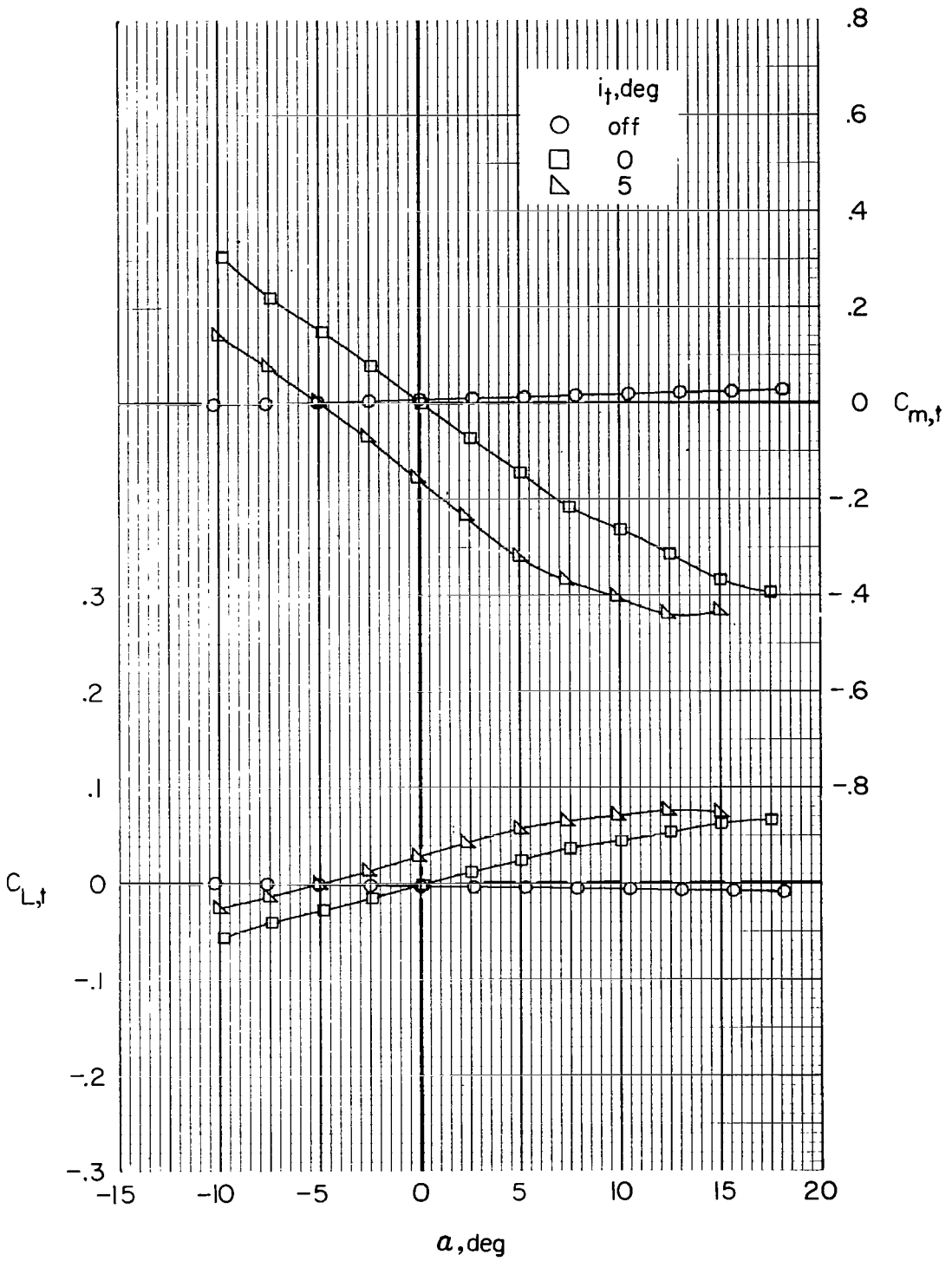

(a) Helicopter tail (F_1VH_H).

Figure 23.- Effect of horizontal-tail incidence on tail longitudinal aerodynamics.

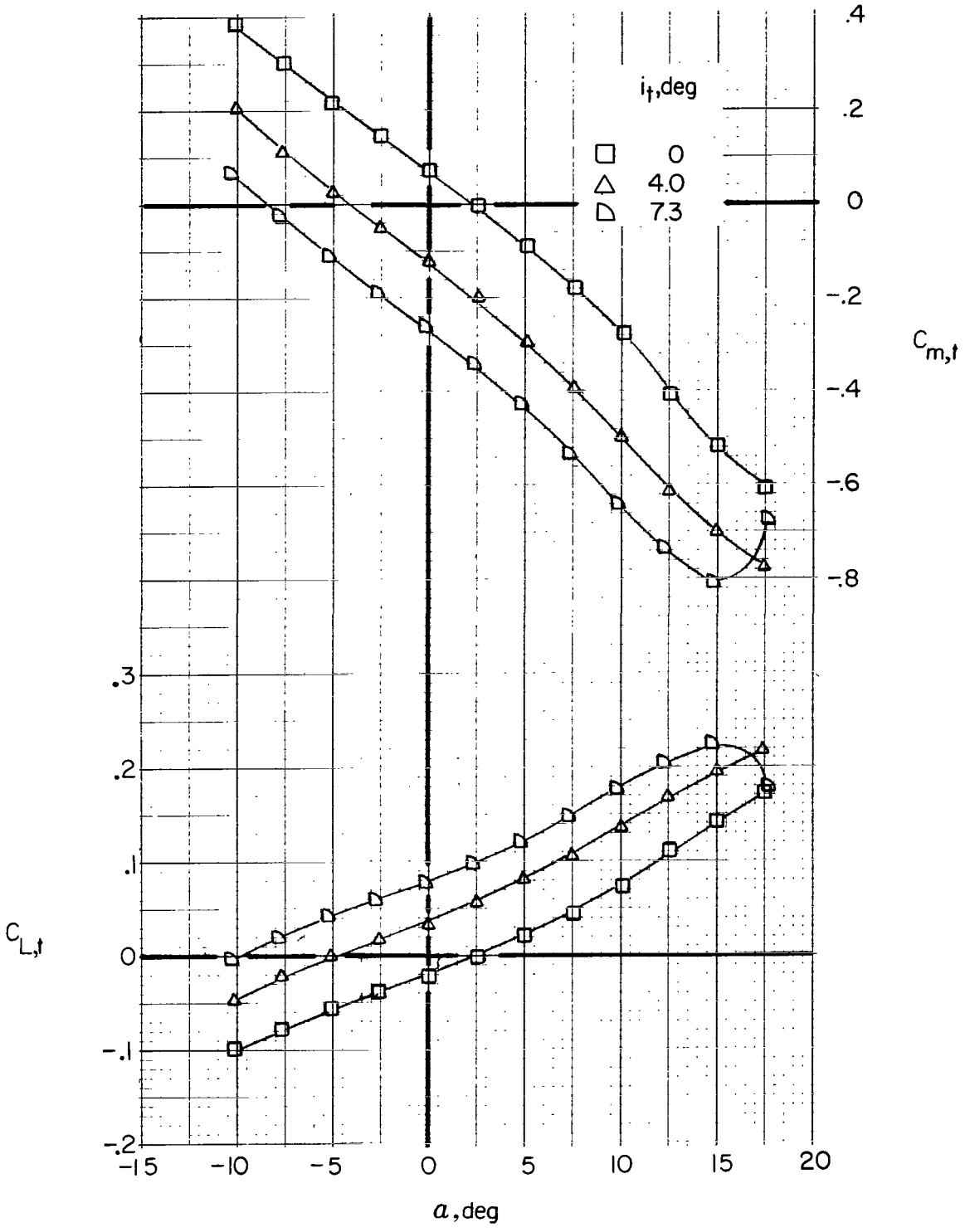

(b) Compound tail ($F_1W_1VH_CJ_2$). $C_{T,J} = 0$.

Figure 23.- Continued.

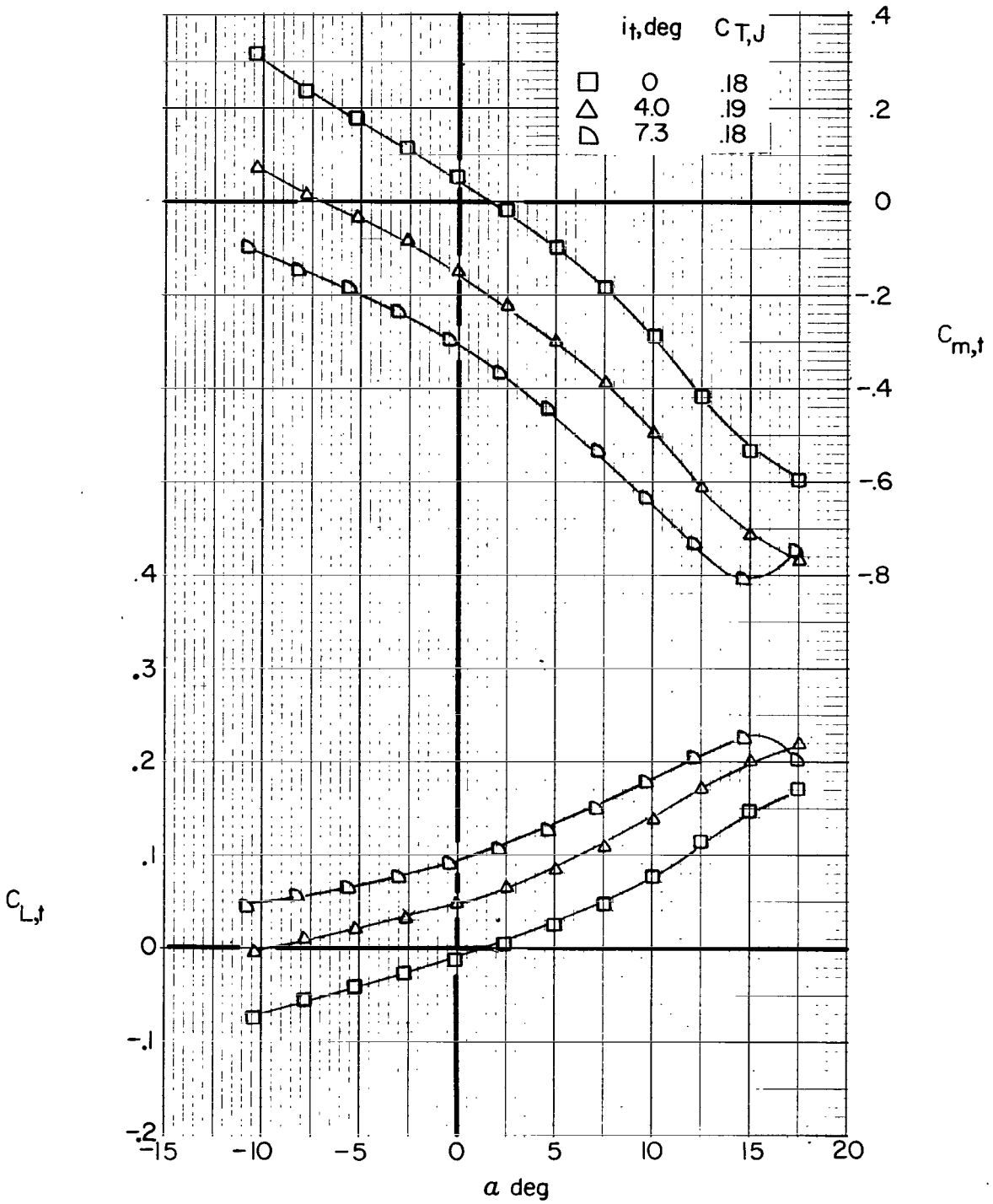

(c) Compound tail ($F_1W_1VH_CJ_2$). Trim thrust.

Figure 23.- Concluded.

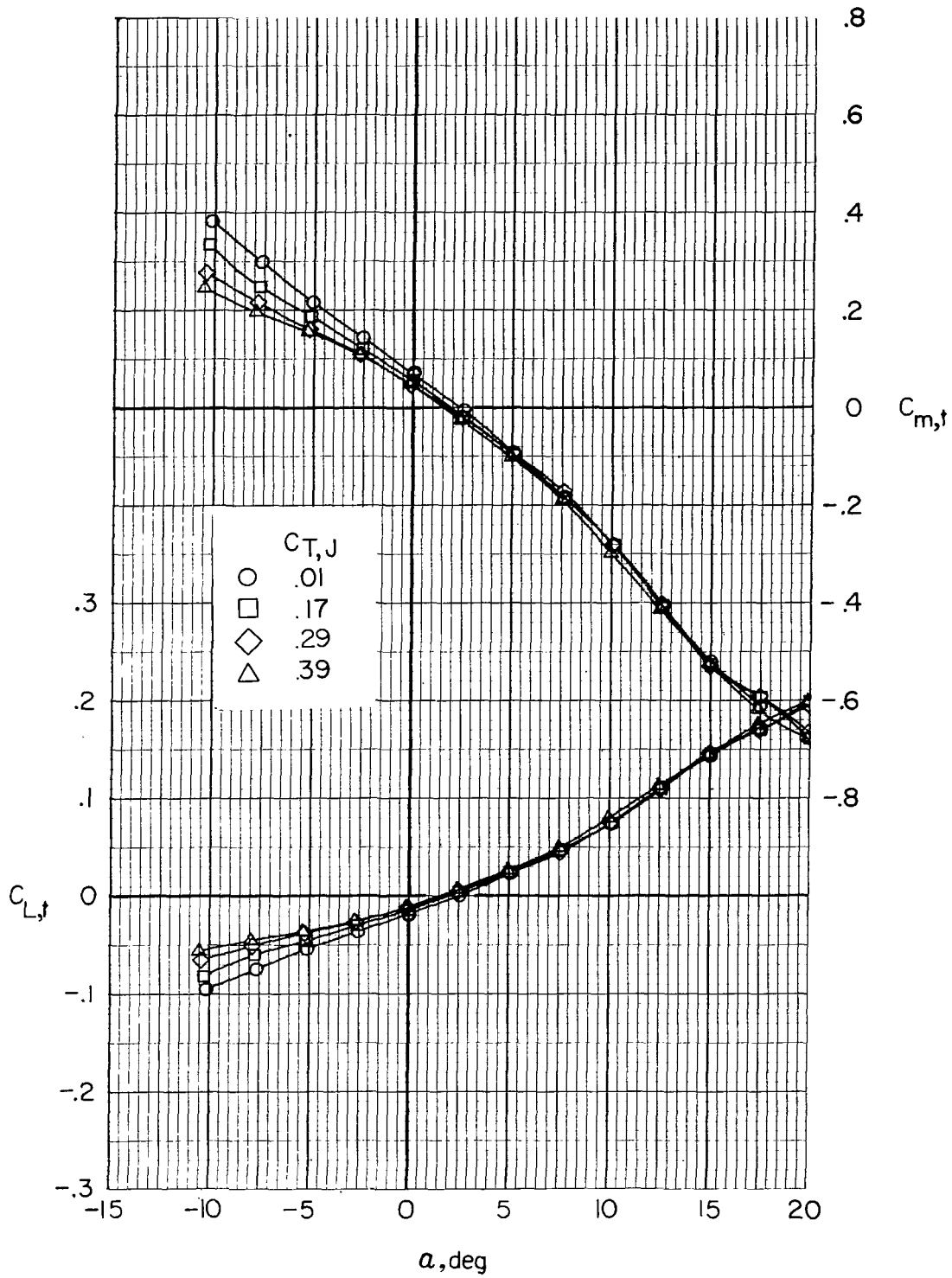

(a) $i_w = 0^o$; $\delta_f = 0^o$.

Figure 24.- Effect of auxiliary engine thrust level on tail longitudinal aerodynamics. $F_1W_xVH_CJ_2$; $i_t = 0^o$.

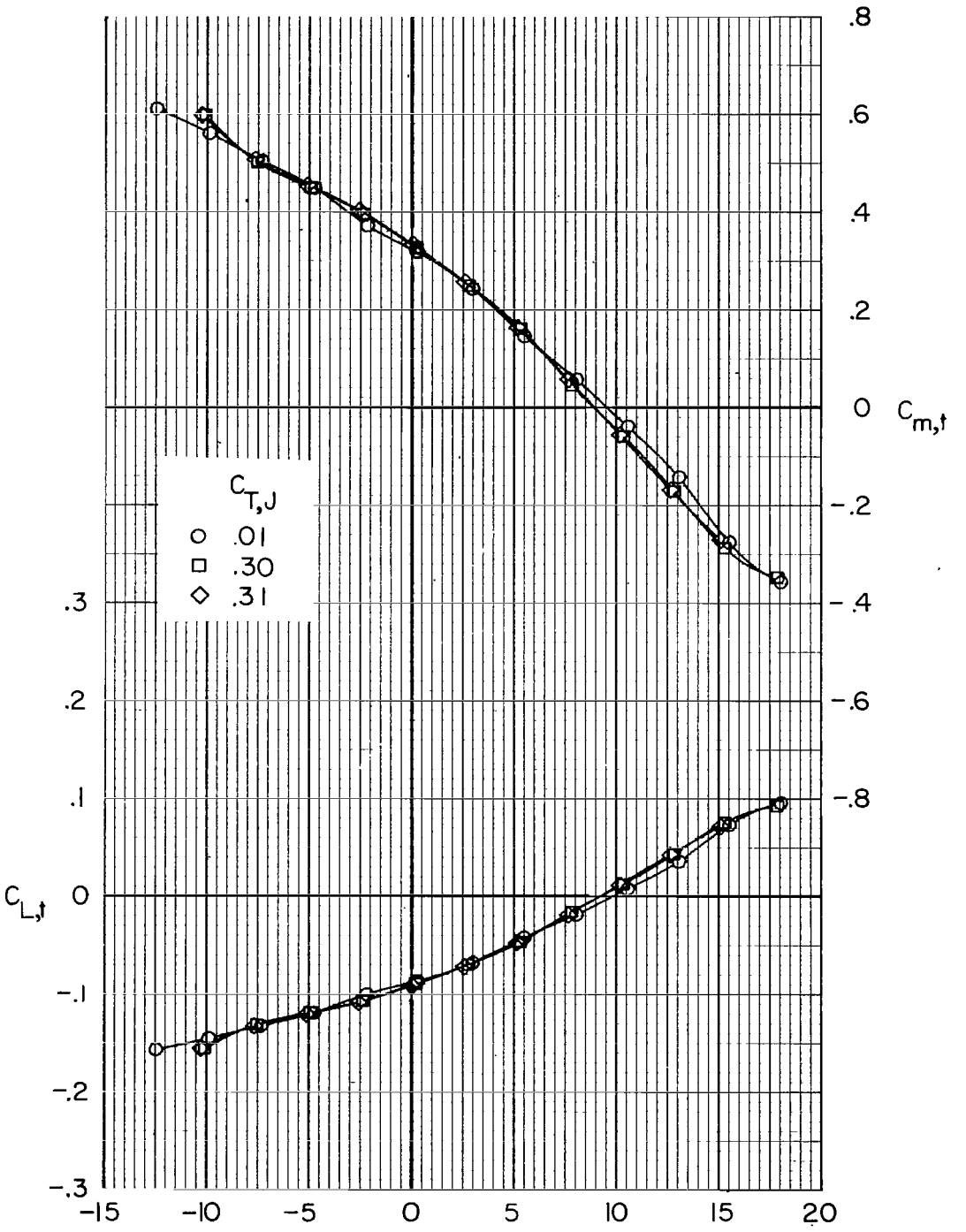

(b) $i_w = 0^\circ$; $\delta_f = 30^\circ$.

Figure 24.- Continued.

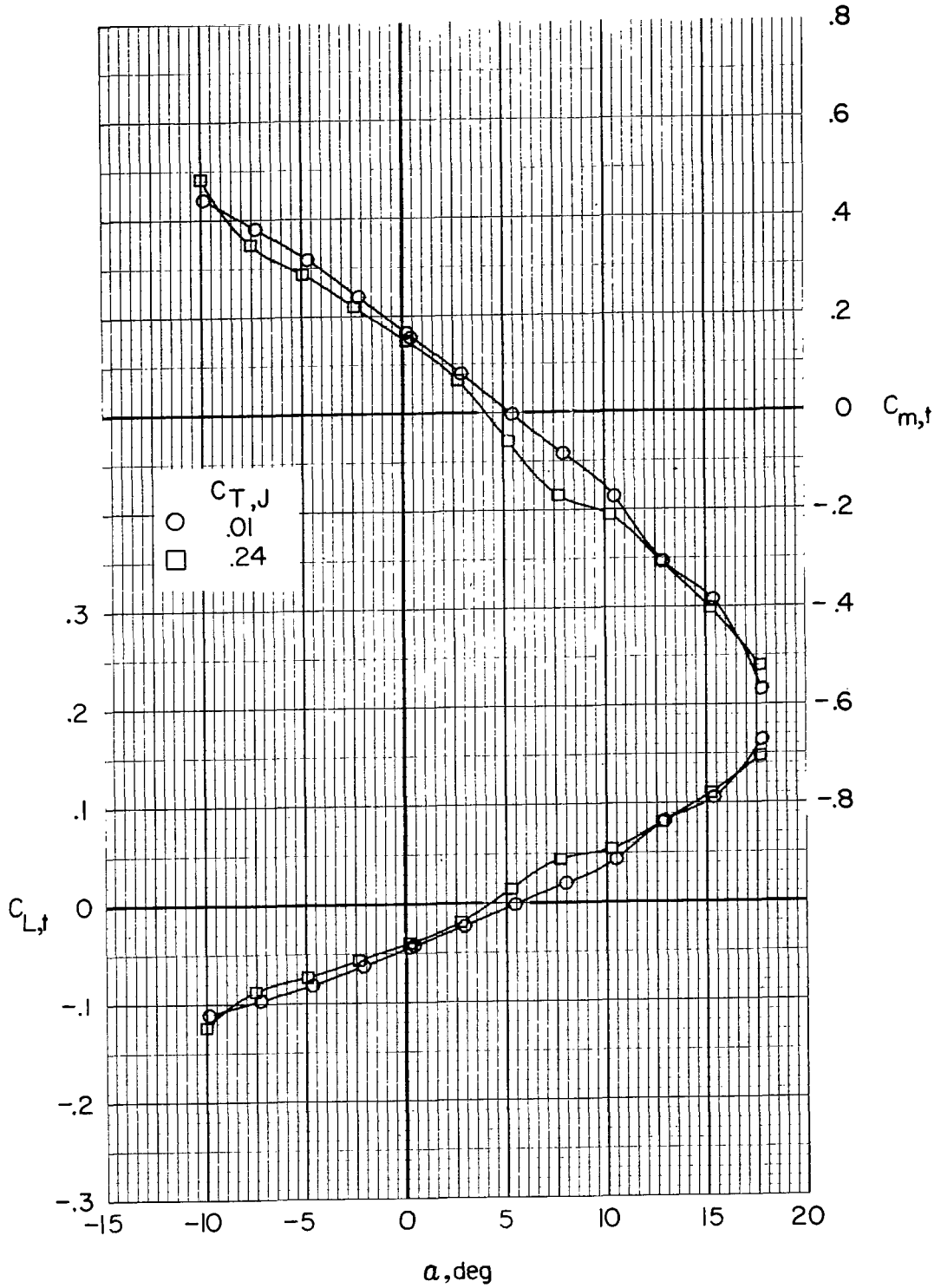

(c) $i_w = 7.5^\circ$; $\delta_f = 0^\circ$.

Figure 24.- Continued.

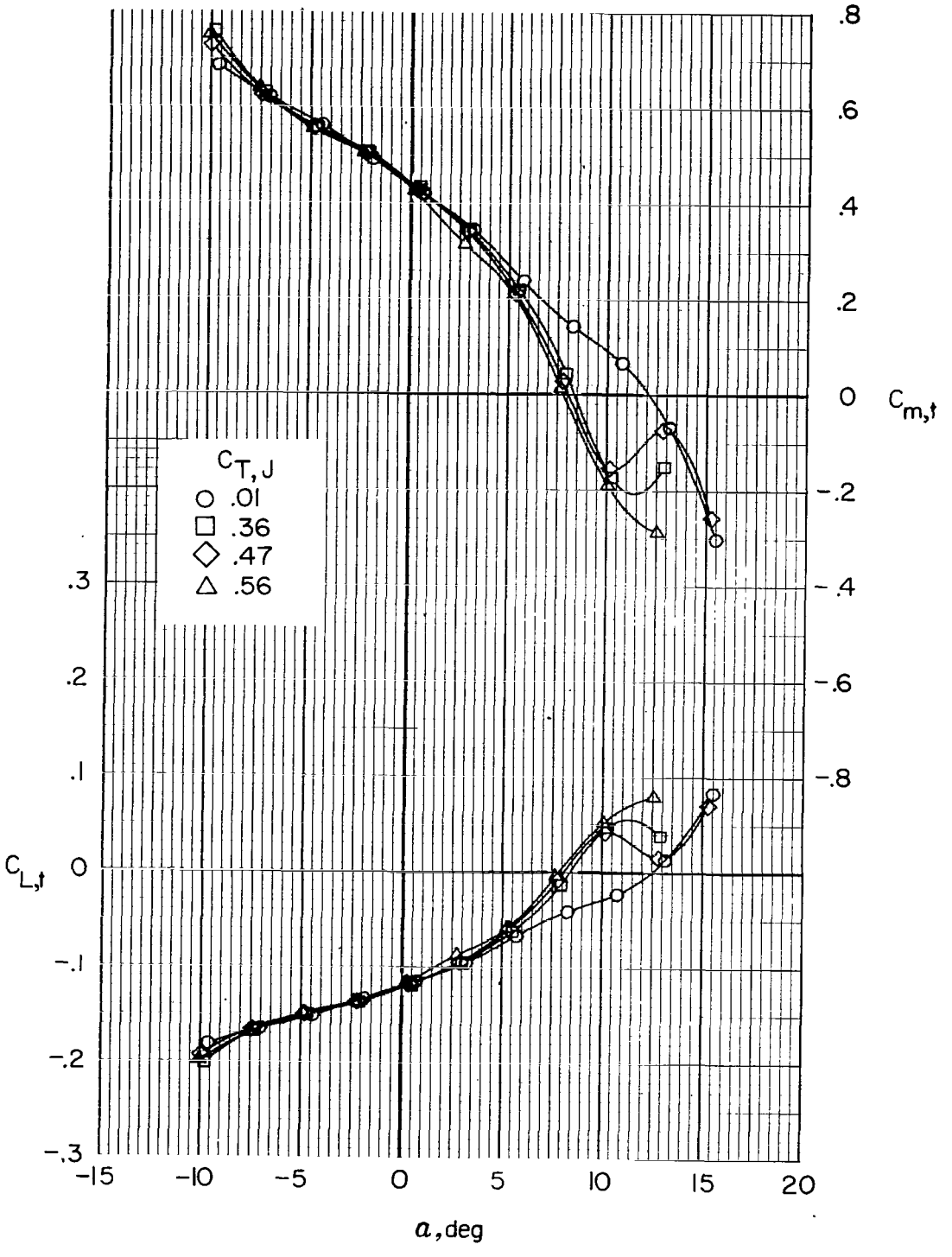

(d) i_w = 7.5°; δ_f = 30°.

Figure 24.- Concluded.

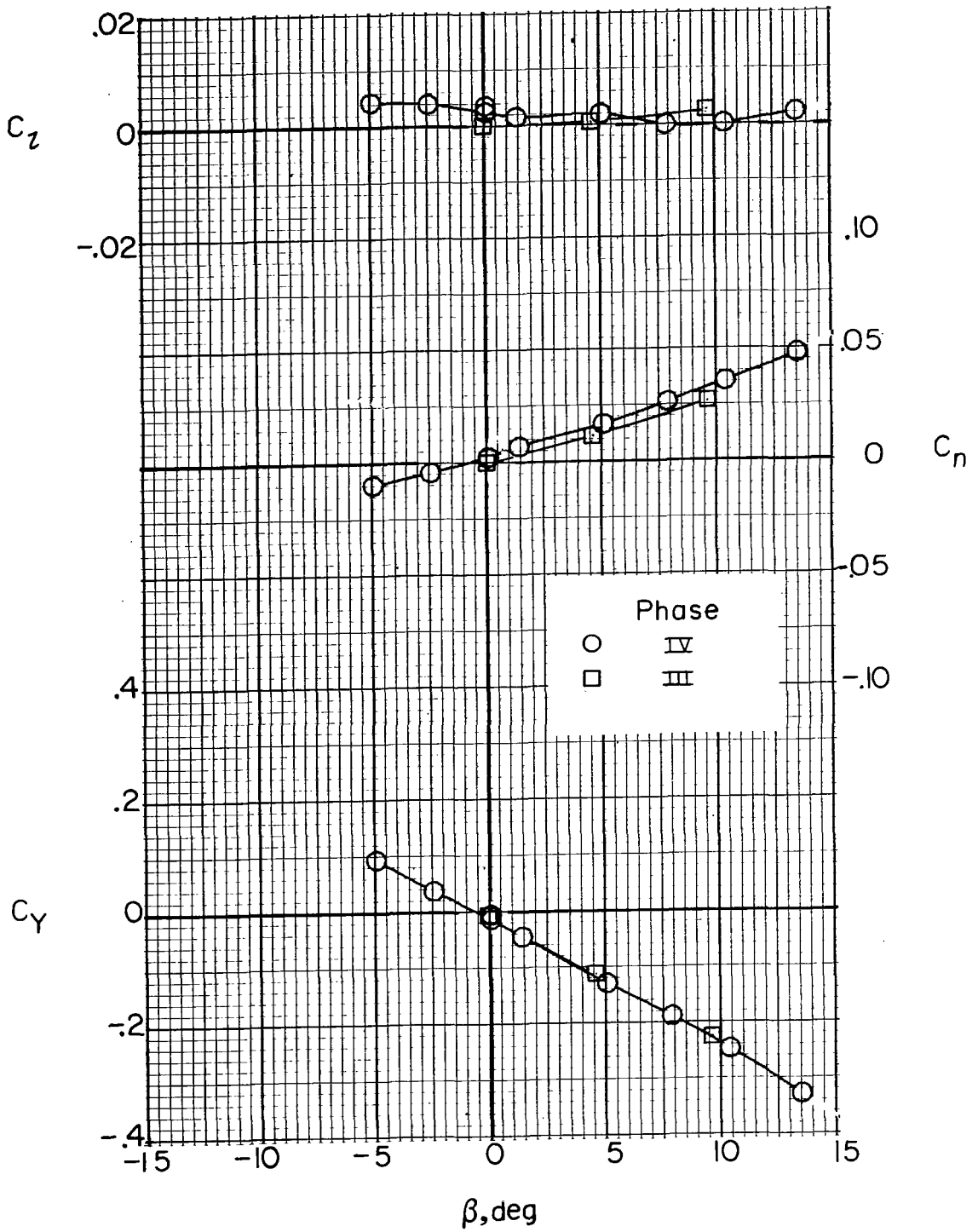

(a) $i_w = 0^o$; $\delta_f = 0^o$; $C_{T,J} = 0$; $\alpha = 0^o$.

Figure 25.- Comparison of lateral aerodynamics from Phase IV and Phase III for compound helicopter ($F_1W_xVH_CJ_2$). $i_t = 0^o$.

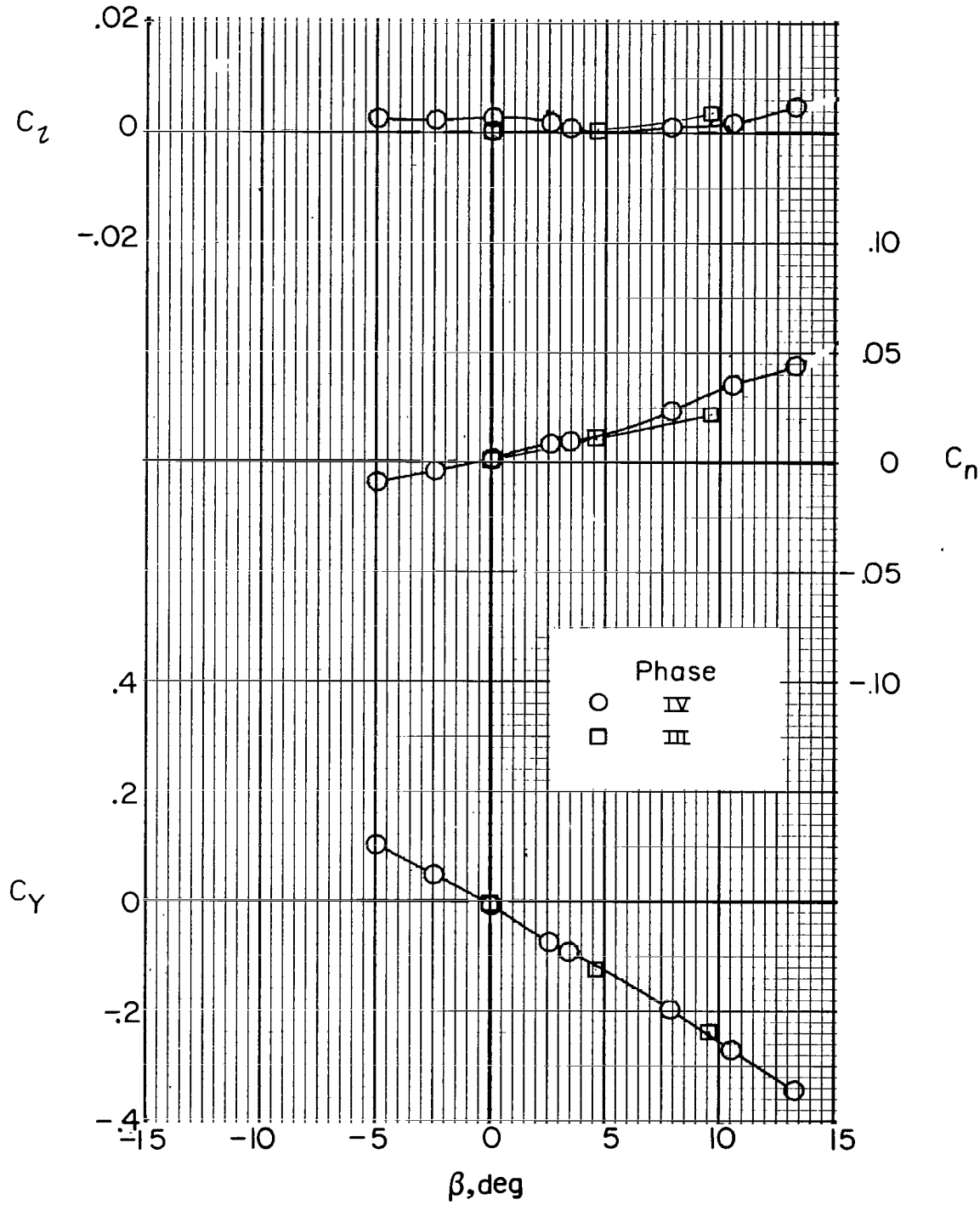

(b) $i_w = 0^o$; $\delta_f = 0^o$; $C_{T,J} = 0.11$; $\alpha = 0^o$.

Figure 25.- Continued.

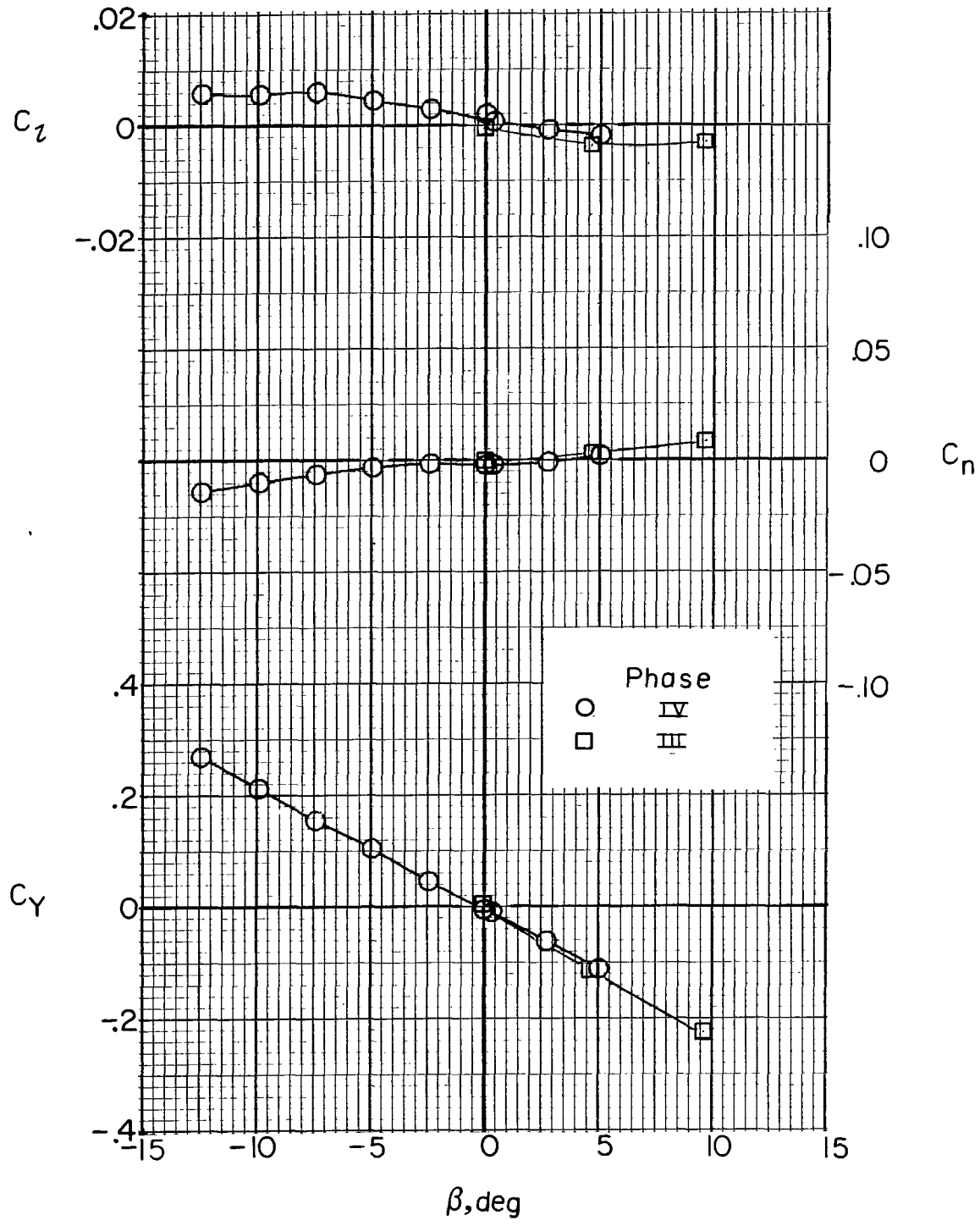

(c) $i_w = 0^\circ$; $\delta_f = 0^\circ$; $C_{T,J} = 0$; $\alpha = 10^\circ$.

Figure 25.- Continued.

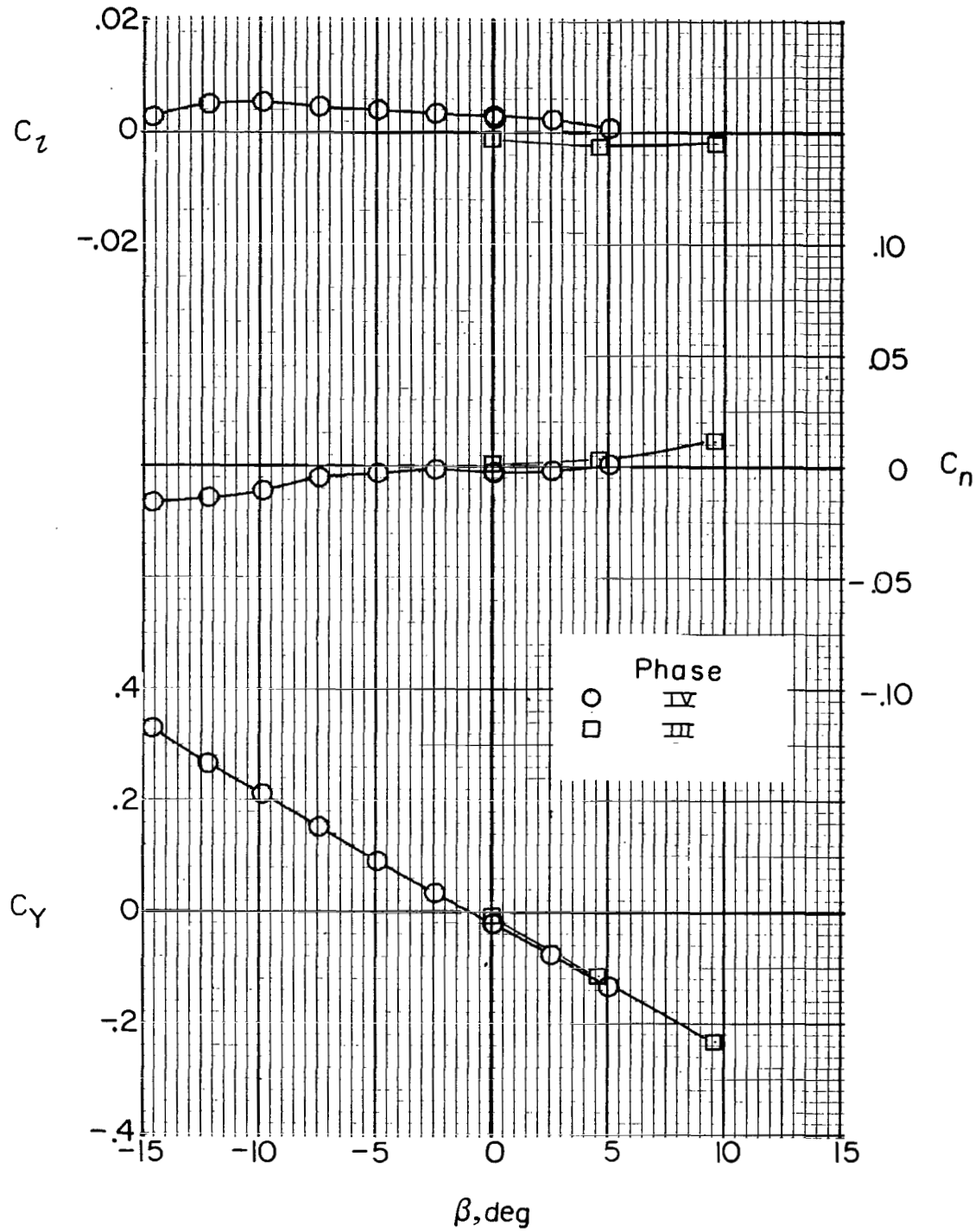

(d) $i_w = 0^o$; $\delta_f = 0^o$; $C_{T,J} = 0.30$; $\alpha = 10^o$.

Figure 25.- Continued.

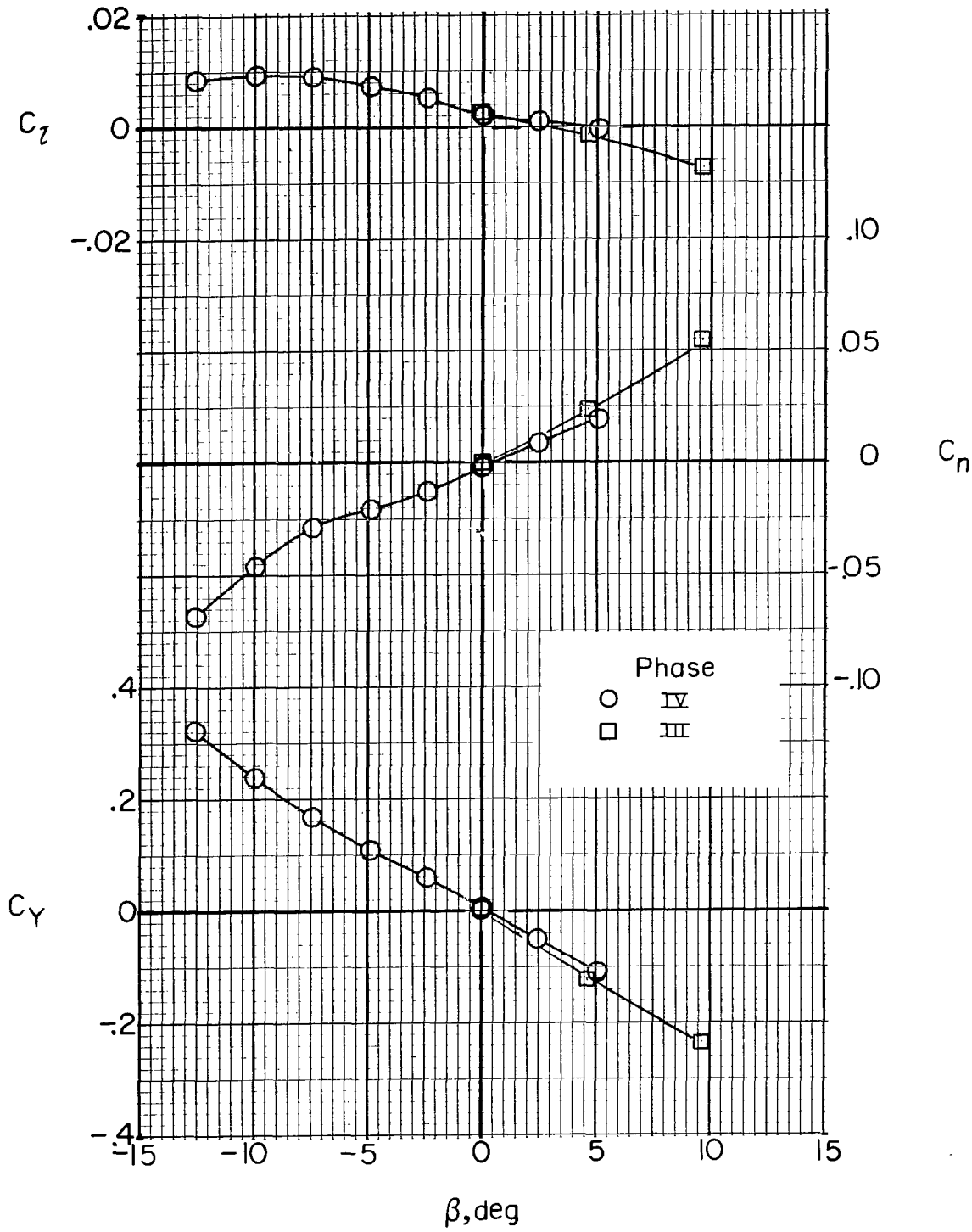

(e) $i_w = 0^o$; $\delta_f = 30^o$; $C_{T,J} = 0$; $\alpha = 0^o$.

Figure 25.- Continued.

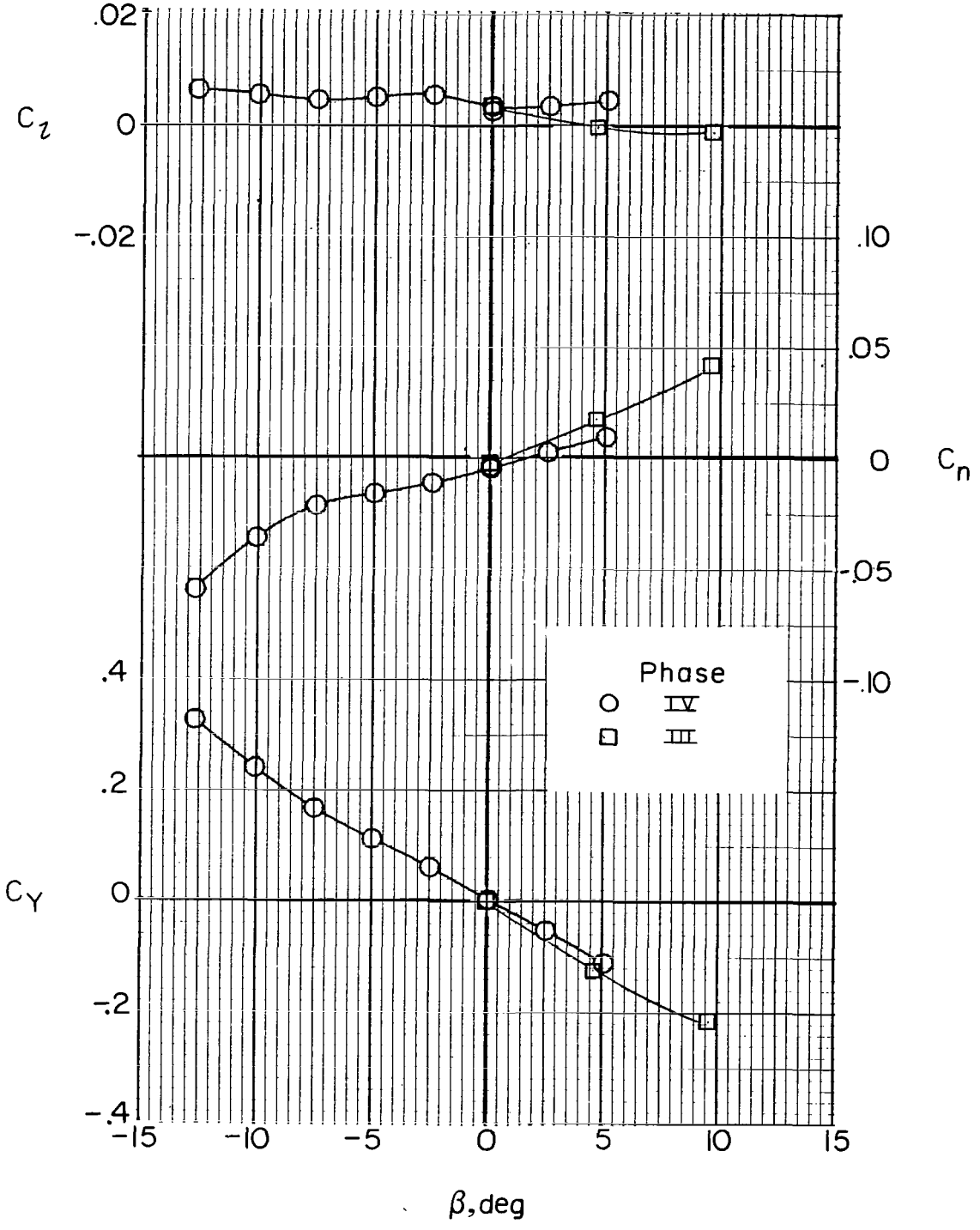

(f) $i_w = 0°$; $\delta_f = 30°$; $C_{T,J} = 0.29$; $\alpha = 0°$.

Figure 25.- Continued.

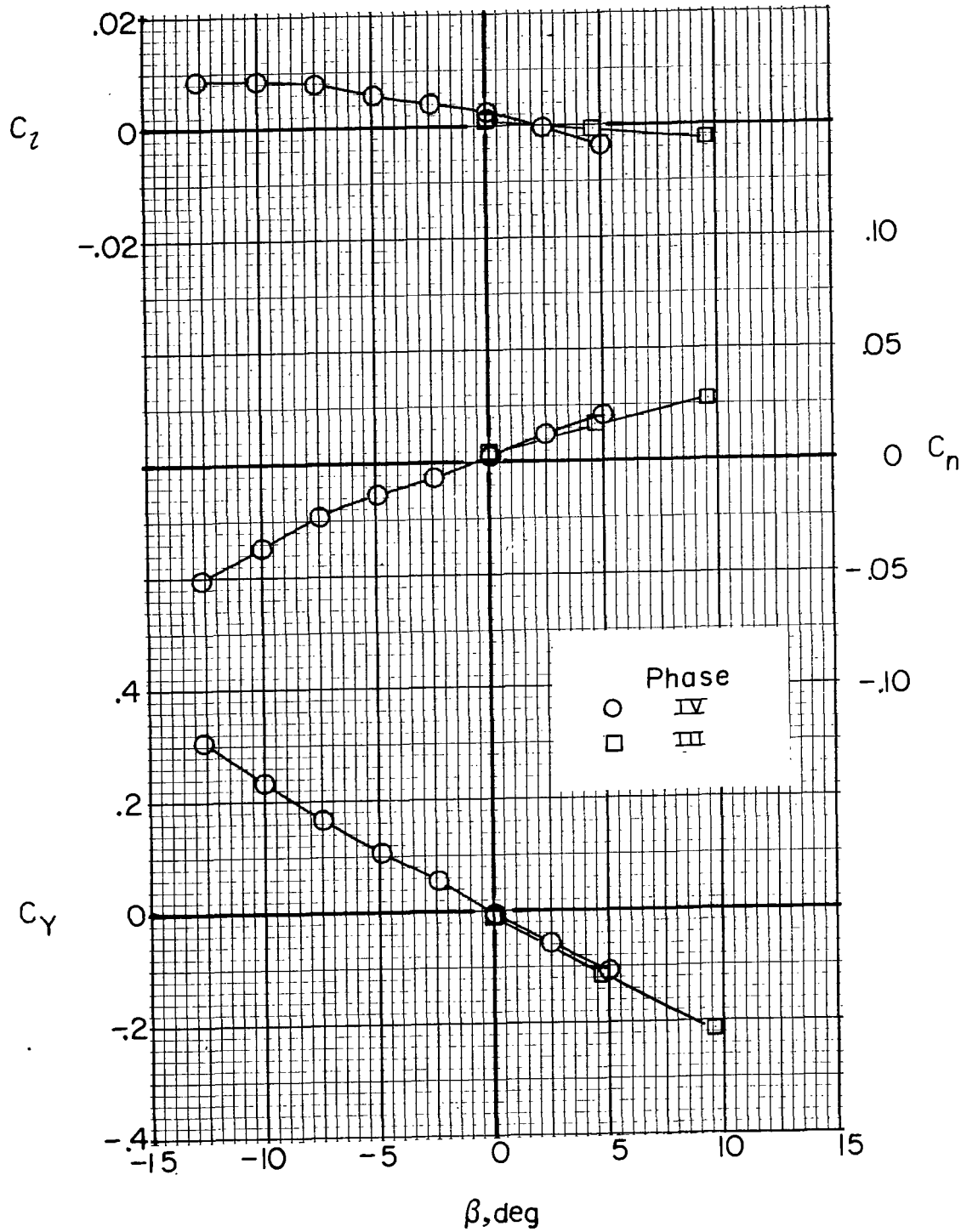

(g) $i_w = 7.5^o$; $\delta_f = 0^o$; $C_{T,J} = 0$; $\alpha = 0^o$.

Figure 25.- Continued.

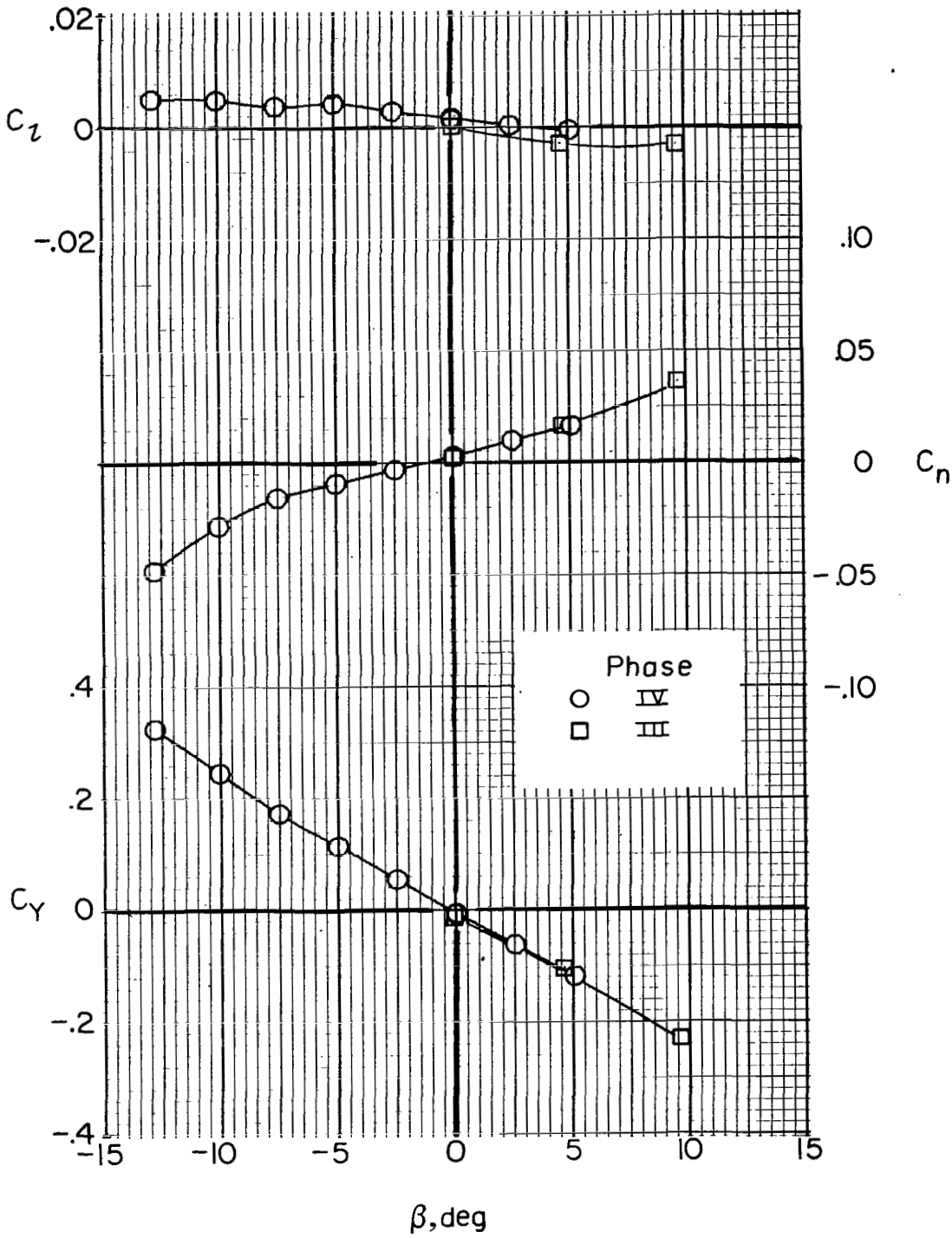

(h) $i_w = 7.5^o$; $\delta_f = 0^o$; $C_{T,J} = 0.23$; $\alpha = 0^o$.

Figure 25.- Continued.

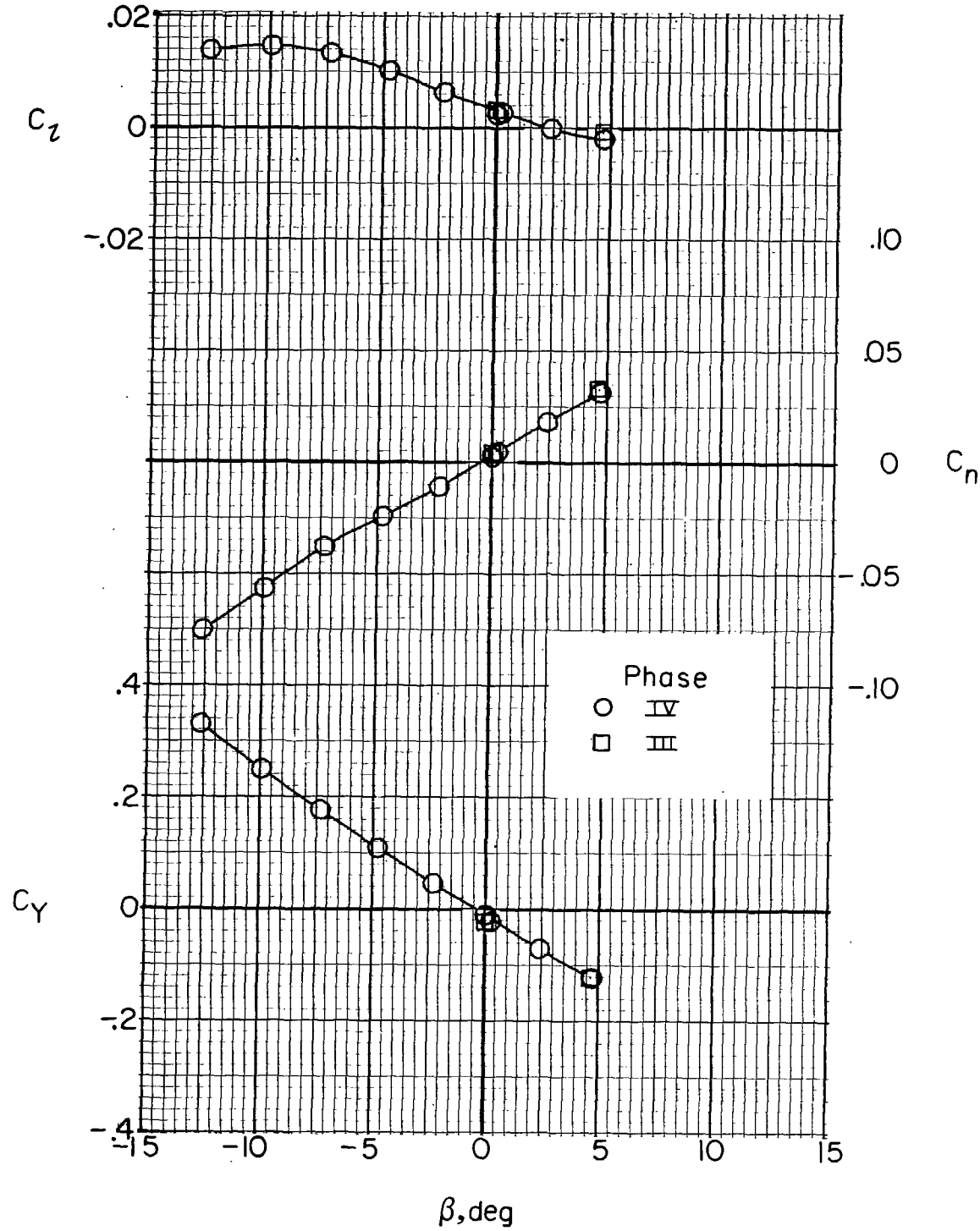

(i) $i_w = 7.5^o$; $\delta_f = 30^o$; $C_{T,J} = 0$; $\alpha = 0^o$.

Figure 25.- Continued.

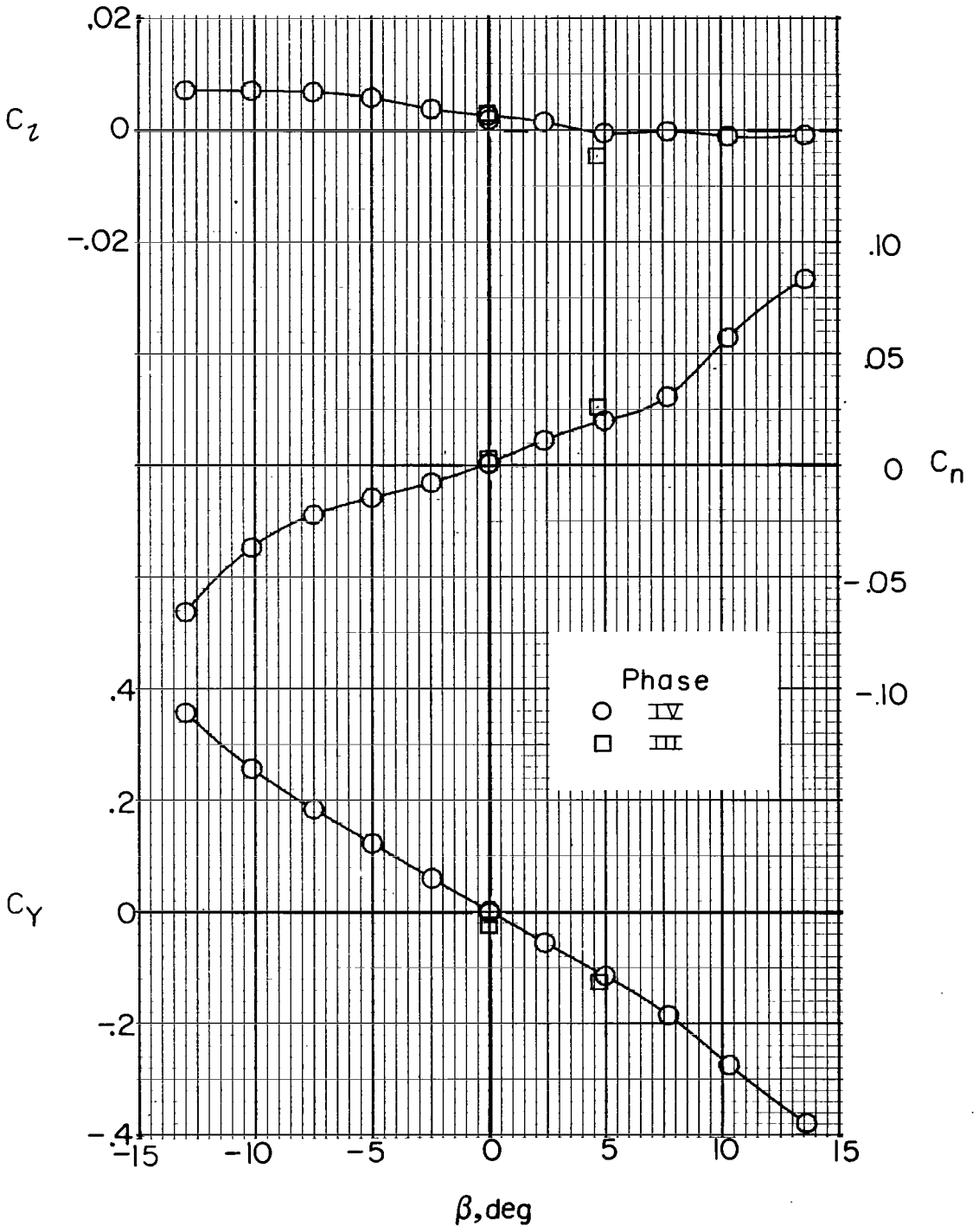

(j) $i_w = 7.5°$; $\delta_f = 30°$; $C_{T,J} = 0.43$; $\alpha = 0°$.

Figure 25.- Concluded.

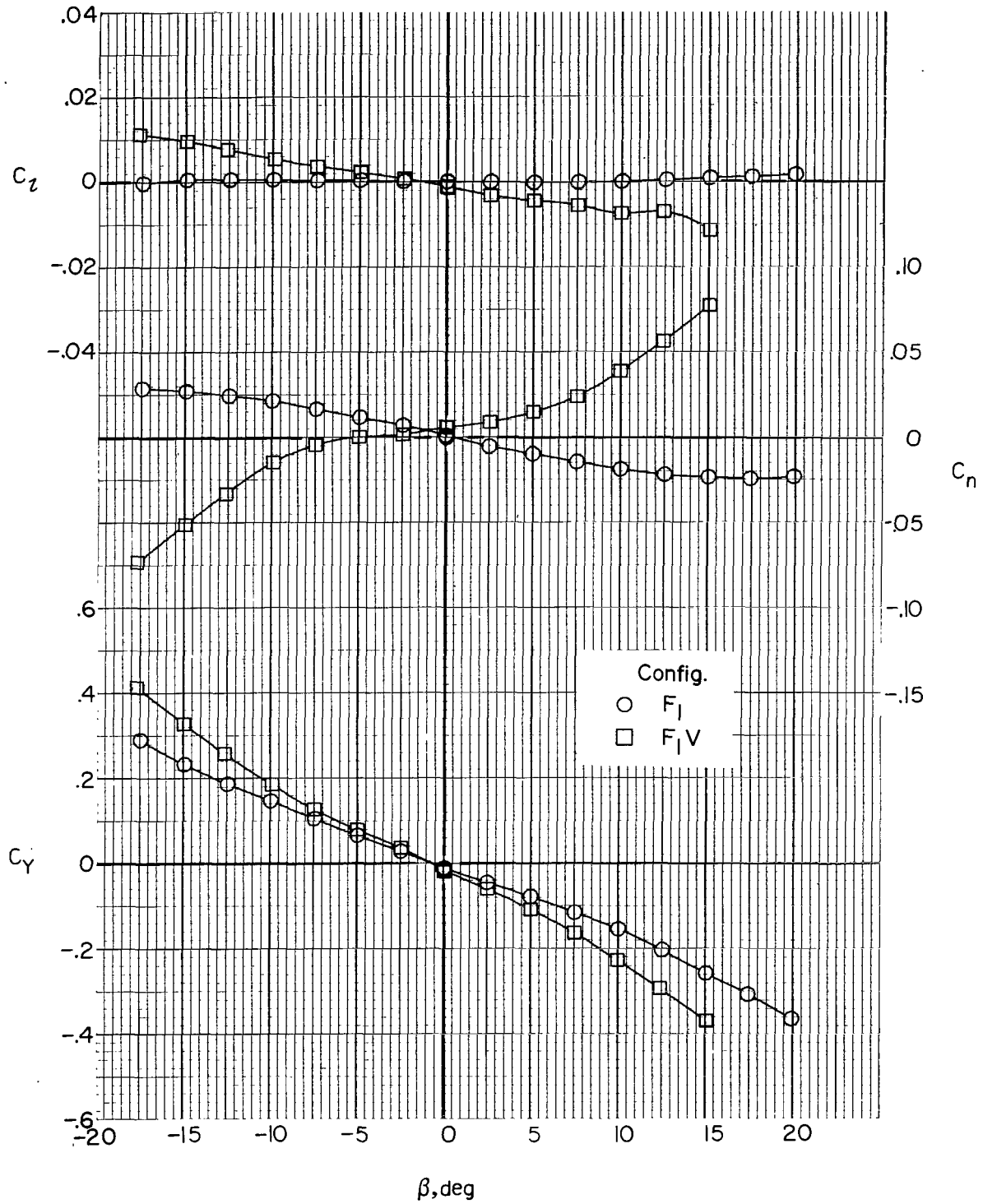

Figure 26.- Effect of vertical tail on airframe lateral aerodynamics. $\alpha = 0^{o}$.

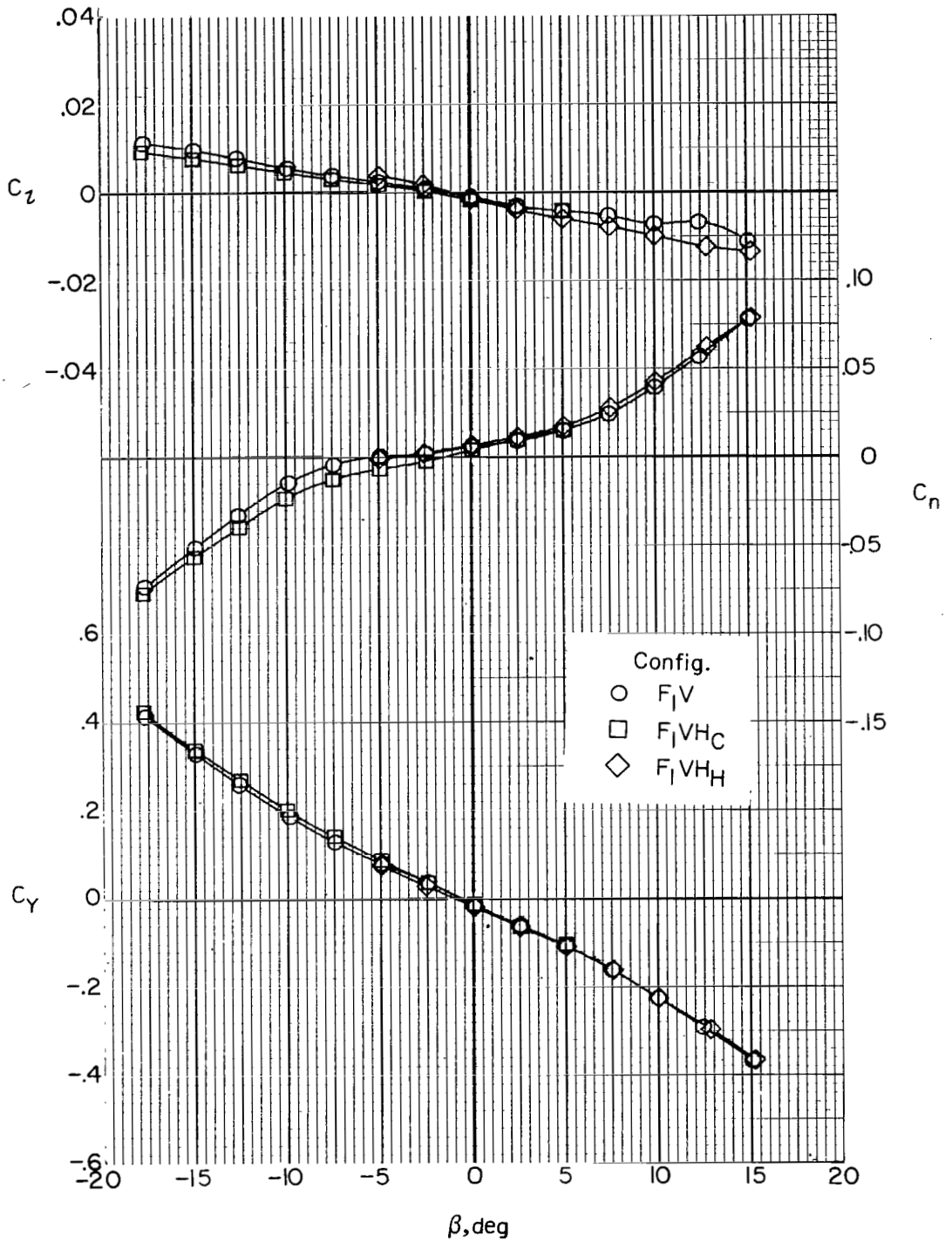

Figure 27.- Effect of horizontal tail on airframe lateral aerodynamics. $\alpha = 0^o$; $i_t = 0^o$.

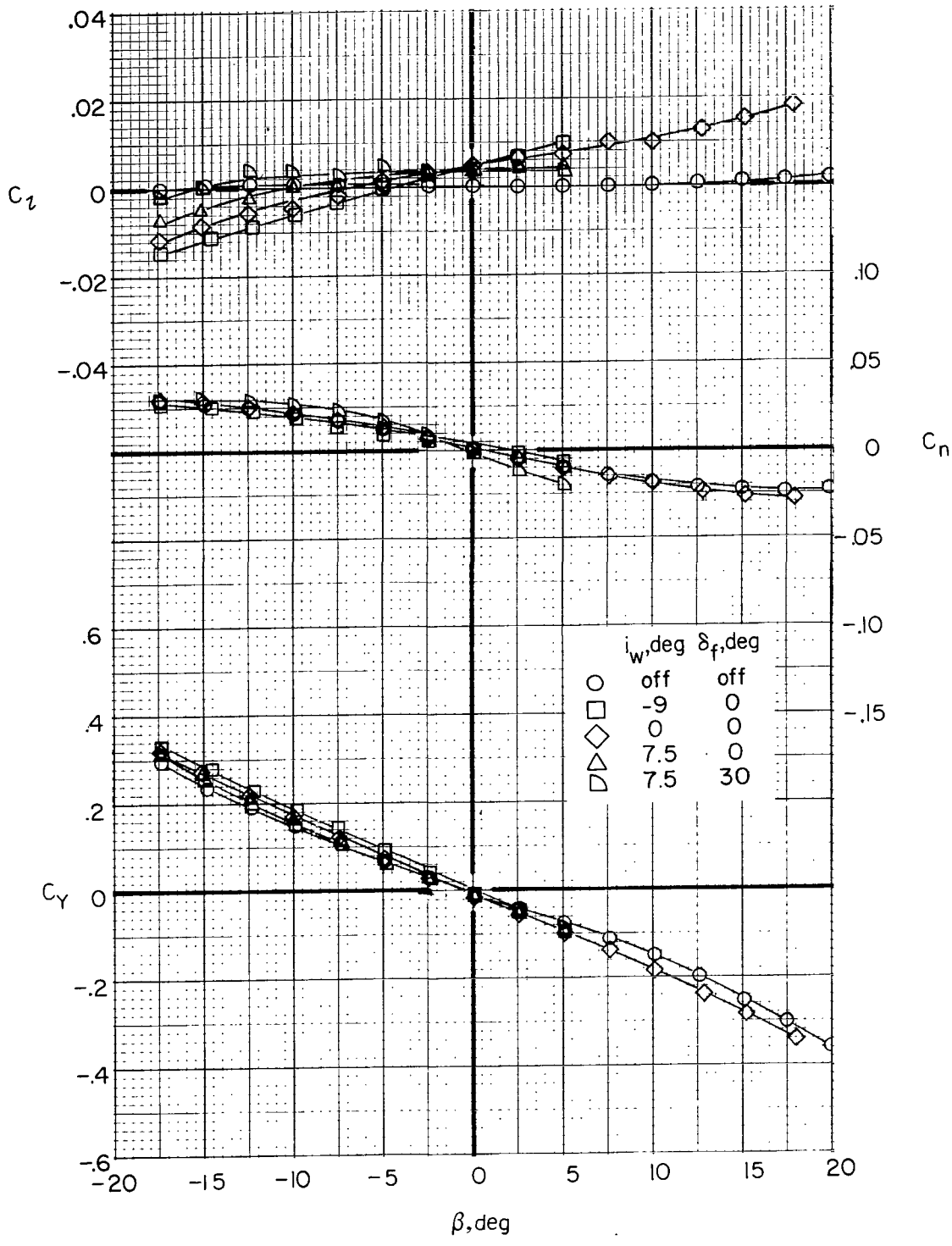

Figure 28.- Effect of wing incidence and flap deflection on airframe lateral aerodynamics with the tail off (F_1W_X). $\alpha = 0^\circ$.

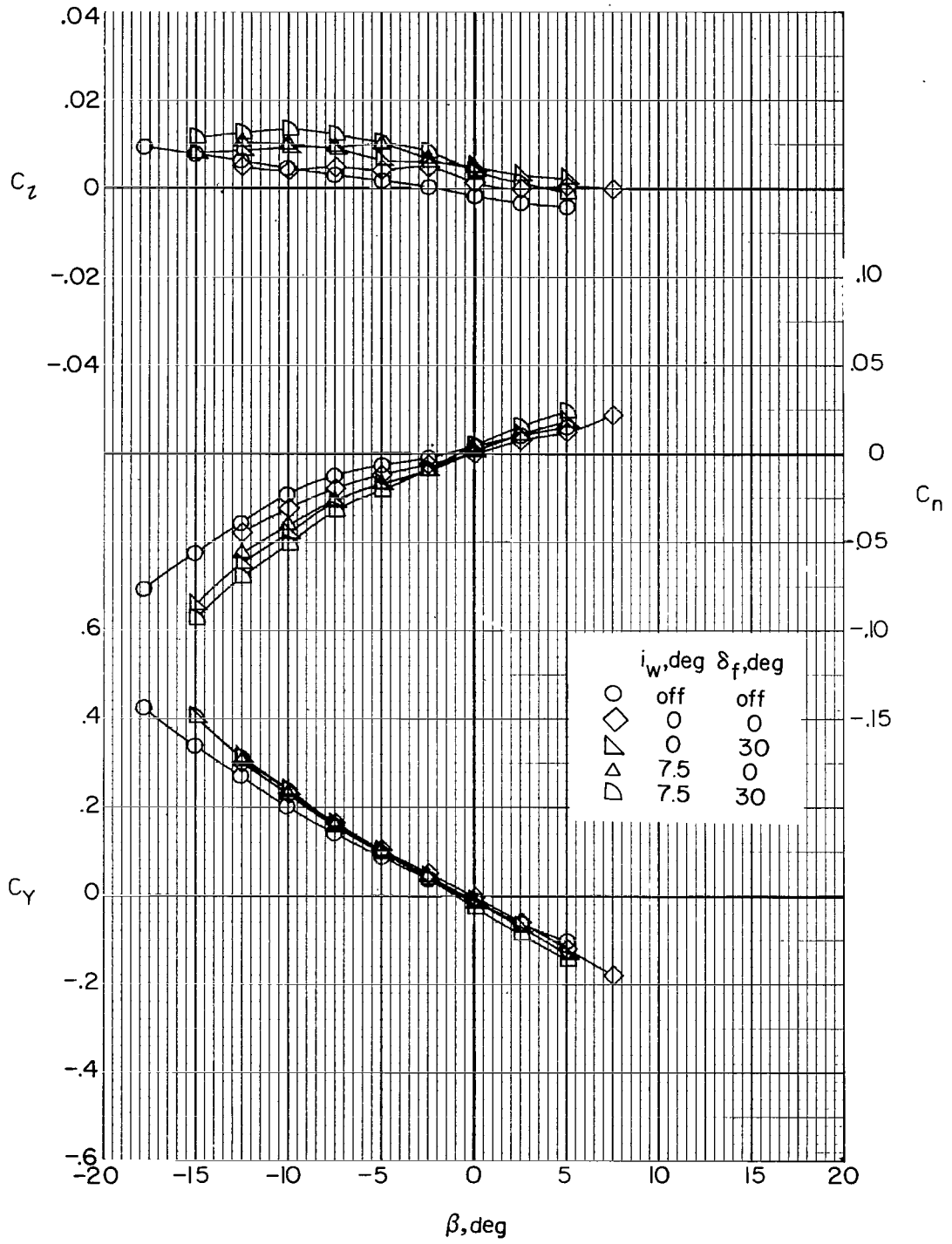

Figure 29.- Effect of wing incidence and flap deflection on airframe lateral aerodynamics with the tail on. $F_1W_xVH_C$; $\alpha = 0^o$; $i_t = 0^o$.

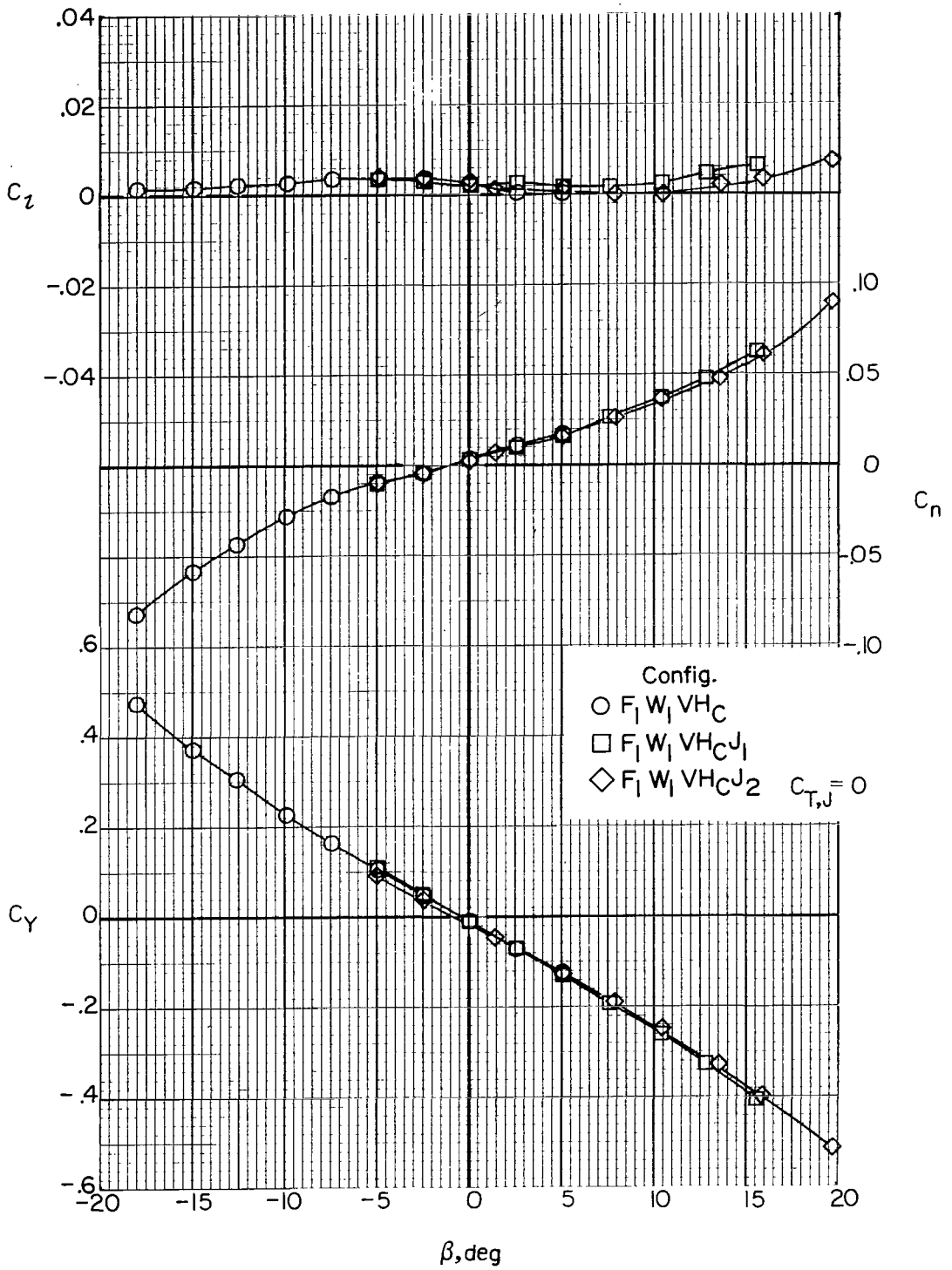

Figure 30.- Effect of auxiliary thrust engine nacelles on airframe lateral aerodynamics. $i_t = 0^o$; $\alpha = 0^o$.

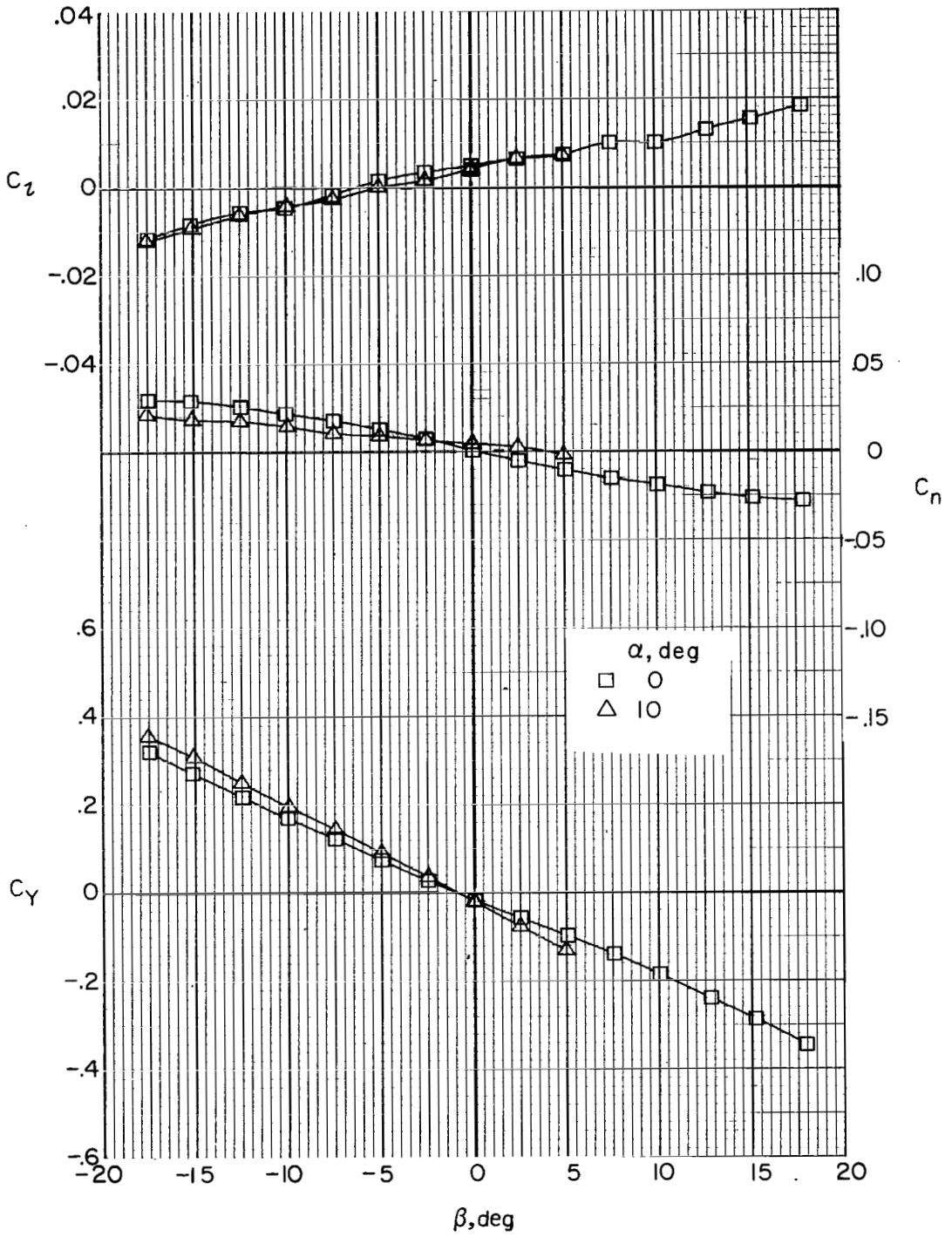

(a) Jets off; tail off (F_1W_1); $i_w = 0^o$; $\delta_f = 0^o$.

Figure 31.- Effect of angle of attack on airframe lateral aerodynamics.

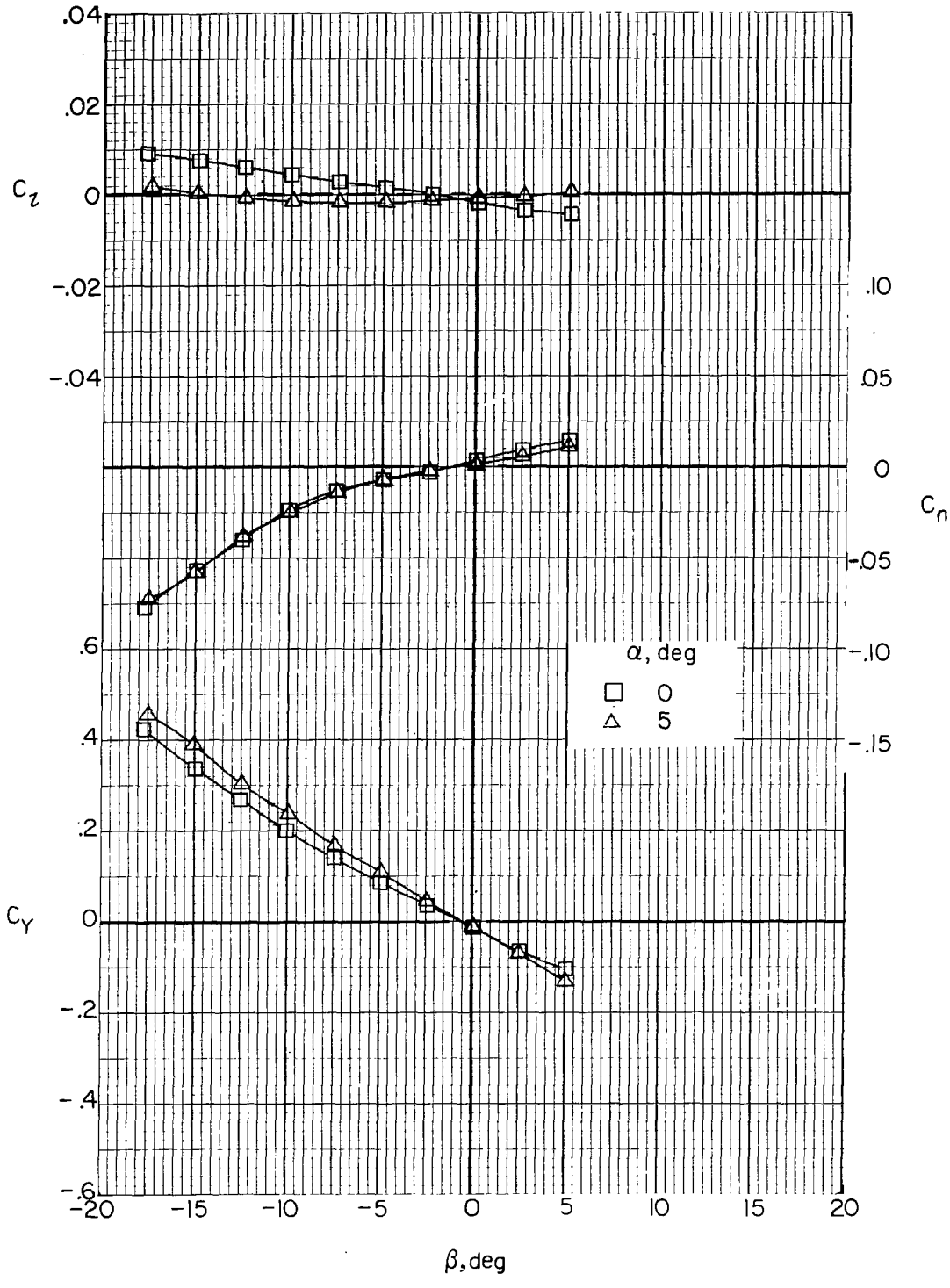

(b) Wing off; jets off; helicopter tail (F_1VH_H).

Figure 31.- Continued.

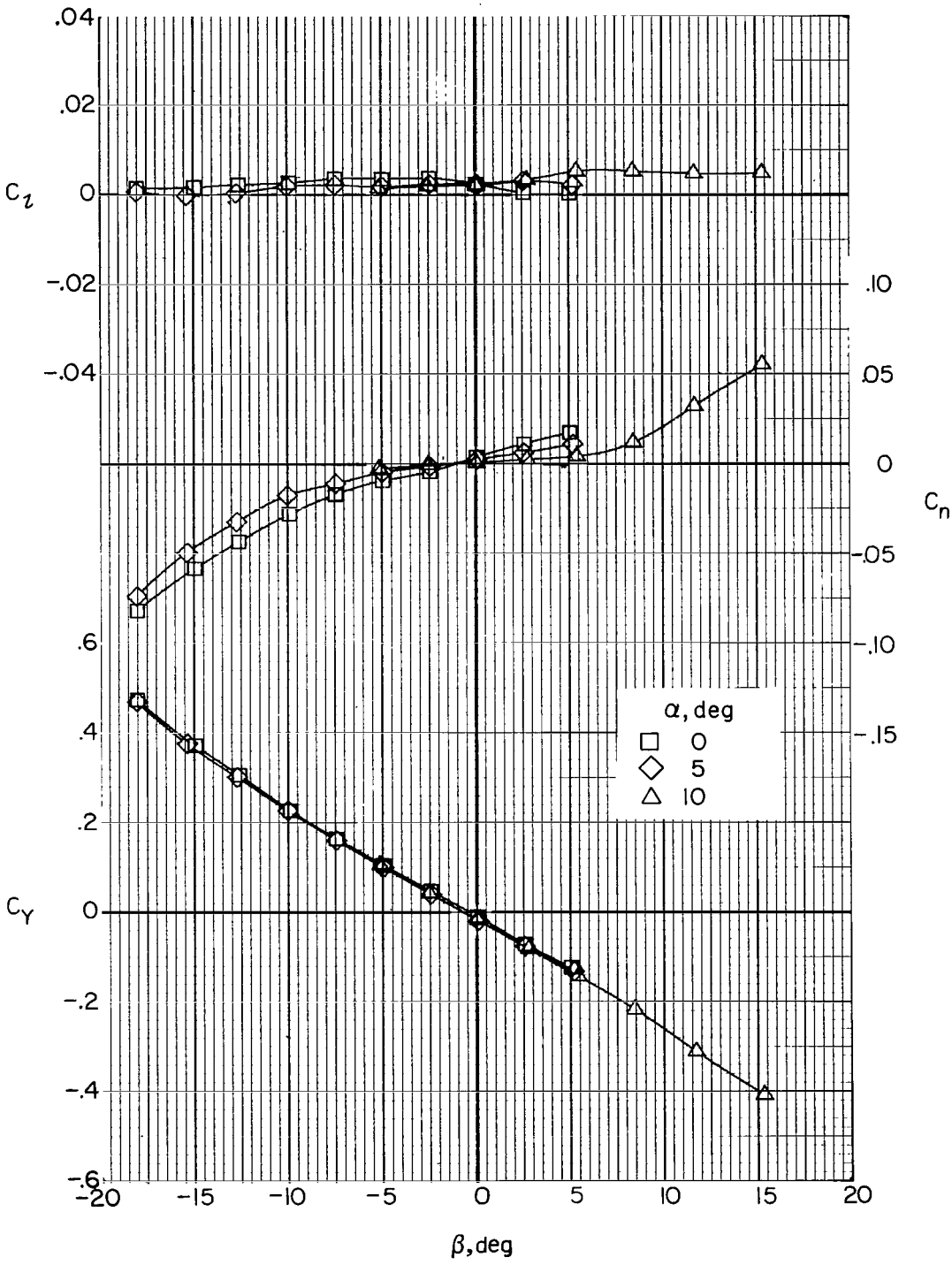

(c) Jets off ($F_1W_1VH_C$); $i_w = 0^o$; $\delta_f = 0^o$.

Figure 31.- Continued.

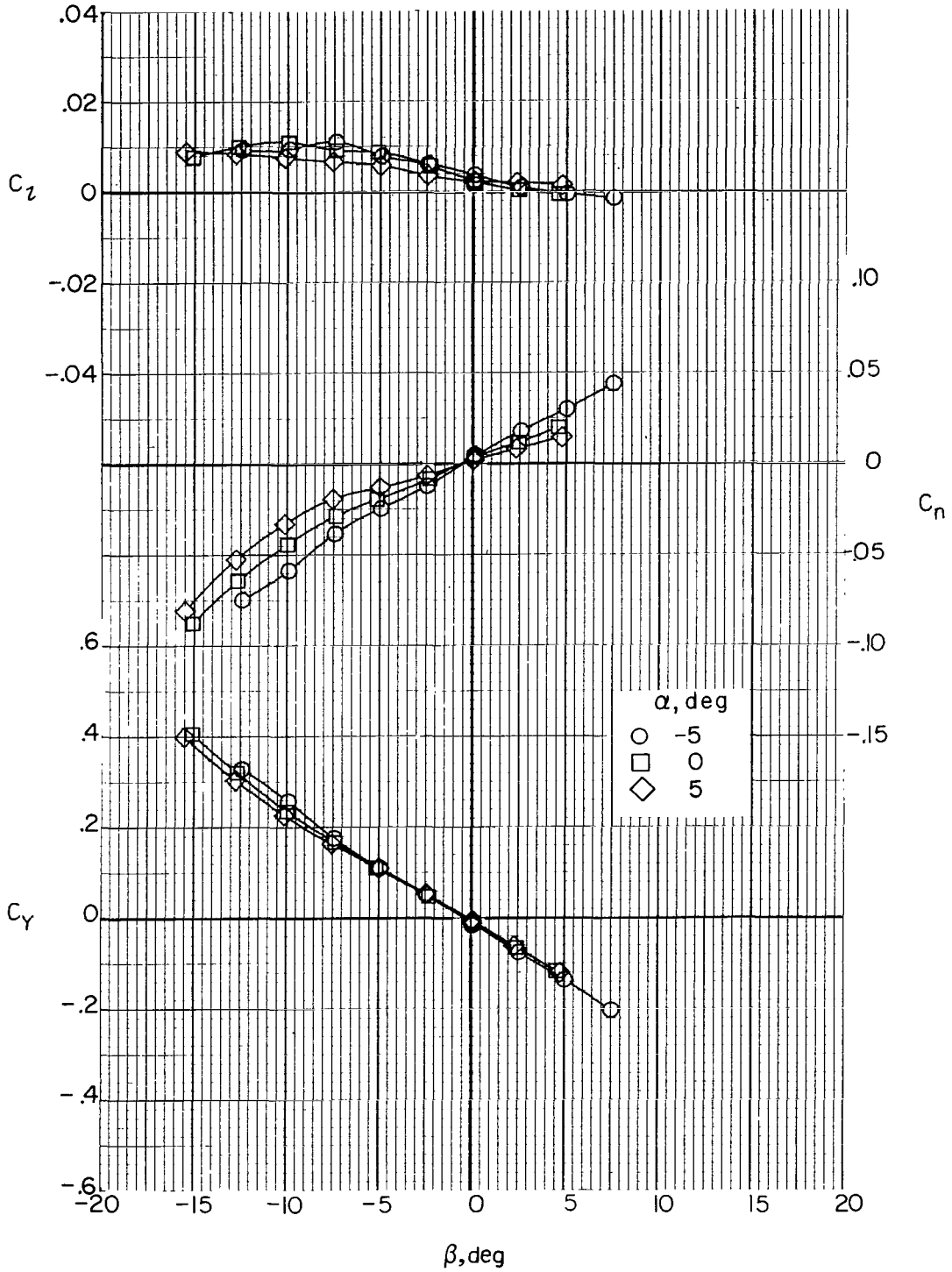

(d) Jets off ($F_1W_6VH_C$); $i_W = 7.5°$; $\delta_f = 30°$.

Figure 31.- Continued.

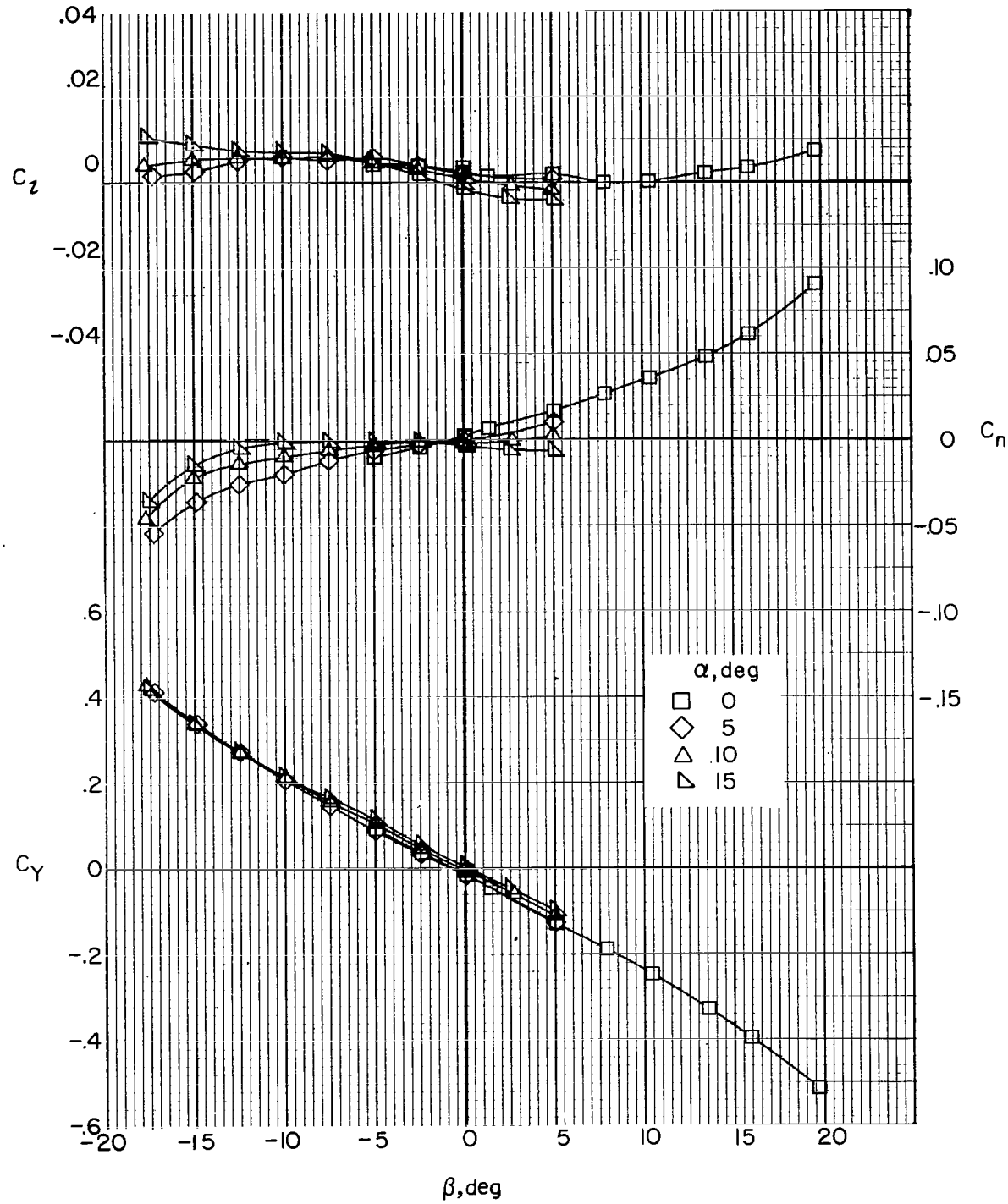

(e) Jets on ($F_1W_1VH_CJ_2$); $C_{T,J} = 0$; $i_W = 0^o$; $\delta_f = 0^o$.

Figure 31.- Continued.

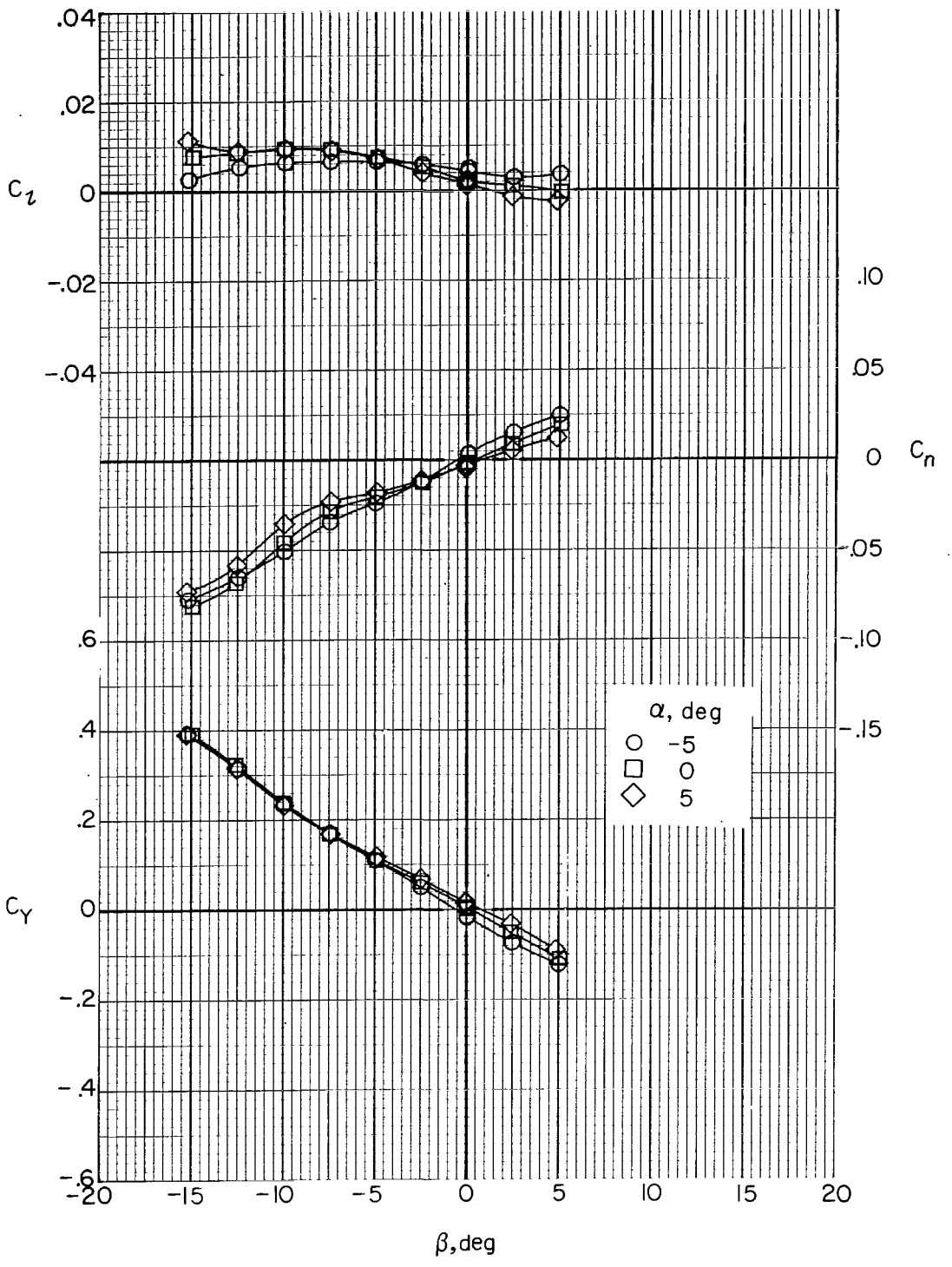

(f) Jets on ($F_1W_5VH_CJ_2$); $C_{T,J} \approx 0$; $i_W = 0°$; $\delta_f = 30°$.

Figure 31.- Continued.

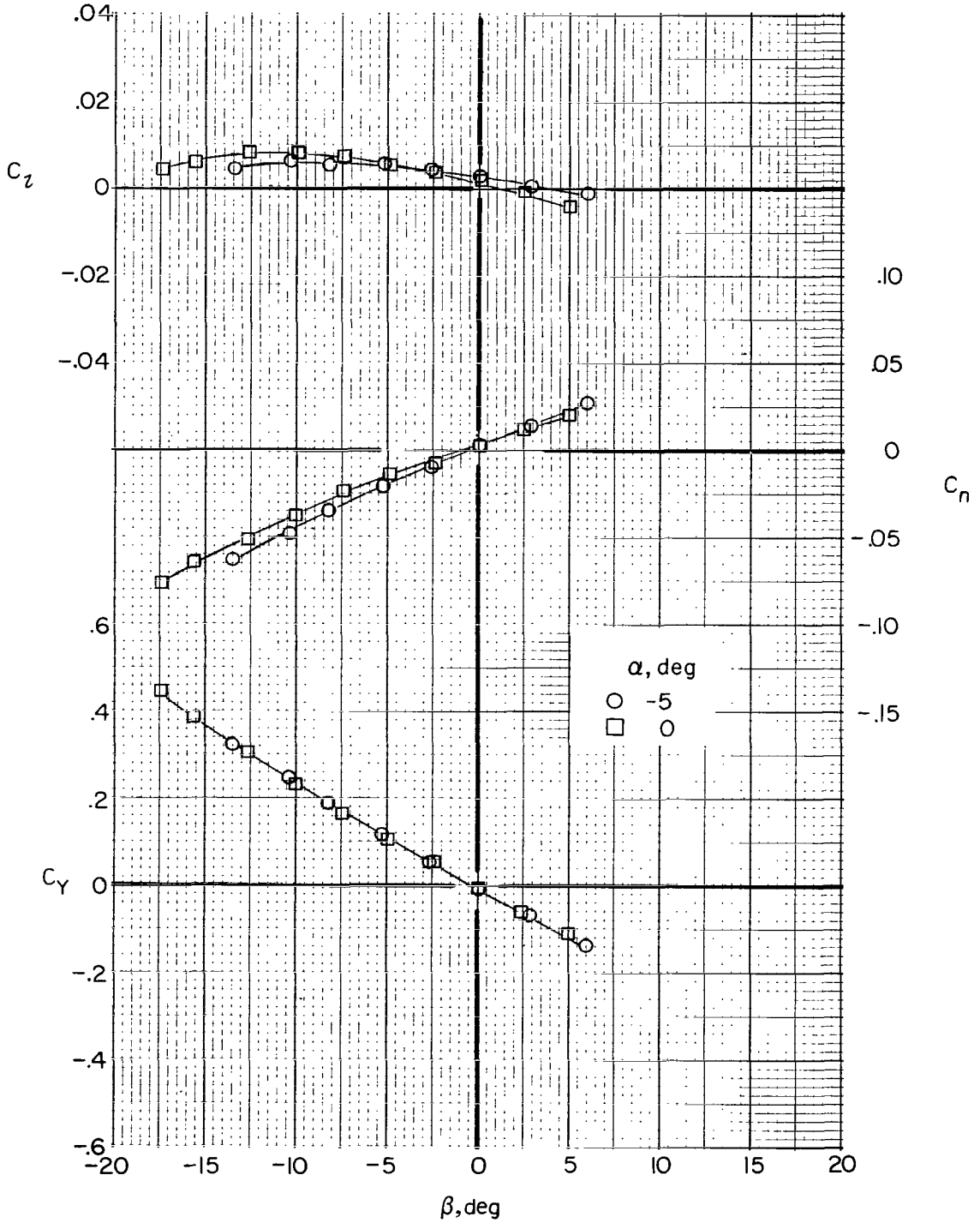

(g) Jets on ($F_1W_2VH_CJ_2$); $C_{T,J} = 0$; $i_w = 7.5^o$; $\delta_f = 0^o$.

Figure 31.- Continued

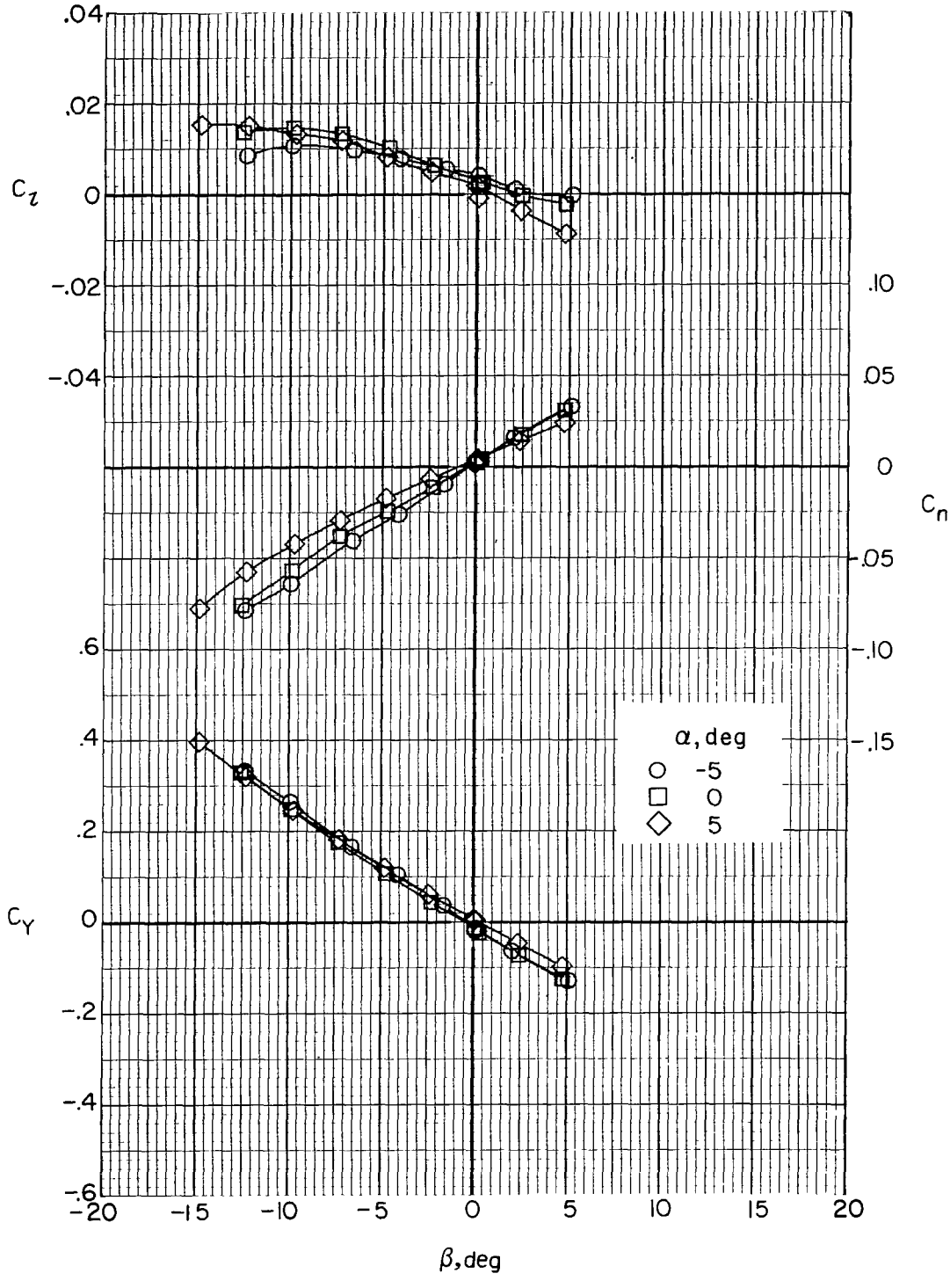

(h) Jets on ($F_1W_6VH_CJ_2$); $C_{T,J} = 0$; $i_w = 7.5^\circ$; $\delta_f = 30^\circ$.

Figure 31.- Concluded.

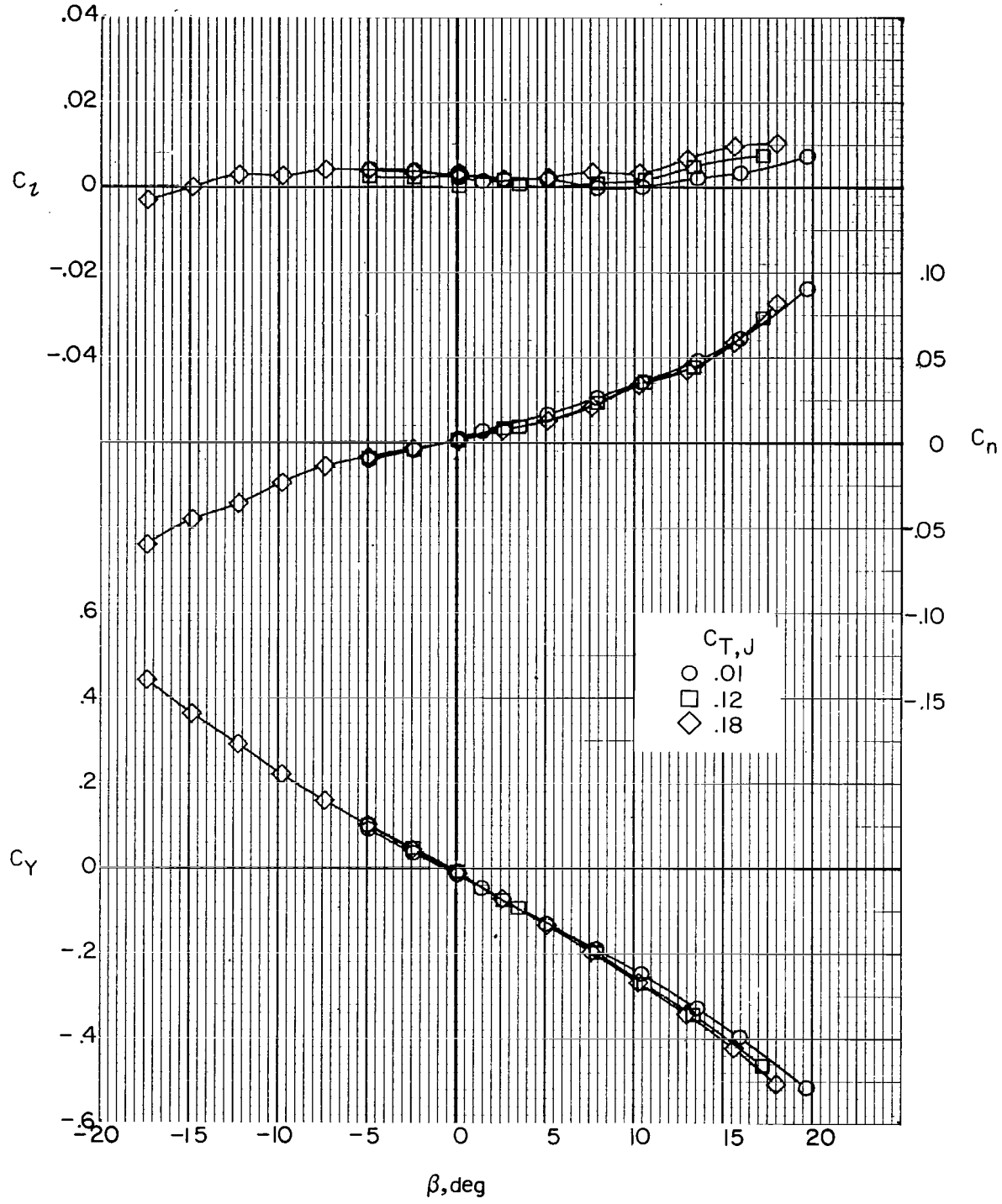

(a) $i_w = 0^o$; $\delta_f = 0^o$; $\alpha = 0^o$; $F_1W_1VH_CJ_2$.

Figure 32.- Effect of auxiliary engine thrust level on lateral aerodynamics. $i_t = 0^o$.

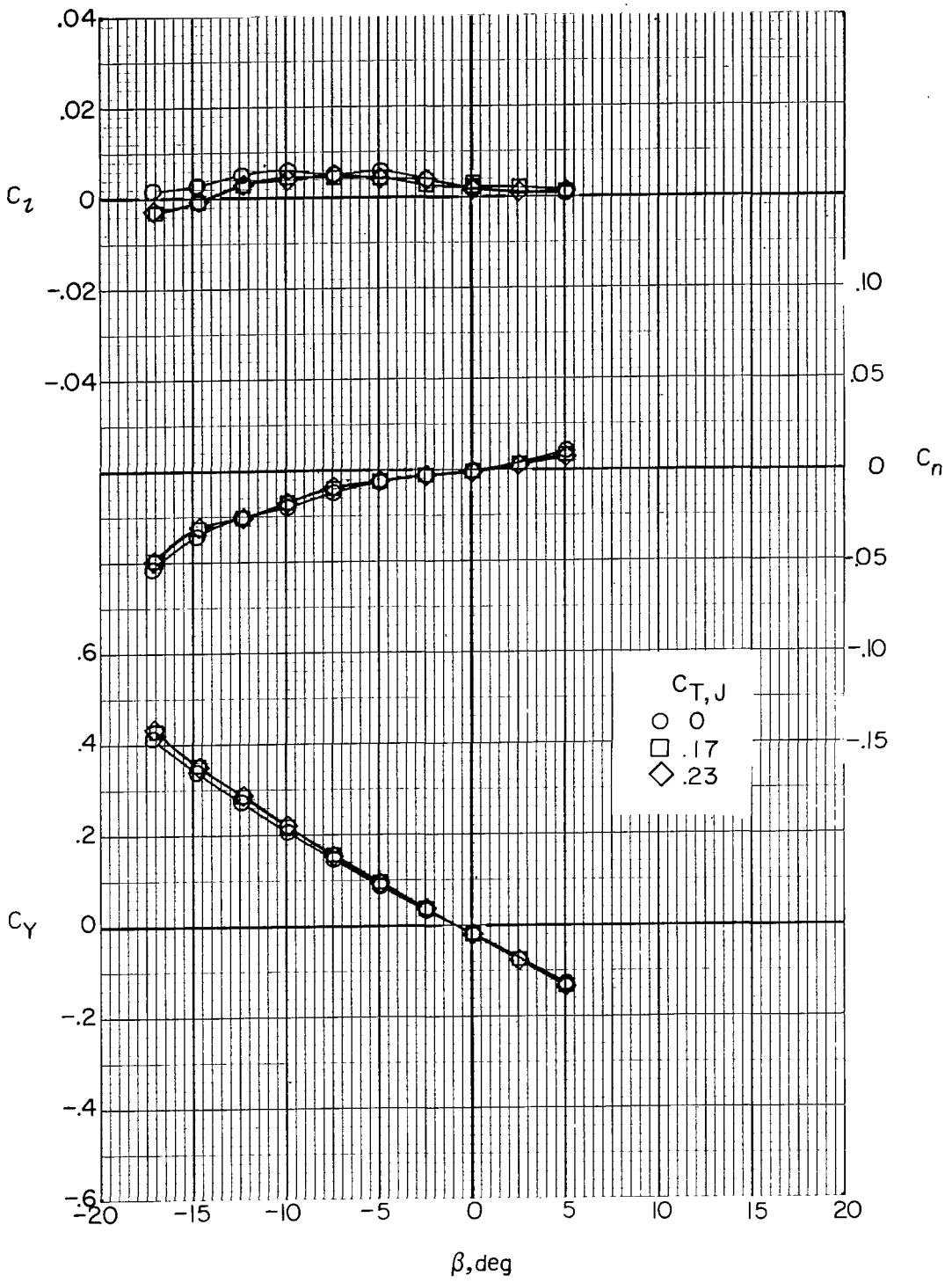

(b) $i_w = 0^o$; $\delta_f = 0^o$; $\alpha = 5^o$; $F_1W_1VH_CJ_2$.

Figure 32.- Continued.

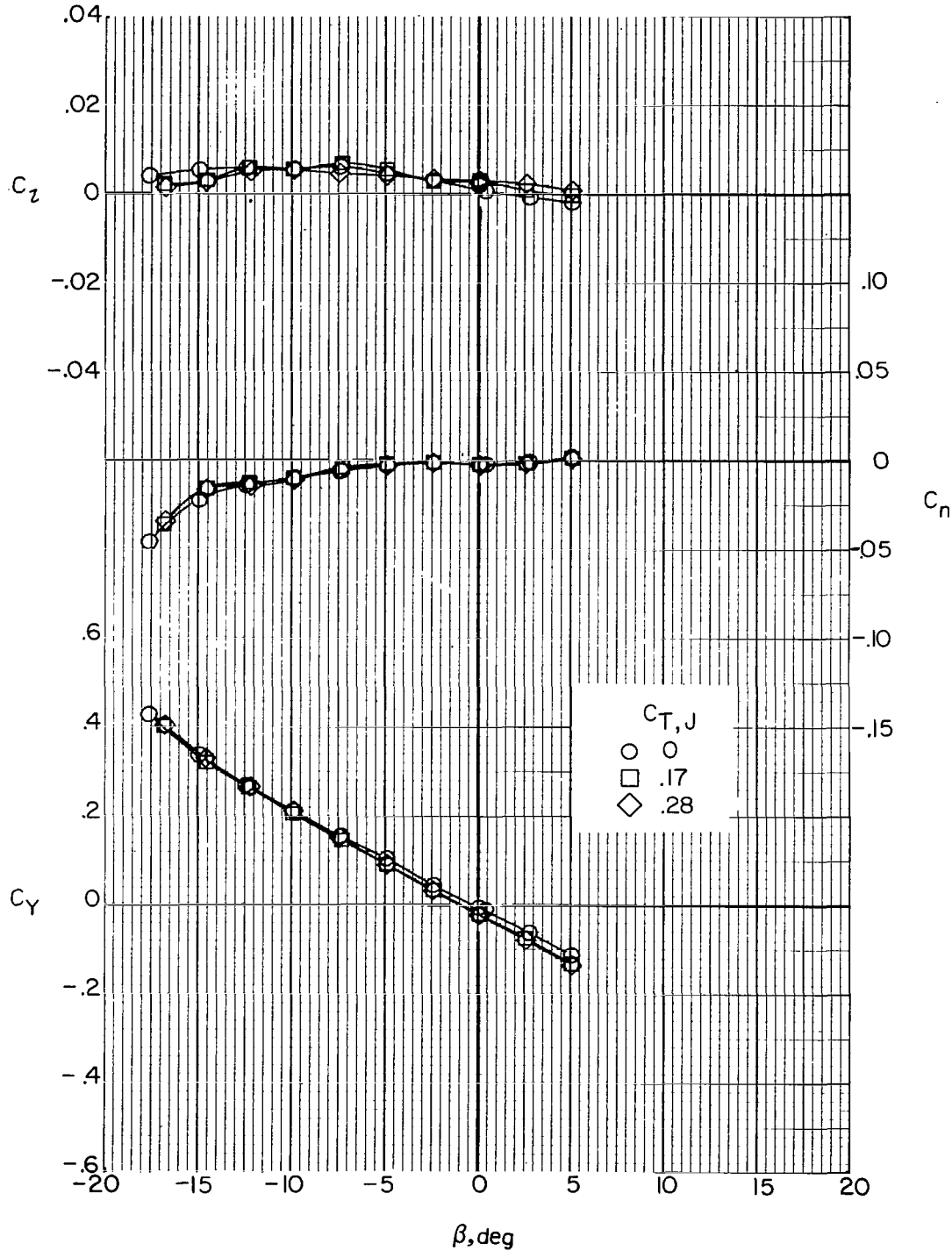

(c) $i_w = 0^o$; $\delta_f = 0^o$; $\alpha = 10^o$; $F_1W_1VH_CJ_2$.

Figure 32.- Continued.

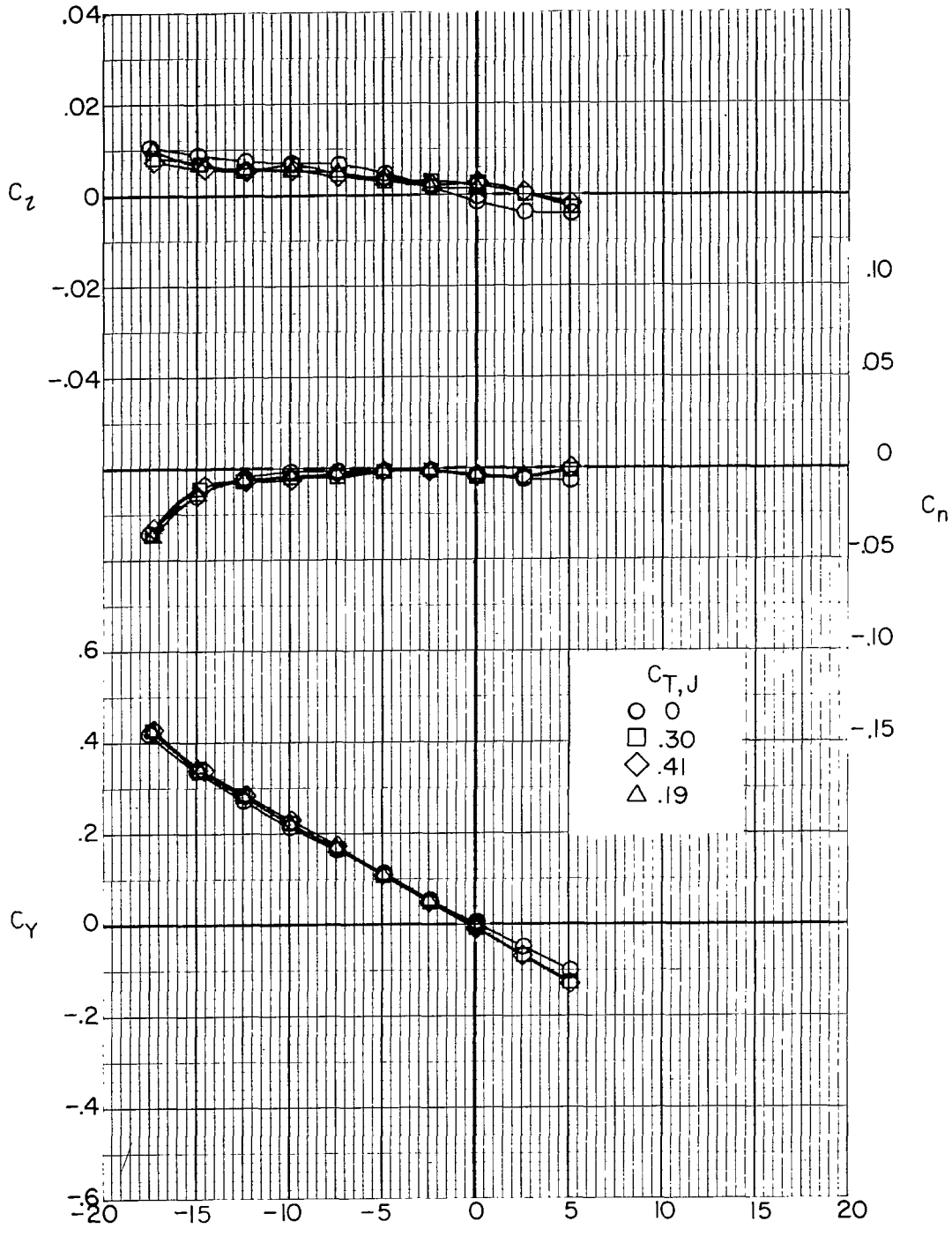

(d) $i_w = 0^o$; $\delta_f = 0^o$; $\alpha = 15^o$; $F_1W_1VH_CJ_2$.

Figure 32.- Continued.

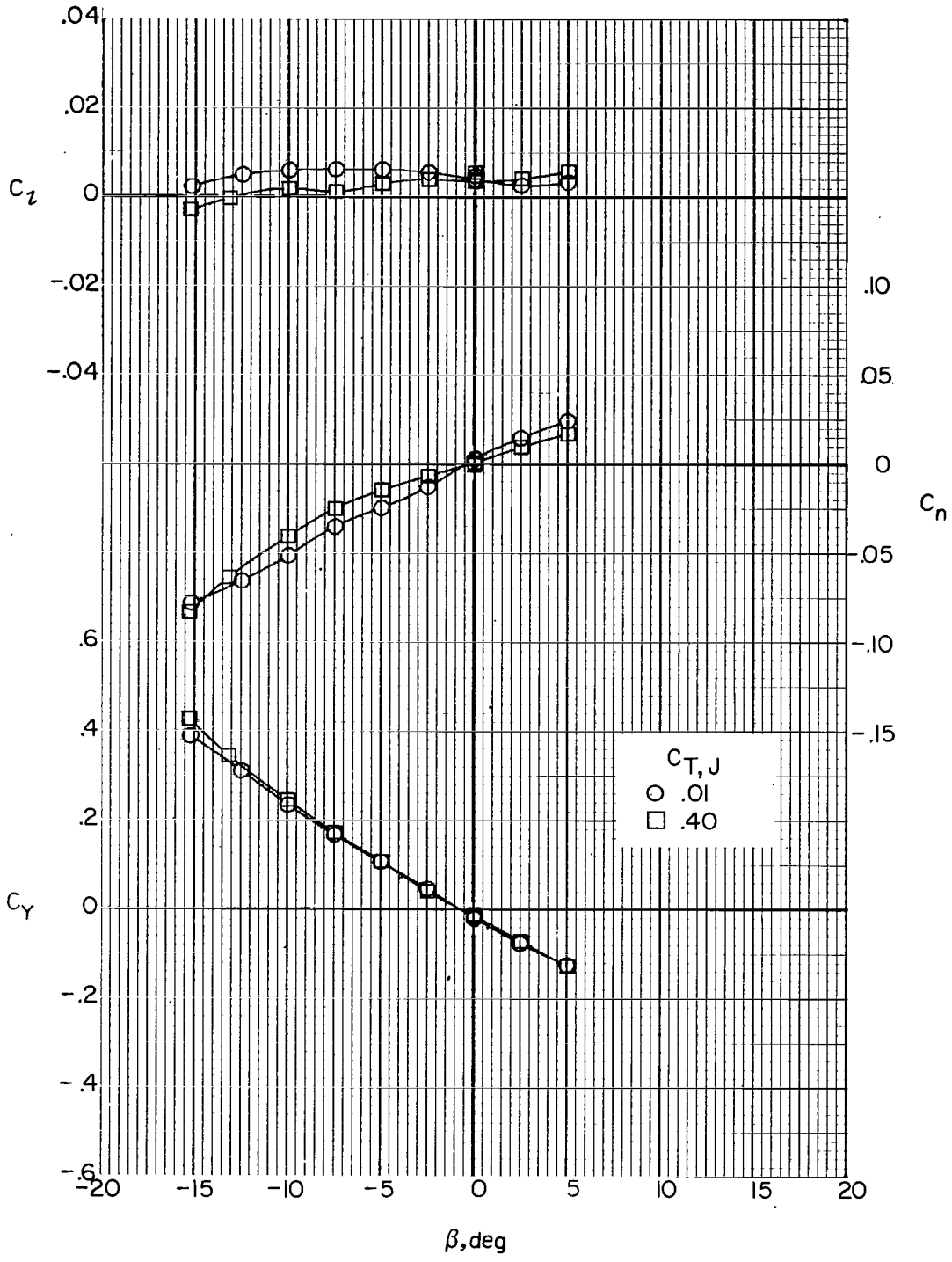

(e) $i_w = 0^o$; $\delta_f = 30^o$; $\alpha = -5^o$; $F_1 W_5 V H_C J_2$.

Figure 32.- Continued.

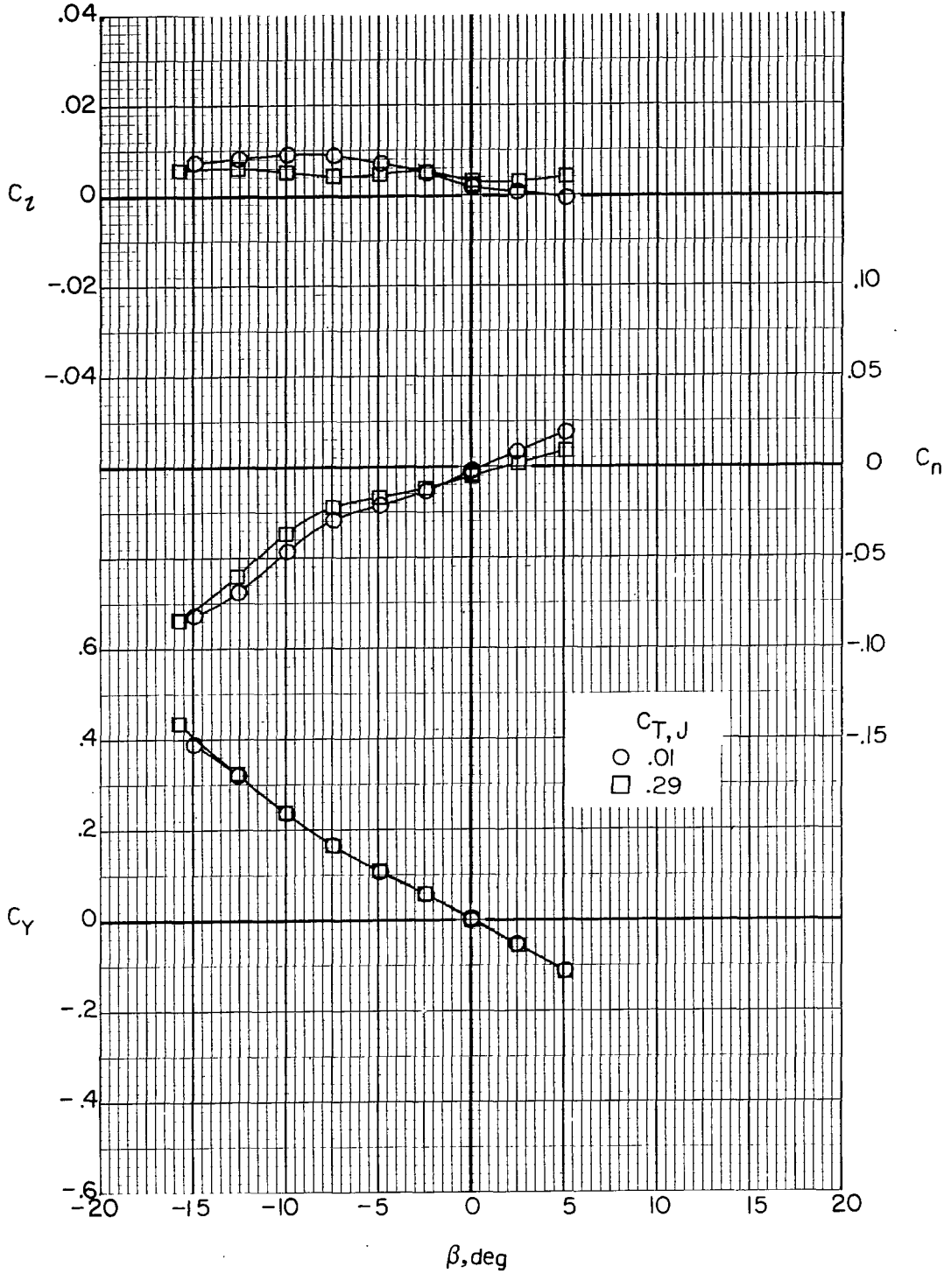

(f) $i_w = 0^o$; $\delta_f = 30^o$; $\alpha = 0^o$; $F_1W_5VH_CJ_2$.

Figure 32.- Continued.

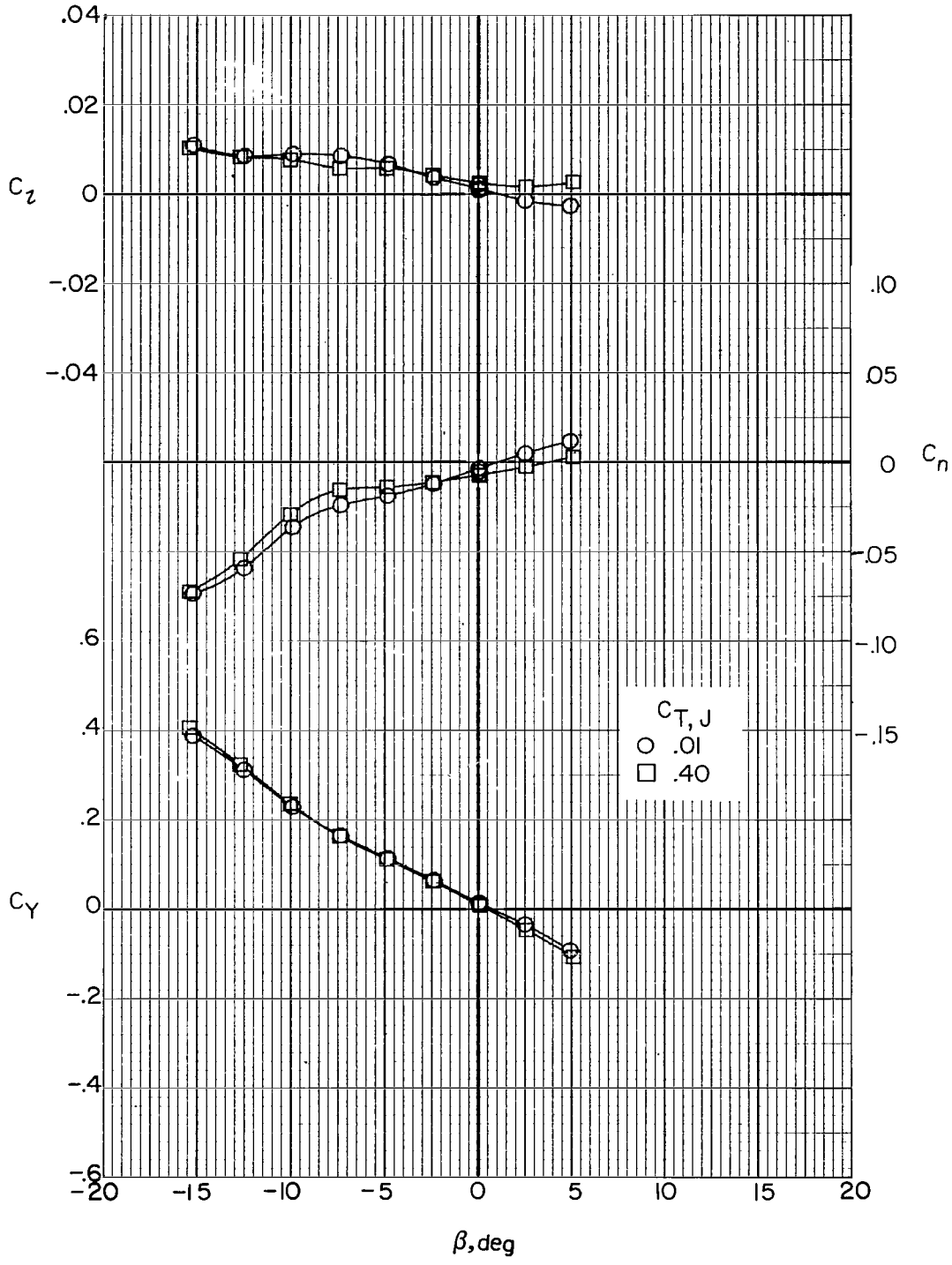

(g) $i_w = 0^o$; $\delta_f = 30^o$; $\alpha = 5^o$; $F_1 W_5 V H_C J_2$.

Figure 32.- Continued.

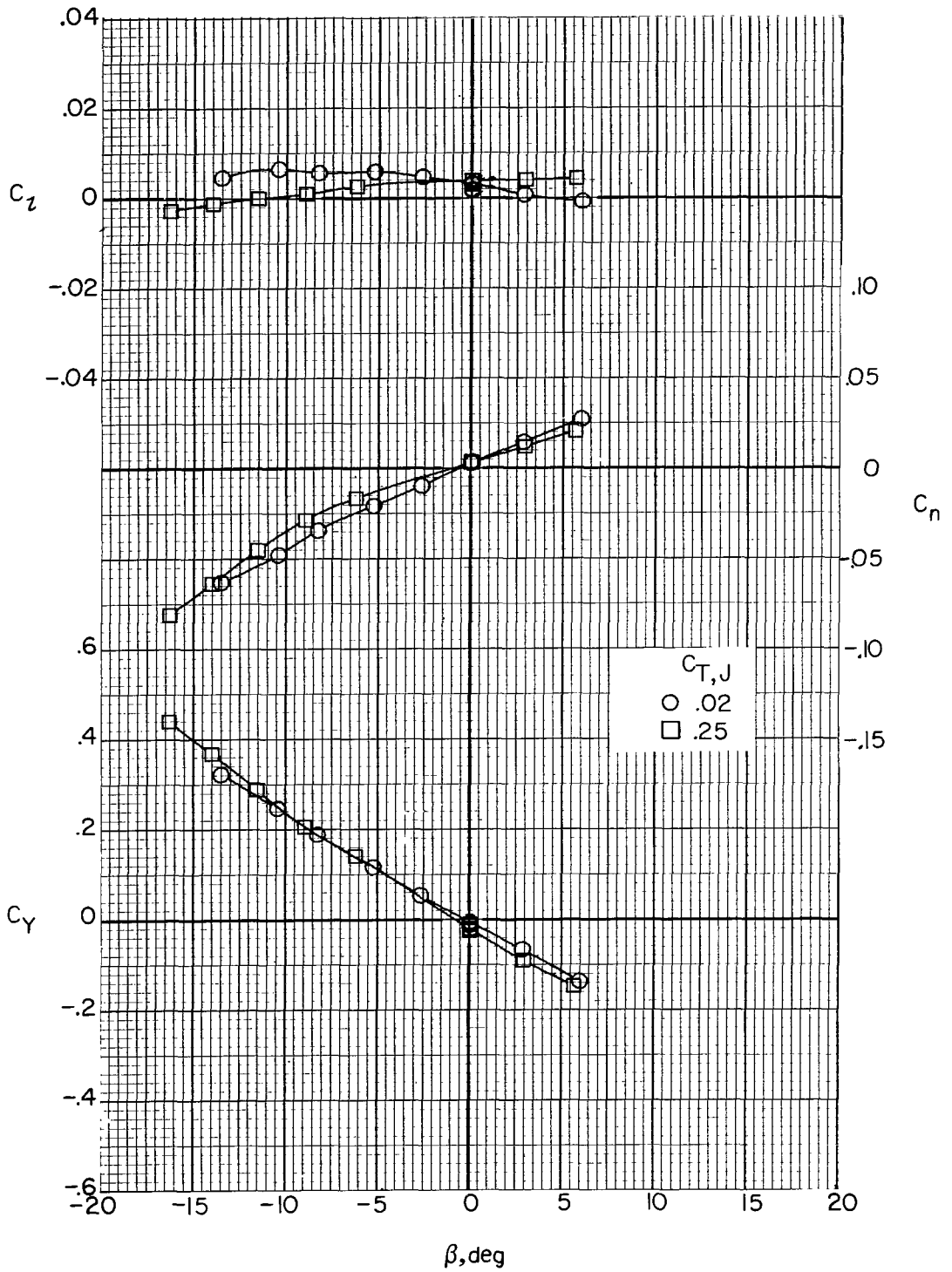

(h) $i_w = 7.5^o$; $\delta_f = 0^o$; $\alpha = -5^o$; $F_1W_2VH_CJ_2$.

Figure 32.- Continued.

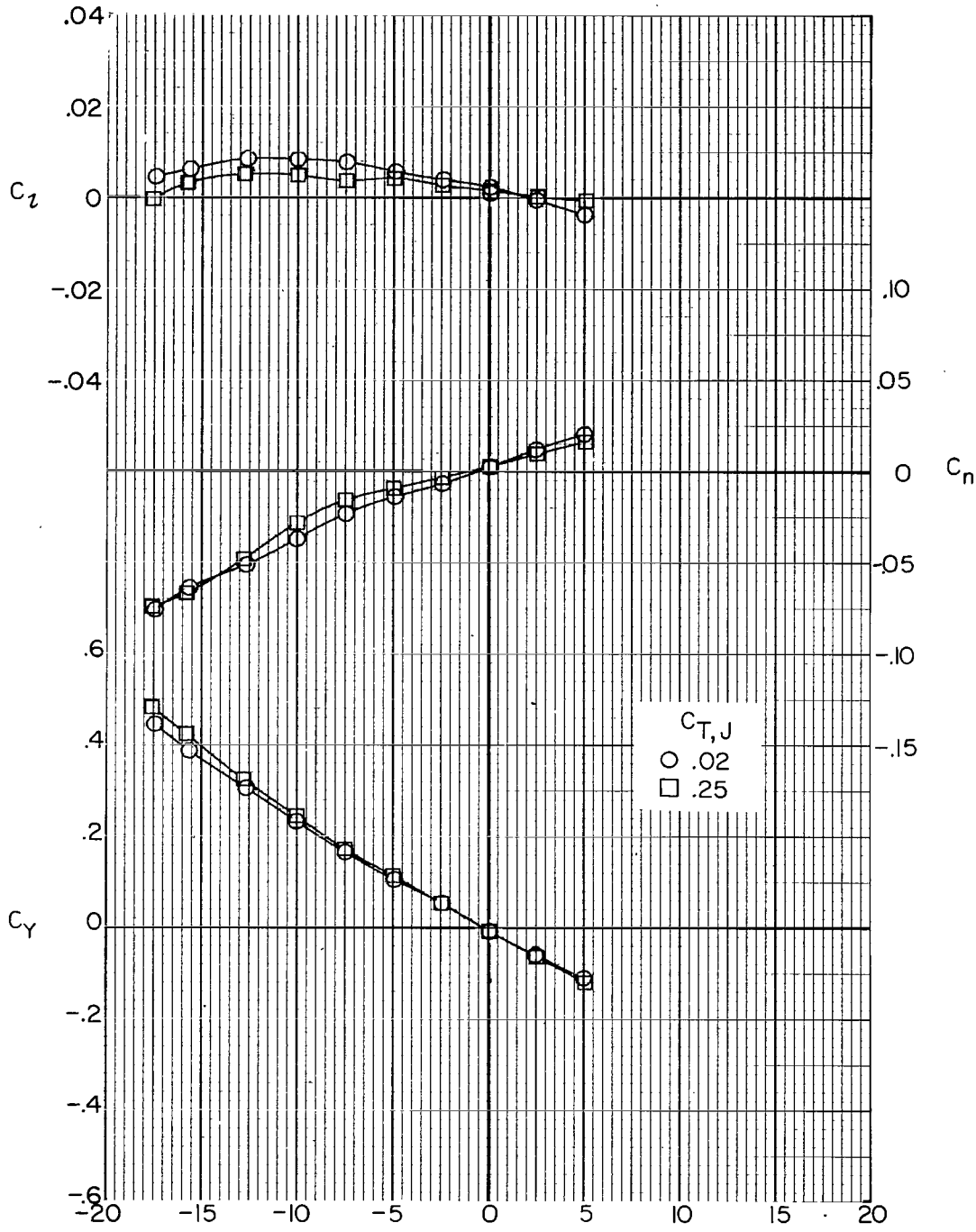

(i) $i_w = 7.5^o$; $\delta_f = 0^o$; $\alpha = 0^o$; $F_1W_2VH_CJ_2$.

Figure 32.- Continued.

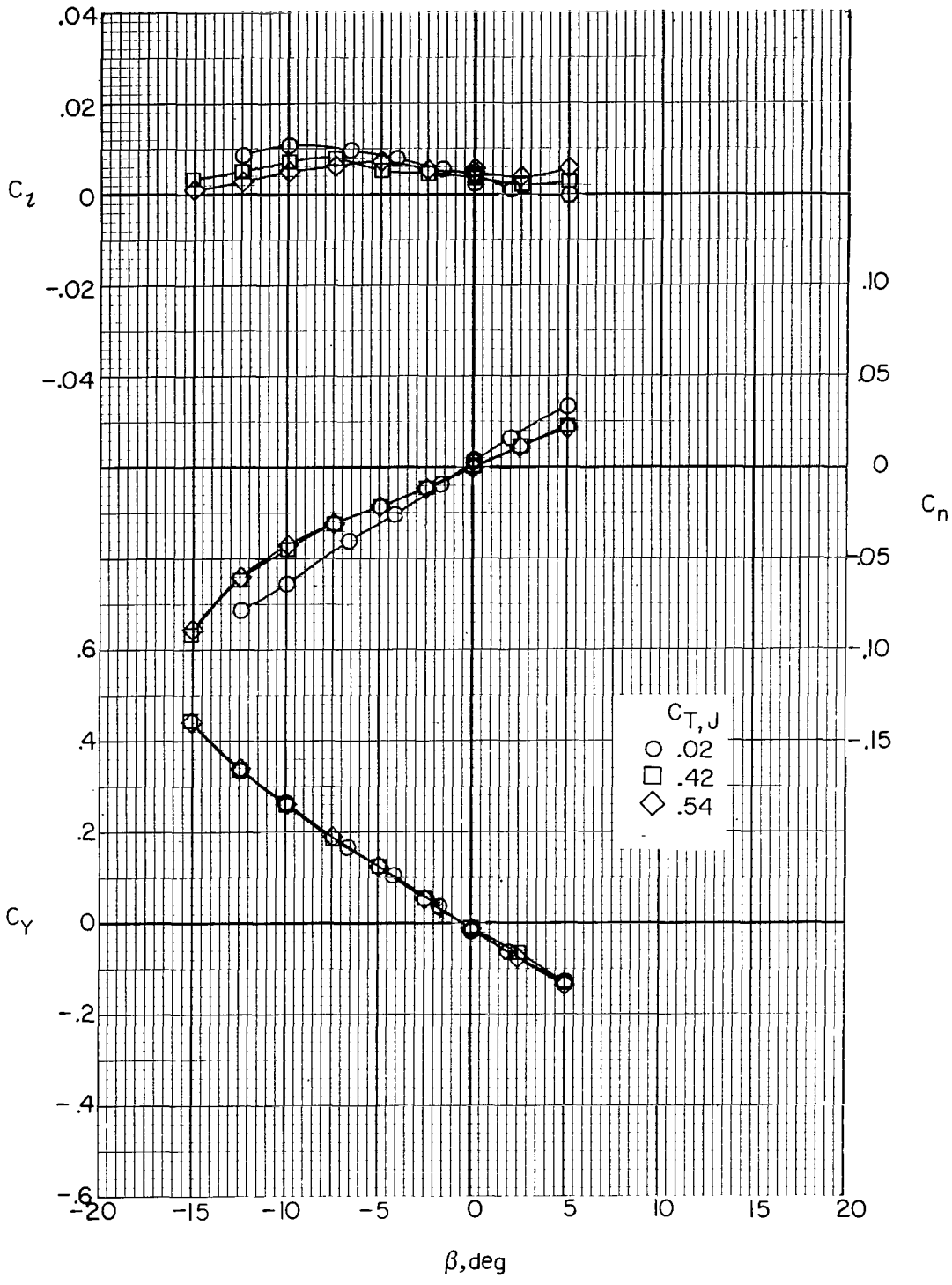

(j) $i_w = 7.5^o$; $\delta_f = 30^o$; $\alpha = -5^o$; $F_1W_6VH_CJ_2$.

Figure 32.- Continued.

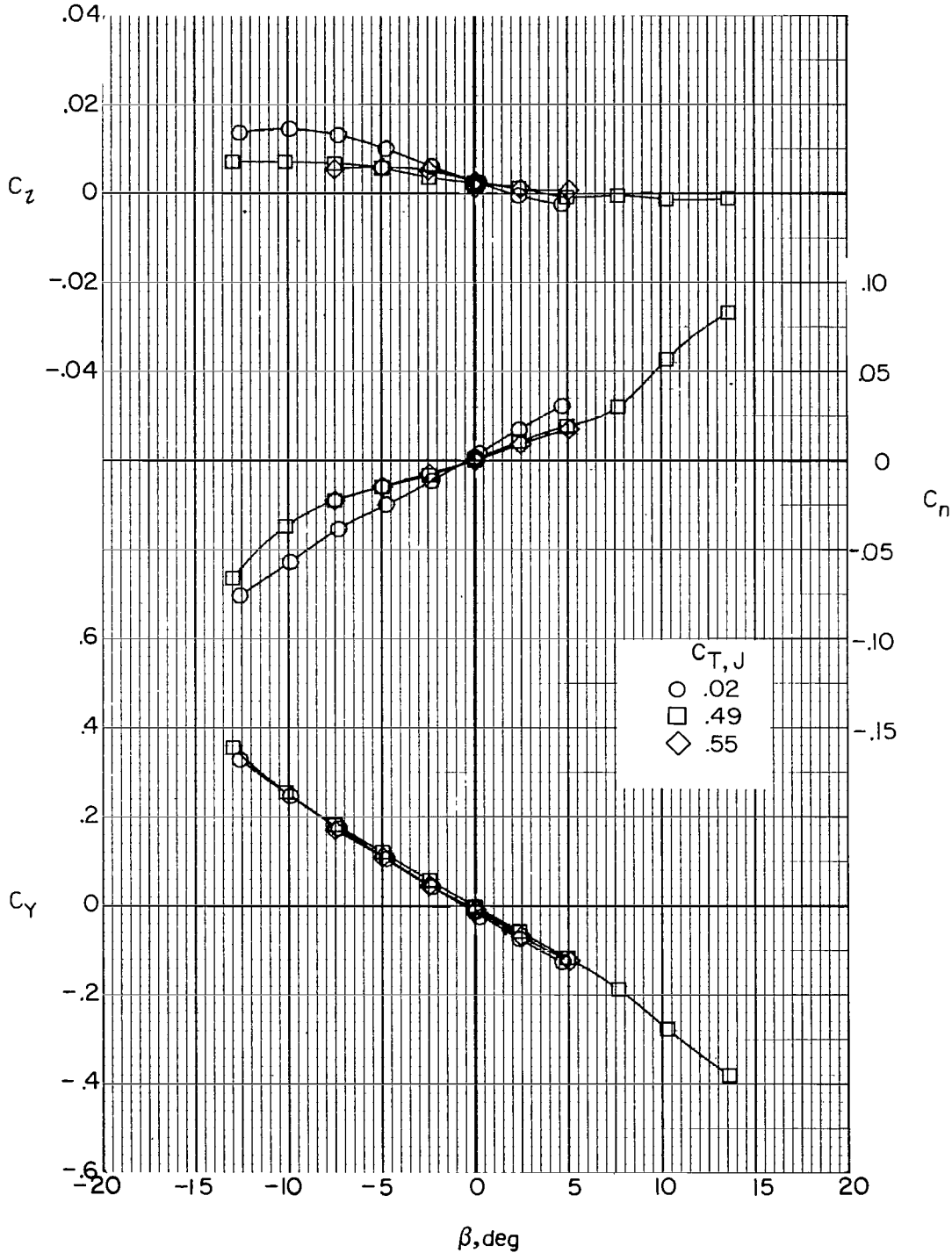

(k) $i_w = 7.5^o$; $\delta_f = 30^o$; $\alpha = 0^o$; $F_1W_6VH_CJ_2$.

Figure 32.- Continued.

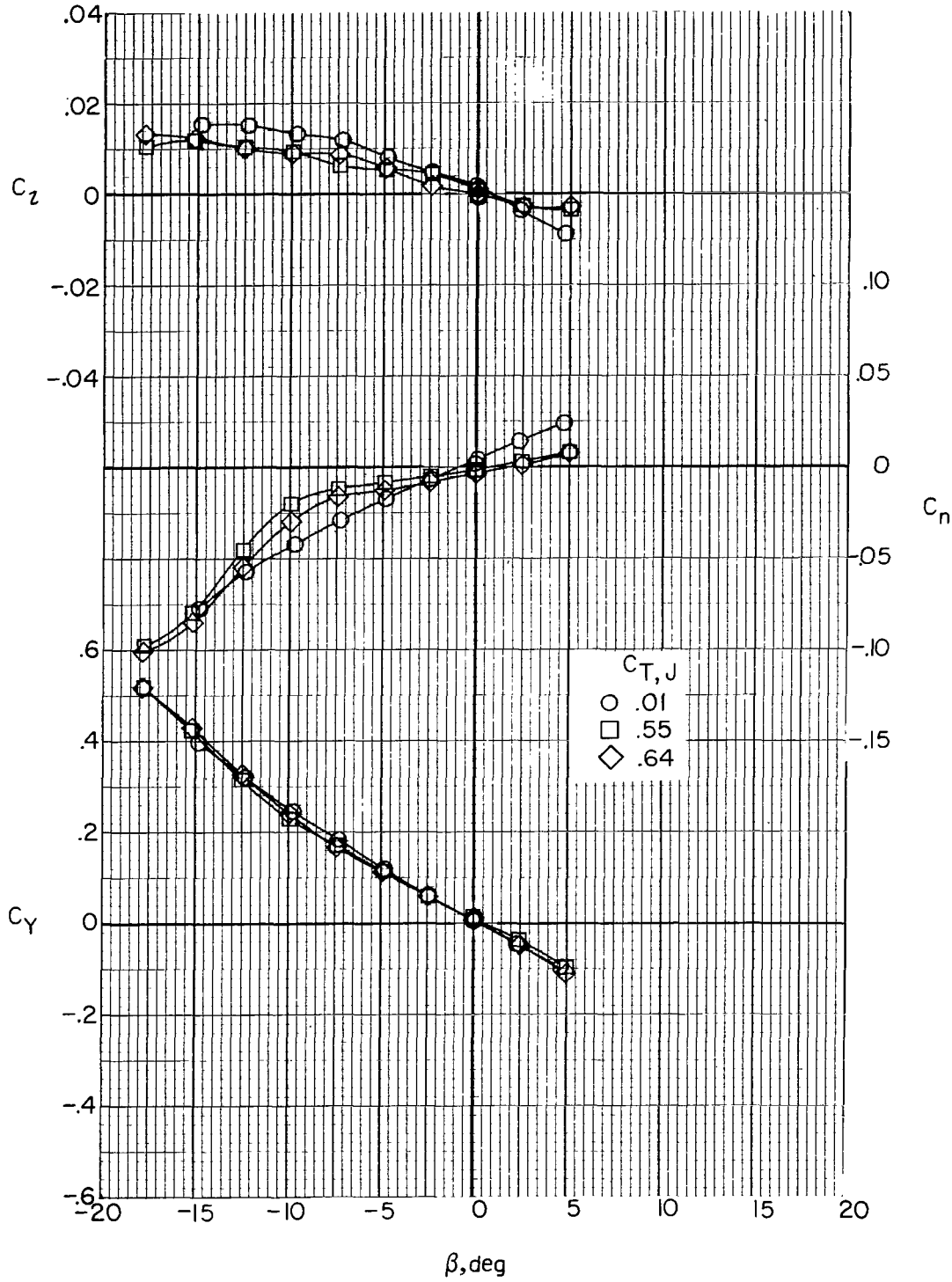

(l) $i_w = 7.5^o$; $\delta_f = 30^o$; $\alpha = 5^o$; $F_1W_6VH_CJ_2$.

Figure 32.- Concluded.

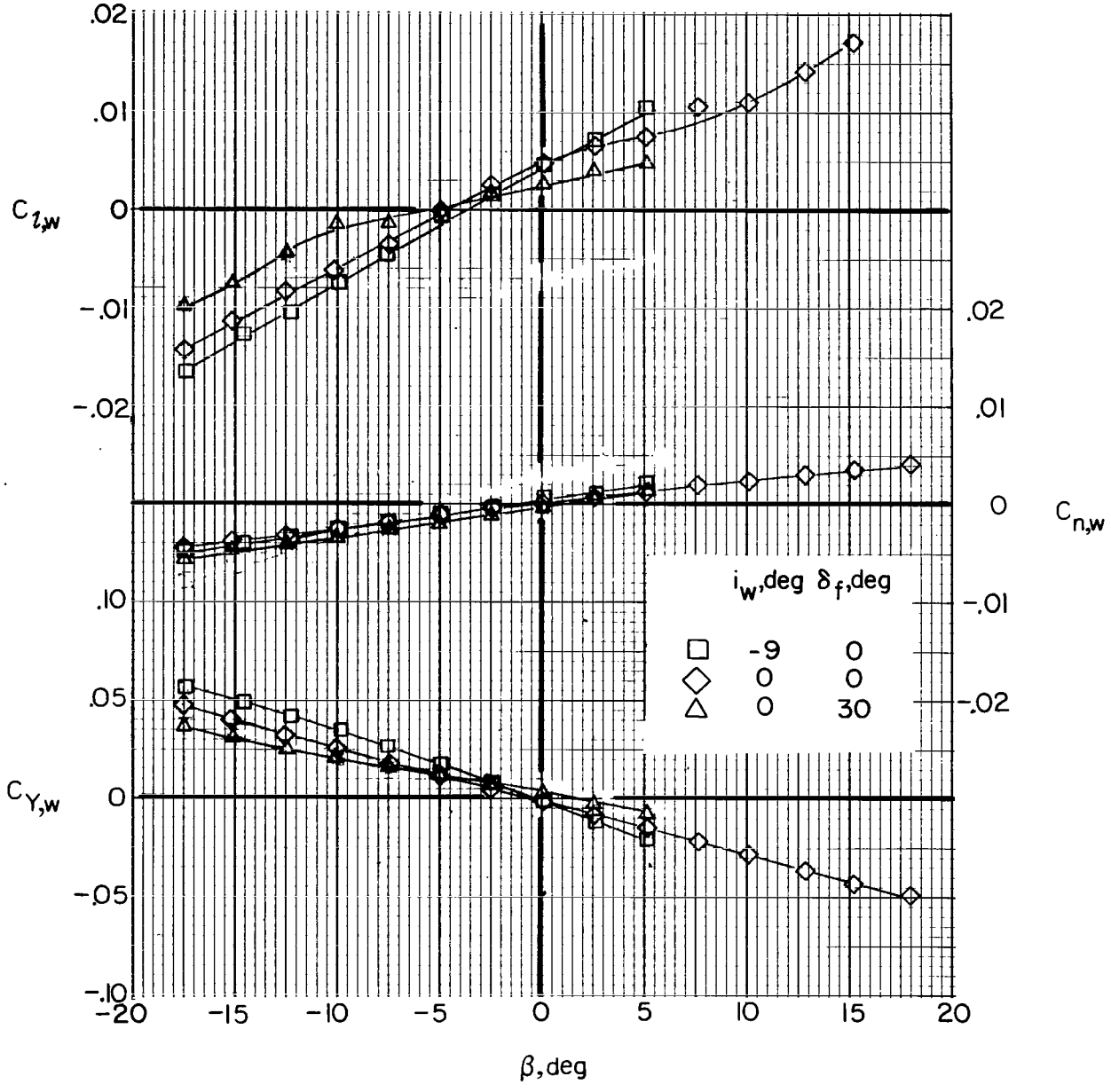

Figure 33.- Effect of wing incidence and flap deflection on wing lateral aerodynamics with the jets removed (F_1W_x). $\alpha = 0^o$.

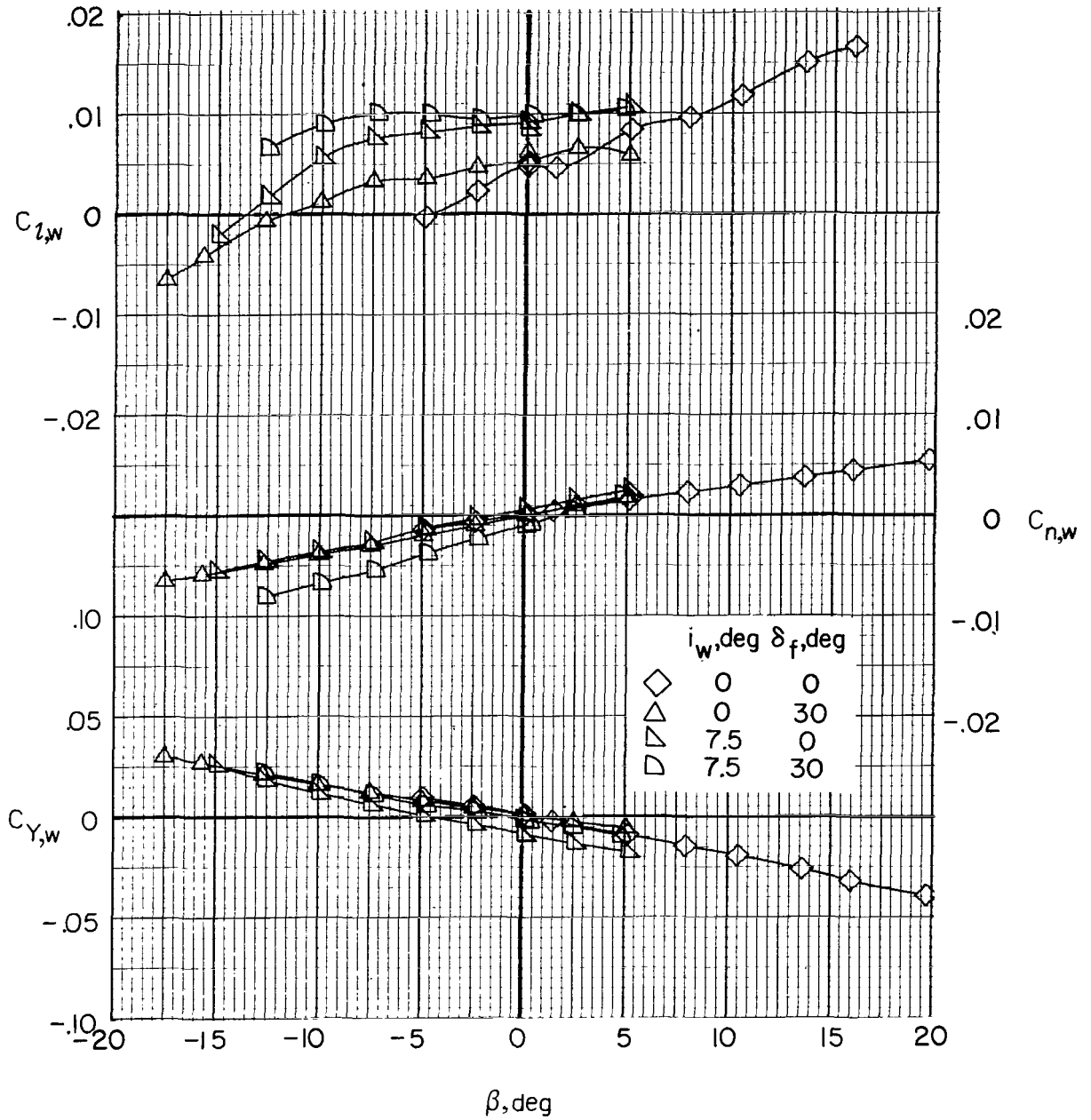

Figure 34.- Effect of wing incidence and flap deflection on wing lateral aerodynamics with the jets on ($F_1 W_X V H_C J_2$). $C_{T,J} = 0$; $\alpha = 0^o$.

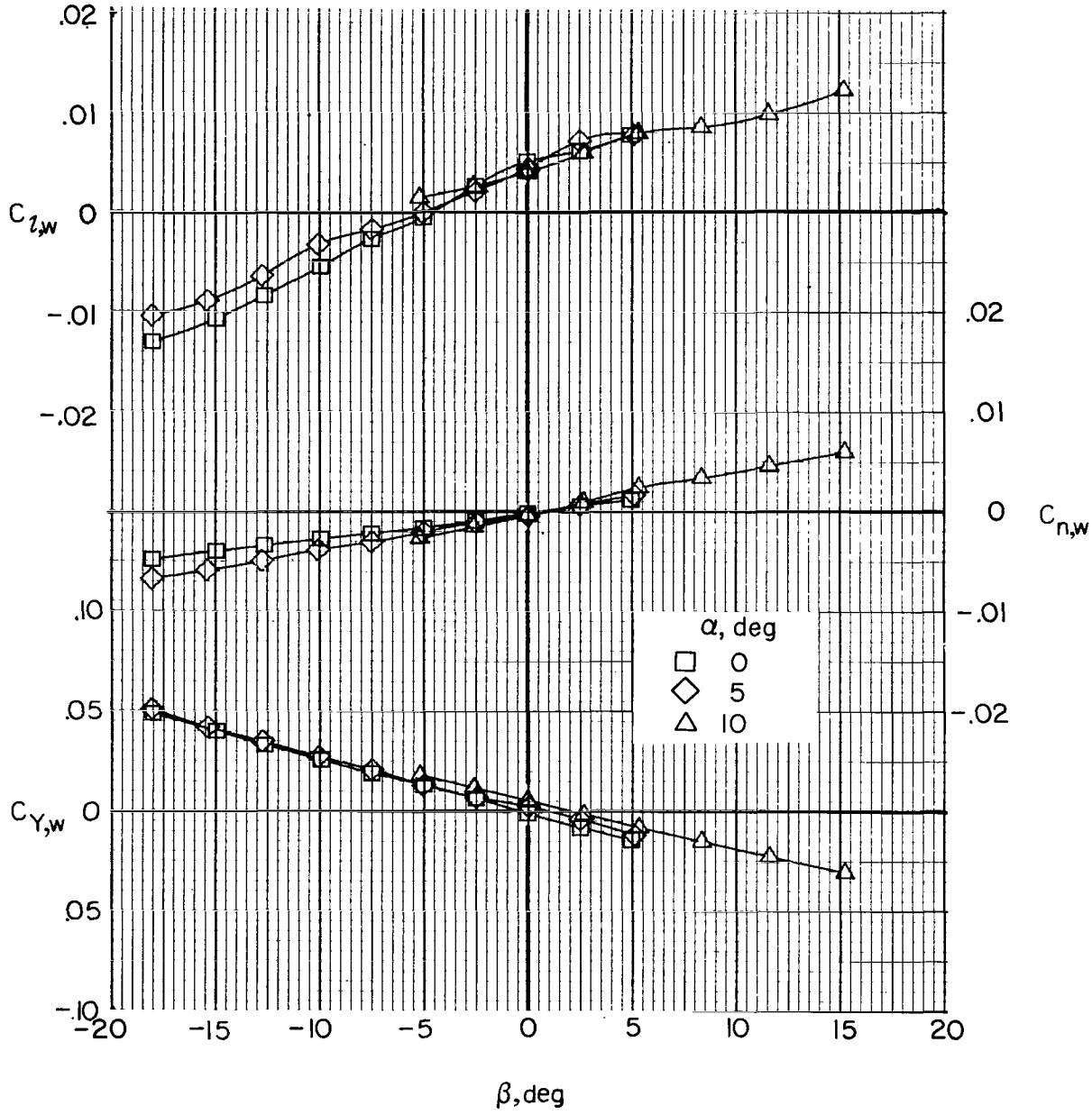

(a) Jets removed ($F_1W_1VH_C$); $i_w = 0^o$; $\delta_f = 0^o$.

Figure 35.- Effect of angle of attack on wing lateral aerodynamics.

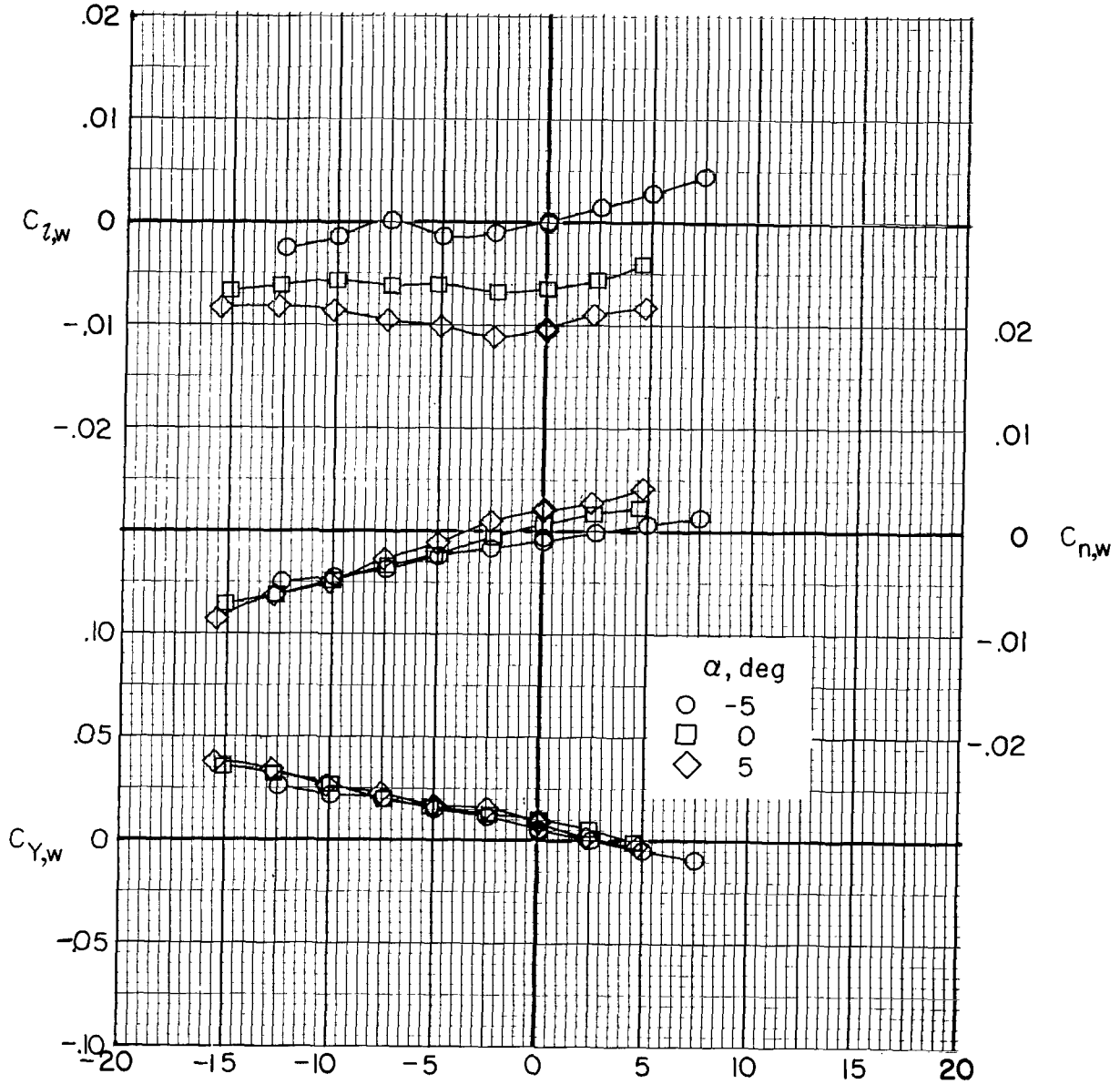

(b) Jets removed ($F_1W_6VH_C$); $i_w = 7.5^o$; $\delta_f = 30^o$.

Figure 35.- Continued.

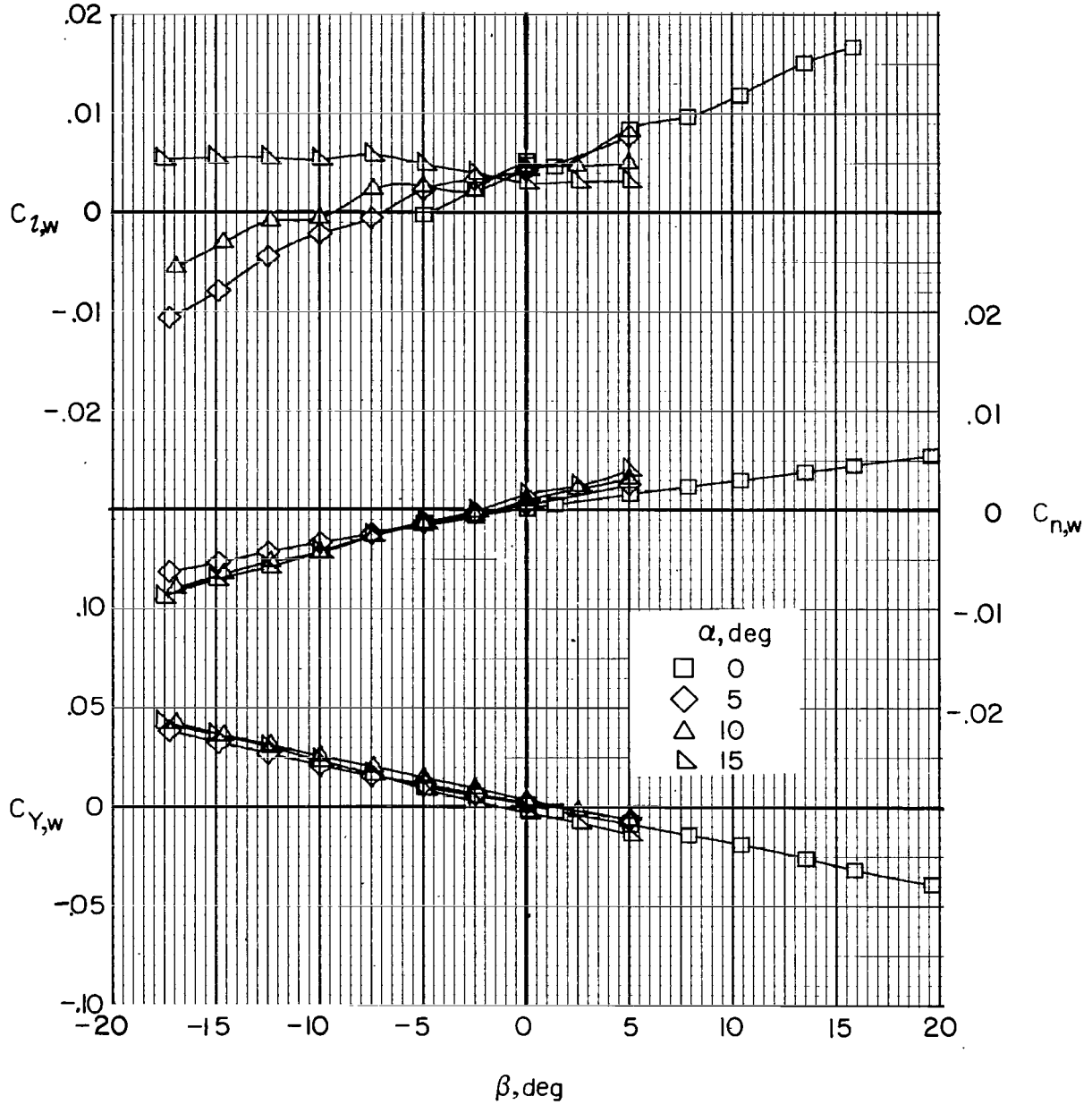

(c) Jets on ($F_1W_1VH_CJ_2$); $C_{T,J} = 0$; $i_w = 0°$; $\delta_f = 0°$.

Figure 35.- Continued.

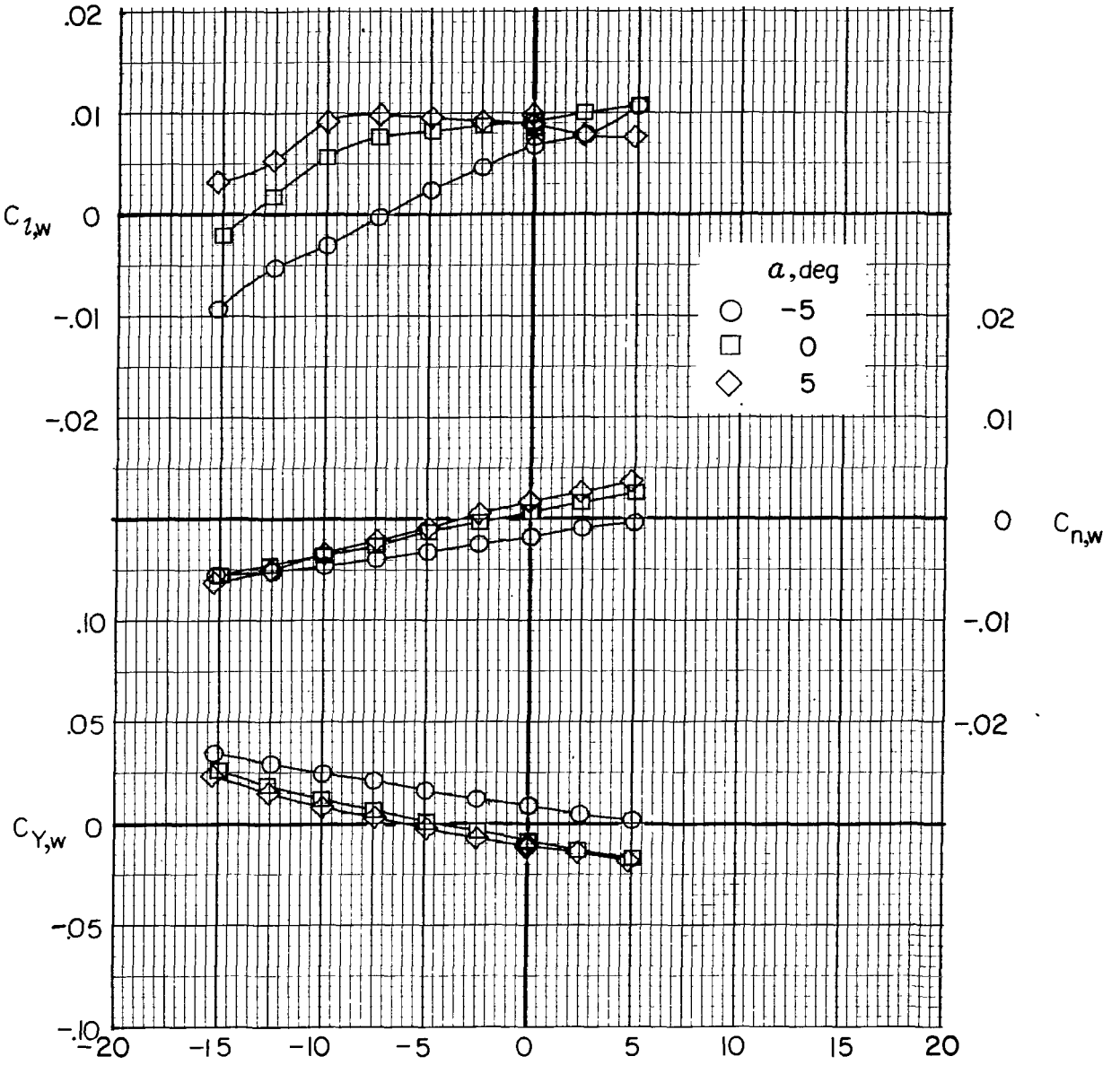

(d) Jets on ($F_1W_5VH_CJ_2$); $C_{T,J} = 0$; $i_W = 0^o$; $\delta_f = 30^o$.

Figure 35.- Continued.

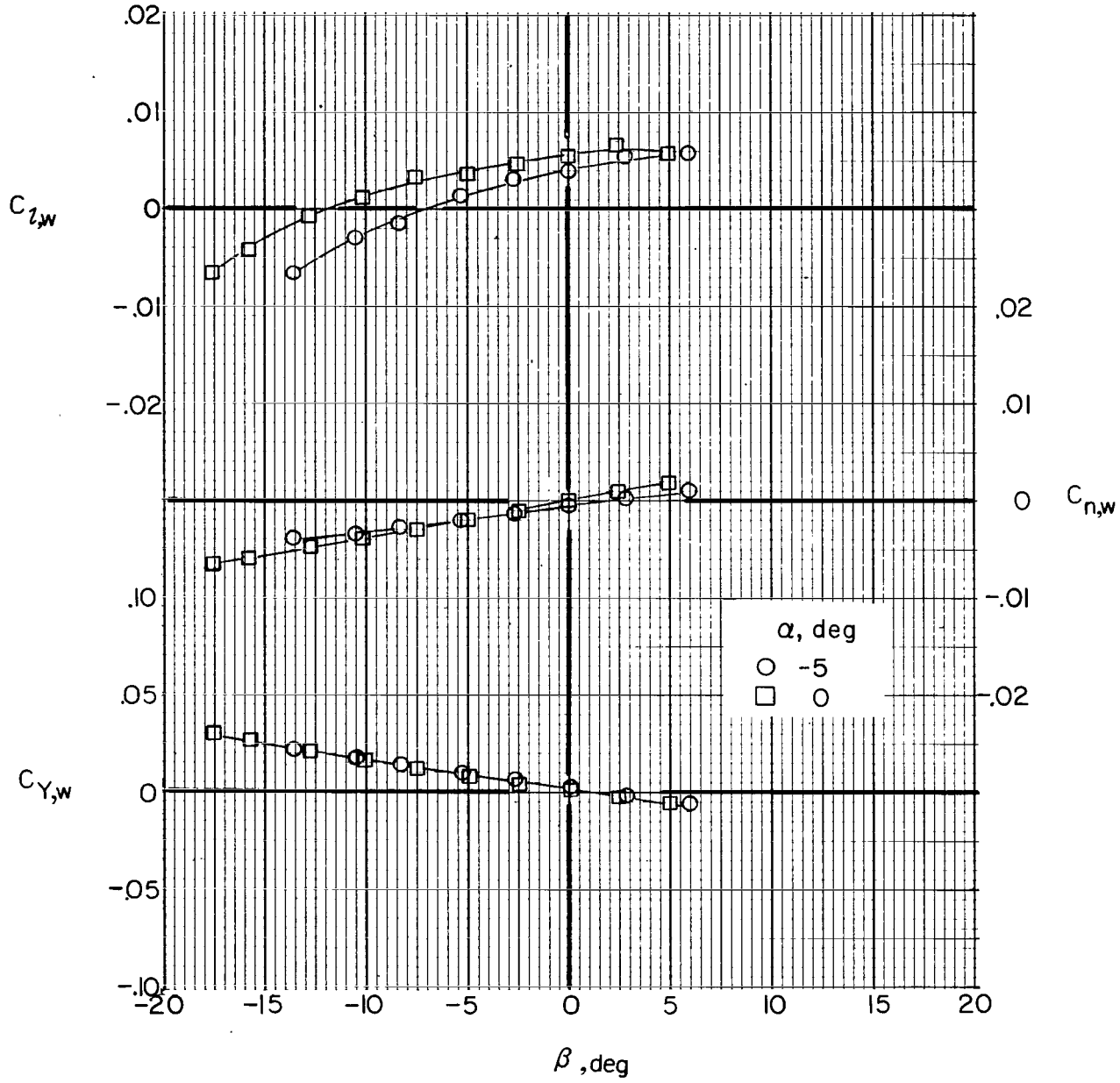

(e) Jets on ($F_1W_2VH_CJ_2$); $C_{T,J} = 0$; $i_w = 7.5°$; $\delta_f = 0°$.

Figure 35.- Continued.

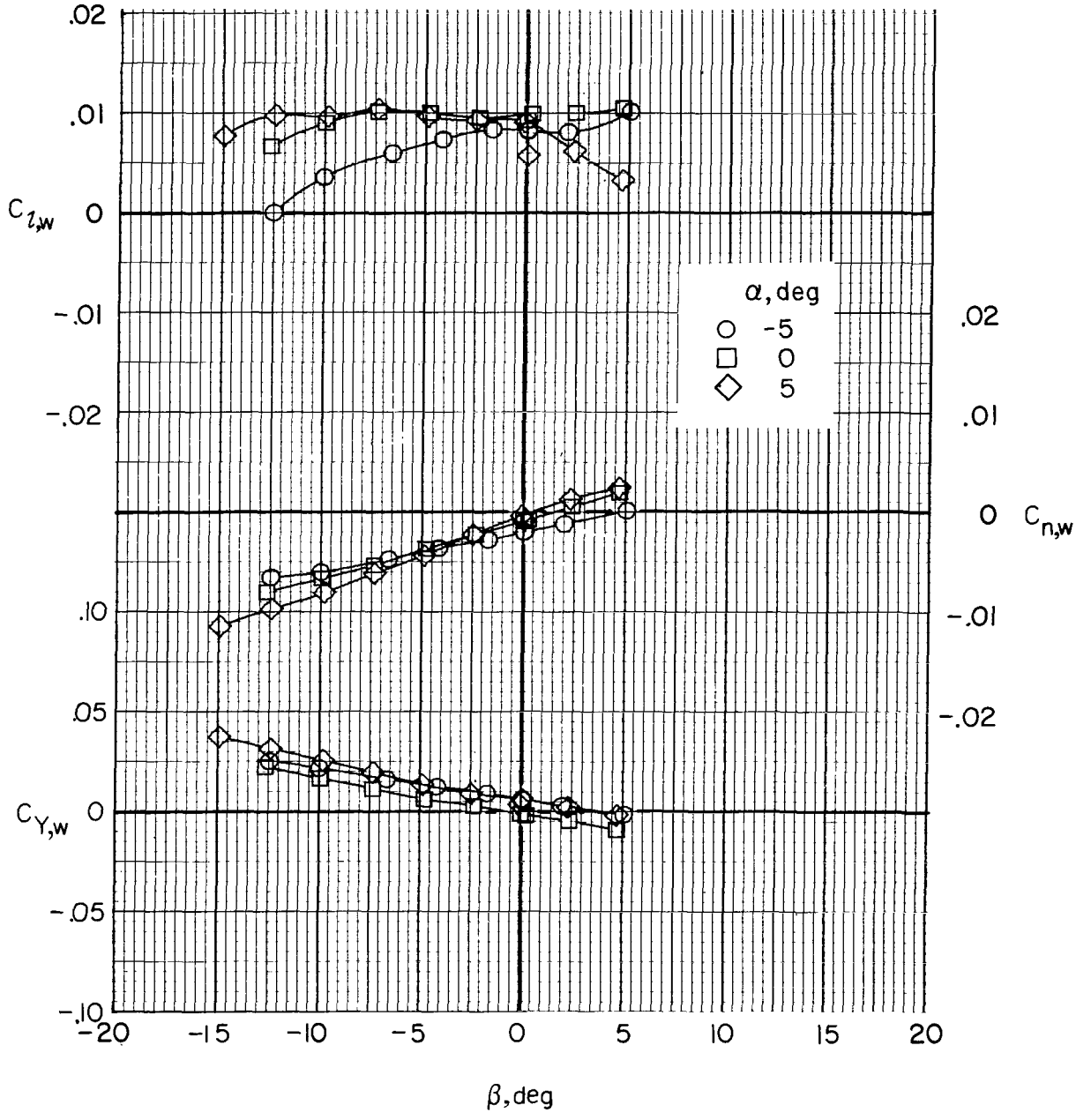

(f) Jets on ($F_1W_6VH_CJ_2$); $C_{T,J} = 0$; $i_W = 7.5^o$; $\delta_f = 30^o$.

Figure 35.- Concluded.

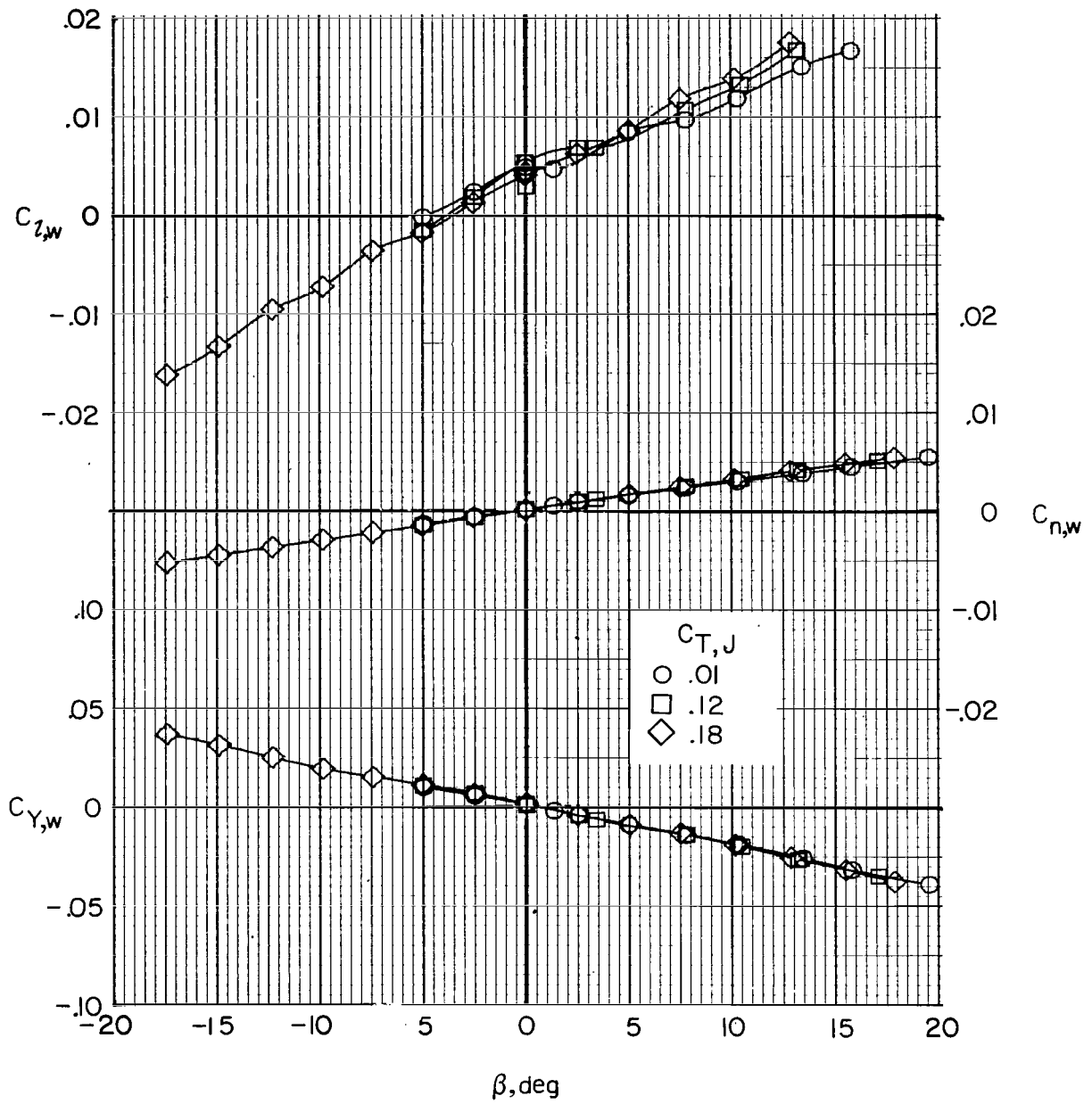

(a) $i_w = 0^o$; $\delta_f = 0^o$; $F_1 W_1 V H_C J_2$.

Figure 36.- Effect of auxiliary engine thrust level on wing lateral aerodynamics. $\alpha = 0^o$.

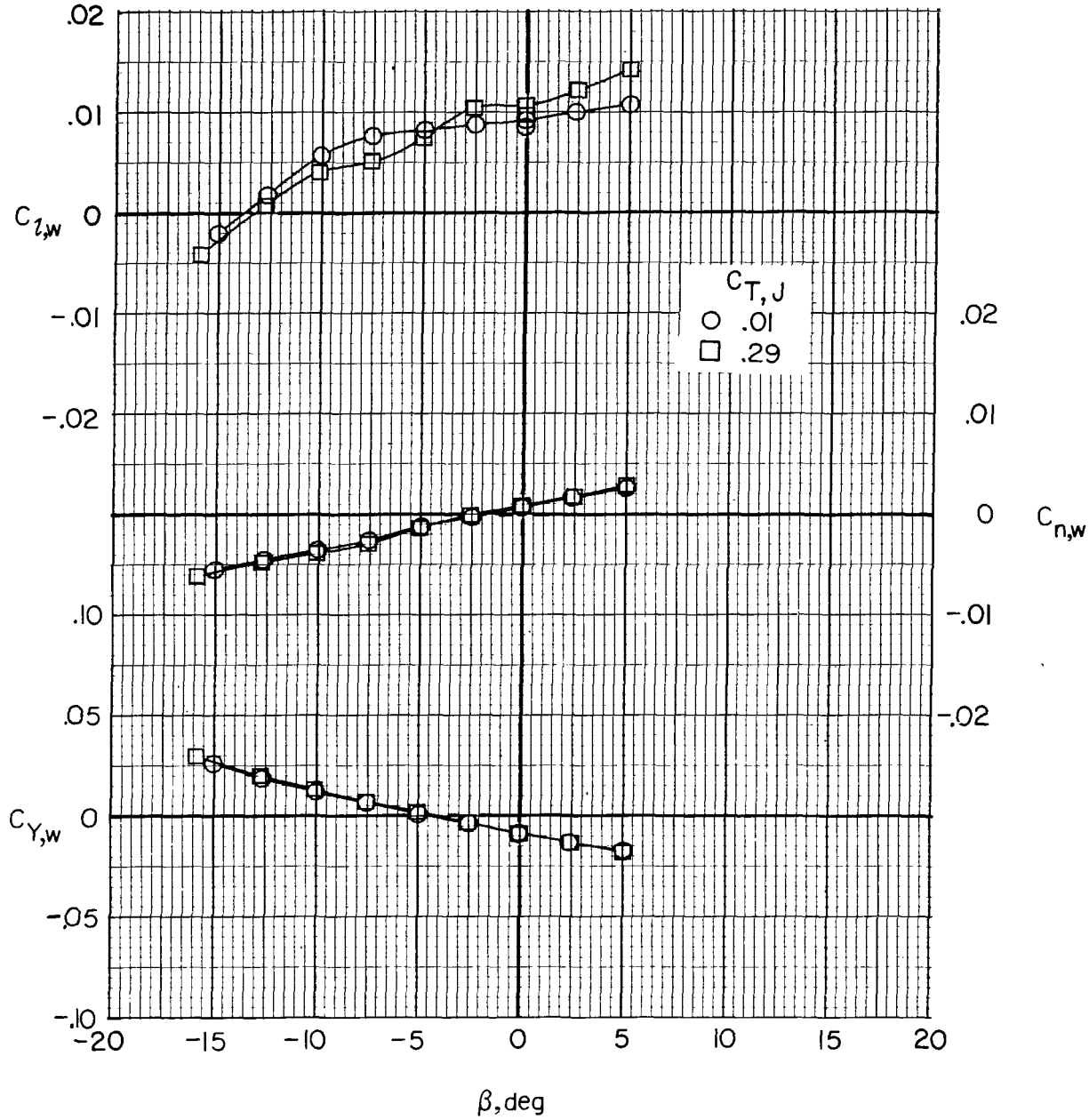

(b) $i_w = 0^o$; $\delta_f = 30^o$; $F_1W_5VH_CJ_2$.

Figure 36.- Continued.

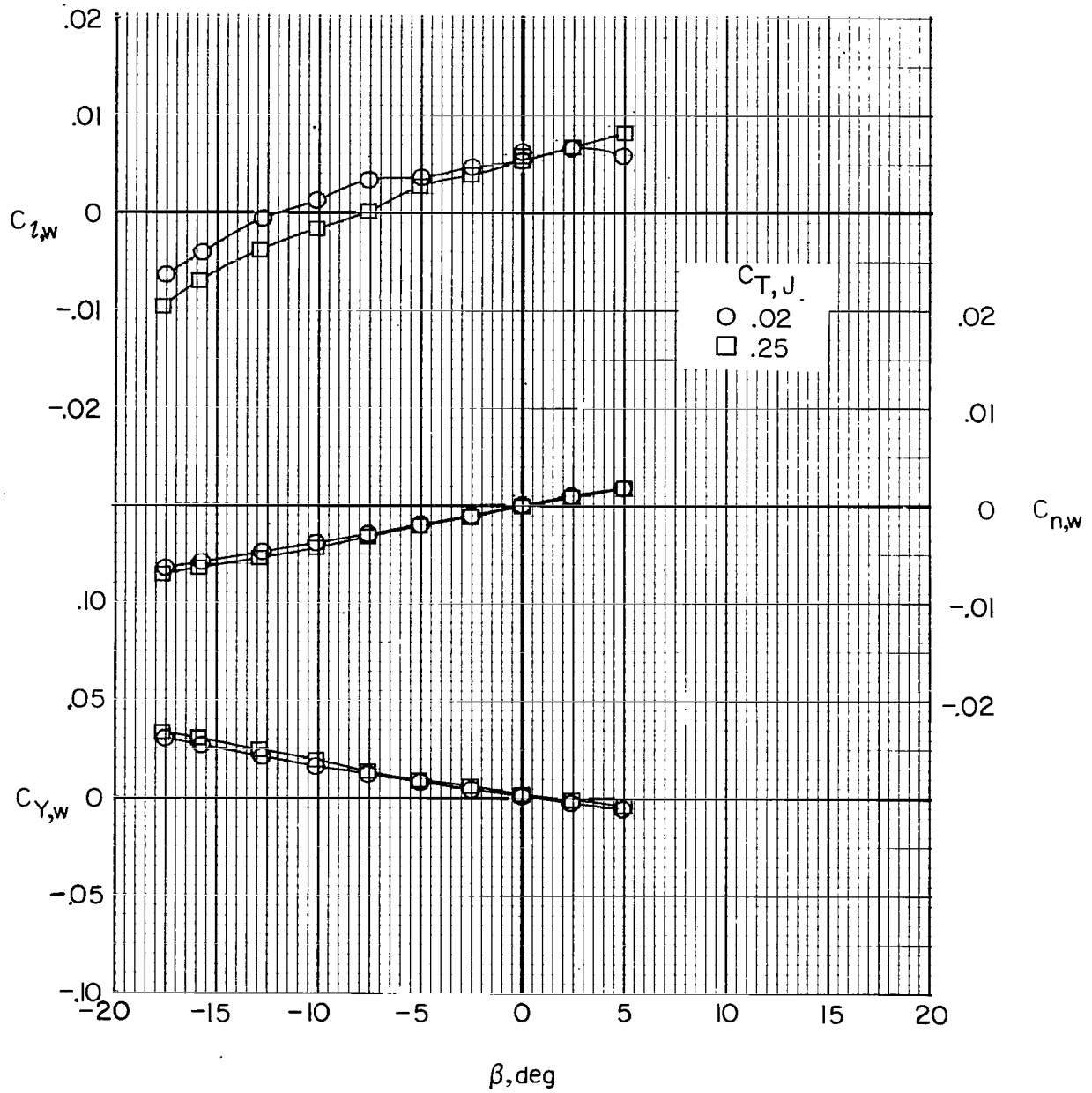

(c) $i_w = 7.5^o$; $\delta_f = 0^o$; $F_1W_2VH_CJ_2$.

Figure 36.- Continued.

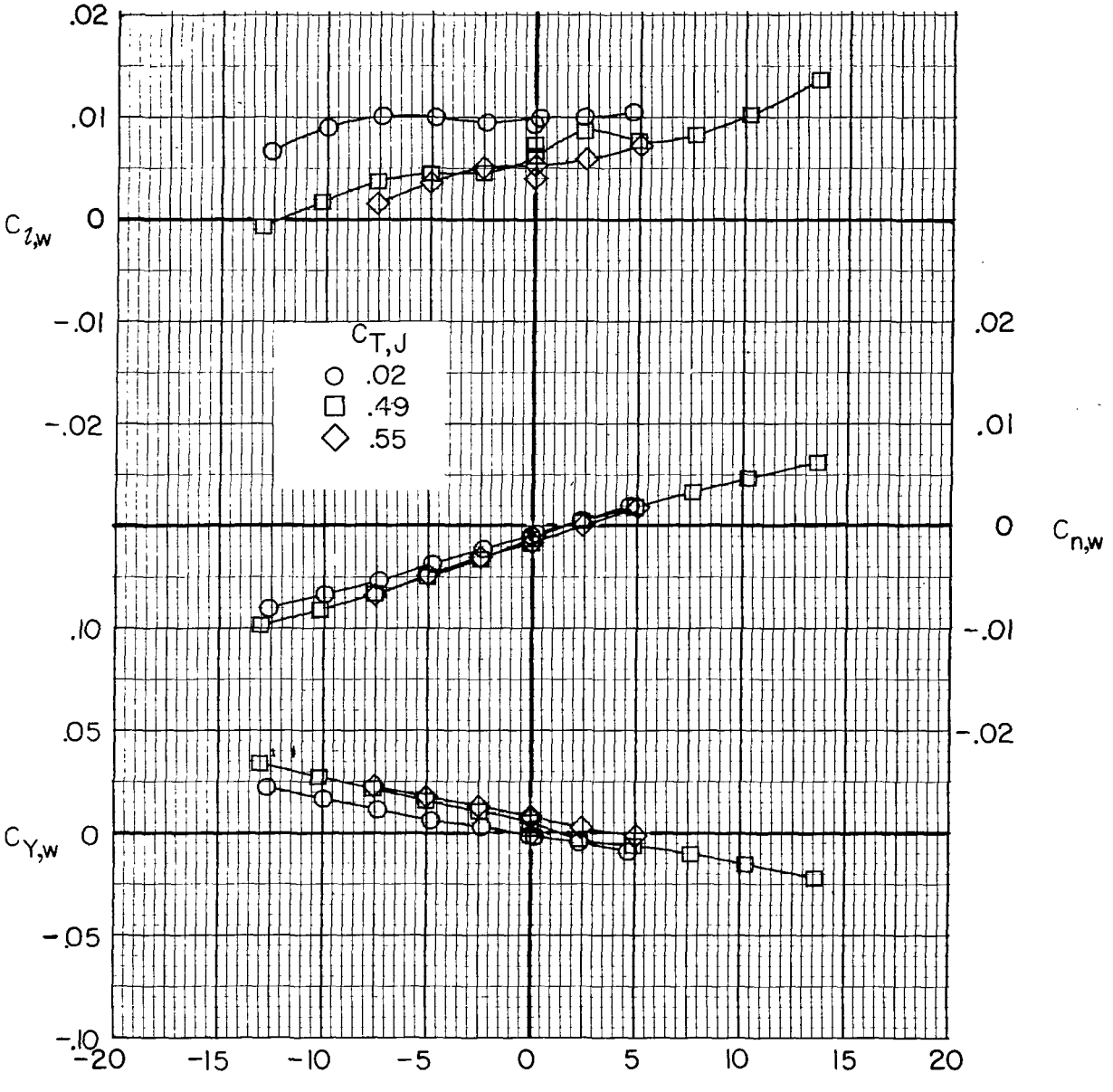

(d) $i_w = 7.5^o$; $\delta_f = 30^o$; $F_1W_6VH_CJ_2$.

Figure 36.- Concluded.

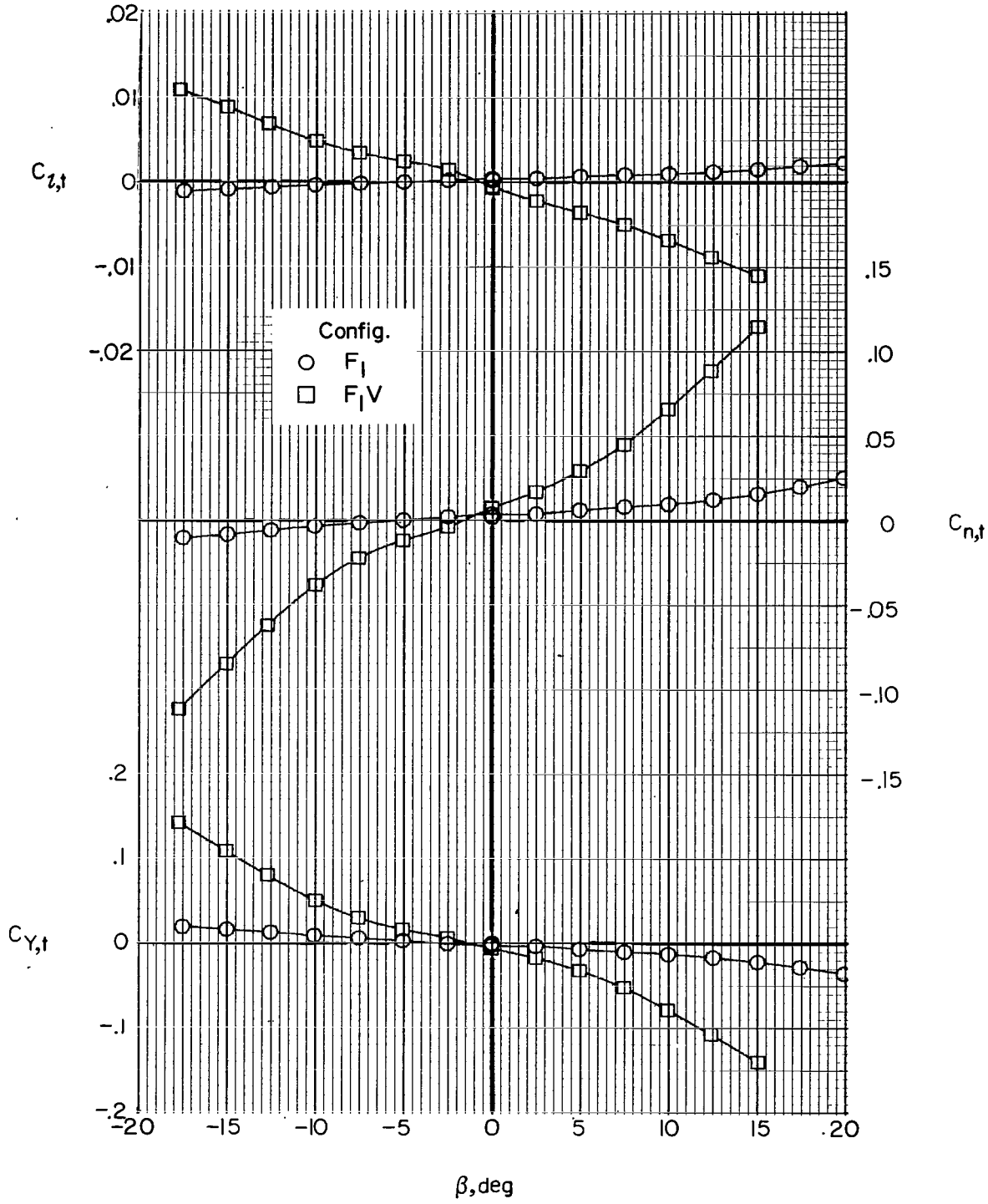

Figure 37.- Effect of vertical tail on tail lateral aerodynamics. $\alpha = 0^{o}$.

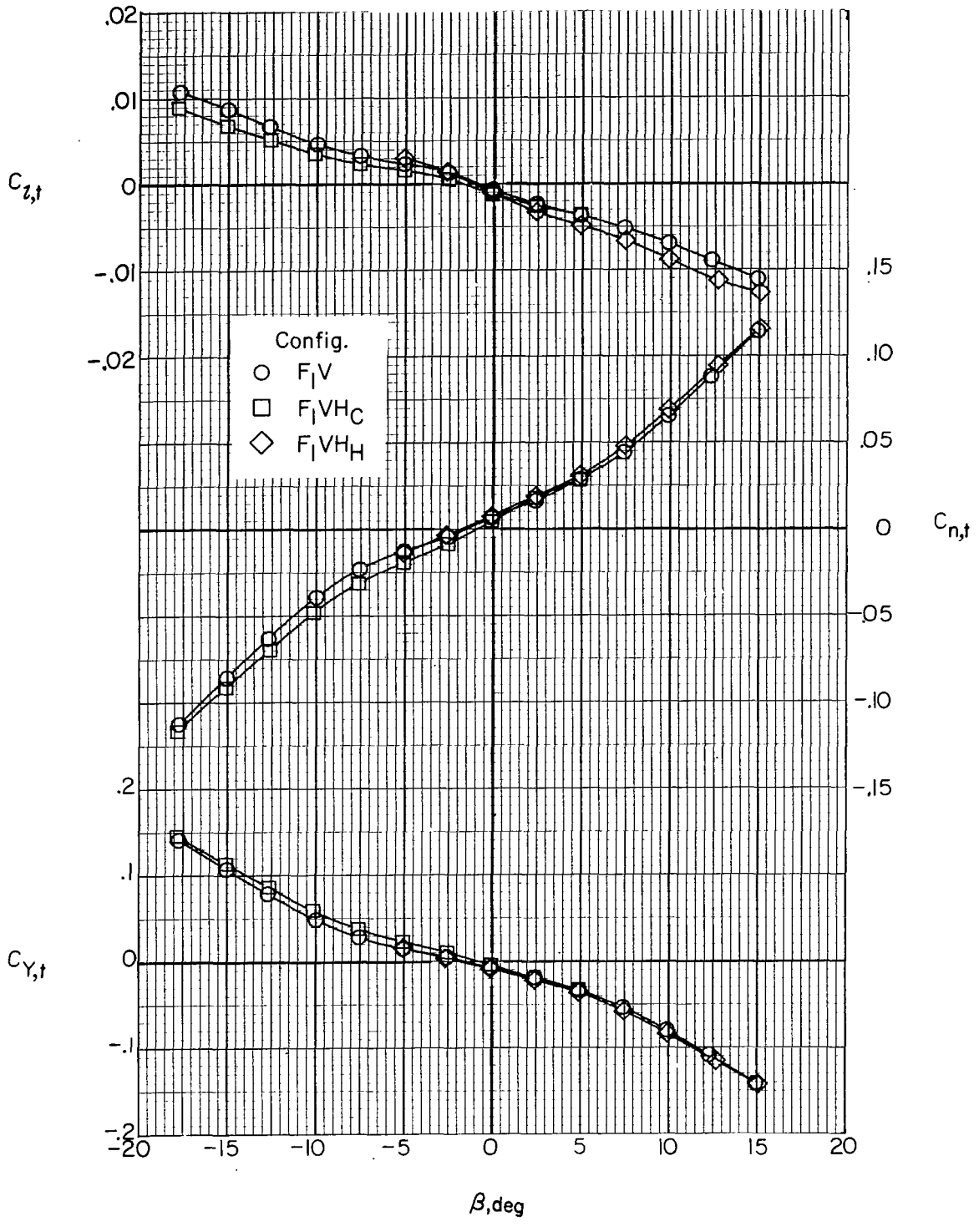

Figure 38.- Effect of horizontal tail on tail lateral aerodynamics. $\alpha = 0^{o}$.

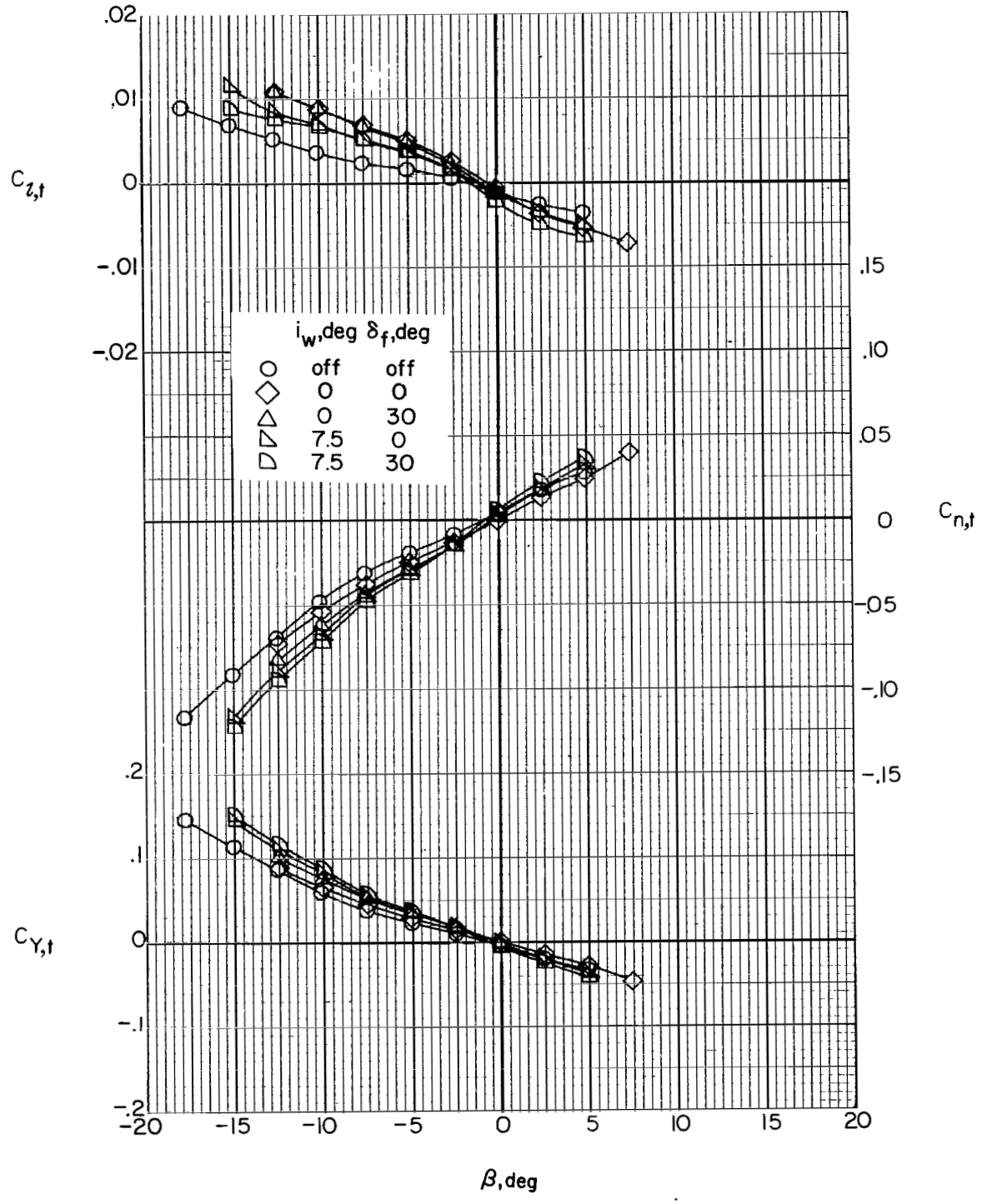

Figure 39.- Effect of wing incidence and flap deflection on tail lateral aerodynamics with the jets off ($F_1W_xVH_C$). $\alpha = 0^o$.

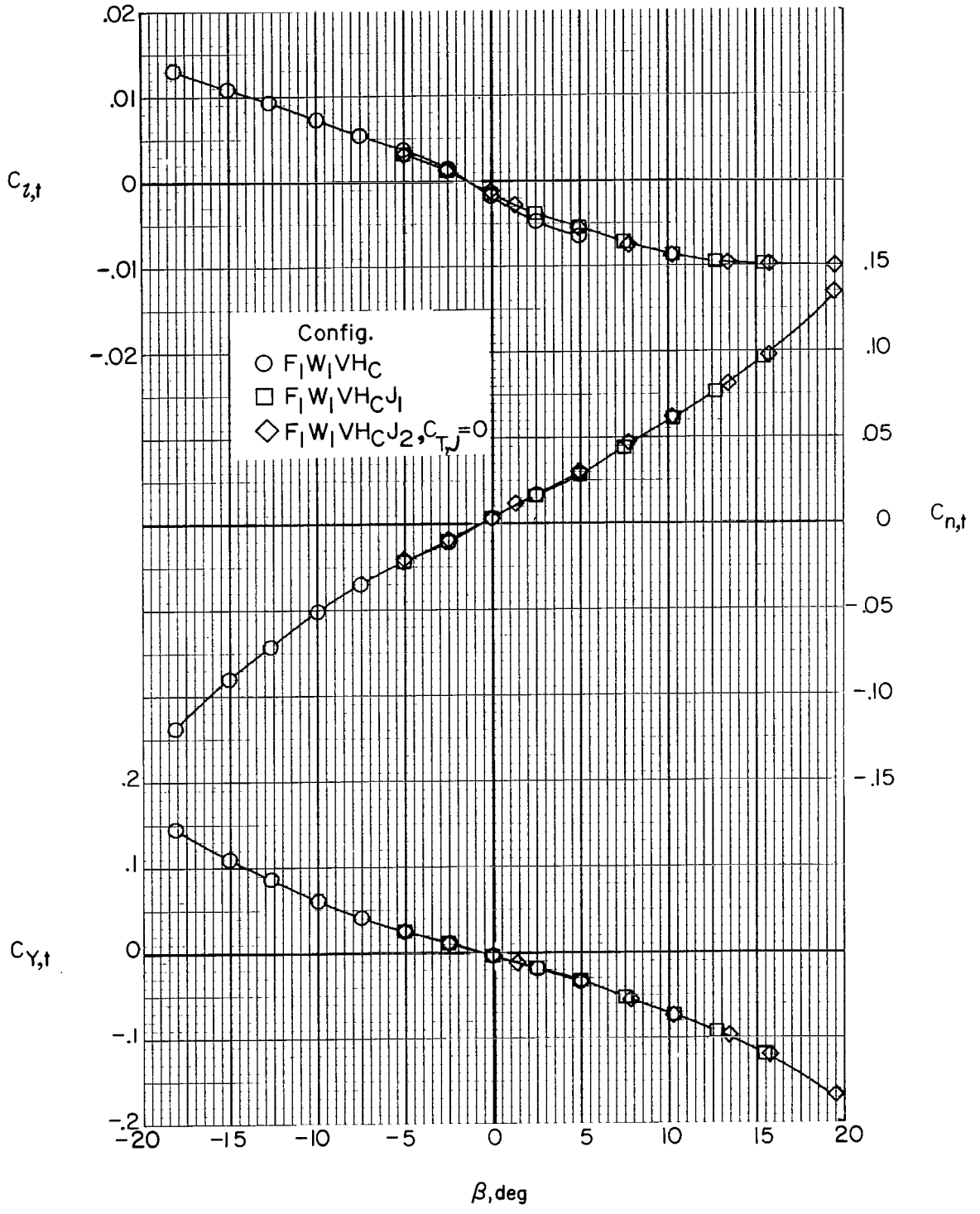

Figure 40.- Effect of auxiliary thrust engine nacelles on tail lateral aerodynamics. $\alpha = 0^{o}$.

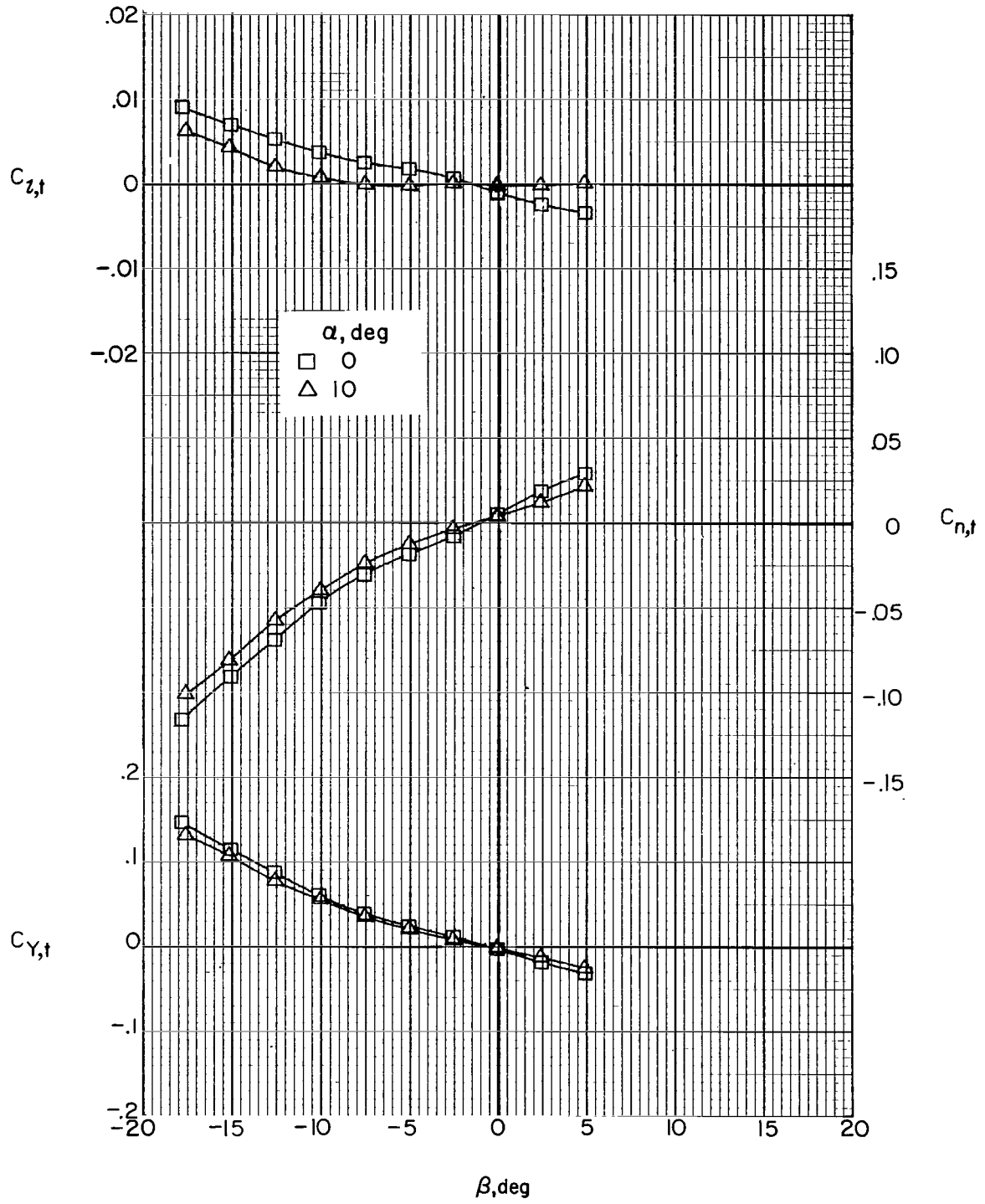

(a) Wing off; jets off (F_1VH_C).

Figure 41.- Effect of angle of attack on tail lateral aerodynamics.

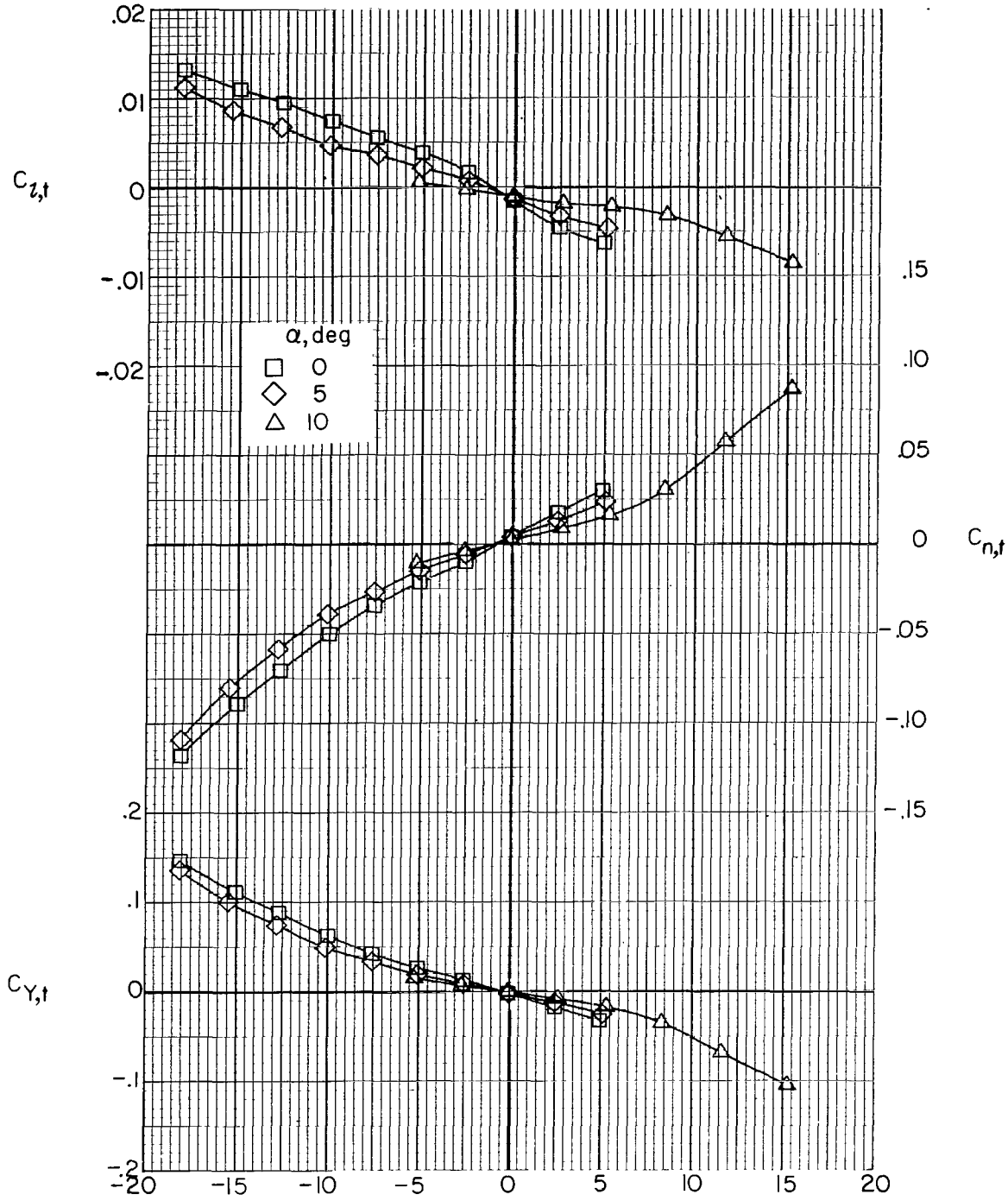

(b) Jets off ($F_1W_1VH_C$); $i_w = 0^o$; $\delta_f = 0^o$.

Figure 41.- Continued.

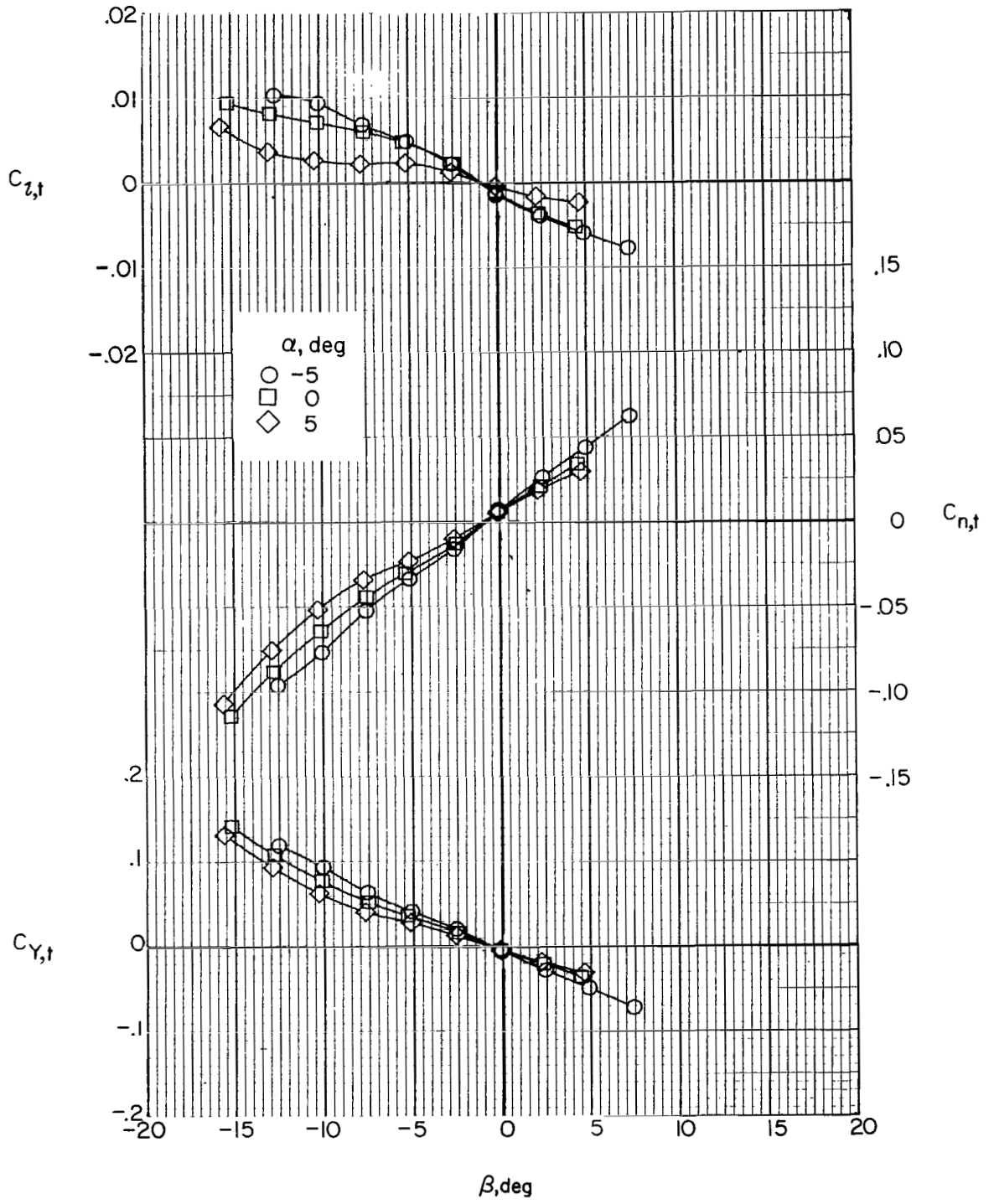

(c) Jets off ($F_1W_6VH_C$); $i_w = 7.5^o$; $\delta_f = 30^o$.

Figure 41.- Continued.

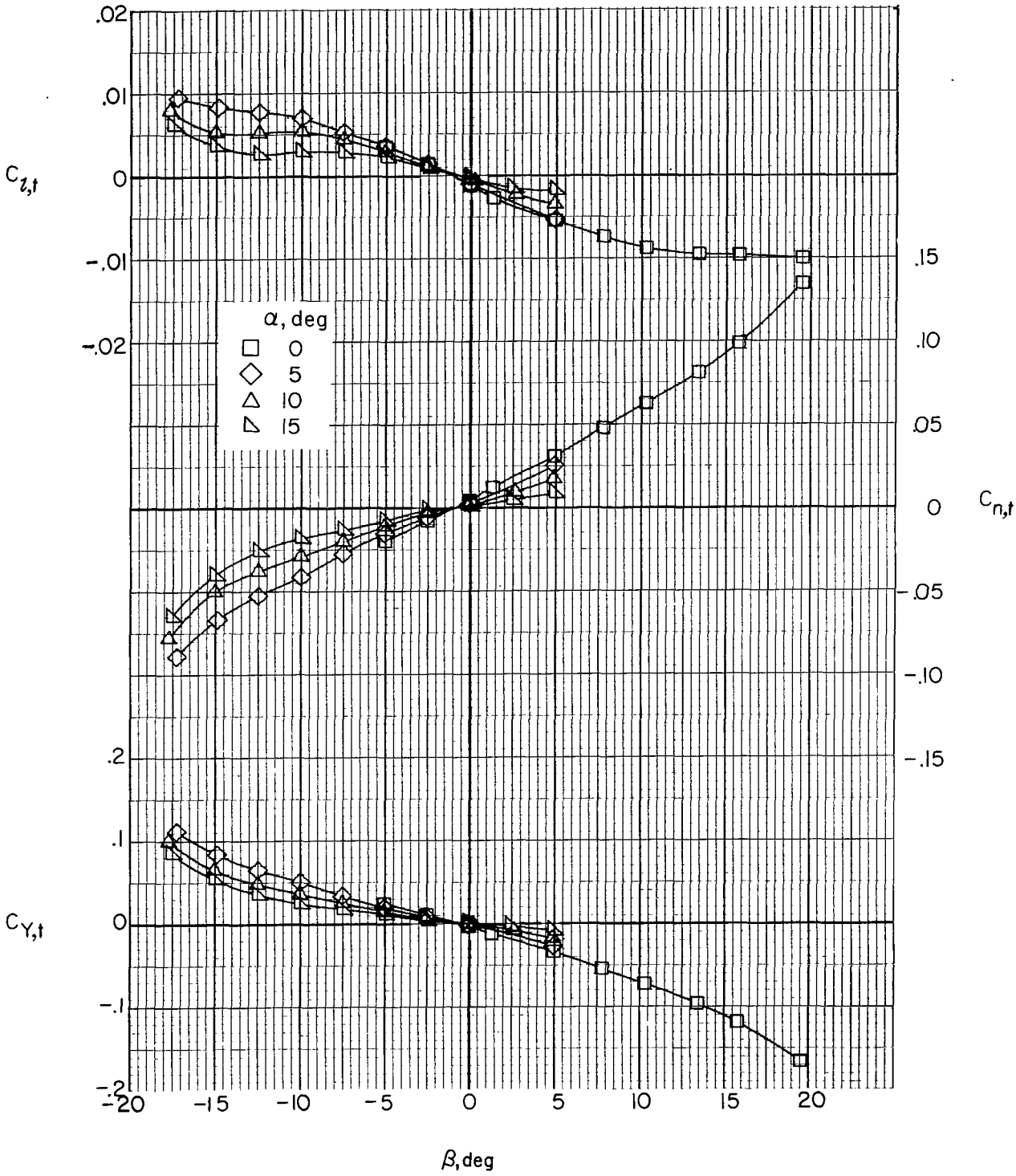

(d) Jets on ($F_1W_1VH_CJ_2$); $C_{T,J} = 0$; $i_W = 0^o$; $\delta_f = 0^o$.

Figure 41.- Continued.

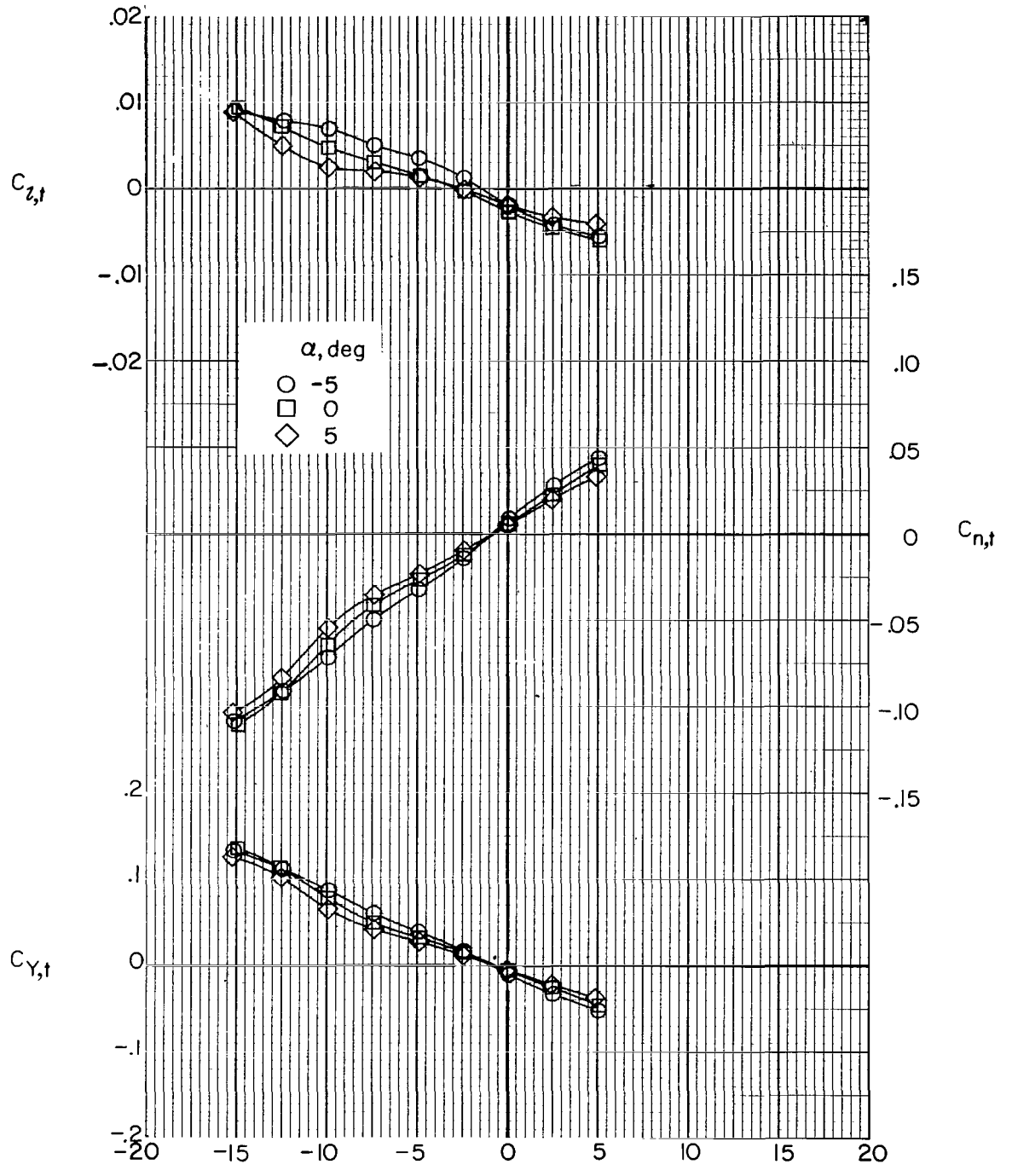

(e) Jets on ($F_1W_5VH_CJ_2$); $C_{T,J} = 0$; $i_W = 0°$; $\delta_f = 30°$.

Figure 41.- Continued.

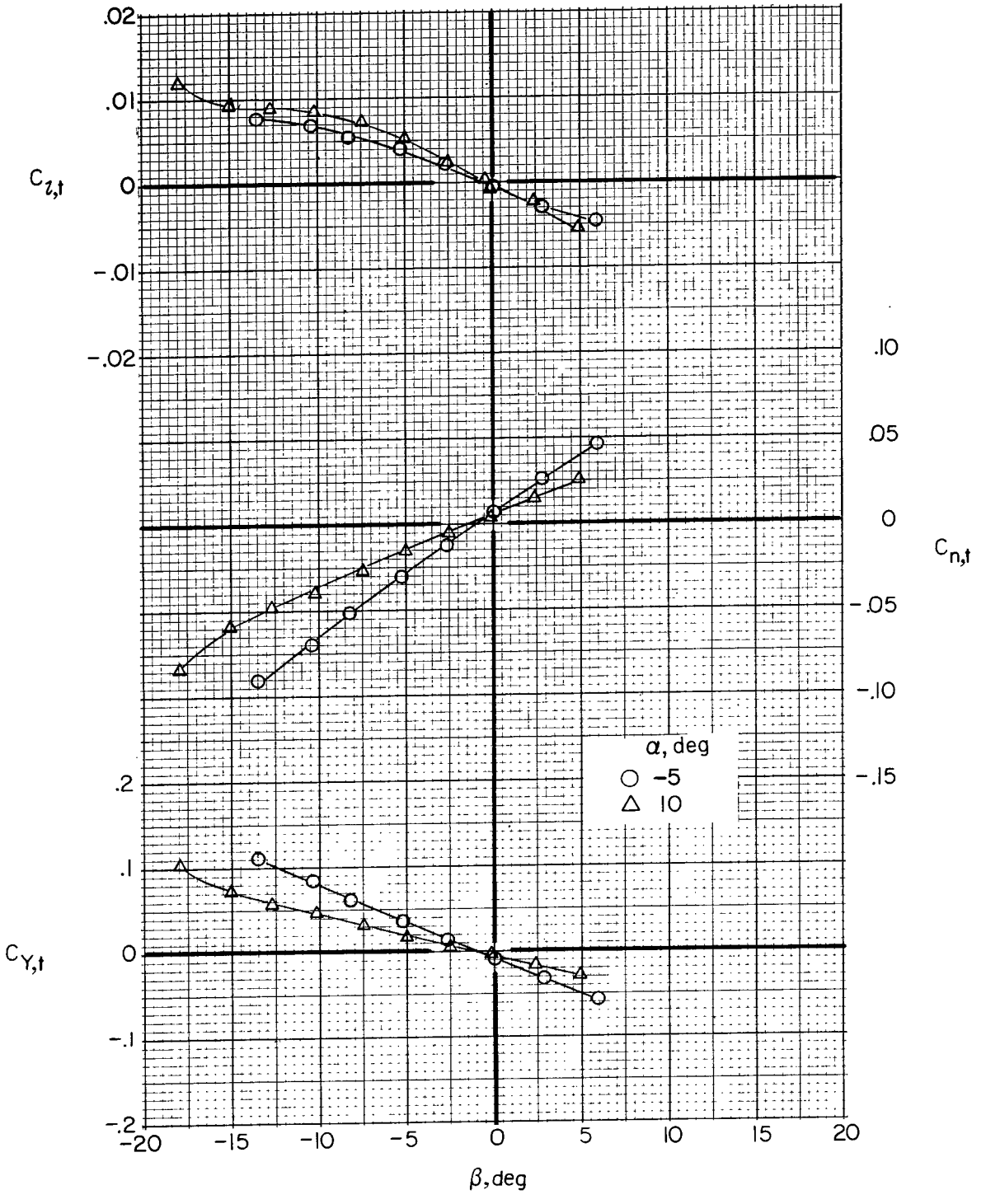

(f) Jets on ($F_1W_2VH_CJ_2$); $C_{T,J} = 0$; $i_W = 7.5^o$; $\delta_f = 0^o$.

Figure 41.- Concluded.

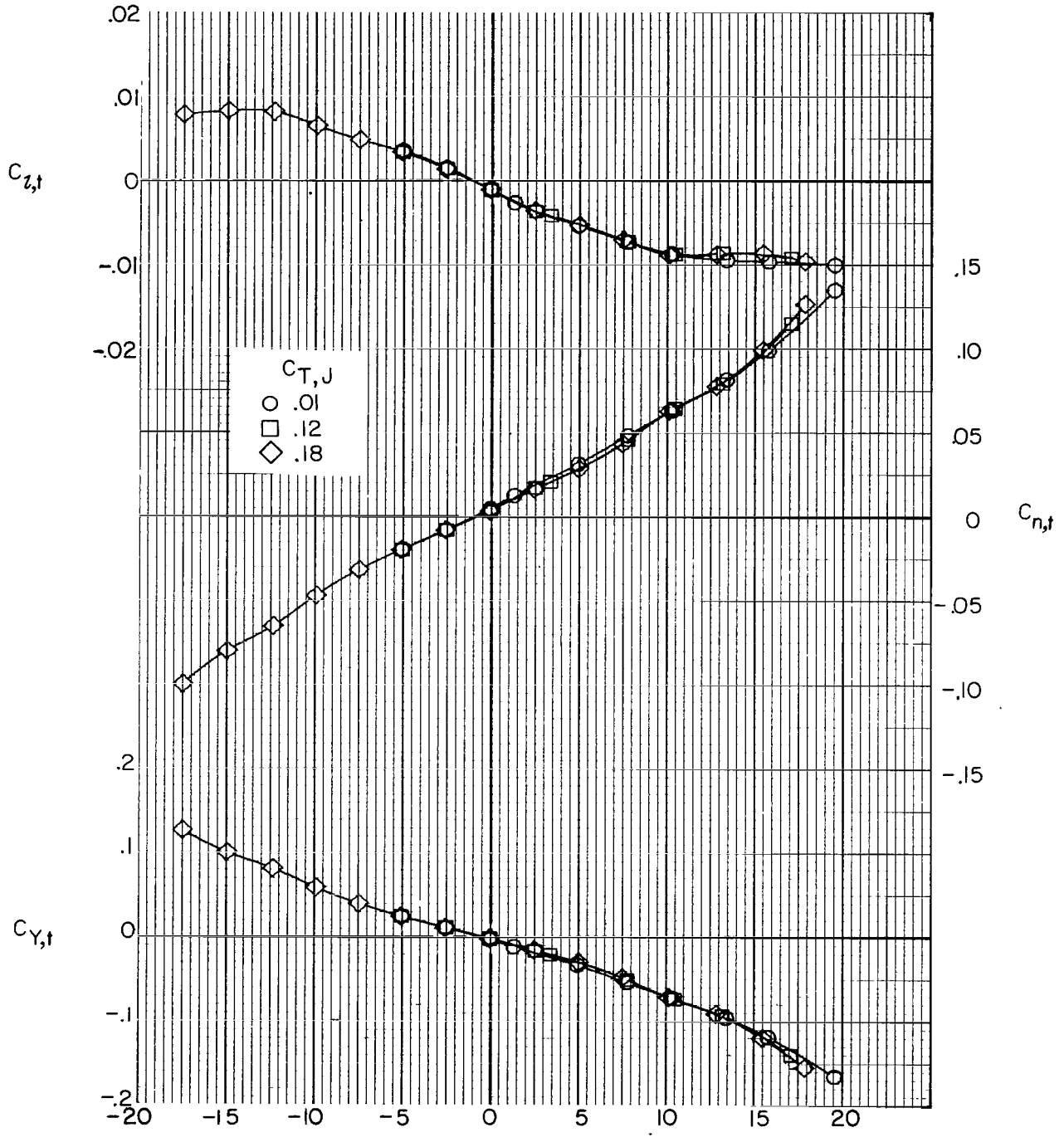

(a) $i_w = 0^o$; $\delta_f = 0^o$; $\alpha = 0^o$.

Figure 42.- Effect of auxiliary engine thrust level on tail lateral aerodynamics. $F_1W_xVH_CJ_2$.

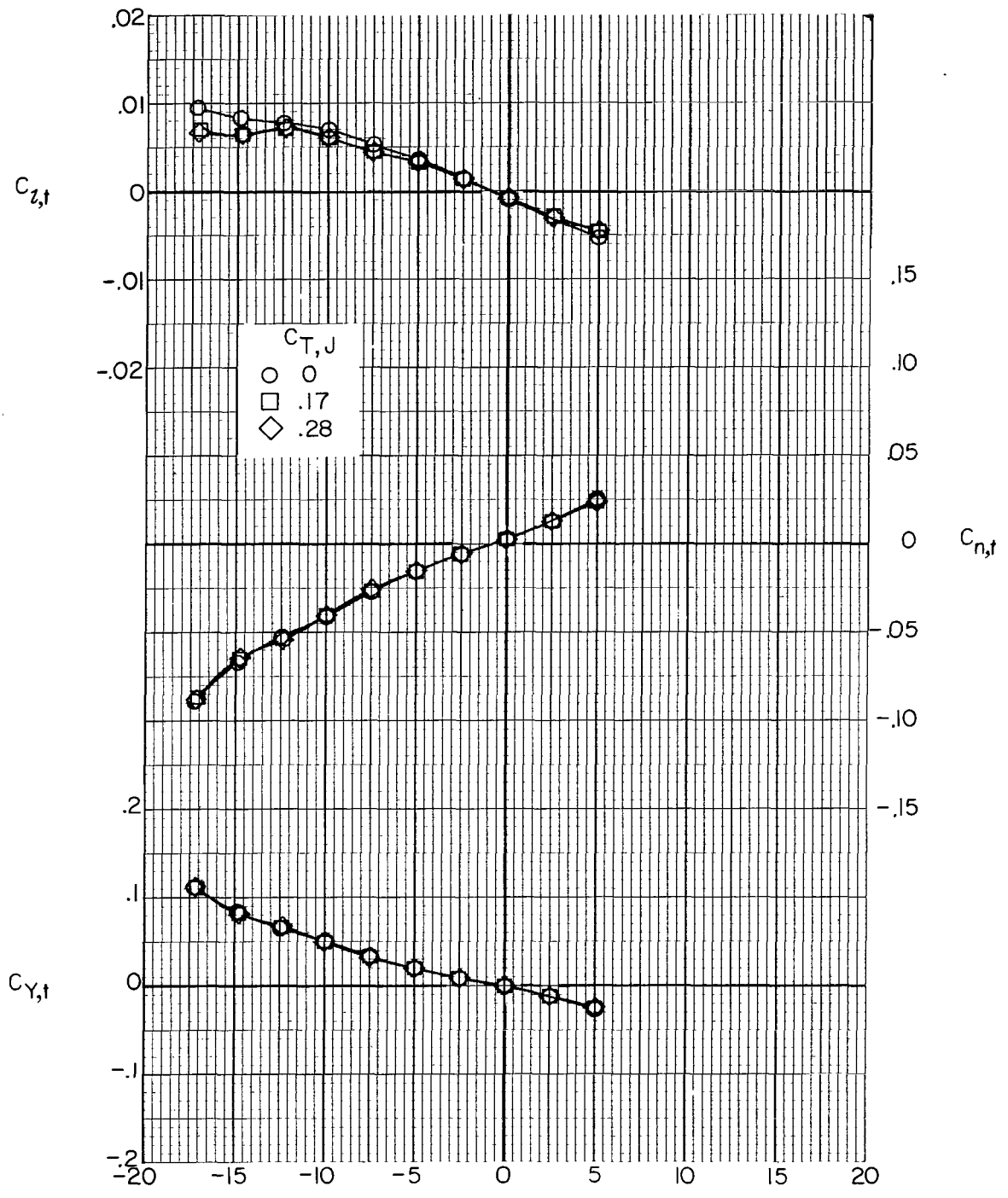

(b) $i_w = 0^o$; $\delta_f = 0^o$; $\alpha = 5^o$.

Figure 42.- Continued.

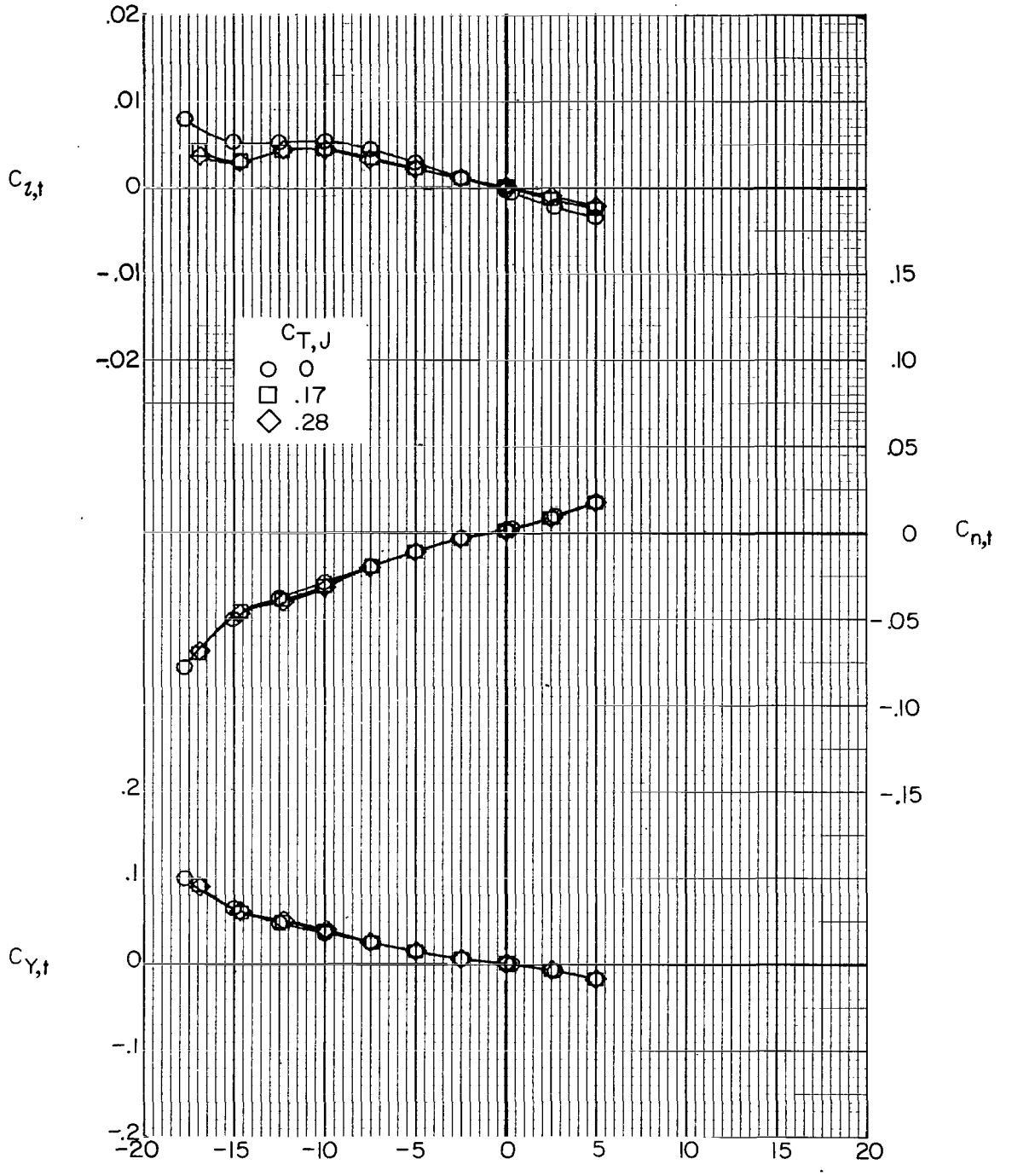

(c) $i_w = 0^o$; $\delta_f = 0^o$; $\alpha = 10^o$.

Figure 42.- Continued.

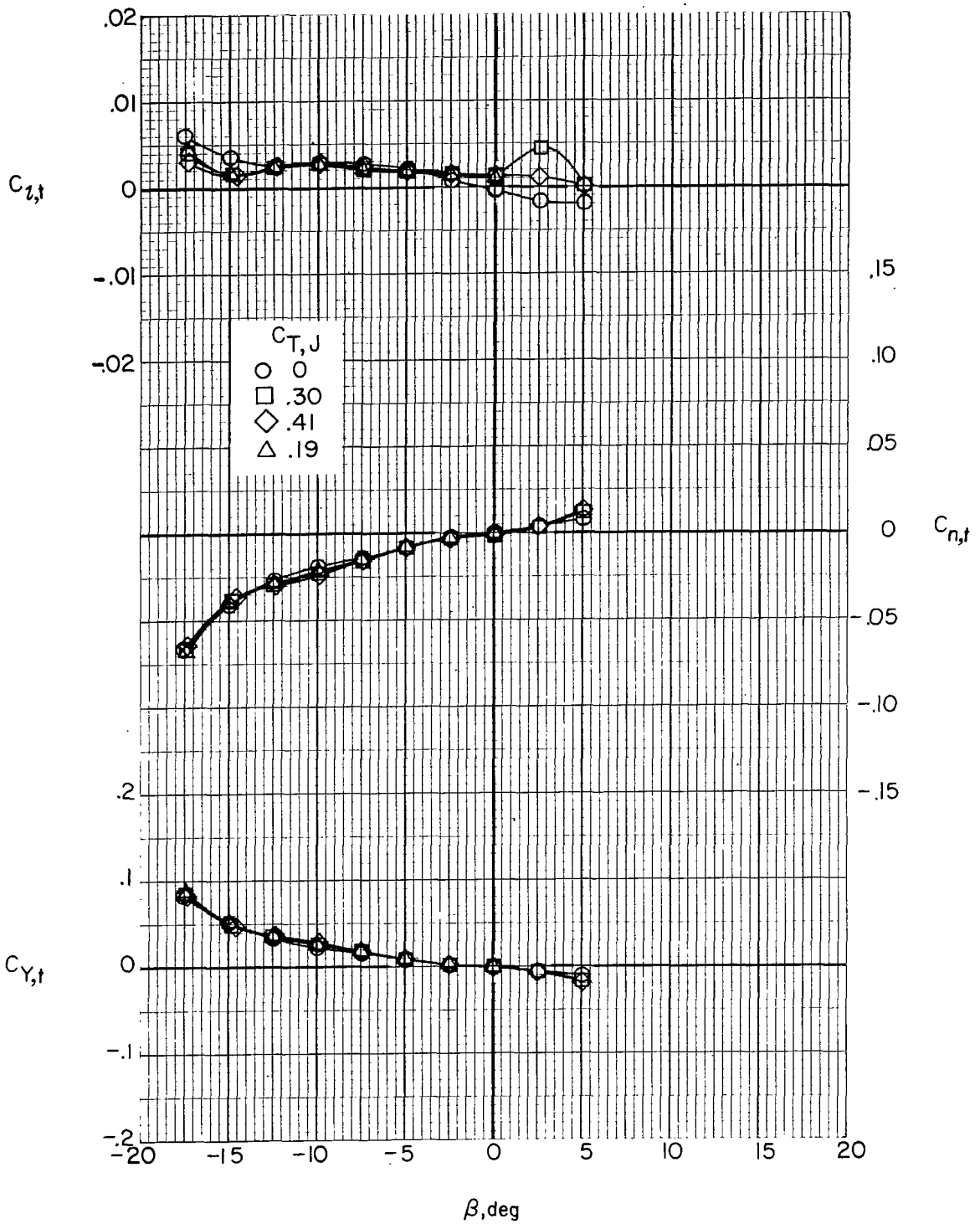

(d) $i_w = 0^o$; $\delta_f = 0^o$; $\alpha = 15^o$.

Figure 42.- Continued.

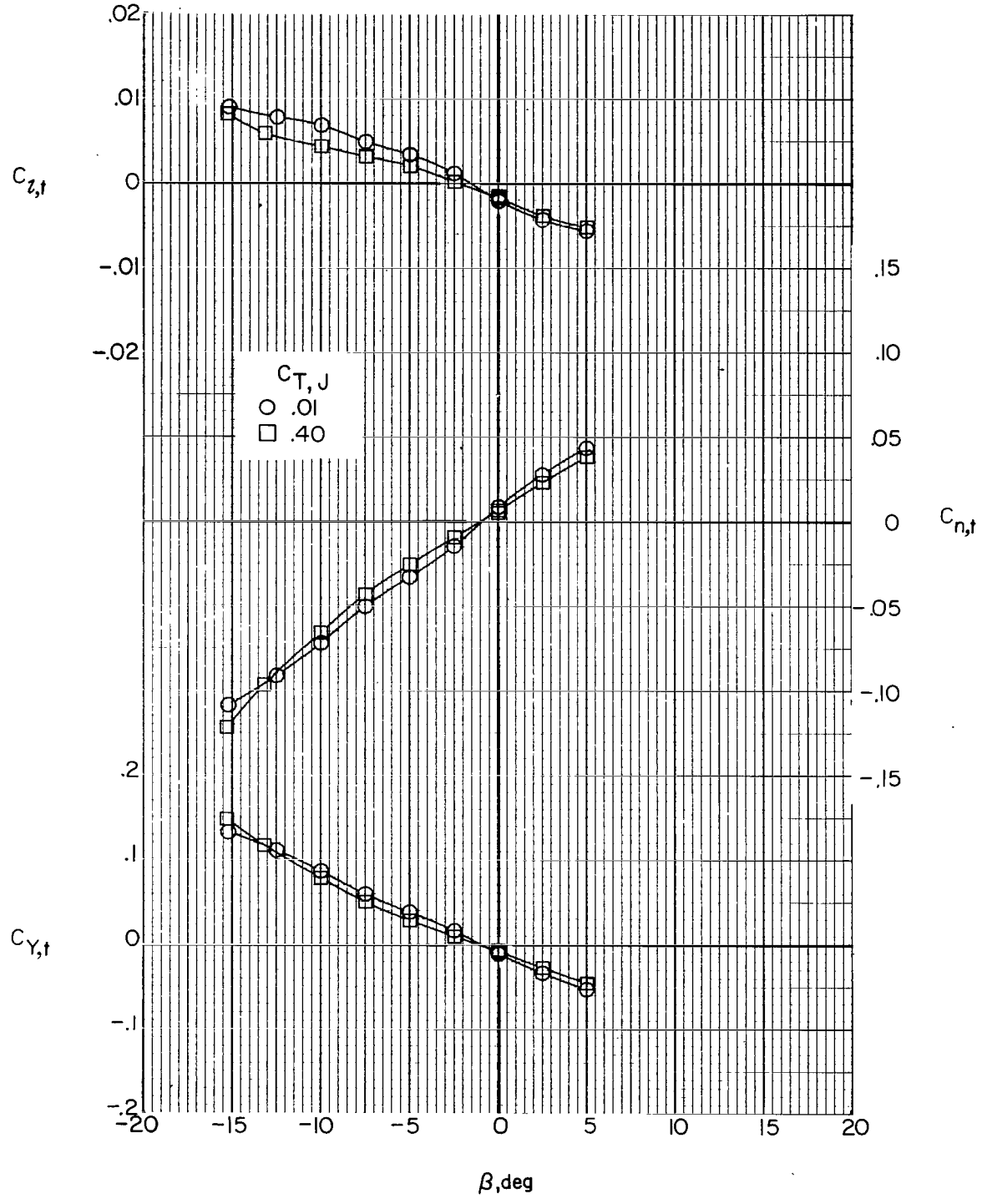

(e) $i_w = 0^o$; $\delta_f = 30^o$; $\alpha = -5^o$.

Figure 42.- Continued.

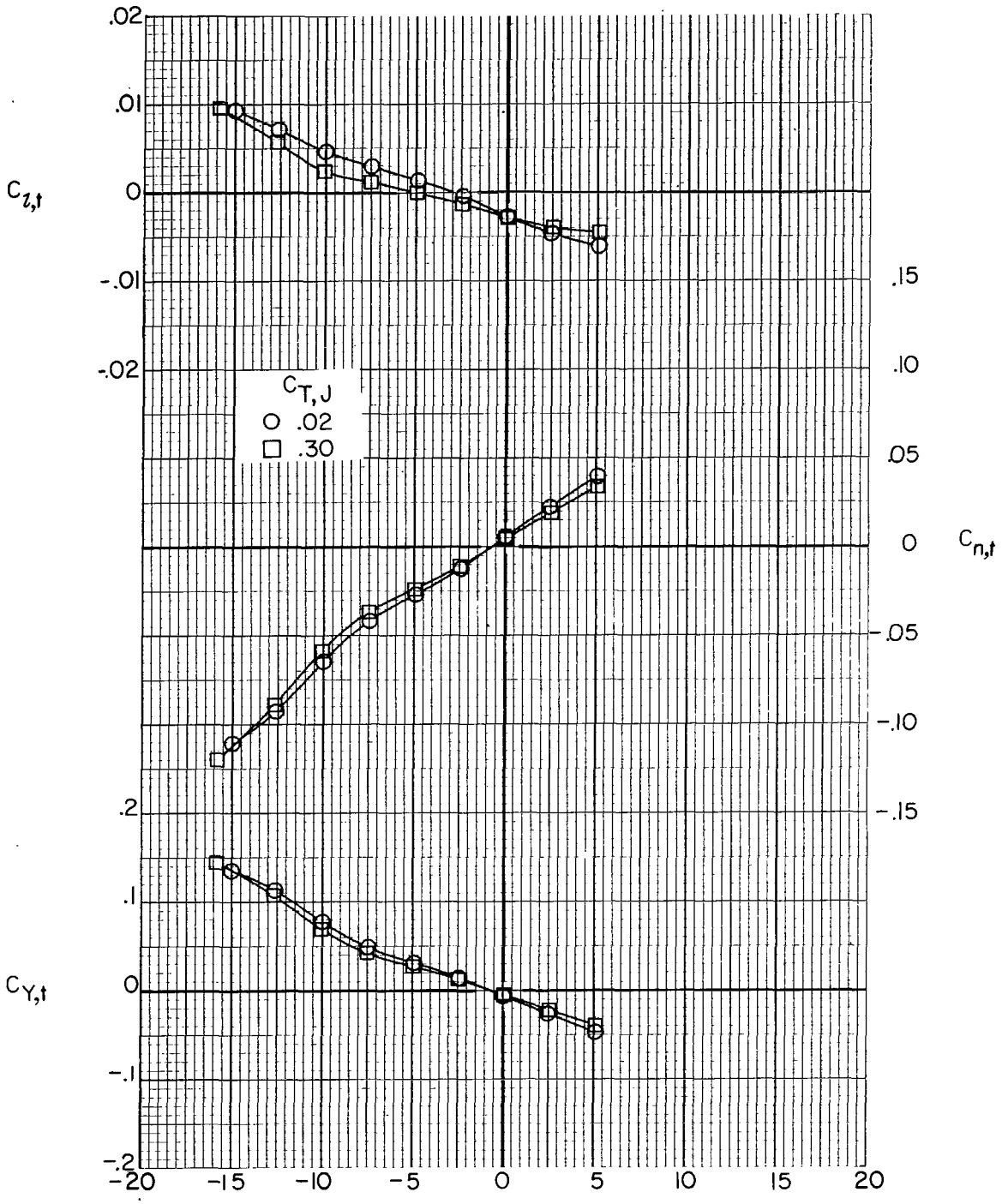

(f) $i_w = 0^o$; $\delta_f = 30^o$; $\alpha = 0^o$.

Figure 42.- Continued.

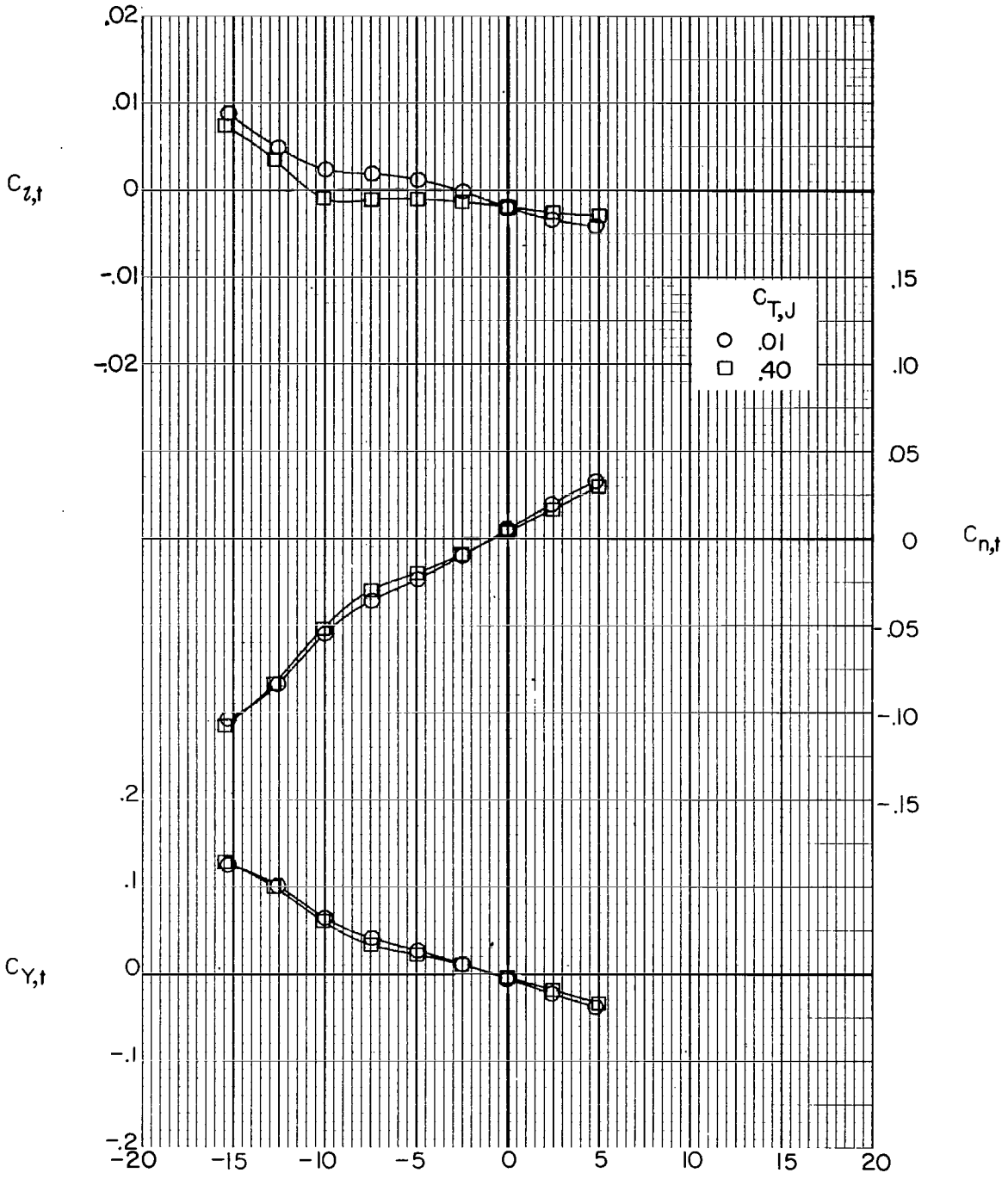

(g) $i_w = 0°$; $\delta_f = 30°$; $\alpha = 5°$.

Figure 42.- Continued.

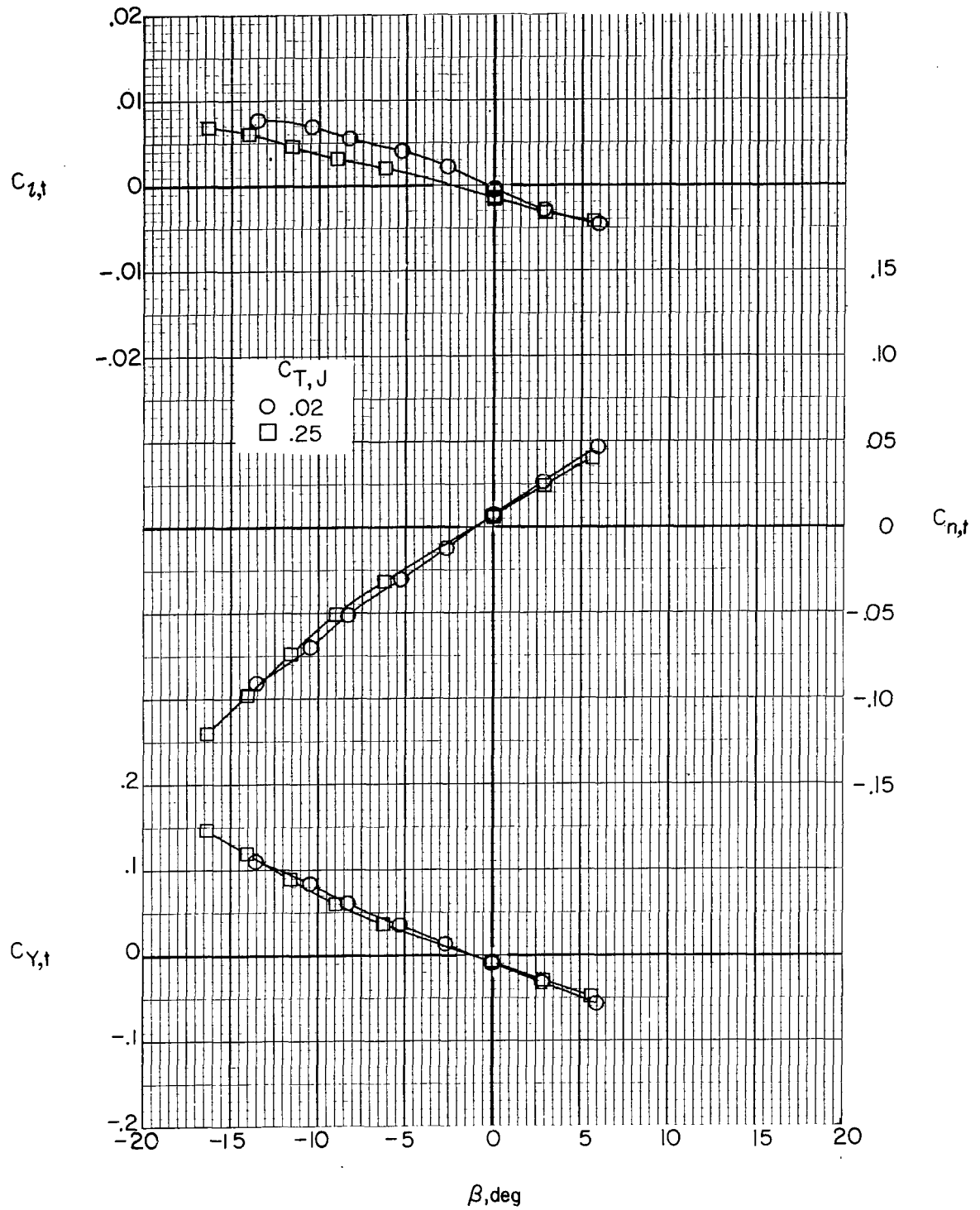

(h) $i_w = 7.5^\circ$; $\delta_f = 0^\circ$; $\alpha = -5^\circ$.

Figure 42.- Continued.

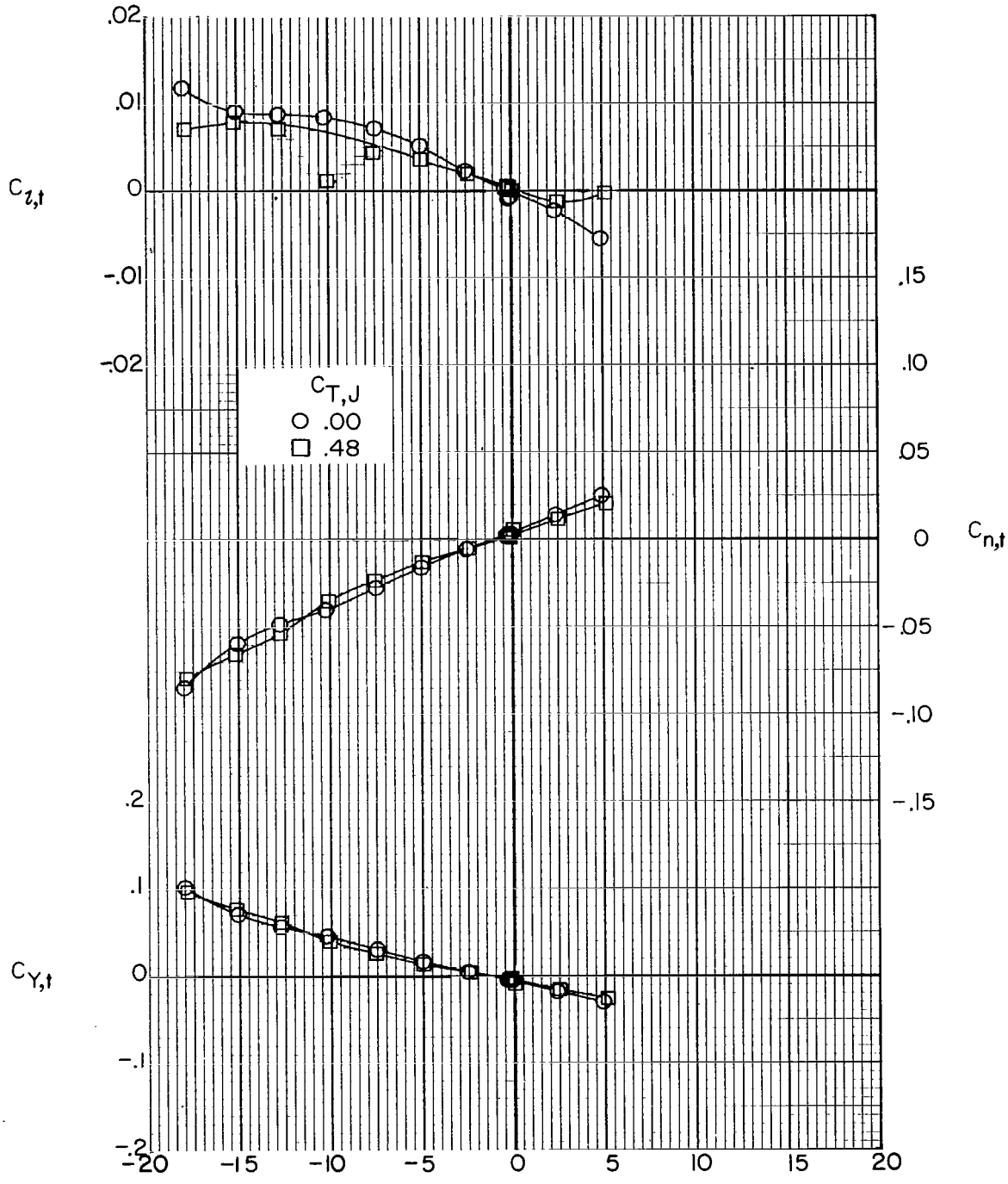

(i) $i_w = 7.5^o$; $\delta_f = 0^o$; $\alpha = 10^o$.

Figure 42.- Concluded.

"The aeronautical and space activities of the United States shall be conducted so as to contribute . . . to the expansion of human knowledge of phenomena in the atmosphere and space. The Administration shall provide for the widest practicable and appropriate dissemination of information concerning its activities and the results thereof."

—NATIONAL AERONAUTICS AND SPACE ACT OF 1958

NASA SCIENTIFIC AND TECHNICAL PUBLICATIONS

TECHNICAL REPORTS: Scientific and technical information considered important, complete, and a lasting contribution to existing knowledge.

TECHNICAL NOTES: Information less broad in scope but nevertheless of importance as a contribution to existing knowledge.

TECHNICAL MEMORANDUMS: Information receiving limited distribution because of preliminary data, security classification, or other reasons. Also includes conference proceedings with either limited or unlimited distribution.

CONTRACTOR REPORTS: Scientific and technical information generated under a NASA contract or grant and considered an important contribution to existing knowledge.

TECHNICAL TRANSLATIONS: Information published in a foreign language considered to merit NASA distribution in English.

SPECIAL PUBLICATIONS: Information derived from or of value to NASA activities. Publications include final reports of major projects, monographs, data compilations, handbooks, sourcebooks, and special bibliographies.

TECHNOLOGY UTILIZATION PUBLICATIONS: Information on technology used by NASA that may be of particular interest in commercial and other non-aerospace applications. Publications include Tech Briefs, Technology Utilization Reports and Technology Surveys.

Details on the availability of these publications may be obtained from:

SCIENTIFIC AND TECHNICAL INFORMATION OFFICE

NATIONAL AERONAUTICS AND SPACE ADMINISTRATION

Washington, D.C. 20546